Numerical Modelling of Compressible Laminar and Turbulent Flow: The Cbs Algorithm

M. Vázquez
R. Codina
O.C. Zienkiewicz

Monograph CIMNE Nº-50, April 1999

Numerical Modelling of Compressible Laminar and Turbulent Flow: The Cbs Algorithm

M. Vázquez
R. Codina
O.C. Zienkiewicz

Monograph CIMNE Nº-50, April 1999

International Center for Numerical Methods in Engineering
Gran Capitán s/n, 08034 Barcelona, Spain

The cover designed by: Jordi Pallí

First published, April 1999

Edited by:
International Center for Numerical Methods in Engineering
C/ Gran Capitán s/n
08034 Barcelona, Spain

ISBN: 84-89925-42-9
Depósito legal: B-22853-99

Contents

Chapter 1

Introduction

This work is about the development of a general algorithm for the numerical solution of flow equations: the Navier - Stokes set. This set of differential equations models the time dependent behavior of fluids. It is formed by continuity, linear momentum and an energy transport equations.[1] The algorithm here described is a *general* one since it can handle equally a great variety of problems, ranging from incompressible to compressible flows, viscous to inviscid, stationary and transient, all of them physically modeled by the same set of differential equations.

As we will see in the following chapters, the introduction of the restriction $\nabla \cdot \boldsymbol{u} = 0$ in the Navier - Stokes equations produces very important effects. Basically, they are derived from the fact that the velocity field can be taken as the only unknown, with the pressure field being further derived from it. On the contrary, in compressible flows, the problem is described in terms of velocity and two thermodynamic variables, pressure and temperature, say, both related through an equation of state. In this case, each of the three fields evolution can be modeled by means of a conservation transport equation of the same kind, namely, the temporal variation of the unknown equal a flux divergence. On numerical grounds, the consequence is that the same algorithm for compressible flow cannot be plainly applied to incompressible problems unless some aspects are considered. In theoretical physics (see for instance [Landau and Lifshitz, 1987]), when solving analitically some simple flow problems, it is usual to consider inompressible flow as a simplification of compressible one. But in computational fluid dynamics, despite of the simplified equations, both problems present a variety of difficulties of their own. Even the solvers are different: while implicit solvers are a must in incompressible flow, explicit ones are widely applied in compressible problems.

[1] The original Navier - Stokes equation is the momentum one. The set including it and the other two is so called by extension.

In the present work, a quest for a general algorithm is described, following one of many possible ways to tackle the problem. In general, this is done extending methods either from compressible to incompressible flows or from incompressible to compressible ones. Recent works following the first line include that of G. Hawke and T. Hughes [Hawke and Hughes, 1998], previously studied in [Hawke, 1995] where its extension to k-ε model is also developed. They propose a finite element method using the Galerkin/Least-Squares technique (GLS), proven to work well as a stabilization technique in both regimes, . The problem is then reformulated in different sets of variables, choosing the entropy and the primitive sets, for solving incompressible and compressible flows. S. Mittal and T. Tezduyar [Mittal and Tezduyar, 1998] modified this method by working with an "augmented" conservation set of variables. Instead of using entropy or primitive sets they propose to use a conservation set adding an equation for the pressure. M. Storti and co-workers [Storti et al., 1997] have developed a method based in Streamline Upwind / Petrov-Galerkin method (SUPG) in which a particular evaluation of the intrinsic times matrix provides the stabilization required by both convective terms and the continuity equation.

Also in the same group, E. Turkel, V. Vatsa and R. Radespiel propose in [Turkel and Radespiel, 1996] (also see [Turkel, 1992]) a preconditioning method which accelerates the convergence of both compressible and incompressible flows. It is mainly devised for compressible flow with low Mach number zones. Within them, the large disparity between local velocity and speed of sound produces very stiff systems. Hence, explicit time advancing can be done only using very small time steps. By preconditioning, the difference between speed of sound and convective velocity is narrowed, thus, improving convergence and with the additional benefit of the presence of a stabilizing artificial viscosity. It is extended to incompressible flow by J. Weiss and W. Smith [Weiss and Smith, 1995] by the addition of artificial compressibility in the continuity incompressible equation. Mixed interpolations, a well known technique in incompressible problems, has also been extended to compressible flows, for example in works of A. Soulaïmani and M. Fortin [Soulaimani and M.Fortin, 1994] or M.O. Bristeau and co-workers [Bristeau et al., 1990]. The former paper propose an algorithm which combines SUPG techniques for stabilizing convective terms and different spaces for density (pressure) and energy (temperature) on one side and velocity on the other one. P1 and P2 respectively is their choice, and a conservative set of variables is suggested. No convective stabilization is needed, as proposed in [Bristeau et al., 1990], if primitive variables are used and if the velocity interpolation space is P1, similarly for the pressure - density - temperature set, but either enriched with bubble functions or defined on a finer spatial tesselation.

On the other hand, S. Karimian and G. Schneider [Karimian and Schneider, 1995] propose an extension to compressible flow of a pressure based method, and was successfully applied to incompressible flows. As we said, the continuity equation is in this case a constraint for the pressure instead of an evolution equation. In this method, by using

control volumes surrounding the nodes they calculate conservation conditions for them. In the continuity equation both pressure/velocity and pressure/density couplings are treated according to each node regime.

The present monograph follows the ideas of O.C. Zienkiewicz and co-workers, introduced in [Zienkiewicz et al., 1990, Zienkiewicz and Wu, 1992] and extended and developed in [Zienkiewicz and Codina, 1995, Zienkiewicz et al., 1995, Codina et al., 1998b] and so on. This method was christened *CBS* for *Characteristic Based Split* algorithm. Its cornerstone corresponds to extending of *splitting* or *fractional step* techniques from incompressible to compressible flow. In CFD context, the concept of *splitting* was first independently introduced by G. Strang in [Strang, 1968] and in a slightly different way by A.J. Chorin and R. Temam in [Chorin, 1967, Temam, 1969]. Splitting techniques are all based in the fractional solution of the momentum equation. In the conservation form, we will see that the linear momentum transport equation has three main terms, divergences of fluxes: convective, diffusive and pressure contributions, which in turn can be segregated from the original equation in order to solve first a fractional momentum equation and then to correct it with the rest of the terms thus obtaining the proper momentum. In the context of incompressible flows, these methods are also called *projection* methods. The fractional momentum does not verify the divergence free condition due to the lacking terms. When completing the right hand side of the original momentum equation is done, the momentum is "projected" on the space of divergence free solutions. In compressible flow, the concept of projection on divergence free solution spaces loses its meaning.

From the name given to the algorithm, the second basic ingredient becomes apparent : the characterisitc based time discretization. This concept was probably addressed for the first time in [Douglas and Russel, 1982, Pironneau, 1982, Loehner et al., 1984]. The idea is to discretize in time not the time partial derivative of the unknonwn but its total or material derivative by reformulating the continuum flow equations in a characteristics co-moving frame. If then the space discretization is done, a consistent artificial diffusion which stabilizes convective terms appears. It is similar in looks and effects to that introduced by other schemes like Streamline Upwind Petrov-Galerkin, Sub Grid Scale, etc. [2] In this case, it basically consists of the convective derivative of the spatial residual multiplied by the time step. If space is discretized using the finite element method and characterisitc based time discretization is used, we talk about a *Characteristic - Galerkin* technique.

Finally, in the case of compressible flows, the presence of strong gradients and / or discontinuities in the problem variables requires the use of an additional artificial diffusion to avoid the presence of spurious overshoots and undershoots in the solution. Again, out of many possibilities, we have chosen one, the anisotropic shock capturing

[2] See references [Pironneau et al., 1992, Codina, 1998a] for a comparison between these methods.

technique of R. Codina [Codina, 1993a, Codina, 1993b].

In the first half of this monograph, the algorithm for laminar flow is presented and its behavior under many conditions and regimes is shown, mainly based on the following papers: [Zienkiewicz and Codina, 1995], [Zienkiewicz et al., 1995], [Codina et al., 1998b], [Vázquez et al., 1996], [Codina et al., 1998c], [Codina et al., 1998a], [Nithiarasu et al., 1998], etc., which trace the evolution of the general algorithm. Once the algorithm was tested in many laminar flow problems, considering all the combinations of compressible / incompressible cases and viscous / inviscid cases, the following step is the extension to turbulent problems. The turbulence model chosen is the k-ε model, original from [Harlow and Nakayama, 1968, Launder and Spalding, 1974]. It is of the kind known as the *two - equation models*. In these models, Navier - Stokes equations are replaced by a set of Averaged Navier - Stokes + two turbulent variables equations. The Averaged Navier - Stokes set is obtained by averaging in some particular way the continuum Navier - Stokes one. Hence, their solutions are no more instantaneous but "mean" fields. The other additional equations are transport ones for the kinetic turbulent energy and, in the case of k-ε , turbulent dissipation, which are derived using a mixture of analytical and phenomenological ideas. CBS extension to turbulent problems is first studied in [Zienkiewicz et al., 1996] for incompressible regime and more extensively in the present dissertation, where compressible turbulent flow is considered.

The last issue addressed in this monograph is the possible way to improve the slow convergence to stationary states of the CBS method, a typical problem in fractional step algorithms. Solving implicitly some terms ([Codina et al., 1998b]), using Multi Grid techniques
([Vázquez and Codina, 1998]) or even through Domain Decomposition (under study) are some of the possible solutions to this problem. Out of these, the first two are treated in this work, and are reflected in a small chapter devoted to Multi Grid techniques.

This monograph is organized as follows. In Chapter 2, the physical problem is set. Chapter 3 introduces the basics of the algorithm for laminar flows. Chapter 4 is a gallery of numerical examples in laminar flow. In Chapter 5, the CBS algorithm extension to turbulent problems is defined and developed. Chapter 6 is again devoted to numerical examples, now for turbulent flow. Chapter 7 presents the Multi Grid ideas applied to CBS. Finally, Chapter 8 sketches some conclusions and future lines of work.

Conventions, notations and definitions:

Spatial vectors are noted in two forms: bold type ($\boldsymbol{u}$) or subindexed italics type (u_i). The form chosen in a given formula responds to neatness criteria. To note n-order tensors (2-order τ_{ij}), n-subindexes are used. Latin subindexes label vector or tensor

components in a Cartesian coordinate system, and for all the mathematical deductions, 3-D space is considered. Vectors of nodal variables are noted by putting an over bar ($\bar{\boldsymbol{E}}$), and greek subindexes are used to label their nodal components. In turbulent problems, the overbar is used also for mean variables, but in these particular chapters care is taken to avoid confusion.

The normals to the domain boundaries are considered pointing outwards and with unitary module.

Einstein summation convention for repeated (both latin and greek) indexes is used:

$$a_i b_{ij} \equiv \sum_i a_i b_{ij},$$

unless explicitly said.

To interpolate continuum fields to discrete finite element spaces, the following procedure is used, according to the character of the fields. Let $W(\boldsymbol{x})$ be the usual scalar piecewise interpolant function, then, for any point $\boldsymbol{x}$ belonging to the domain, we discriminate between scalar and vector fields as follows:

- *Scalar fields V:* Let

$$\bar{\boldsymbol{W}}(\boldsymbol{x}) = [W_1(\boldsymbol{x}), \ldots, W_M(\boldsymbol{x})]\,,$$

  where M is the number of nodes of a finite element partition. Then, if $\bar{\boldsymbol{V}}$ is the vector of nodal values of function V,

$$V(\boldsymbol{x}) = \bar{\boldsymbol{W}}(\boldsymbol{x}) \cdot \bar{\boldsymbol{V}} \tag{1.1}$$

- *3-D Vector fields $\boldsymbol{v}$:* Let

$$\boldsymbol{W}(\boldsymbol{x}) = [\boldsymbol{W}_1(\boldsymbol{x}), \ldots, \boldsymbol{W}_M(\boldsymbol{x})]$$

where

$$\overline{\boldsymbol{W}}_a(\boldsymbol{x}) = \begin{bmatrix} W_a(\boldsymbol{x}) & 0 & 0 \\ 0 & W_a(\boldsymbol{x}) & 0 \\ 0 & 0 & W_a(\boldsymbol{x}) \end{bmatrix}$$

and again

$$\boldsymbol{v}(\boldsymbol{x}) = \boldsymbol{W}(\boldsymbol{x}) \cdot \overline{\boldsymbol{v}} \tag{1.2}$$

The spatial derivatives of interpolated fields are calculated as follows:

$$\frac{\partial \boldsymbol{x}}{\partial x_i} = \frac{\partial \tilde{\boldsymbol{W}}(\boldsymbol{x})}{\partial x_i} \cdot \overline{\boldsymbol{v}} \tag{1.3}$$

where

$$\frac{\partial \tilde{\boldsymbol{W}}(\boldsymbol{v})}{\partial x_i} = \left[\frac{\partial W_1(\boldsymbol{x})}{\partial x_i}, \ldots, \frac{\partial W_M(\boldsymbol{x})}{\partial x_i} \right].$$

Acknowledgement

This work has been done under the contract "Solution algorithms for high speed compressible flows. NASA Ames Research Center, NAGW/2127, Ames control number 90-144, from USA. One of the authors (M. Vázquez) thanks the Ministry of Education of Spain for the FPI scholarship enjoyed while doing this work.

Chapter 2

The Navier-Stokes Equations

2.1 The physical problem

Starting from a few hypothesis and general conservation principles, a set of equations known as Navier - Stokes equations can be derived. It is the set of differential equations that models the dynamic behavior of a fluid [Batchelor, 1967], [Faber, 1995] or [Landau and Lifshitz, 1987]. Two great classes of flows can be identified, described both by the same set. On one hand, incompressible and compressible flows, on the other hand, viscous and inviscid flows.

In the former case, when the flow is incompressible, changes in pressure do not follow changes in density, and no state law is needed. Most of the time, density remains constant, with the exception of atmospheric problems where density is allowed to vary slightly according to some thermal dilatational law, but keeping pressure changes independent. Leaving aside these atmospheric types of problems and considering the density constant, the flow is velocity divergence free. Also, the thermal problem is decoupled from the mechanical one. In compressible flow, thermodynamic and mechanical problems are strongly coupled through the energy equation, due to compressibility effects and the state law, which relates the state variables. The flow is no longer velocity divergence free.

Viscous and inviscid flows present also very different characteristics. If viscosity effects are neglected (in this case the governing equations are known as Euler equations) the only force which can be exerted by or upon flow is pressure, apart from body forces. Discontinuities and shocks are allowed by the solutions of Euler equations. Continuity and permanent thermodynamic equilibrium reigns for all times within the system are the two basic hypotheses. In inviscid flow when shocks are present, these two hypotheses are not verified, at least in the vicinity of shocks ([Courant and Friedrichs, 1948]).

Fortunately, and as far as has been tested, it looks like the region where this fact could have any influence is comparatively very small, and its effects remain local. The Euler equations give the correct solution to discontinuous problems relying only on continuum hypothesis and thermodynamic equilibrium outside this small region and on the energy, momentum and mass continuity conditions across the jump. The additional entropy increasing rule bans shocks that would otherwise violate the Second Thermodynamics Law.

The solution of inviscid problems seems to agree very well with more realistic cases, where the viscosity is very small. But the effect of viscosity, even for very high Reynolds numbers, introduces very important changes in the equations: physical no-slip conditions can be prescribed, for the second order derivative terms now included in the momentum equation, allowing the presence of boundary layers. Boundary layers are the foremost source of vorticity, which in turn is responsible for the onset of turbulence. Also, the continuum hypothesis is deeper imposed on the equations through the definition of the stress tensor. The presence of diffusive processes precludes the formation of discontinuities. Shocks now have an extension normal to them, which depends on molecular viscosity and thermal diffusion.

2.1.1 The Navier - Stokes equations of flow

Let us picture a fluid contained in a given domain Ω. Its *velocity* $\boldsymbol{u} = \boldsymbol{u}(\boldsymbol{x}, t)$ can be described by means of a vectorial function of position $\boldsymbol{x}$, within Ω, and time t, within $[0, \infty)$. To complete the dynamic description, two of the following three variables are needed: $\rho = \rho(\boldsymbol{x}, t)$, $p = p(\boldsymbol{x}, t)$ and $T = T(\boldsymbol{x}, t)$ *density*, *pressure* and *temperature* respectively, which describe its thermodynamic state. The *linear momentum*

$$U_i := \rho u_i, \tag{2.1}$$

and the *total energy*

$$E := \rho e, \tag{2.2}$$

where the *total energy per unit mass*

$$e := e_o + \frac{1}{2} u_i u_i, \tag{2.3}$$

can be defined as above. Here, the first term e_o is the *internal energy*, and the second one, the *kinetic energy*. For an ideal gas, the state variables are related according to the following state law:

$$p = \rho RT, \tag{2.4}$$

where R is the universal gas constant. Besides, if the gas is polytropic, the internal energy is dependent only upon T linearly

$$e_o = C_v T, \tag{2.5}$$

with the constant of proportionality C_v, the *specific heat at constant volume*.

The set of Navier - Stokes equations consists of a continuity, a linear momentum transport and an energy transport equations. The first and the third ones represent mass and energy conservation, and are both scalar equations. The second is the Newton's law linear momentum conservation vectorial equation. In its pure conservative form, the Navier - Stokes equations can be written:

$$\frac{\partial \boldsymbol{V}}{\partial t} + \frac{\partial \boldsymbol{C}_i}{\partial x_i} + \frac{\partial \boldsymbol{D}_i}{\partial x_i} + \boldsymbol{S} = 0, \tag{2.6}$$

where the *conservative variables*

$$\boldsymbol{V}^T = (\rho, \rho u_1, \rho u_2, \rho u_3, \rho e) \tag{2.7}$$

are transported by means of convection, through the *convective fluxes*:

$$\boldsymbol{C}_i^T = (\rho u_i, \rho u_i u_1 + \delta_{i1} p, \rho u_i u_2 + \delta_{i2} p, \rho u_i u_3 + \delta_{i3} p, u_i(\rho e + p)) \tag{2.8}$$

and of diffusion, through the *diffusive fluxes*:

$$\boldsymbol{D}_i^T = (0, -\tau_{i1}, -\tau_{i2}, -\tau_{i3}, q_i - \tau_{ij}u_j). \tag{2.9}$$

The source is

$$\boldsymbol{S}^T = (0, \rho g_1, \rho g_2, \rho g_3, \rho(g_i u_i + r)), \tag{2.10}$$

where g_i is the acceleration due to gravity, points vertically downwards, and r is the heat source per unit mass.

The thermal flux is assumed proportional to temperature gradients, i.e. it is assumed the *Fourier law*:

$$q_i = -k(\boldsymbol{x})\frac{\partial T}{\partial x_i}, \tag{2.11}$$

where $k(\boldsymbol{x})$ is the *thermal conductivity*.

The deviatoric (i.e. excluding pressure isotropic term) stress tensor τ_{ij} is related linearly to velocity gradients as is usual in Newtonian fluids. In its most general form, it can be written as

$$\tau_{ij} = 2\mu(s_{ij} - \frac{1}{3}\theta\delta_{ij}) + \zeta\theta\delta_{ij} \tag{2.12}$$

where the *strain rate* tensor and the *dilatation* are

$$\begin{aligned} s_{ij} &= \frac{1}{2}(\frac{\partial u_i}{\partial x_j} + \frac{\partial u_j}{\partial x_i}), \\ \theta &= \frac{\partial u_k}{\partial x_k}, \end{aligned} \tag{2.13}$$

$\mu = \rho\nu$ is the *viscosity*, being ν the *kinematic viscosity* and ζ is often called the *second viscosity*. It can be shown that these viscosity coefficients are positive. For all the types of flow considered in this work, ζ is taken as zero. This is not true, for instance,

for polyatomic gases, not studied here, where the internal energy is not only function of the thermal agitation but also of the rotational degrees of freedom of the molecules forming the gas.

For some types of flow, viscosity is found to be temperature dependent through the *Sutherland law*:

$$\frac{\mu}{\mu_{\text{ref}}} = \frac{T_{\text{ref}} + 110.3K}{T + 110.3K} \left(\frac{T}{T_{\text{ref}}}\right)^{3/2} \tag{2.14}$$

where subindex "ref" means reference values. This empirical law holds between $100K$ and $1900K$. For a narrower range, $150K$ and $500K$, it can be simplified to

$$\frac{\mu}{\mu_{\text{ref}}} = \left(\frac{T}{T_{\text{ref}}}\right)^{0.76} \tag{2.15}$$

([Ames Research Staff, 1953] cited in [Smits and Dussauge, 1996]).

Some dimensionless numbers can be defined:

- *Reynolds number:*

$$Re = UL/\nu,$$

  where U and L are a velocity module and a length respectively, characteristic of the problem,

- *Prandtl number:*

$$Pr = \mu C_p/k,$$

  where C_p is the *specific heat at constant pressure*, and

- *Mach number:*

$$M = u/c,$$

where $c = \sqrt{dp/d\rho}$ is a positive quantity, known as the *speed of sound*, at a given point and $u = \sqrt{u_i u_i}$ is the module of the fluid velocity.

The Mach number, which is defined locally, gives an idea of the compressibility of the flow at any given point as was said before. When incompressible flows are considered, density gradients are not related to pressure ones. In fact, it is taken as a constant. In this case, the speed of sound can be considered as a constant, much larger than the local convective velocity. On the other hand, in compressible flow it is a quantity that varies in space following changes in thermodynamic properties. The Mach number allows a classification of flows: if larger than one, the flow is *supersonic*; if smaller, *subsonic*; if comparable, *transonic*. Sometimes, when the Mach number is great than 3, flows are called *hypersonic*.

Each of the Navier-Stokes equations can be written as follows:

- CONTINUITY EQUATION:

$$\frac{\partial \rho}{\partial t} + \frac{\partial}{\partial x_i}(U_i) = 0, \tag{2.16}$$

- MOMENTUM CONSERVATION EQUATION:

$$\frac{\partial U_j}{\partial t} + \frac{\partial}{\partial x_i}(u_i U_j) + \frac{\partial}{\partial x_i}(\delta_{ij} p - \tau_{ij}) + \rho g_j = 0, \tag{2.17}$$

- TOTAL ENERGY CONSERVATION EQUATION:

$$\frac{\partial E}{\partial t} + \frac{\partial}{\partial x_i}(u_i E) + \frac{\partial}{\partial x_i}(u_i p - k\frac{\partial T}{\partial x_i} - \tau_{ij} u_j) + \rho(u_i g_i + r) = 0. \tag{2.18}$$

2.1.2 Boundary conditions

To solve the strongly coupled set formed by (2.16), (2.17) and (2.18), proper boundary and initial conditions are needed. Boundary conditions for Navier-Stokes equations are

still an open question. By the order of the derivatives, it is clear that, if the contour is partitioned $\Gamma = \Gamma_D \cup \Gamma_N \cup \Gamma_M$, the following is required to solve the equations:

1. Initial conditions at time $t = 0$ for the unknowns (ρ, U_j, E) defined in all the domain Ω.
2. Dirichlet boundary conditions for the unknowns at contour Γ_D.
3. Neumann boundary conditions for the fluxes normal component at Γ_N.
4. Mixed boundary conditions, i.e. a linear combination of unknowns and normal fluxes, at Γ_M.

It is not at all clear whether these partitions of the boundary should be coincident for each of the equations (for instance, where ρ is prescribed, also U_j and E are duly imposed) or not. Also boundary conditions could be imposed on the primitive variables rather than on conservative ones.

The initial-boundary value problem of the Navier-Stokes equations is very complicated, and as said before, still unsolved [Higdon, 1986, Oliger and Sundstrom, 1978]. The theory is developed by H.O. Kreiss and others ([Kreiss, 1970] cited in [Higdon, 1986] for instance, or [Hirsch, 1990]). Let us consider that neither viscosity nor diffusion is present. Hyperbolic systems of equations can be reformulated along their characteristic curves. By doing so, certain quantities v_j that are conserved as they travel along these curves can be identified. Well-posedness of the problem relies mainly in evaluating their behavior at the contours of the spatial domain: boundary conditions should be imposed only in incoming modes through the equations of the general kind

$$v_j(x_{|in}, t) = S_{ij} v_i(x_{|out}, t) + h_j(t) \tag{2.19}$$

where S_{ij} is a sort of reflection matrix, $h_j(t)$ is a function of time and subscripts "in" and "out" label incoming and outgoing parts of the boundaries. Outgoing modes are left free. When the system is linear, hyperbolic and scalar, both the proofs on the necessary conditions for the well posedness and the physics behind are clear and direct ([Higdon, 1986]). But from that point to the Navier - Stokes set studied here there is a long way of increasing complexity, due to the appearance of non linear terms, loss of hyperbolicity and multidimensional character, the latter allowing the appeareance of tangential modes [Oliger and Sundstrom, 1978].

For the sake of simplicity, suppose a 1-D system. Incoming and outgoing modes are identified through the Jacobian matrix $\dfrac{\partial \boldsymbol{F}}{\partial \boldsymbol{V}}$ of the symetrized (1-D) problem,

$$\frac{\partial \boldsymbol{V}}{\partial t} + \frac{\partial \boldsymbol{F}}{\partial \boldsymbol{V}} \frac{\partial \boldsymbol{V}}{\partial x} + \boldsymbol{D}(\boldsymbol{V}) = 0, \tag{2.20}$$

where $\boldsymbol{F}$ is the flux vector and $\boldsymbol{D}(\boldsymbol{V})$ a given function of $\boldsymbol{V}$ (likely non - linear). For hyperbolic problems, it has a set of real eigenvalues λ_j. Suppose they are ordered increasingly

$$\lambda_1 < \cdots < \lambda_l < \quad 0 \quad < \lambda_{l+1} < \cdots < \lambda_n.$$

Then, an incoming boundary condition of the form (2.19) is required for the first l equations. The other $(n-l)$ are set free there.

Boundary impositions can be done in many ways over different sets of variables. In the context of differences schemes the problem is reviewed in [Harten et al., 1983] and [Sloan, 1980], and in finite element methods in [Shakib et al., 1991]. In this monograph, through many numerical experiments we have chosen the primitive variables for Dirichlet conditions, whether the conservative or primitive set is used. The Mach number at a given contour is the indicator of its character according to the following:

- When $M < 1$: two conditions at inlets (u,T), one condition at outlets (ρ or p);
- When $M \geq 1$: three conditions at inlets (u,T,ρ or p), none at outlets.

The prescribed variables are the velocity (a scalar in 1-D), the temperature and the density (or pressure). The first two are always imposed at the inflow while the density (or pressure) can either be prescribed at the inflow or at the outflow alternatively. In compressible problems, we generally prescribe the density rather than the pressure in subsonic outflows, being non-physical reflections not developed. Many authors have warned against using the pressure because of the appearance of these kind of effects, and have devised non-reflecting boundary conditions, [Hedstrom, 1979] or [Rudy and Strikwerda, 1980]. However, density prescription in subsonic outflows seems to be all right, at least for the problems we have faced.

The same criteria are extrapolated to multidimensional Navier-Stokes problems. The main differences are that, now, the velocity is a vector and that solid walls with zero velocity prescriptions are present. For inflows and outflows at different Mach numbers, the same conditions are maintained:

- When $M < 1$: two conditions at the inlets ($\boldsymbol{u}$,T), one condition at the outlets (ρ or p);

- When $M \geq 1$: three conditions at the inlets ($\boldsymbol{u}$,T,ρ or p), none at the outlets.

If the velocity is a vector, as in 2-D or 3-D cases, the problem is still well posed if one velocity component is prescribed in some boundaries instead of the whole vector. At the walls, the normal velocity component is prescribed to zero.

Initial conditions are set on the velocity field, the temperature and the density (or the pressure), the initial conservative variables can be further derived.

This is also accepted for full Navier-Stokes equations. An additional boundary condition is in this case the *no-slip condition* (i.e. velocity fixed to zero) which is itself imposed at the walls. There, the temperature is prescribed to a stagnation value T_{stag}. If the flow is restricted to the incompressible case ($\nabla \cdot \boldsymbol{u} = 0$), boundary conditions are set on the velocity (and/or on its derivatives) and on the pressure (at a point, or at a whole boundary). This point will be considered later when the weak form of the equations is derived.

2.1.3 Shock waves

As said before, a characteristic feature of supersonic flows is the *shock wave*. Under this flow regime, when the viscosity is absent, some of the physical variables describing the problem can present

discontinuities in their distribution, forming discontinuity surfaces or shock waves (cf. [Courant and Friedrichs, 1948, Landau and Lifshitz, 1987]). For the case of non steady flows, usually the shocks are not fixed, but move with some speed U_i^s. Crossing these surfaces, jump conditions, known as the *Rankine - Hugoniot 's*, are verified. They can be derived from conservation principles of mass, momentum and energy fluxes, and can be breafly written in the following form:

$$r_i \left(\boldsymbol{C}_i^{\mathrm{L}}(\boldsymbol{V}) - \boldsymbol{C}_i^{\mathrm{R}}(\boldsymbol{V}) \right) = r_i U_i^s \left(\boldsymbol{V}^{\mathrm{L}} - \boldsymbol{V}^{\mathrm{R}} \right), \tag{2.21}$$

where superscripts "L" and "R" mean left and right to the shock, r_i is any of the unitary vectors which form a orthonormal Cartesian basis for the space, and $\boldsymbol{V}$ and $\boldsymbol{C}_i$ are the variables and fluxes appearing in (2.6). Usually, this basis is the canonical one, within a reference frame which coincides with the shock at a given time, allowing one of the versors to be normal to the shock.

Shocks are, unlike sound, non-linear waves. For that reason, they do not propagate at a fixed velocity derived from local thermodynamic properties of the flow, the speed

of sound c, but at different velocities, maybe greater than c. Also, being a non-linear phenomenon, when shocks are superimposed, the pressure can rise up to very high values. Theoretical, numerical and experimental studies have been carried out exhaustively, specially with the advent of transonic and supersonic flights, and more recently, the atmospheric re-entry of space vehicles and shuttles. Usually these kind of practical problems involve high Reynolds numbers (more than 10^6), Mach numbers values ranging from slightly lower than one to 20 or more. Shock interaction with themselves and with boundary layers, strong adverse pressure gradients, tubulent boundary layers and wakes are their typical features. See for instance the book [Smits and Dussauge, 1996] or the wide review [Spina et al., 1994].

2.2 Incompressible flows

In these flows, the restriction $\nabla \cdot \boldsymbol{u} = 0$ is imposed on the velocity field. All along this work, when incompressible flows are considered, density is taken constant. Leaving aside the thermal problem, Navier - Stokes equations can be reduced to

$$\begin{aligned} &\frac{\partial u_j}{\partial t} + \frac{\partial}{\partial x_i}(u_i u_j) + \frac{1}{\rho}\frac{\partial}{\partial x_i}(\delta_{ij} p - \tau_{ij}) + g_j = 0 \\ &\frac{\partial}{\partial x_i}(u_i) = 0 \end{aligned} \tag{2.22}$$

with, if, for simplicity $\Gamma = \Gamma_{\mathrm{D}} \cup \Gamma_{\mathrm{N}}$

$$\begin{aligned} &\boldsymbol{u}(\boldsymbol{x}, 0) := \boldsymbol{u}_0(\boldsymbol{x}), && \text{for all } \boldsymbol{x} \in \Omega \\ &\boldsymbol{u}(\boldsymbol{x}, t) := \tilde{\boldsymbol{u}}(t), && \text{for all } \boldsymbol{x} \in \Gamma_{\mathrm{D}} \\ &\boldsymbol{\sigma} \cdot \boldsymbol{n} := \tilde{\boldsymbol{t}}(t), && \text{for all } \boldsymbol{x} \in \Gamma_{\mathrm{N}}, \end{aligned}$$

where $\boldsymbol{n}$ is the exterior normal versor and $\boldsymbol{\sigma}$ is defined as

$$\sigma_{ij} = \tau_{ij} - p\,\delta_{ij}.$$

As sketched in the introduction, pressure here is not a thermodynamic variable. It is a quantity which establishes the equilibrium of forces for each volume element, defined as the mean normal stress and with a minus sign. Density and internal energy retain their thermodynamic meaning, but there is no state law for relating pressure to them, like in the case of compressible flows. When the problem is static, it coincides with the hydrostatic pressure.

By taking the curl of the momentum equation in (2.22) the pressure can be eliminated. Once the equation for the velocity is solved, the pressure can be obtained from it by taking the divergence of (2.22). This character is inherent to incompressible flows.

2.3 Summary

Flow dynamics is physically modeled by the set known as Navier - Stokes equations (viscous problems) or Euler equations (inviscid problems). It is formed by two scalar equations for mass and energy transport and a third vectorial equation, for the linear momentum transport. The conservative form, which is very useful for numerical treatment, can be written

$$\begin{aligned}
&\frac{\partial \rho}{\partial t} + \frac{\partial}{\partial x_i}(U_i) = 0, \\
&\frac{\partial U_j}{\partial t} + \frac{\partial}{\partial x_i}(u_i U_j) + \frac{\partial}{\partial x_i}(\delta_{ij} p - \tau_{ij}) + \rho g_j = 0, \\
&\frac{\partial E}{\partial t} + \frac{\partial}{\partial x_i}(u_i E) + \frac{\partial}{\partial x_i}(u_i p - k\frac{\partial T}{\partial x_i} - \tau_{ij} u_j) + \rho(u_i g_i + r) = 0.
\end{aligned} \tag{2.23}$$

They can describe many different types of flow: incompressible and compressible, viscous and inviscid. Non linearities due to compressibility produce discontinuities known as shocks. Also, boundary conditions must be carefully imposed according to the compressibility character of the contour, evaluated using the Mach number. Those contours are classified as subsonic or supersonic inlets or outlets.

The incompressibility restriction, uncouples the thermal problem from the mechanical one, which in turn is modeled by

$$\frac{\partial u_j}{\partial t} + \frac{\partial}{\partial x_i}(u_i u_j) + \frac{1}{\rho}\frac{\partial}{\partial x_i}(\delta_{ij} p - \tau_{ij}) + g_j = 0$$

$$\frac{\partial}{\partial x_i}(u_i) = 0 \tag{2.24}$$

with proper boundary and initial conditions. In this case, the pressure field has a different character than in compressible flows in that it is obtained from the velocity field.

Chapter 3

The CBS Algorithm. Laminar Flow

As said in the introduction, the present monograph follows the ideas of O.C. Zienkiewicz and co-workers, introduced in [Zienkiewicz et al., 1990, Zienkiewicz and Wu, 1992] and [Zienkiewicz and Codina, 1995, Zienkiewicz et al., 1995, Codina et al., 1998b]. In this section we describe the algorithm and its main ingredients and how they are concocted together. The convective stabilization produced by the Characteristic-Galerkin technique, a fractional step method applied to the momentum equation and an anisotropic shock capturing diffusion allow to solve many different flow problems like those shown in chapter 4.

3.1 Characteristic based schemes

Convection - diffusion equations are very common in Physics. The equations forming the Navier - Stokes set, for instance, are of this kind. It is well known (cf. [Zienkiewicz, 1977, Hughes, 1987]) that when convection strongly dominates over diffusion, numerical problems can arise, resulting in spurious and purely numerical oscillations. Many methods have been proposed since long ago for stabilizing the convective term effects. Out of these, there is a whole family of techniques in the context of finite element methods. Although they come from different principles, the same kind of answer is reached. In them, the stabilization is due to additional terms in the weak form of the equations, consisting of a certain operator applied to the test functions, which in turn weights the residual multiplied by some factors. Both operators and factors are different in each case, the best known being perhaps the Streamline-Upwind/Petrov-Galerkin (SUPG) [Brooks and Hughes, 1982], the Galerkin / Least-

Squares (GLS) [Hughes and Mallet, 1986], the Taylor-Galerkin (TG) [Donea, 1984], the Characteristic-Galerkin (CG) [Loehner et al., 1984],[Douglas and Russel, 1982] or [Pironneau, 1982] and more recently the Sub-Grid Scale (SGS) [Hughes, 1995].

SUPG is based on the fact that for stabilizing the convective terms additional numerical diffusion is needed along the streamlines. The operator applied to the test function is then the convective one, in its non conservative form. In GLS method the operator chosen is the convective one, now conservative, plus the diffusive one. The appearance of the pressure gradient in the operator gives this method the bonus of stabilizing the continuity equation, allowing equal interpolation for both pressure and velocity. In the case of TG, a Taylor expansion in time before the Galerkin method is used to discretize the space hence producing the desired numerical effect. SGS starting point is different from the rest. It is based on the assumption that the finite element discrete solution is exact on the inter-element boundaries, meaning that the sub grid scales, which cannot be resolved by the discrete method with a given spatial grid, vanish at these boundaries. The outcome is the same as in the GLS method, but with changed sign in the diffusion operator. Each of the methods aforementioned requires an adequate evaluation of the factors which multiply the stabilization terms [Codina, 1998a].

Characteristic - Galerkin (CG) is a characteristic based scheme (reviewed in [Roe, 1986]) embedded in the context of finite element methods. Probably, the first references on this idea are those of J. Douglas and T. Russel [Douglas and Russel, 1982], O. Pironneau [Pironneau, 1982] and R. Loehner, K. Morgan and O.C. Zienkiewicz [Loehner et al., 1984]. All of them are based in the time discretization of the material instead of the partial time derivatives, which is equivalent to solve the equations in a reference frame "bonded" to the fluid particles. Thus, as we will show, a scalar equation of the form

$$\frac{\partial V}{\partial t} + u_i \frac{\partial V}{\partial x_i} - D(V) + S = 0 \tag{3.1}$$

on $\Omega \times (0,T)$ / $\Omega \subset \mathbb{R}^n$, with $n = 1, 2, 3$, can be written as

$$\frac{d\tilde{V}}{dt} - D(\tilde{V}) + S = 0 \tag{3.2}$$

on Ω, where $\tilde{V}$ means that is V evaluated in the *co-moving* (with the fluid) reference frame, and discretized as

$$\frac{1}{\Delta t}\left(\tilde{V}^{n+1} - \tilde{V}^{n}\right) - D(\tilde{V}^{n+\theta}) + S = 0 \tag{3.3}$$

on Ω^{n+1}, being $\tilde{V}^{n+\theta} = (1-\theta)\tilde{V}^{n} + \tilde{V}^{n+1}$ with $0 \leq \theta \leq 1$. In this co-moving reference frame, convective terms disappear and Galerkin method is optimal with no spurious numerical oscillations (at least those produced by convective instability) expected to appear.

How to evaluate (3.3) is the difference between CG schemes. In [Pironneau, 1982] (see also [Pironneau et al., 1992] for a comparison with space-time GLS) it is proposed to evaluate (3.3) by first integrating backwards the trajectories of the flow particles, then by identifying the element of Ω^{n+1} where the particle was at time n, and finally by calculating $\tilde{V}$ at that position. Typically the integrals inherent to the finite element method are solved by numerical integration, and so, in this case, the trajectories traced back are those that at time $n+1$ are coincident with integration points.

On the other hand, as shown below, we follow the lines set on [Loehner et al., 1984] (see also [Lee et al., 1987]) and further developed in [Zienkiewicz and Codina, 1995, Zienkiewicz et al., 1995], etc. Here, $\tilde{V}$ is calculated from a Taylor expansion. By doing this, the search of the integration points in neighboring elements is avoided. Next, we describe the procedure.

3.1.1 The co-moving system

Consider a general convection-diffusion equation. In it, convective fluxes can be written as $\boldsymbol{C}_i = u_i \boldsymbol{V}$. For that reason

$$\frac{\partial \boldsymbol{V}}{\partial t} + \frac{\partial (u_i \boldsymbol{V})}{\partial x_i} + \frac{\partial \boldsymbol{D}_i(\boldsymbol{V})}{\partial x_i} + \boldsymbol{S} = 0 \tag{3.4}$$

can be re written as

$$\frac{\partial \boldsymbol{V}}{\partial t} + u_i \frac{\partial \boldsymbol{V}}{\partial x_i} + \boldsymbol{V}\frac{\partial u_k}{\partial x_k} + \frac{\partial \boldsymbol{D}_i(\boldsymbol{V})}{\partial x_i} + \boldsymbol{S} = 0. \tag{3.5}$$

solved on $\Omega \times (0,T)$ / $\Omega \subset \mathbb{R}^n$, with $n = 1, 2, 3$ as we said.

Now consider each component of them separately. The first two terms of (3.5) compose the *material derivative* of V (now a scalar):

$$\frac{dV}{dt} := \frac{\partial V}{\partial t} + u_i \frac{\partial V}{\partial x_i}, \tag{3.6}$$

A *material derivative* of variable V means that the rate of change of V, as observed from a reference system in which the fluid is locally and instantaneously at rest: the co-moving reference frame. In this frame, the convective terms disappear. As mentioned earlier, the equations containing convective terms often are satisfied by non-smooth solutions. In this case, the usual Galerkin finite element method loses accuracy and can produce a numerical solution with spurious effects, very far away from the physical one (cf. [Johnson, 1987, Eriksson et al., 1996]). But if we want to solve the transport equation for the variable V taking advantage of the fact that the convective term vanishes in a different coordinate frame, the equation must be wholy reformulated in the co-moving system. If we note

$$L(V) := \frac{\partial D_i(V)}{\partial x_i} + V \frac{\partial u_k}{\partial x_k}, \tag{3.7}$$

then (3.5) is simplified to

$$\frac{dV}{dt} + L(V) + S = 0. \tag{3.8}$$

Until the end of the section we consider the source S as zero to simplify the algebra. Labeling a particle and following it as it wanders within the fluid, its motion can be described by the *characteristics equation*

$$\frac{d\tilde{\boldsymbol{x}}(t)}{dt} = u(\tilde{\boldsymbol{x}}(t)), \tag{3.9}$$

where the tilde means "the trajectory of a particle of fluid that was at a reference point $\boldsymbol{x}_{\text{ref}}$ at a reference time t_{ref}". This statement is in fact the initial condition for the equation (3.9):

$$\tilde{\boldsymbol{x}}(t_{\text{ref}}) = \boldsymbol{x}_{\text{ref}}. \tag{3.10}$$

Time integrating this ordinary differential equation with its initial condition would solve the problem of tracking particles of fluid, the "carriers" of co-moving frames. Doing so, the equation (3.8) can be restated in that frame. Let $\mathcal{S}$ be the fixed reference spatial system, whose origin is pinned at $\boldsymbol{x}_{\text{ref}}$. Let $\mathcal{S}'$ be the co-moving frame (fig. 3.1.1). If the origin of $\mathcal{S}'$ coincides at time t_{ref} with that of $\mathcal{S}$, i.e., $\boldsymbol{x}_{\text{ref}}$, then

$$\frac{dV}{dt}(\tilde{\boldsymbol{x}}(t),t)\Big|_{\boldsymbol{x}_{\text{ref}},t_{\text{ref}}} = \left[\frac{\partial V}{\partial t} + u_i \frac{\partial V}{\partial x_i}\right]\Big|_{\boldsymbol{x}_{\text{ref}},t_{\text{ref}}}, \tag{3.11}$$

so that

$$\frac{dV}{dt}(\tilde{\boldsymbol{x}}(t),t) + L(V(\tilde{\boldsymbol{x}}(t),t)) = 0. \tag{3.12}$$

This equation can be time-discretized using the *trapezoidal rule*:

$$\begin{aligned}\frac{1}{\Delta t}(V(\tilde{\boldsymbol{x}}^{n+1},t^{n+1}) - V(\tilde{\boldsymbol{x}}^{n},t^{n})) + \\ \theta L(V(\tilde{\boldsymbol{x}}^{n+1},t^{n+1})) + \quad (1-\theta)L(V(\tilde{\boldsymbol{x}}^{n},t^{n})) = 0,\end{aligned} \tag{3.13}$$

where

$$\begin{aligned}\Delta t &= t^{n+1} - t^{n}, \\ \tilde{\boldsymbol{x}}^{n+1} &\simeq \tilde{\boldsymbol{x}}(t^{n+1}), \\ \tilde{\boldsymbol{x}}^{n} &\simeq \tilde{\boldsymbol{x}}(t^{n}).\end{aligned} \tag{3.14}$$

Once the time-discretization is done, it is necessary to choose the pair $\boldsymbol{x}_{\text{ref}}$, t_{ref} according to it. If $\mathcal{S}'$ coincides with $\tilde{\boldsymbol{x}}^n$, the trajectory of our particle of fluid is integrated forward in time using the values obtained at $\tilde{\boldsymbol{x}}^n$. And backwards if $\boldsymbol{x}_{\text{ref}} := \tilde{\boldsymbol{x}}^{n+1}$, expanding from the values at $\tilde{\boldsymbol{x}}^{n+1}$. A point between them can be used too. In fact, any point lying in the linear approximation of the trajectory can be chosen, this generalization is analyzed in [Codina, 1998b]. In this case, we choose $\boldsymbol{x}_{\text{ref}} := \tilde{\boldsymbol{x}}^{n+1}$. The Galerkin

method is going to be used to discretize the space because in the co-moving frame the convective terms disappear. For that reason, the space convergence for Galerkin method is optimal in the frame $\mathcal{S}'$ (i.e.$(\Delta x')^2$). If $\theta = 1/2$ is chosen (*Crank-Nicholson*) in (3.13), the trapezoidal rule gives the highest possible order in time: $O(\Delta t^2)$. Then, as $(\Delta x')^2 = (\Delta x)^2 + (u\Delta t)^2$, second order in space in $\mathcal{S}$ (i.e. $O(\Delta x^2)$) is reached in the streamline direction.

Through four successive steps, a second order time-discretized transport equation can be obtained in the co-moving frame, but with values obtained at the same point in the same, fixed, reference frame. For that reason, each approximation is evaluated around that point $\boldsymbol{x}_{\text{ref}} := \tilde{\boldsymbol{x}}^{n+1}$ according to our choice:

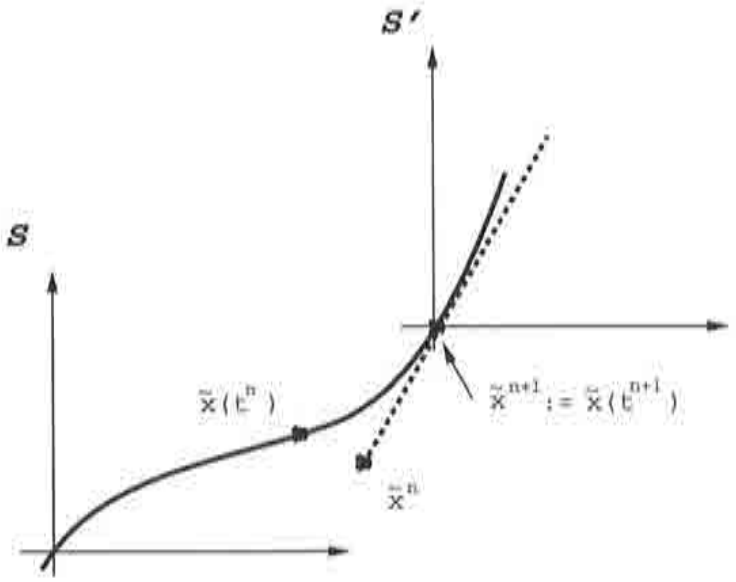

Figure 3.1: Co - moving reference frame.

1. Integrate trajectory backwards, with $O(\Delta t^2)$:

$$\begin{aligned} \tilde{\boldsymbol{x}}^n &= \tilde{\boldsymbol{x}}^{n+1} - \Delta t \boldsymbol{u}(\tilde{\boldsymbol{x}}^{n+1}, t^n) + O(\Delta t^2) \\ &= \boldsymbol{x} - \Delta t \boldsymbol{u}^n + O(\Delta t^2), \end{aligned} \tag{3.15}$$

As the choice for the reference point has no privileged position, let us note $\tilde{\boldsymbol{x}}^{n+1} = \boldsymbol{x}$.

2. Approximate velocity of this particle at $(\tilde{\boldsymbol{x}}^n, t^n)$:

$$\begin{aligned} \boldsymbol{u}(\tilde{\boldsymbol{x}}^n, t^n) &= \boldsymbol{u}\left(\boldsymbol{x} - \Delta t \boldsymbol{u}^n + O(\Delta t^2)\,,\ t^n\right) \\ &= \boldsymbol{u}^n - \Delta t u_i^n \frac{\partial \boldsymbol{u}^n}{\partial x_i} + O(\Delta t^2). \end{aligned} \tag{3.16}$$

3. Integrate trajectory backwards, now with $O(\Delta t^3)$:

$$\begin{aligned} \tilde{\boldsymbol{x}}^n &= \tilde{\boldsymbol{x}}^{n+1} - \frac{\Delta t}{2}\left[\boldsymbol{u}(\tilde{\boldsymbol{x}}^{n+1}, t^{n+1}) + \boldsymbol{u}(\tilde{\boldsymbol{x}}^n, t^n)\right] + O(\Delta t^3) \\ &= \boldsymbol{x} - \frac{\Delta t}{2}\boldsymbol{u}^{n+1} - \frac{\Delta t}{2}\boldsymbol{u}^n + \frac{\Delta t^2}{2} u_i^n \frac{\partial \boldsymbol{u}^n}{\partial x_i} + O(\Delta t^3) \\ &= \boldsymbol{x} - \Delta t \boldsymbol{u}^{n+1/2} + \frac{\Delta t^2}{2} u_i^n \frac{\partial \boldsymbol{u}^n}{\partial x_i} + O(\Delta t^3), \end{aligned} \tag{3.17}$$

where $\boldsymbol{u}^{n+1/2} = \left(\boldsymbol{u}^{n+1} + \boldsymbol{u}^n\right)/2$.

4. Calculate the variable V at $(\tilde{\boldsymbol{x}}^n, t^n)$:

$$\begin{aligned} V(\tilde{\boldsymbol{x}}^n, t^n) &= V\left(\boldsymbol{x} - \Delta t \boldsymbol{u}^{n+1/2} + \frac{\Delta t^2}{2} u_i^n \frac{\partial \boldsymbol{u}^n}{\partial x_i} + O(\Delta t^3)\,, t^n\right) \\ &= V^n - \Delta t u_j^{n+1/2} \frac{\partial V^n}{\partial x_j} \\ &\quad + \frac{\Delta t^2}{2}\left[u_i^n \frac{\partial u_j^n}{\partial x_i}\frac{\partial V^n}{\partial x_j} + u_i^{n+1/2} u_j^{n+1/2} \frac{\partial^2 V^n}{\partial x_i \partial x_j}\right] \\ &\quad + O(\Delta t^3). \end{aligned} \tag{3.18}$$

As $\boldsymbol{u}^{n+1/2} = \boldsymbol{u}^n + O(\Delta t)$ and

$$u_i^n u_j^n \frac{\partial^2 V^n}{\partial x_i \partial x_j} = u_i^n \frac{\partial}{\partial x_i}\left(u_j^n \frac{\partial V^n}{\partial x_j}\right) - u_i^n \frac{\partial u_j^n}{\partial x_i}\frac{\partial V^n}{\partial x_j},$$

we have for the variable V:

$$V(\bar{\boldsymbol{x}}^n, t^n) = V^n - \Delta t u_j^{n+1/2}\frac{\partial V^n}{\partial x_j} + \frac{\Delta t^2}{2} u_i^n \frac{\partial}{\partial x_i}\left(u_j^n \frac{\partial V^n}{\partial x_j}\right) + O(\Delta t^3). \tag{3.19}$$

To find an approximation for $L(V(\bar{\boldsymbol{x}}^n, t^n))$, it is done

$$\begin{aligned} L(V(\bar{\boldsymbol{x}}^n, t^n)) &= L\left(V^n - \Delta t u_j^n \frac{\partial V^n}{\partial x_j} + O(\Delta t^2)\right) \\ &= L(V^n) - \Delta t u_j^n \frac{\partial L(V^n)}{\partial x_j} + O(\Delta t^2) \end{aligned} \tag{3.20}$$

Finally, using (3.19) and (3.20) in (3.13)

$$\begin{aligned} V^{n+1} - V^n &= -\Delta t\left[u_j^{n+1/2}\frac{\partial V^n}{\partial x_j} + L(V^{n+1/2})\right] \\ &\quad + \frac{\Delta t^2}{2}\left[u_i \frac{\partial}{\partial x_i}\left(u_j \frac{\partial V}{\partial x_j} + L(V)\right)\right]^n \end{aligned} \tag{3.21}$$

which can be now safely approximated to

$$\begin{aligned} V^{n+1} - V^n &= -\Delta t\left[u_j^n \frac{\partial V^n}{\partial x_j} + L(V^n)\right] \\ &\quad + \frac{\Delta t^2}{2}\left[u_i \frac{\partial}{\partial x_i}\left(u_j \frac{\partial V}{\partial x_j} + L(V)\right)\right]^n + O(\Delta t^2) \end{aligned} \tag{3.22}$$

evaluating all the right hand side explicitly. All the terms of this equation are evaluated in the original, fixed reference frame. The key of the method is to identify its origin at

a given point along the characteristic curve. By combining this with time integration of the characteristic equation, we finally obtain equation (3.22), a time discretized equation where all the terms are evaluated in the fixed reference frame and which can be treated by the Galerkin method. We recall the effect of the convective terms was erased by formulating it in the co-moving frame.

In brief, if we note

$$R(V) := -u_i \frac{\partial V}{\partial x_i} - L(V) \tag{3.23}$$

the continuum equation

$$\frac{\partial V}{\partial t} = R(V) \tag{3.24}$$

is discretized in time, according to the methodology hitherto exposed, as:

$$\Delta V = \Delta t R(V)^n - \frac{\Delta t^2}{2} u_i^n \frac{\partial R(V)^n}{\partial x_i} \tag{3.25}$$

that is: *time-discretization of transport equation (3.24) using this method has led us to conclude that temporal variation of V is controlled by both the residual of the equation (at first order) and its convective derivative (at second order).*

3.1.2 Characteristic - Galerkin.

Now, as our transport equation is time-discretized, in order to find a numerical solution, we are going to discretize it in space, using the finite element method. Space discretization itself is treated in next sections. Here, a previous step is taken: the weak form.

Consider the operator $L(V)$ purely as diffusive, only to define the main guidelines. Then, we want to solve the following continuous problem: find V on $\Omega \times (0,T)$ such that

$$\begin{cases} \dfrac{\partial V}{\partial t} + u_i \dfrac{\partial V}{\partial x_i} - \epsilon \dfrac{\partial^2 V}{\partial x_k \partial x_k} = f & \text{in } \Omega \\ V = V_0 & \text{in } \Gamma_D \\ \epsilon \dfrac{\partial}{\partial n} V = g & \text{in } \Gamma_N \\ \quad + \text{an initial condition} \end{cases} \tag{3.26}$$

where Γ_D and Γ_N means respectively contours with a Dirichlet's condition (i.e. a condition over the unknown) and with a Neumann's condition (i.e. a condition over the normal derivative of the unknown). Also, ϵ is a positive diffusion coefficient, say, constant throughout the domain. If it approaches to zero, the convective terms become dominant, and as was said above, the Galerkin methods could lose accuracy. The time-discretized equation can be projected first on the usual space of the test functions (cf. Introduction or [Johnson, 1987, Hughes, 1987])

$$\begin{aligned} V^{n+1} - V^n &= -\Delta t \left[u_j \frac{\partial V}{\partial x_j} - \epsilon \frac{\partial^2 V}{\partial x_i^2} \right]^n \\ &\quad + \frac{\Delta t^2}{2} \left[u_i \frac{\partial}{\partial x_i} \left(u_j \frac{\partial V}{\partial x_j} - \epsilon \frac{\partial^2 V}{\partial x_k \partial x_k} \right) \right]^n \end{aligned} \tag{3.27}$$

Let W belong to such a space. Projecting equation (3.27) yields

$$\begin{aligned} \int_\Omega W V^{n+1} d\Omega &= \int_\Omega W V^n d\Omega \\ &\quad - \Delta t \left[\int_\Omega W u_i \frac{\partial V}{\partial x_i} d\Omega - \int_\Omega W \epsilon \frac{\partial^2 V}{\partial x_i^2} d\Omega \right]^n \\ &\quad + \frac{\Delta t^2}{2} \left[\int_\Omega W u_j \frac{\partial}{\partial x_j} \left(u_i \frac{\partial V}{\partial x_i} - \epsilon \frac{\partial^2 V}{\partial x_i^2} \right) d\Omega \right]^n , \end{aligned} \tag{3.28}$$

for all test function W. As usual, integrals of spatial second order derivatives are integrated by parts

$$- \int_\Omega W \frac{\partial^2 V}{\partial x_i^2} d\Omega = \int_\Omega \frac{\partial W}{\partial x_i} \frac{\partial V}{\partial x_i} d\Omega - \int_\Gamma W \frac{\partial}{\partial n} V d\Gamma \tag{3.29}$$

and because the residual of the equation is considered to vanish at the boundaries, the weak form is

$$\begin{aligned}\int_\Omega W u_i \frac{\partial R(V)}{\partial x_i} d\Omega &= \overbrace{\int_\Gamma n_i W u_i R(V) d\Gamma}^{0} - \int_\Omega \frac{\partial}{\partial x_i}(W u_i)\ R(V) d\Omega \\ &= -\int_\Omega (u_i \frac{\partial W}{\partial x_i})\ R(V) d\Omega - \int_\Omega (W \frac{\partial u_i}{\partial x_i})\ R(V) d\Omega \end{aligned} \tag{3.30}$$

for all test function W, where $R(V)$ is defined as follows

$$R(V) := u_i \frac{\partial V}{\partial x_i} - \epsilon \frac{\partial^2 V}{\partial x_i^2}. \tag{3.31}$$

Then

$$\begin{aligned}\int_\Omega W V^{n+1} d\Omega &= \int_\Omega W V^n d\Omega \\ &- \Delta t \left[\int_\Omega W u_j \frac{\partial V}{\partial x_j} d\Omega + \int_\Omega \epsilon \frac{\partial W}{\partial x_j} \frac{\partial V}{\partial x_j} d\Omega\right]^n \\ &- \frac{\Delta t^2}{2} \left[\int_\Omega (u_i \frac{\partial W}{\partial x_i})\ R(V) d\Omega + \int_\Omega (W \frac{\partial u_i}{\partial x_i})\ R(V) d\Omega\right]^n \\ &+ \Delta t \int_{\Gamma_N} W g d\Gamma \end{aligned} \tag{3.32}$$

for all test function W, using

$$\int_\Gamma W \epsilon \frac{\partial V}{\partial n} d\Gamma = \overbrace{\int_{\Gamma_D} W \epsilon \frac{\partial V}{\partial n} d\Gamma}^{0} + \int_{\Gamma_N} W g d\Gamma$$

The main features of this last equation are the following. First, the terms linear in Δt are integrals evaluated over all the domain + boundary terms that, at least in principle,

cannot be dismissed. Second, the terms quadratic in Δt are SUPG-like term (different only in that the *intrinsic time* (τ) of SUPG is here replaced by a linear function of time) + a term which depends on the velocity divergence, and for that reason, mainly active in the case of compressible flows.

3.1.3 A Discontinuity Capturing Technique

The method proposed adds artificial diffusion which is needed when the physical diffusion vanishes in the differential equations of the type considered here. However, this numerical diffusion could not be enough to smooth out all spurious oscillations. Localized overshoots and undershoots can appear around the strong discontinuities which are likely to be present in the solution. For that reason, some techniques have been developed in order to deal with them consistently (for a review of different techniques see for instance [Van den Burg et al., 1992] or [Nithiarasu et al., 1998]).

One of these techniques (proposed in [Codina, 1993a, Codina, 1993b]) consists of adding an anisotropic diffusion tensor in those particular places where the streamline diffusion of the Characteristic–Galerkin method is insufficient. It is based on two concepts. First, to preserve consistency, this diffusion tensor must be proportional to the residual of the equation evaluated within each of the elements. Second, it must be small where the convection is small.

If a convection–diffusion–reaction (CDR) equation

$$\frac{\partial V}{\partial t} + u_i \frac{\partial V}{\partial x_i} - \nu \frac{\partial^2 V}{\partial x_k \partial x_k} + sV = Q, \tag{3.33}$$

is considered, to the artificial elementary diffusion due to the Characteristic–Galerkin (CG) method, given by

$$\nu_{\rm cg} = \frac{1}{2}\frac{\Delta t}{2} u^2,$$

where $u^2 = u_i u_i$, we propose to add a numerical, discontinuity capturing elementary diffusion

$$\nu_{\rm dc} = \frac{1}{2}\alpha_{\rm dc} h \frac{|R(V^{\rm h})|}{|\nabla V^{\rm h}|},$$

where $R(V^h)$ is the residual (only spatial terms considered) of (3.33) and

$$\alpha_{dc} = \max\left(0, C - \frac{2\nu|\nabla V^h|}{hR(V^h)}\right).$$

C is a constant depending on the interpolation order (0.7 if linear and 0.35 if quadratic). Supraindex "h" means that it belongs to the discretized usual FEM space.

But while the former only acts along the streamlines, the latter do it in all directions, taking into account both of the previous concepts. Like the streamline CG diffusion, the final discontinuity capturing tensor diffusion is not diagonal: in the streamline direction it is compared to the CG effect. Hence, once space discretization in N_{el} elements is done, the terms added to the right hand side of equation (3.1.2) are:

$$\sum_{e=1}^{N_{el}} \int_{\Omega^e} \left[\nu_{dc} \frac{\partial W^h}{\partial x_i} \delta_{ij} \frac{\partial V^h}{\partial x_j} \right.$$
$$\left. + \quad (\nu_{sl} - \nu_{dc}) \frac{\partial W^h}{\partial x_i} \left(\frac{u_j u_i}{u^2} \right) \frac{\partial V^h}{\partial x_j} \right] d\Omega, \tag{3.34}$$

where $\nu_{sl} = \max(0, \nu_{dc} - \nu_{cg})$.

As in the preceding section, in order to apply these concepts to Navier-Stokes equations, they must be rewritten in a CDR form. Then, those same identifications can be done. Later, we will come back to these matters.

3.2 Fractional Step Techniques

As previously said, in incompressible flow, the unknowns velocity and pressure are not modeled by the same kind of continuum differential equations. What is seemed as a simplification of Navier - Stokes equations for searching analytical solutions (when possible), in discretizations based on the weak form of the equations brings to light some problems generated by the fact that different regularity properties are required to both the solution spaces. In the finite element context, once the spatial discretization of the weak problem is done and the Galerkin method is plainly applied, some compatibility conditions should be satisfied between interpolation spaces: the well known *Babuška - Brezzi* conditions (cf. [Brezzi and Bathe, 1990]). For that reason, a finite element

general algorithm should use either mixed interpolation spaces verifying this or equal interpolation, but circumventing in some way the compatibility restrictions. In the introduction, we have cited some of the many solutions suggested. Fractional step techniques comprise an important group.

Two distinct procedures are based on this concept, both of them commonly known under this denomination. The transport equations that model flow dynamics has the same structure: they can be written in *conservative form*, meaning that the temporal derivative of the unknown is equal to the divergence of convective, diffusive and / or reactive fluxes. Strang's viscous splitting (c.f. [Strang, 1968]) is designed to separate convective from diffusive effects, present in the same equation. In this approach, the effects of convective terms are considered in one step and the viscous boundary layer treatment is faced in another, allowing particular kind of schemes for each branch of the splitting according to their own numerical properties. See for instance [Demkowicz et al., 1990]. On the other hand, A.J. Chorin [Chorin, 1967] and R. Temam [Temam, 1969] split also, but doing the surgery in a different place, for their objective is different too. They proposed to solve firstly the momentum equation with no pressure gradient term, then the continuity equation, and finally to correct the momentum. The fractional momentum contribution in the continuity equation produces a double benefit for incompressible problems: to stabilize the pressure and to allow equal interpolation for both velocity and pressure. It has been proposed also to combine both ideas by doing a triple split, like in [Laval and Quartapelle, 1990]. In the context of incompressible flow, to calculate the new pressure and use it to correct the momentum can be seen as a *projection* over the space of free divergence velocity field, which in turn is a Poisson equation for the pressure and a explicit correction for the momentum [Guermond and Quartapelle, 1995].

In this work, we follow the idea first suggested in [Chorin, 1967, Chorin, 1969, Temam, 1969]. It can be seen that the projection step introduces some terms in the continuity equation that stabilizes the pressure and allows the use of equal interpolations for velocity and pressure fields. The idea is to extend these concepts to compressible flows in order to have only one algorithm that can work equally well in both regimes, using the same interpolation spaces for all the unknowns, and allowing to resolve the incompressible limit, in particular for the case of compressible flow problems with regions of low compressibility, like boundary layers. Another important subject regarding this equation and its fractional step discretization is what boundary conditions are to be put.

The choice of the set of unknowns is also addressed here. Many times it is read that as conservative variables are clearly not suitable for solving pure incompressible problems, then they are useless if a general algorithm is what we are looking for. In this case, this set must be left aside, favoring one in which pressure is one of the unknowns, like the primitive, non conservative set. We think that this reasoning should

not be taken into account to a priori avoid conservation variables in a general algorithm context. The pressure appearing in incompressible problems is not at all the same kind of variable than that of compressible flow. It is not a thermodynamic variable, there is no state law which couples it with the thermal problem. In incompressible flow is wholy determined by the velocity field, apart from a reference value: in the absence of volume forces and velocity gradients, it equals to that reference value, no matter any temperature change, contrary to what happens in compressible flow. Therefore, this difference is not a matter of any numerical method, but of the physics of the problem. It follows: what is the reason for discarding a conservative set for a general algorithm? May be the convenience from the programmer point of view [Hansbo, 1994], or the advantages for implementing a given algorithm [Shakib et al., 1991], or even the beauty and symetry of the equations. We believe that the real challenge for a general algorithm is that it can solve well the incompressibility limit, both in fully incompressible problems or in compressible problems with a broad Mach number range keeping the same algorithm structure, being the set of variables chosen flexible enough and dependent on the physics of the problem.

In this section, we firstly present the split and its action. Then, we study each equation at a time. Their weak form, being the base of the FEM method, instead of the differential equations themselves is chosen for the analysis. To start with, we tackled the fractional momentum equation, addressing also to its boundary conditions. Next, the continuity equation. It can be solved either explicitly or implicitly. Besides, either pressure or density could be the unknown. Which is the best combination? An additional comment on boundary conditions is worth to mention. Then the momentum correction. And finally, both total energy conservation and heat transport equations are treated.

3.2.1 The split

Let us write the conservation equations for the momentum U_i and the density ρ (continuity equation) as

$$\frac{\partial U_i}{\partial t} = M_i - \frac{\partial p}{\partial x_i} =: R_i, \tag{3.35}$$

$$\frac{\partial \rho}{\partial t} = -\frac{\partial U_i}{\partial x_i}. \tag{3.36}$$

where R_i is the i-th component of the steady-state residual and we have used the abbreviation

$$M_i := -\frac{\partial}{\partial x_j}\left(\rho u_i u_j - \tau_{ij}\right) - \rho g_i. \tag{3.37}$$

As said before, the convective contribution $u_j \partial(\rho u_i)/\partial x_j$ appearing in M_i could lead to numerical instabilities if the standard Galerkin formulation is used to discretize the space. In order to stabilize this effect, we first discretize (3.35) in time along the characteristics of the total derivative $\partial/\partial t + u_j \partial/\partial x_j$ as explained in the previous section. This leads to the following equations:

$$\frac{\Delta U_i^n}{\Delta t} = M_i^{n+\theta_3} - \frac{\partial p^{n+\theta_2}}{\partial x_i} - \frac{\Delta t}{2} u_k^n \frac{\partial R_i^n}{\partial x_k}, \tag{3.38}$$

$$\frac{\Delta \rho^n}{\Delta t} = -\frac{\partial U_i^{n+\theta_1}}{\partial x_i}, \tag{3.39}$$

where Δt is the time step size (assumed to be constant for simplicity), the superscripts denote time step level, $\theta_1, \theta_2, \theta_3 \in [0,1]$ and we use the notation $f^{n+\theta} = \theta f^{n+1} + (1-\theta) f^n$, $\Delta f^n = f^{n+1} - f^n$ for any function f and $\theta \in [0,1]$.

While the second order term coming from the time discretization along the characteristics is evaluated explicitly, the supraindexes θ_2 and θ_3 mean that pressure and convective - diffusive fluxes terms can be evaluated implicitly. Also, once the momentum is known at time step $n+1$,the continuity equation can be solved also implicitly. If we want to solve implicitly all the first order terms, then we get stuck with the fact that we must know the new pressure *before* the continuity equation is solved. Or if we solve first this equation, then it happens the same, now with the knew momentum. A possible way out of this is to take out the pressure terms from the momentum equation, solve it, solve the continuity equation and finally correct the momentum using the new variables. This introduces some first order splitting errors, which we shall study.

But if the same approach is used and all the terms are solved explicitly, no splitting error is present. Of course when dealing with incompressible problems the fully explicit scheme is not possible. On the other hand, when compressible problems are considered many possibilities appear: solving all the terms explicitly gives no splitting error but slower convergence rate speed, and on the other hand, when convective and / or diffusive terms are implicit the error appears but it can be faster to converge.

Let

$$\Delta\tilde{U}_i^n := \Delta U_i^n + \Delta t \frac{\partial p^{n+\theta_2}}{\partial x_i}. \tag{3.40}$$

Having introduced this new variable, (3.38) and (3.39) can be written as

$$\frac{\Delta\tilde{U}_i^n}{\Delta t} = M_i^{n+\theta_3} - \frac{\Delta t}{2} u_k^n \frac{\partial R_i^n}{\partial x_k}, \tag{3.41}$$

$$\frac{\Delta\rho^n}{\Delta t} = -\frac{\partial}{\partial x_i}\left(U_i^n + \theta_1 \Delta\tilde{U}_i^n - \theta_1 \Delta t \frac{\partial p^{n+\theta_2}}{\partial x_i}\right), \tag{3.42}$$

$$\frac{\Delta U_i^n}{\Delta t} = \frac{\Delta\tilde{U}_i^n}{\Delta t} - \frac{\partial p^{n+\theta_2}}{\partial x_i}. \tag{3.43}$$

Hereafter, we shall refer to $\tilde{U}_i^{n+1} := U_i^n + \Delta\tilde{U}_i^n$ as the *fractional momentum*.

A deeper insight of the implicit treatment of M_i can be achieved by separating its convective and viscous parts. We define them respectively as

$$M_{c,i} := -\frac{\partial}{\partial x_j}\left(u_j U_i\right), \tag{3.44}$$

$$M_{v,i} := \frac{\partial}{\partial x_j}\tau_{ij}, \tag{3.45}$$

so that

$$M_i = M_{c,i} + M_{v,i} - \rho g_i.$$

In order to avoid the need for solving a nonlinear problem within each time step, we take

$$M_{c,i}^{n+\theta_3} = -\frac{\partial}{\partial x_j}\left(u_j^n U_i^{n+\theta_3}\right), \tag{3.46}$$

that is, the convective velocity is evaluated at the previous time step. This approach is used for example in [Simo and Armero, 1994] for incompressible flows.

In principle, the term $M_i^{n+\theta_3}$ in (3.41) must be computed using U_j^{n+1}. If this is done, (3.41), (3.42) and (3.43) are exactly equivalent to (3.38) and (3.39) for the continuous in space problem that we consider for the moment. However, the use of U_j^{n+1} in (3.41) prevents from the possibility of computing directly the fractional momentum from this equation. This can be avoided by replacing $M_i^{n+\theta_3}$ by $\tilde{M}_i^{n+\theta_3}$, which is obtained by computing M_i with $\tilde{U}_j^{n+1}$ instead of U_j^{n+1}. This introduces of course a splitting error.

This error, coming from the fact that the convective contribution to M_i is computed with the fractional momentum and not with the momentum itself, can be eliminated. Using (3.46) and (3.40), second order accuracy for the pressure term can be achieved,

$$\begin{aligned} M_{c,i}^{n+\theta_3} &= -\frac{\partial}{\partial x_j}\left(u_j^n U_i^n\right) - \theta_3 \frac{\partial}{\partial x_j}\left(u_j^n \Delta\tilde{U}_i^n\right) + \theta_3 \Delta t \frac{\partial}{\partial x_j}\left(u_j^n \frac{\partial p^n}{\partial x_i}\right) \\ &= \tilde{M}_{c,i}^{n+\theta_3} + \theta_3 \Delta t \frac{\partial}{\partial x_j}\left(u_j^n \frac{\partial p^n}{\partial x_i}\right). \end{aligned} \tag{3.47}$$

The last term corrects the splitting error in the convective fluxes and only that corresponding to the viscous fluxes will remain. This original idea, in particular related to incompressible flows, but which can be used in compressible regime is firstly exposed in [Codina et al., 1998b].

If in (3.41) $M^{n+\theta_3}$ is replaced by $\tilde{M}^{n+\theta_3}$, using the correction given by (3.47) or not, we obtain an equation for the fractional momentum alone, which can be solved. Once this is done, (3.42) may be used to compute either ρ^{n+1} if $\theta_2 = 0$ or p^{n+1} if $\theta_2 > 0$. In this last case, the equation of state is needed to express ρ^{n+1} in terms of p^{n+1}. This point is treated in the following section.

Finally, (3.43) can be used to compute the momentum U_i^{n+1}. The important point is the substitution of $\Delta\tilde{U}_i^n$ in (3.42) using the definition (3.40), all this at the continuous level. This will lead to a stabilizing pressure dissipation term in the discrete finite element scheme that allows to use this scheme for incompressible flows with the same velocity-pressure finite element interpolation if the semi-implicit version of the algorithm is used.

In brief, the complete set of Navier - Stokes, time discretized according to the preceding section and combined with the fractional step technique is depicted in table 3.1. A special treatment for $M_{v,i}$ is proposed in the next section, which also can be treated implicitly (in fact, a part of it). Some terms in the energy equation can be treated implicitly, a fact that will be addressed also in the next section. By the

moment, we write the energy equation residual as $R_{\mathrm{E}}^{n+\theta_4}$ to remember this.

$$
\begin{aligned}
\frac{\Delta \tilde{U}_i^n}{\Delta t} &= \tilde{M}_{\mathrm{v},i} + \tilde{M}_{\mathrm{c},i}^{n+\theta_3} \\
&\quad +\theta_3 \Delta t \frac{\partial}{\partial x_j}\left(u_j^n \frac{\partial p^n}{\partial x_i}\right) - \frac{\Delta t}{2} u_k^n \frac{\partial R_i^n}{\partial x_k}, \\
\frac{\Delta \rho^n}{\Delta t} &= -\frac{\partial}{\partial x_i}\left(U_i^n + \theta_1 \Delta \tilde{U}_i^n - \theta_1 \Delta t \frac{\partial p^{n+\theta_2}}{\partial x_i}\right), \\
\frac{\Delta U_i^n}{\Delta t} &= \frac{\Delta \tilde{U}_i^n}{\Delta t} - \frac{\partial p^{n+\theta_2}}{\partial x_i}, \\
\frac{\Delta E^n}{\Delta t} &= R_{\mathrm{E}}^{n+\theta_4} - \frac{\Delta t}{2} u_k^n \frac{\partial R_{\mathrm{E}}^n}{\partial x_k}.
\end{aligned}
$$

Table 3.1: Weak form of the CBS algorithm for Navier-Stokes equations.

3.2.2 Fractional momentum equation

Let us obtain now the weak form of (3.41), (3.42) and (3.43). Considering first (3.41), let $\tilde{W}_i$ be the i-th component of the test function for the fractional momentum. We shall compute it in the problem domain Ω and also on its boundary $\Gamma = \partial\Omega$, and therefore $\tilde{W}_i$ is subject to no conditions. Multiplying (3.41) by $\tilde{W}_i$, integrating over Ω and integrating the viscous term and the term coming for the discretization along the characteristics by parts we get

$$\begin{aligned}\int_\Omega \tilde{W}_i \frac{\Delta \tilde{U}_i^n}{\Delta t} d\Omega &= \int_\Omega \tilde{W}_i \tilde{M}_{c,i}^{n+\theta_3} d\Omega - \theta_3 \Delta t \int_\Omega \frac{\partial \tilde{W}_i}{\partial x_j} u_j^n \frac{\partial p^n}{\partial x_i} d\Omega \\ &+ \theta_3 \Delta t \int_\Gamma n_j u_j^n \tilde{W}_i \frac{\partial p^n}{\partial x_i} \, \mathrm{d}\Gamma + \int_\Omega \tilde{W}_i \rho g_i - \int_\Omega \frac{\partial \tilde{W}_i}{\partial x_j} \tau_{ij}^{n+\theta_3} d\Omega \\ &+ \int_\Gamma \tilde{W}_i n_j \tau_{ij}^{n+\theta_3} \, \mathrm{d}\Gamma + \frac{\Delta t}{2} \int_\Omega \frac{\partial}{\partial x_k} (u_k^n \tilde{W}_i) R_i^n d\Omega, \end{aligned} \tag{3.48}$$

where $\boldsymbol{n}$ is the unit outward normal to Γ and we have assumed that $R_i^n = 0$ on Γ. The first three terms correspond to the modification introduced in (3.47).

The terms containing the viscous stresses must be computed at $n + \theta_3$. Again, if $\theta_3 = 0$, the term is calculated explicitly. But if not, τ_{ij} must be evaluated from the momentum at $n+1$ but in the equation which calculates the fractional mometum, not the momentum itself. For that reason, in the implicit terms we could take

$$\tau_{ij}^{n+1} \approx \bar{\tau}_{ij}^{n+1}$$

which is simply τ_{ij} but computed using the fractional momentum instead. If this is done so, the viscous stresses should be all computed at $n + \theta_3$, coupling all the components of the fractional momentum, that is to say, it is a system of d coupled scalar equations and d unknowns, $d = 2$ or 3 being the number of space dimensions. In order to avoid this coupling, we propose to evaluate the part of the viscous stresses that couples the d equations explicitly. Also, in order to avoid the need for using the density at $n + \theta_3$ (which is unknown at the moment of solving (3.48)) we also evaluate it explicitly. After doing this, the viscous stresses are approximated by

$$\bar{\tau}_{ij}^{n+\theta_3} \approx \frac{\mu}{\rho^n} \frac{\partial \tilde{U}_i^{n+\theta_3}}{\partial x_j} - \frac{\mu}{(\rho^n)^2} \tilde{U}_i^{n+\theta_3} \frac{\partial \rho^n}{\partial x_j} + \mu \left(\frac{\partial u_j^n}{\partial x_i} - \frac{2}{3} \frac{\partial u_k^n}{\partial x_k} \delta_{ij} \right). \tag{3.49}$$

This will keep the splitting error corresponding to the viscous terms but it will allow to increase the time step when viscous effects are present.

Boundary conditions

Integration by parts has led us to the boundary integral of the deviatoric stress tensor contracted with the normal at the contours. We have seen that, for the case of New-

tonian fluids, τ_{ij} is a linear combination of the velocity's first derivatives. Therefore, any condition imposed through this boundary integral would be a Neumann condition. On the other hand, as was said above we *do not* impose any boundary condition on $\tilde{W}_i$, the test function for the fractional momentum. From a physical point of view, we free the fractional momentum because it is not a physical variable but just an artificial, mathematical concept. Also, the real equation for the momentum is the sum of both the fractional momentum and the correction equations, so in principle, we could impose the Dirichlet condition later in the momentum correction equation, after the continuity equation is solved.

We propose here ([Codina et al., 1995], previously considered by Papanastasiou et al. in [Papanastasiou et al., 1992] but in a different context) to leave $\tilde{\tau}_{ij}n_i$ free not only in Γ_D but in Γ_N too in the weak form, that is to say, to evaluate for the whole contour the boundary integral in (3.48) with no imposition on fractional momentum. It must be remarked that this is done weakly. This boundary condition is treated only in the equation for the fractional momentum, because it carries the Neumann's boundary contribution. Apart from it, no other unknown is fixed at the contours in equation (3.48): fractional momentum is free at the whole domain. The solutions obtained doing this in all the examples tested so far are correct, even no Dirichlet condition are imposed in this step, where the fractional momentum is the unknown. Probably, this is so due to the fact that all is done weakly. An alternative (heuristic) interpretation can be found in [Papanastasiou et al., 1992].

Neumann boundary conditions can be (weakly) imposed through the boundary integral in (3.48) and expressed in terms of traction, which is defined as

$$t_i = -pn_i + \tilde{\tau}_{ij}n_j$$

Suppose the boundary is divided in two: $\Gamma = \Gamma_T \cup \Gamma_F$. Hence, we can divide also the boundary integral:

$$\int_\Gamma W_j \tilde{\tau}_{ij} n_i d\Gamma = \int_{\Gamma_F} W_j \tau_{ij} n_i d\Gamma + \int_{\Gamma_T} W_j \left(t_j + pn_j\right) d\Gamma. \tag{3.50}$$

This allows us to impose the following Neumann boundary conditions:

1. Γ_T: The whole traction is prescribed

$$-pn_i + n_j\tilde{\tau}_{ij} = t_i.$$

So, there

$$\int_{\Gamma_T} \tilde{W}_i n_j \tilde{\tau}_{ij}^{n+\theta_3}\, \mathrm{d}\Gamma = \int_{\Gamma_T} \tilde{W}_i \left(t_i + pn_i\right)\, \mathrm{d}\Gamma$$

2. Γ_F: Free part of the boundary, where the integral is computed as it appears in the original equation.

For instance, in an outflow, if $\boldsymbol{t} = 0$ is imposed, the fluid there is allowed to escape freely, being that boundary a "physical" one: the streamlines are curved toward the center of the outflow hole right before crossing it and then they spread in the opposite direction. On the other hand, the open boundary condition as set in (3.48) is nothing but a "numerical" boundary, which releases us from constructing extremely large domains to study regions that are physically far away from open outlets. It is worth to mention that no condition on the traction or the pressure is implicit in (3.48). For that reason, it is said that the boundary is "numerical" and can become "physical" by naturally imposing a physical condition on the traction. Instead, other methods carry implicitly the $\boldsymbol{t} = 0$ prescription (like in [Gresho, 1990]). Equation (3.48) is the second and last step in calculating the linear momentum at time $n + 1$. Once this is done, $\boldsymbol{U}$ is imposed at the Dirichlet's boundary, according to the physical considerations made at section 2., and taking into account the kind of flow (supersonic or subsonic) at the given contour.

In brief, what is here proposed for the boundary treatment of the weak form of the linear momentum equation is:

i. Neumann's boundary condition on $\boldsymbol{U}$: (eventually) imposed on equation (3.48) using (3.50), and

ii. Dirichlet's boundary condition on $\boldsymbol{U}$: imposed on equation (3.48).

3.2.3 Continuity Equation

Let us consider now (3.42) and weight it by a test function W_p. We have that

$$\int_\Omega W_p \frac{\Delta\rho^n}{\Delta t} d\Omega = -\int_\Omega W_p \frac{\partial U_i^n}{\partial x_i} d\Omega$$
$$+ \quad \theta_1 \int_\Omega \frac{\partial W_p}{\partial x_i} \left(\Delta\tilde{U}_i^n - \Delta t \frac{\partial p^{n+\theta_2}}{\partial x_i} \right) d\Omega$$
$$- \quad \theta_1 \int_\Gamma W_p n_i \left(\Delta\tilde{U}_i^n - \Delta t \frac{\partial p^{n+\theta_2}}{\partial x_i} \right) \mathrm{d}\Gamma. \tag{3.51}$$

The continuity equation as written down here is the core of the algorithm, the key of its general character. Additional to its numerical advantages is the fact that it easily allows us to change the unknown, chosing either the density (e.g. in compressible flow) or the pressure (in both compressible and incompressible), using to eliminate the other one the state law. We shall come back to this point later.

Boundary conditions

As a boundary condition, we impose that the normal component of (3.43) be also verified on Γ, a condition equivalent to impose that the normal component of the momentum equation (3.38) be verified on Γ. This leads to

$$n_i \left(\Delta\tilde{U}_i^n - \Delta t \frac{\partial p^{n+\theta_2}}{\partial x_i} \right) = n_i \Delta U_i^n. \tag{3.52}$$

Let us recall the boundary division done for the fractional momentum equation. We keep Γ_T, but we sub divide Γ_P in three:

$$\Gamma = \Gamma_\mathrm{T} \cup \Gamma_\mathrm{P} \cup \Gamma_{\Delta\mathrm{U}} \cup \Gamma_{\mathrm{FP}}.$$

In the first two sets of Γ, Dirichlet boundary conditions for the pressure are prescribed. In Γ_T we impose direct conditions on the pressure through the equation $p = n_i \tilde{\tau}_{ij} n_j - n_i t_i$, where t_i is given and used in the Neumann prescription for the fractional momentum. In Γ_P a given value is imposed to the continuity momentum unknown, either the pressure or the density. In $\Gamma_{\Delta\mathrm{U}}$, a Neumann condition is imposed weakly through the boundary integral in (3.51). There, in the nodes with Dirichlet

conditions for the momentum, $\Delta U = f(\boldsymbol{x}, t)$ where $f(\boldsymbol{x}, t)$ is a given function. Finally, Γ_{FP} is a free contour for this equation.

It is remarkable what happens in boundary contours of the kind Γ_{T}. Suppose that we are dealing with an incompressible problem. This boundary is a Neumann contour for the momentum equation and a Dirichlet one for the continuity equation. For that reason, we take the fixed pressure at the nodes belonging to it as $p = n_i \tilde{\tau}_{ij}^n n_j - n_i t_i$, where the values of $\tilde{\tau}_{ij}$ must be extrapolated to the nodes themselves, for they were evaluated at integration points. Also, the tensor $\tilde{\tau}_{ij}$ is that evaluated at time step n, introducing this fact a $O(\Delta t)$ error.

Then, using (3.52) and the approximations just described, (3.51) can be written as

$$\begin{aligned}
\int_\Omega W_p \frac{\Delta \rho^n}{\Delta t} d\Omega &= -\int_\Omega W_p \frac{\partial U_i^n}{\partial x_i} d\Omega \\
&+ \theta_1 \int_\Omega \frac{\partial W_p}{\partial x_i} \left(\Delta \tilde{U}_i^n - \Delta t \frac{\partial p^{n+\theta_2}}{\partial x_i} \right) d\Omega \\
&- \theta_1 \int_{\Gamma_{\Delta U}} W_p n_i \Delta U_i^n \, \mathrm{d}\Gamma. \qquad (3.53)
\end{aligned}$$

This is the weak form of the continuity equation that we use, either if the unknown is the pressure or the density. As we said before, in the second case, the pressure may be considered known where the density is given by using the equation of state and a guess for the temperature, if required.

3.2.4 Momentum equation

For (3.43) we have that

$$\int_\Omega W_i \frac{\Delta U_i^n}{\Delta t} d\Omega = \int_\Omega W_i \frac{\Delta \tilde{U}_i^n}{\Delta t} d\Omega - \int_\Omega W_i \frac{\partial p^{n+\theta_2}}{\partial x_i} d\Omega, \qquad (3.54)$$

where W_i is the i-th component of the test function. In this equation all the components of the momentum can be prescribed. This is possible due to the fact that the fractional momentum has been computed precisely by imposing that (3.43) be also satisfied on the boundary.

3.2.5 Energy Equation: Total Energy or Temperature

Total Energy Conservation Equation. Taking from 3.1 the discretized equation of the energy, its weak form can be calculated. Weighting this equation by a test function W_{E}, integrating the diffusion and heat generation terms by parts, setting $R_{\mathrm{E}} = 0$ on the boundary and prescribing the total heat flux (from heat generation and from conduction) to H on a part of the boundary Γ_{H} we get

$$\begin{aligned}\int_{\Omega} W_{\mathrm{E}} \frac{\Delta E^n}{\Delta t} d\Omega \;=\; & -\int_{\Omega} W_{\mathrm{E}} \frac{\partial}{\partial x_i} \left[u_i \left(E+p\right)\right]^{n+\theta_4} d\Omega \\ & -\int_{\Omega} \frac{\partial W_{\mathrm{E}}}{\partial x_i} \left(k \frac{\partial T}{\partial x_i} + \tau_{ij} u_j\right)^n d\Omega + \frac{\Delta t}{2} \int_{\Omega} \frac{\partial}{\partial x_k} \left(u_k^n W_{\mathrm{E}}\right) R_{\mathrm{E}}^n d\Omega \\ & + \int_{\Gamma_{\mathrm{H}}} W_{\mathrm{E}} H \, \mathrm{d}\Gamma. \end{aligned} \tag{3.55}$$

On $\Gamma - \Gamma_{\mathrm{H}}$ we assume that $W_{\mathrm{E}} = 0$, that is, the energy is known there. Again, θ_4 and is a parameter for apply the trapezoidal rule like in the preceeding equations. See that in this case, in the convective term, velocity and pressure at time step $n+1$ could be already known depending on the set of variables used. The unknown is E, but placing new values of the other unknowns in the right hand side can be an advantage for faster convergence. Then, it is possible to choose in terms like

$$\left[u_i \left(E+p\right)\right]^{n+\theta_4} \simeq \left[u_i' \left(E^{n+\theta_4} + p'\right)\right] \tag{3.56}$$

the following:

$$\begin{aligned} u_i' &= \left(U_i/\rho\right)^{n+1} \\ p' &= p^n \end{aligned}$$

if ρUE set is used, or

$$u_i' = \left(U_i^{n+1}/\rho^n\right)$$

$$p' = p^{n+1}$$

if pUE set is used. In the diffusive terms involving the velocity and velocity gradients, like the Joule effect term, u_i' can be taken as above. Heat transport term either is evaluated at time n for simplicity or an iterative scheme should be used. In this case, $T^{n+1,0} := T^n$ can be taken as first guess and some iterations on the energy equation should be done.

As for the momentum, the total energy is not normally prescribed, but instead of this the temperature is given. In this case, we prescribe the total energy using the values already known of velocity and density and the prescribed temperatures.

Heat Transport Equation. An alternative to the total energy conservation equation is the heat transport one. The main reason for choosing it is the needing of the temperature at the new time step in certain stages of the algorithm when semi-implicit options are used for the continuity equation. As from the total energy equation T^{n+1} can't be evaluated unless we have ρ^{n+1}, the heat transport equation is a good choice in spite of its non-conservative character. However, the solution must be free of shocks because its numerical solution can place them in wrong position.

Heat transport equation is

$$\frac{\partial T}{\partial t} = R_{\mathrm{T}} := -u_i \frac{\partial T}{\partial x_i} + \frac{1}{C_v \rho}\left(\frac{\partial}{\partial x_i}\left(k\frac{\partial T}{\partial x_i}\right)\right) + \frac{1}{C_v \rho}\left(\sigma_{ij}\frac{\partial u_i}{\partial x_j}\right) \tag{3.57}$$

where

$$\sigma_{ij} := \tau_{ij} - p\delta_{ij} \tag{3.58}$$

Let us weight now this equation by a test function W_{T}, integrate the diffusion term by parts, set $R_{\mathrm{T}} = 0$ on the boundary and prescribe the conduction heat flux to H on a part of the boundary Γ_{H}. The result is

$$\int_\Omega W_{\rm T}\frac{\Delta T^n}{\Delta t}d\Omega = \int_\Omega W_{\rm T}\left[\left(-u_i+\frac{k}{C_v\rho^2}\frac{\partial\rho}{\partial x_i}\right)\frac{\partial T}{\partial x_i}\right]^{n+\theta_4}d\Omega$$
$$+\int_\Omega W_{\rm T}\left[\frac{1}{C_v\rho}\sigma_{ij}\frac{\partial u_i}{\partial x_j}\right]^{n}d\Omega-\int_\Omega\frac{\partial W_{\rm T}}{\partial x_i}\left(\frac{k}{C_v\rho}\frac{\partial T}{\partial x_i}\right)^{n+\theta_4}d\Omega$$
$$+\frac{\Delta t}{2}\int_\Omega\frac{\partial}{\partial x_k}\left(u_k^n W_{\rm T}\right)R_{\rm T}^n d\Omega+\int_{\Gamma_{\rm H}}\frac{1}{C_v\rho^n}W_{\rm T}H\ {\rm d}\Gamma. \qquad (3.59)$$

The temperature is assumed to be known on $\Gamma-\Gamma_{\rm H}$. As for the energy, θ_4 indicates whether any term is implicit. Unlike in E equation, the unknown T is explicitly written in both convective and diffusive terms. Therefore both terms can be advanced implicitly, using some guesses for density and velocity like those for the energy equation. In any case, by taking $\theta_4=0$, either total energy or heat transport equation are advanced explicitly.

3.3 Discrete Problem and Solution Strategies

With the weak form of the differential equations already established, we can proceed to discretize the space. We do this using the standard Galerkin method, since the term coming from the discretization in time along the characteristics will stabilize the convective terms. This means that we take all the test functions $\tilde{W}_i$, W_p, $W_{\bar{v}}$, W_E and $W_{\rm T}$ equal to the shape functions. Also, some additional shock-capturing viscosity will be needed in the presence of discontinuities or sharp gradients of the solution, as explained in Section 3.2.

Let us consider first the equations for the fractional momentum (3.48) and for the end-of-step momentum (3.54). For the sake of simplicity, we take $\theta_3=0$ in what follows. Once the spatial discretization has been performed, the discrete version of these equations can be written in matrix form, the structure of which is

$$\boldsymbol{M}\frac{\Delta\tilde{\bar{\boldsymbol{U}}}^n}{\Delta t} = \boldsymbol{F}_1-\boldsymbol{K}\bar{\boldsymbol{U}}^n, \qquad (3.60)$$

$$\boldsymbol{M}_0\frac{\Delta\bar{\boldsymbol{U}}_0^n}{\Delta t} = \boldsymbol{M}_0\frac{\Delta\tilde{\bar{\boldsymbol{U}}}_0^n}{\Delta t}-\boldsymbol{G}_0\bar{\boldsymbol{p}}^{n+\theta_2}+\boldsymbol{F}_2. \qquad (3.61)$$

Vectors of nodal unknowns have been indicated by a boldface character and an overbar. Matrices $\boldsymbol{M}$, $\boldsymbol{K}$ and $\boldsymbol{G}$ are the standard mass matrix for vector fields, the matrix coming

from the viscous and convective terms in the equation for the fractional momentum and the matrix coming from the gradient operator, respectively. Subscript naught in the previous equations refers to not prescribed degrees of freedom for the momentum (in the sense indicated above), and $\boldsymbol{F}_2$ contains precisely the contribution from $\Delta\tilde{\bar{U}}^n$ and $\Delta\bar{U}^n$ corresponding to the prescribed degrees of freedom for the latter. Here and below we use $\boldsymbol{F}$ with subscripts to denote a vector which is known at the moment of solving a particular equation.

The discrete version of the energy equation written in conservation form (3.55) or the heat equation (3.59) can be solved at the beginning or at the end of the time step. These equations have the structure

$$\boldsymbol{M}_{\mathrm{s},0}\frac{\Delta\bar{\boldsymbol{T}}^n}{\Delta t}+\boldsymbol{K}_{\mathrm{T}}\bar{\boldsymbol{T}}^{n+\theta_4}=\boldsymbol{F}_{\mathrm{T}}\quad\text{and}\quad\boldsymbol{M}_{\mathrm{s},0}\frac{\Delta\bar{\boldsymbol{E}}^n}{\Delta t}+\boldsymbol{K}_{\mathrm{E}}\bar{\boldsymbol{E}}^{n+\theta_4}=\boldsymbol{F}_{\mathrm{E}},\tag{3.62}$$

where $\boldsymbol{M}_{\mathrm{s}}$ is the mass matrix for scalar unknowns and $\boldsymbol{M}_{\mathrm{s},0}$ its modification to account for Dirichlet boundary conditions. $\boldsymbol{K}_{\mathrm{T}}$ and $\boldsymbol{K}_{\mathrm{E}}$ are the matrices coming from viscous and convective fluxes, discretizing the weak form of the total energy and heat transport equations respectively.

It remains to write the discrete version of the continuity equation (3.53). We consider different cases according to the type of flow being analyzed. We will see that it is useful to introduce the matrices $\boldsymbol{M}_\alpha$ and $\boldsymbol{L}_\beta$, of components

$$M_{\alpha,ij}=\int_\Omega \alpha N_i N_j d\Omega,$$
$$L_{\beta,ij}=\int_\Omega \beta\frac{\partial N_i}{\partial x_k}\frac{\partial N_j}{\partial x_k}d\Omega,$$

where N_i is the shape function associated to the i-th node of the finite element mesh with which we assume that all the variables are interpolated and α and β are functions that depend on the type of flow.

3.3.1 Incompressible and slightly compressible flows

These two types of flows can be defined by the relation

$$\Delta\rho^n = \alpha\Delta p^n, \tag{3.63}$$

with $\alpha = 0$ for fully incompressible flows and $\alpha = 1/c^2$ (a positive constant) for slightly compressible flows. In this case, (3.53) can be written as

$$\begin{aligned}
&\int_\Omega \alpha W_p \frac{\Delta p^n}{\Delta t} d\Omega + \theta_1 \Delta t \int_\Omega \frac{\partial W_p}{\partial x_i} \frac{\partial p^{n+\theta_2}}{\partial x_i} d\Omega = \\
&- \int_\Omega W_p \frac{\partial U_i^n}{\partial x_i} d\Omega + \theta_1 \int_\Omega \frac{\partial W_p}{\partial x_i} \Delta \tilde{U}_i^n d\Omega \\
&- \theta_1 \int_{\Gamma_D} W_p n_i \Delta U_i^n \, d\Gamma,
\end{aligned} \tag{3.64}$$

Once the finite element discretization of this equation has been done, the matrix form of the discrete problem is

$$\boldsymbol{M}_\alpha \frac{\Delta \bar{\boldsymbol{p}}^n}{\Delta t} + \theta_1 \Delta t \boldsymbol{L}_\beta \bar{\boldsymbol{p}}^{n+\theta_2} = \boldsymbol{F}_C, \tag{3.65}$$

with α the parameter appearing in (3.63) and $\beta = 1$ in this case. In (3.65) we have introduced

$$\boldsymbol{F}_C := -\boldsymbol{D}\bar{\boldsymbol{U}}^n + \theta_1 \boldsymbol{G}^t \Delta \bar{\tilde{\boldsymbol{U}}}^n + \boldsymbol{F}_D,$$

where $\boldsymbol{F}_D$ is the vector coming from the last term in (3.64) that is, from the boundary values of the momentum, and $\boldsymbol{D}$ is the matrix coming from the divergence operator. Dirichlet boundary conditions for the pressure are assumed to be included in (3.65).

Of special interest is the case of fully incompressible flows, that is, $\alpha = 0$. It is well known that in this case the velocity and pressure finite element interpolations must satisfy the Babuška-Brezzi conditions when the classical $\boldsymbol{U}$-p approach is used. This is not the case using the type of fractional step methods that we are considering. We justify this in the following. To simplify the discussion, we assume that $\boldsymbol{U}$ is prescribed to zero on the whole boundary Γ.

Omitting the subscript β for a moment (it is 1), the matrix form of (3.60), (3.61) and (3.65) can be written as

$$\begin{aligned}
\boldsymbol{M}_0 \frac{\Delta \tilde{\bar{\boldsymbol{U}}}_0^n}{\Delta t} &= \boldsymbol{F}_1^* - \boldsymbol{K}_0 \bar{\boldsymbol{U}}_0^n, && (3.66)\\
\theta_1 \Delta t \boldsymbol{L} \bar{\boldsymbol{p}}^{n+\theta_2} &= -\boldsymbol{D}_0 \bar{\boldsymbol{U}}_0^n + \theta_1 \boldsymbol{G}_0^{\mathrm{t}} \Delta \tilde{\bar{\boldsymbol{U}}}_0^n + \boldsymbol{F}^*, && (3.67)\\
\boldsymbol{M}_0 \frac{\Delta \bar{\boldsymbol{U}}_0^n}{\Delta t} &= \boldsymbol{M}_0 \frac{\Delta \tilde{\bar{\boldsymbol{U}}}_0^n}{\Delta t} - \boldsymbol{G}_0 \bar{\boldsymbol{p}}^{n+\theta_2} + \boldsymbol{F}_2. && (3.68)
\end{aligned}$$

Now subscript naught refers to degrees of freedom of interior nodes. Matrices $\boldsymbol{D}_0$ and $\boldsymbol{G}_0^{\mathrm{t}}$ are the submatrices of $\boldsymbol{D}$ and $\boldsymbol{G}^{\mathrm{t}}$ corresponding to these nodes. They are related by $\boldsymbol{D}_0 = -\boldsymbol{G}_0^{\mathrm{t}}$. Vectors $\boldsymbol{F}_1^*$ and $\boldsymbol{F}^*$ have been introduced to take into account the boundary values of the fractional momentum.

From (3.68) we get that

$$\Delta \tilde{\bar{\boldsymbol{U}}}_0^n = \Delta \bar{\boldsymbol{U}}_0^n + \Delta t \boldsymbol{M}_0^{-1} \boldsymbol{G}_0 \bar{\boldsymbol{p}}^{n+\theta_2} - \Delta t \boldsymbol{M}_0^{-1} \boldsymbol{F}_2,$$

and using this in (3.66) and (3.67) we obtain

$$\begin{aligned}
&\boldsymbol{M}_0 \frac{\Delta \bar{\boldsymbol{U}}_0^n}{\Delta t} + \boldsymbol{K}_0 \bar{\boldsymbol{U}}_0^n + \boldsymbol{G}_0 \bar{\boldsymbol{p}}^{n+\theta_2} = \boldsymbol{F}_1^* + \boldsymbol{F}_2,\\
&\boldsymbol{D}_0 \bar{\boldsymbol{U}}_0^{n+\theta_1} + \theta_1 \Delta t \left(\boldsymbol{L} - \boldsymbol{G}_0^{\mathrm{t}} \boldsymbol{M}_0^{-1} \boldsymbol{G}_0 \right) \bar{\boldsymbol{p}}^{n+\theta_2} = \boldsymbol{F}_{\mathrm{C}}^*,
\end{aligned} \qquad (3.69)$$

with

$$\boldsymbol{F}_{\mathrm{C}}^* := \boldsymbol{F}^* - \theta_1 \Delta t \boldsymbol{G}_0^{\mathrm{t}} \boldsymbol{M}_0^{-1} \boldsymbol{F}_2.$$

Clearly, we must have $\theta_1 > 0$ and $\theta_2 > 0$ in order to have a solvable problem.

The important point in (3.69) is the presence of the matrix $\boldsymbol{B} := \boldsymbol{L} - \boldsymbol{G}_0^t \boldsymbol{M}_0^{-1} \boldsymbol{G}_0$, that can be understood as the difference between two discrete Laplacian operators. This matrix provides additional stability and, in particular, allows to use equal velocity pressure finite element interpolations in the incompressible case, as it had been noticed for example in [Schneider et al., 1978] and [Kawahara and Ohmiya, 1985]. This is so because this matrix is *positive semidefinite*. The proof of this fact can be found in in the Appendix and in [Codina et al., 1998b].

3.3.2 Barotropic flows

Let us consider now the flow of compressible barotropic fluids, that is to say, fluids for which there is an equation of state that involves only the density and the pressure, and not the temperature. In general, we write this equation as $p = p(\rho)$, but we will particularize it to the case

$$p = A\rho^{\gamma}, \tag{3.70}$$

where A and γ, the *adiabatic exponent*, are physical constants. This situation is found for example in the case of isentropic flow of perfect gases.

In the case of incompressible or slightly compressible flows we have formulated the continuity equation in terms of the pressure only. However, now we have the possibility of choosing either the density or the pressure as unknown of the problem. Let us start with the former option:

Density as variable If we choose to write the continuity equation (3.53) using the density we have to express the pressure gradient in terms of the density. For this we use the approximation

$$\frac{\partial p^{n+\theta_2}}{\partial x_i} = \left(\frac{\mathrm{d}p}{\mathrm{d}\rho}\right)^n \frac{\partial \rho^{n+\theta_2}}{\partial x_i} = \frac{\gamma p^n}{\rho^n} \frac{\partial \rho^{n+\theta_2}}{\partial x_i}. \tag{3.71}$$

The approximation relies on the fact that we evaluate the derivative of p with respect to ρ (the square of the speed of sound) at n instead of at $n+\theta_2$. This may be thought of as a linearization of the problem.

Using (3.71) in (3.53), it is found that the discrete continuity equation can be written in this case as:

$$\boldsymbol{M}_\alpha \frac{\Delta \bar{\boldsymbol{\rho}}^n}{\Delta t} + \theta_1 \Delta t \boldsymbol{L}_\beta \bar{\boldsymbol{\rho}}^{n+\theta_2} = \boldsymbol{F}_C, \tag{3.72}$$

now with $\alpha = 1$ and $\beta = \gamma p^n/\rho^n$. Observe that this equation has the same structure as (3.65) but with the density being the unknown instead of the pressure.

Pressure as variable If instead of using the density we use the pressure, the approximation that we employ is

$$\Delta \rho^n = \left(\frac{\mathrm{d}\rho}{\mathrm{d}p}\right)^n \Delta p^n$$

which is of order $O((\Delta p^n)^2)$. This approximation leads to

$$\frac{\Delta \rho^n}{\Delta t} = \left(\frac{\mathrm{d}\rho}{\mathrm{d}p}\right)^n \frac{\Delta p^n}{\Delta t} = \frac{\rho^n}{\gamma p^n} \frac{\Delta p^n}{\Delta t},$$

and the discrete continuity equation can now be written again as

$$\boldsymbol{M}_\alpha \frac{\Delta \bar{\boldsymbol{p}}^n}{\Delta t} + \theta_1 \Delta t \boldsymbol{L}_\beta \bar{\boldsymbol{p}}^{n+\theta_2} = \boldsymbol{F}_C, \tag{3.73}$$

that is, exactly as (3.65), but now with $\alpha = \rho^n/(\gamma p^n)$ and $\beta = 1$.

For this type of flows, unlike the incompressible case, the continuity equation (3.72) or (3.73) can be solved explicitly ($\theta_2 = 0$) also. The fully explicit form of the algorithm allows very fast calculations at each time step, for matrix inversions are avoided. On the other hand, smaller time increments are to be used which leads to a poorer convergence rate to stationary states.

3.3.3 Perfect gases

In this case the equation of state involves not only the pressure and the density, but also the temperature, as it is described in the introduction. The appearance of the temperature in it complicates a little the treatment of the continuity equation. As before, we may use either the density or the pressure as variables.

Density as variable Again, if $\theta_2 > 0$ we need to relate the pressure gradient to the density. We have that

$$\frac{\partial p^{n+\theta_2}}{\partial x_i} = \frac{\partial \rho^{n+\theta_2}}{\partial x_i} R T^{n+\theta_2} + \rho^{n+\theta_2} R \frac{\partial T^{n+\theta_2}}{\partial x_i}. \tag{3.74}$$

Clearly, if $\theta_2 = 0$ the pressure gradient term is on the right hand side (RHS) of the continuity equation, and it is entirely evaluated in the previous time step explicitly. But for $\theta_2 > 0$, if we use directly this expression in (3.53) the continuity equation will be coupled to the energy (or heat) conservation equation. In order to avoid this, for the implicit solution of this equation we use an iterative strategy based on assuming that $T^{n+\theta_2}$ is known and then correcting it. There is also another aspect that is computationally inconvenient. If we take $\rho^{n+\theta_2}$ as unknown in the second term of the RHS of (3.74) this will lead to a non-symmetric matrix (see (3.53)). This can be circumvented if we also assume that $\rho^{n+\theta_2}$ is known and then we correct it.

Let then T_{g} be a guess for $T^{n+\theta_2}$ within the time step under consideration and ρ_{g} a guess for $\rho^{n+\theta_2}$. Equation (3.74) may be replaced by

$$\frac{\partial p^{n+\theta_2}}{\partial x_i} = \frac{\partial \rho^{n+\theta_2}}{\partial x_i} R T_{\mathrm{g}} + \rho_{\mathrm{g}} R \frac{\partial T_{\mathrm{g}}}{\partial x_i}$$

The second term in this equation contributes to the RHS of the discrete continuity equation. If we denote by $\boldsymbol{F}_\rho$ this contribution, this discrete equation is

$$\boldsymbol{M}_\alpha \frac{\Delta \bar{\boldsymbol{\rho}}^n}{\Delta t} + \theta_1 \Delta t \boldsymbol{L}_\beta \bar{\boldsymbol{\rho}}^{n+\theta_2} = \boldsymbol{F}_{\mathrm{C}} + \boldsymbol{F}_\rho. \tag{3.75}$$

with $\alpha = 1$ and $\beta = RT_{\mathrm{g}}$. This equation is similar to (3.72). Apart from the coefficients α and β, the only difference is the term $\boldsymbol{F}_\rho$, which comes from the spatial derivative of the temperature.

Pressure as variable As for the case of barotropic flows, we may also use the pressure as the unknown of the continuity equation. For that we only need to use the equation of state, from which we have

$$\rho^{n+1} = \frac{p^{n+1}}{RT^{n+1}}. \tag{3.76}$$

As in the previous case, we need to guess the value of T^{n+1} by T_g in order to uncouple the resulting continuity equation and the energy equation. We may then write

$$\Delta\rho^n = \frac{\Delta p^n}{RT_g} + \left[\frac{p^n}{RT_g} - \frac{p^n}{RT^n}\right].$$

The bracketed term term contributes to the RHS of the discrete continuity equation with a vector $\boldsymbol{F}_p$. This equation can be written as

$$\boldsymbol{M}_\alpha \frac{\Delta\bar{\boldsymbol{p}}^n}{\Delta t} + \theta_1 \Delta t \boldsymbol{L}_\beta \bar{\boldsymbol{p}}^{n+\theta_2} = \boldsymbol{F}_C + \boldsymbol{F}_p, \tag{3.77}$$

with $\alpha = 1/(RT_g)$ and $\beta = 1$. Again, this equation has the same structure as (3.73) with a modification of the RHS due to the variation (now in time) of the temperature.

From numerical experiments we have found that this approach doesn't work well in the presence of strong shocks, in the sense that we haven't been able to obtain a converged steady state solution in these cases. We attribute this to the appearence of the temperature as a denominator in the function α. This makes the coefficients of $\boldsymbol{M}_\alpha$ difficult to evaluate numerically and with possibly high variations from one time step to the other in the vicinity of shocks.

3.3.4 General expression of the continuity equation

For all the type of flows considered we have written the continuity equation in a very similar way. Using the pressure as variable the general form is

$$\boldsymbol{M}_\alpha \frac{\Delta\bar{\boldsymbol{p}}^n}{\Delta t} + \theta_1 \Delta t \boldsymbol{L}_\beta \bar{\boldsymbol{p}}^{n+\theta_2} = \boldsymbol{F}'_C,$$

according to the following table:

Pressure as unknown

Coefficient	Incomp.	Slightly comp.	Barot.	Compress.
α	0	$\frac{1}{c^2}$	$\frac{\rho^n}{\gamma p^n}$	$\frac{1}{RT_g}$
β	1	1	1	1

In the RHS, $\boldsymbol{F}'_{\mathrm{C}} = \boldsymbol{F}_{\mathrm{C}}$, except in the case of perfect gases, for which $\boldsymbol{F}'_{\mathrm{C}} = \boldsymbol{F}_{\mathrm{C}} + \boldsymbol{F}_{\rho}$.

On the other hand, the density can be used as variable only for barotropic fluids and perfect gases. In this case the discrete continuity equation is

$$\boldsymbol{M}_{\alpha}\frac{\Delta\bar{\boldsymbol{\rho}}^n}{\Delta t} + \theta_1\Delta t\boldsymbol{L}_{\beta}\bar{\boldsymbol{\rho}}^{n+\theta_2} = \boldsymbol{F}'_{\mathrm{C}},$$

and the coefficients are calculated according to the table:

Density as unknown

Coefficient	Incomp.	Slightly comp.	Barot.	Perf. gas
α	1	1	1	1
β	-	-	$\frac{\gamma p^n}{\rho^n}$	RT_g

Sources are $\boldsymbol{F}'_{\mathrm{C}} = \boldsymbol{F}_{\mathrm{C}}$ for barotropic fluids and $\boldsymbol{F}'_{\mathrm{C}} = \boldsymbol{F}_{\mathrm{C}} + \boldsymbol{F}_{\rho}$ for perfect gases.

In all the cases, the matrix of the algebraic system of equations to be solved is symmetric and positive-definite (for incompressible confined flows a pressure needs to

be specified). We use the conjugate gradient method to solve it. In general, very few iterations are needed to converge, since the unknown at the previous time step is a good initial guess for its value at the current one.

3.4 Programming Notes

The complete set of discretized equations that we are going to solve is briefly written down in table 3.2. There, $\bar{\boldsymbol{X}}_{\text{cont}}$ and $\bar{\boldsymbol{X}}_{\text{heat}}$ account for the chosen continuity and energy transport equation unknown.

From things exposed in the previous section it can be inferred easily that a characteristic of the algorithm is the multiple set of solving procedure possibilities. This should be controlled by the programmer and at later step, by the user. We distinguished two main options: SIM or EXP, for "Semi Implicit" and "Explicit", according to whether the continuity equation is solved implicitly or explicitly, being the rest of the equations advanced explicitly. Also, it is possible to, within each of these general schemes, solve implicitly some terms in the fractional momentum or energy equations in order to increase the speed of convergence to stationary states. Finally, different groups of variables can be alternatively used as unknowns. This is sketched in the following lines.

Forms and variables

Algorithm forms = { SIM , EXP }

Sets of variables = { ρUT , ρUE , pUT , pUE }

Programming schemes

- EXP Form As it was said above, this is the computationally cheapest option. For each time step , it is as follows:

  Scheme A:
  Set of variables: ρUE or ρUT
  A.1. Calculate time increment Δt.
  A.2. Calculate fractional momentum $\tilde{\boldsymbol{U}}^{n+1}$, with or without implicit terms.
  A.3. Calculate $[\rho,\ \boldsymbol{U}\ ,\ E\ \ (or\ T)]^{n+1}$ using $\tilde{\boldsymbol{U}}^{n+1}$ and the rest of the variables at n step.

$$\boldsymbol{M}\frac{\tilde{\boldsymbol{U}}^{n+1}}{\Delta t} + \boldsymbol{K}\tilde{\boldsymbol{U}}^{n+\theta_3} = \boldsymbol{M}\frac{\bar{\boldsymbol{U}}^{n}}{\Delta t} + \boldsymbol{F}_1,$$

$$\boldsymbol{M}_\alpha\frac{\bar{\boldsymbol{X}}_{\text{cont}}^{n+1}}{\Delta t} + \theta_1\Delta t\boldsymbol{L}_\beta\bar{\boldsymbol{X}}_{\text{cont}}^{n+\theta_2} = \boldsymbol{M}_\alpha\frac{\bar{\boldsymbol{X}}_{\text{cont}}^{n}}{\Delta t} + \boldsymbol{F}_{\text{cont}},$$

$$\boldsymbol{M}_0\frac{\bar{\boldsymbol{U}}_0^{n+1}}{\Delta t} = \boldsymbol{M}_0\frac{\tilde{\boldsymbol{U}}_0^{n+1}}{\Delta t} - \boldsymbol{G}_0\bar{\boldsymbol{p}}^{n+\theta_2} + \boldsymbol{F}_2,$$

$$\boldsymbol{M}_{s,0}\frac{\bar{\boldsymbol{X}}_{\text{heat}}^{n+1}}{\Delta t} + \boldsymbol{K}_{\text{heat}}\bar{\boldsymbol{X}}_{\text{heat}}^{n+\theta_4} = \boldsymbol{M}_{s,0}\frac{\bar{\boldsymbol{X}}_{\text{heat}}^{n}}{\Delta t} + \boldsymbol{F}_{\text{heat}},$$

Table 3.2: Complete set of discretized CBS equations.

A.4. Assign new variables to old ones and go back to step 1.

- SIM Form This form is more expensive, but stationary states can be reached faster. However, in the case of incompressible flow, it is not possible to use the fully explicit form. For each time step, two strategies can be described:

Scheme B:
Set of variables: pUT or *ρUT*
B.1. Calculate time increment Δt.
B.2. Calculate fractional momentum $\tilde{\boldsymbol{U}}^{n+1}$, with or without implicit terms.
B.3. Calculate new temperature T^{n+1}.
B.4. Solve for p^{n+1} (*or* ρ^{n+1}) using T^{n+1},
B.5. Calculate $\boldsymbol{U}^{n+1}$.
B.6. Assign new variables to old ones and go back to step 1.

Scheme C:
Set of variables: pUE or *ρUE*
C.1. Calculate time increment Δt.
C.2. Calculate fractional momentum $\tilde{\boldsymbol{U}}^{n+1}$, with or without implicit terms.
C.3. Set counter $i = 0$ and assign $T^{n+1,0} := T^n$.
C.4. Solve for $p^{n+1,i}$ (*or* $\rho^{n+1,i}$),
C.5. Calculate $\boldsymbol{U}^{n+1,i}$, $E^{n+1,i}$ and $T^{n+1,i}$.
C.6. Increment counter i and go back to step 4 until a certain convergence criterion is accomplished.
C.7. Assign new variables to old ones and go back to step 1.

Scheme A is simplified in the case of barotropic flow, where as we have seen in the precedent section, the constant entropy condition allows us not to solve the energy transport equation and calculate the temperature directly from the density and pressure obtained. Obviously, this scheme is forbidden to solve incompressible flow problems.

SIM Schemes B and C are more general although more complex. In incompressible or barotropic flow, the two schemes are basically the same. In the first case, the thermal problem is decoupled and a temperature equation is solved at the end of the time step. On the other hand, the trivial constant entropy equation allows not to solve any transport equation for the energy or the heat. Out of both the SIM Schemes, Scheme B is more direct: T is updated explicitly *before* p (or ρ). In scheme C, there is a price to pay for using a full set of conservative variables: to update p (or ρ), T must be guessed. To get the right answer, an iterative loop can be programmed. Its first guess is simply the old T^n, the following ones come from the variables on which depend the temperature (through the state law, for example) at the actual iteration. This is done,

until some convergence condition is reached. This inner iterative cycle can slow down seriously the performance of the code, but it was observed that in studying stationary states, no inner iterations are needed, specially when reaching the stationary regime. For transient problems, as the other explicit equations rule the time step, T^{n+1} cannot vary that much from T^n. Therefore, a limited number of iterations is needed in any case.

Time step: Based on stability criteria, the time increment can be calculated for Convection-diffusion-reaction (CDR) equations [Hindmarsh et al., 1984, Codina, 1993a]. Then, to be used here, Navier-Stokes terms must be identified with the analogue terms in a CDR equation. In this case, for the whole set of equations we use the same time increment. This is evaluated for each node using the following:

$$\Delta t = \frac{F^{\mathrm{TI}}}{\left(\frac{1}{\Delta t_{\mathrm{c}}} + \frac{1}{\Delta t_{\mathrm{u}}}\right)} \tag{3.78}$$

where Δt_{c} is the "crosswind" time increment, calculated using the diffusive limit for the 1-D CDR equation and Δt_{u} is the "upwind" one, calculated using the general form of for the 1-D CDR equation, which depends on a ratio between diffusion and convection (through Péclet or Reynolds number). F^{TI} is a factor that for explicit advance can be considered as a safety factor, always lower than 1.0. For implicit treatment this factor can be larger than 1.0. In the numerical diffusion which comes from Characteristic - Galerkin method the Δt which appears divided by two is evaluated using $F^{\mathrm{TI}} = 1.0$ in all cases.

We have seen that if time-discretization is done according to the method here exposed, i.e.

$$V^{n+1} = V^n + \Delta t_{\mathrm{ext}} \left[R - \frac{\Delta t_{\mathrm{int}}}{2} u_i \frac{\partial R}{\partial x_i} \right]^n$$

where V is any variable and R is the residual of the original transport equation, two time increments Δt appear. One, which is named here "ext" for "external", comes from the derivative discretization. The other one, named "int" for "internal", comes from the integration of fluid particles trajectories. We suggest to use the same Δt obtained using (3.78), except for the safety factor: in the internal time step F^{TI} is fixed to 1.0, while in the external one it varies from 0.0 to 1.0 [Codina, 1998b].

Fractional momentum: It is advanced in two steps. First, boundary integrals are evaluated. This is done by means of a loop over all the elements for which, at least, one of the edges belongs to a certain boundary. Then, its contribution is assembled to the complete RHS of fractional momentum equation. The second step is to calculate the rest of the residual and to advance fractional momentum itself. This second step is done evaluating the remaining RHS at time n according to the matrix form of the fractional momentum equation in table 3.2, and / or evaluating the left hand side matrix contribution of the implicit terms. In this case, the iterative method chosen is the GMRES for the non - symetrical type of the problem matrix when convective terms are included.

Transient and stationary problems: A good approximation here is to use $\boldsymbol{M}_L^{-1}$ in place of $\boldsymbol{M}^{-1}$. Matrix $\boldsymbol{M}_L$ is a diagonalized mass matrix, the *lumped mass matrix*. It is obtained by nodal integration, i.e. through closed numerical integration. This procedure is used every time an explicit time advance is needed, unless when studying transient problems. In this case, the consistent mass matrix is required, and the time advance is done iteratively, for instance using a Jacobi method. In that case, if the equation to solve is $\boldsymbol{M}\boldsymbol{U}^{n+1} + \boldsymbol{b} = 0$ then

$$\boldsymbol{\Delta U}_{i+1}^{n+1} = \boldsymbol{M}_L^{-1}\left(\boldsymbol{M}\boldsymbol{U}_i^{n+1} + \boldsymbol{b}\right) \tag{3.79}$$

where $\boldsymbol{\Delta U}_{i+1}^{n+1} = \boldsymbol{U}_{i+1}^{n+1} - \boldsymbol{U}_i^{n+1}$ and $\boldsymbol{U}_o^{n+1} = \boldsymbol{U}^n$.

The solver problem: SIM Form (schemes 2 and 3) involves the solution of a problem:

$$\boldsymbol{K}_{SIM}\boldsymbol{x} = \boldsymbol{f} \tag{3.80}$$

for the continuity equation, where $\boldsymbol{K}_{SIM}$ can be a quite big matrix. This could be a great disadvantage if there exists any kind of stability restriction in the time increment. In our algorithm, this restriction comes from the terms (convective, diffusive, reactive) left explicit in fractional momentum and energy equations. However, matrix $\boldsymbol{K}_{SIM}$ of the method here proposed is "polite" in the sense that it can be decomposed as:

$$\boldsymbol{K}_{SIM} = \boldsymbol{M}_{\text{type}} + \boldsymbol{L}_{\text{type}} \tag{3.81}$$

where $\boldsymbol{M}_{\text{type}}$ means any mass matrix type (product of shape functions) and $\boldsymbol{L}_{\text{type}}$ means any Laplacian matrix type (product of gradients of shape functions): both symmetric and positive definite matrixes. Therefore, any iterative method (e.g. preconditioned conjugate gradients) can be used.

"Total" vs. "Incremental" fractional step: In the original incompressible formulation and in many following papers, the fractional momentum evolution equation is calculated without any pressure contribution, and thus, the momentum correction step is done by adding the new pressure gradient. However, some researchers have proposed to do it in an incremental way, that is,

$$\frac{1}{\Delta t}M(\tilde{U}^{n+1}-U^n)+K\tilde{U}^{n+1}+\gamma GP^n=F$$

$$\frac{1}{\Delta t}M(U^{n+1}-\tilde{U}^{n+1})+GP^{n+1}-\gamma GP^n=0$$

$$DU^{n+1}=0$$

(see for instance [Guermond and Quartapelle, 1995, Guermond, 1994]. By placing $\gamma = 0.0$ it is recovered the "total" approach. And $\gamma = 1.0$ produces the "incremental" approach. Here, $K\tilde{U}^{n+1}$ comprises convective and diffusive terms. Clearly, the incremental approach, is $O(\Delta t^2)$, instead of the $O(\Delta t)$ of the total one, because in this way the term GP^n in the right hand side of the fractional momentum equation corrects the first order fractional step error produced by evaluating $K\tilde{U}^{n+1}$ using the *compressible* fractional momentum, i.e. prior to the projection step is done. However, the incremental approach has the disadvantage that when the steady state is reached, $GP^{n+1}-\gamma GP^n = 0$ and the fractional step stabilization fades out and hence additional stabilizing terms should be used. In any case, the incremental or total approaches differences disapears when $K\tilde{U}^{n+1}$ is evaluated explicitly, i.e. when θ_3 factor is zero (see 3.1), or when only convective terms are implicitly evaluated and the correction (3.47) is used.

Set of variables: After numerical experiments with some variables combinations, we can conclude that, as this algorithm is described here, the choice of the set of variables depends on the physics of the problem considered. For fully incompressible problems, out of the options here studied, pUT set is the only one that can be used. On the other hand, for compressible problems, the perspective is wider. The most flexible one is ρUE , having shown its effectiveness in this regime, with or without viscosity and for low, transonic or high M numbers. If shocks are present, they are placed properly

and verifying jump conditions. Non conservative sets, like pUT or ρUT does not work well in supersonic regimes, but fairly good in transonic or subsonic ones. Whereas when solving with sets including pressure as the unknown of the continuity equation the shocks produce instabilities which spoils the steady state result, the ρUT set gives rather nice solutions except for the fact that shocks aren't properly placed. In the case of subsonic problems, non conservative sets behave correctly, both accurate and converging fast to stateady states. In the barotropic case, the use of $s(\boldsymbol{x}, t) = s_o$, being s the entropy and s_o a constant, as a third equation to complement those for ρ and U_i also is a very good choice due to its computational simplicity.

Numerical parameters: Numerical strategies are controlled through few parameters: the θ's set, constant C of the shock capturing and time step factor F^{TI}. In the first case, the set corresponds to each time trapezoidal rule is applied. Except from θ_1, which distributes new fractional momentum and old momentum in continuity equation, a value different than zero leads to implicit solutions. We have experimented different θ combinations, restricted to three possibilities: 0, 1/2 or 1, for being the most representative values. θ_1 is either 1/2 or 1. If it is 1/2, more accuracy is achieved, and 1 corresponds to more numerical diffusion. The rest of the set is either 0, placing all the term on the RHS, or 1, on the LHS.

Shock capturing constant C is always 0.7 (linear) or 0.35 (quadratic). Although this value was obtained for a simplified problem, it seems that when more complex Navier - Stokes equations are solved this value still holds as correct. Finally, factor F^{TI} varies whether explicit or implicit forms of the scheme are used. As said before, in the former case it is a safety factor. Being studied many different problems with this algorithm, some of them presented in this work and some not, we can conclude that in this case it goes from 0.9 in incompressible cases to 0.3 in compressible ones. On the other hand, when viscous or convective terms are solved implicitly, its value depends on the problem. We could reach values of 500 still obtaining proper solutions.

3.5 Summary

The FEM general algorithm called Characteristic Based Split (CBS) is described. On one hand, time discretization is done along the characteristics, which allows the stabilization of convective instabilities inherent to Galerkin method. Its effect is to add terms of the form of convective derivative of the residual multiplied by the half the time increment and the outcome is similar to other convective stabilization techniques. On the other hand, pressure stabilization is attained through time splitting of the linear momentum equation, also allowing the use of equal interpolation spaces for all the variables. This technique comes from incompressible flow and in this work the concept

is extended to compressible problems, the same scheme being used for particular incompressible or compressible cases and also in mixed problems, presenting regions of the two kinds. All of this is done by changing a few parameters which controls the algorithm. Different sets of unknowns, solution of transient and stationary problems, implicit solution of some terms or spatial higher order elements can be tested.

Chapter 4

Laminar Flow: Numerical Examples

In this section we present some numerical examples which validate the general algorithm. The examples cover a wide variety of regimes, all of them laminar. Taken from other researchers' previous work, they are academic and in most of them, we used even the same spatial grids. Since no refinement issues are studied in this monograph, grids are generally not flow adapted. On the other hand, we focus our interest in testing different order elements. The numerical results presented here can be divided in two main groups: incompressible and compressible flow. For each group, Euler and Navier - Stokes equations are solved.

4.1 Incompressible Inviscid Flow

Incompressible flow problems include: an inviscid NACA 0012 tilted profile, a driven cavity flow at $Re = 1000$ and $Re = 5000$, a backwards facing step at $Re = 200$. All these examples are stationary. Finally, an oscillatory solution of a flow passing a cylinder at $Re = 100$ is studied. The continuity equation is solved implicitly and fractional momentum explicitly, except for the cavity flow and the NACA 0012 tilted profile, where tests upon the implicit fractional momentum solver is done.

4.1.1 Flow passing a tilted NACA 0012 profile

In this example (fig. 4.1) inviscid flow passing a NACA 0012 airfoil, placed at an attack angle of 5° is modeled. It is well known (see, for instance, [Hirsch, 1990]) that although no condition is imposed in the circulation around the airfoil (the so called

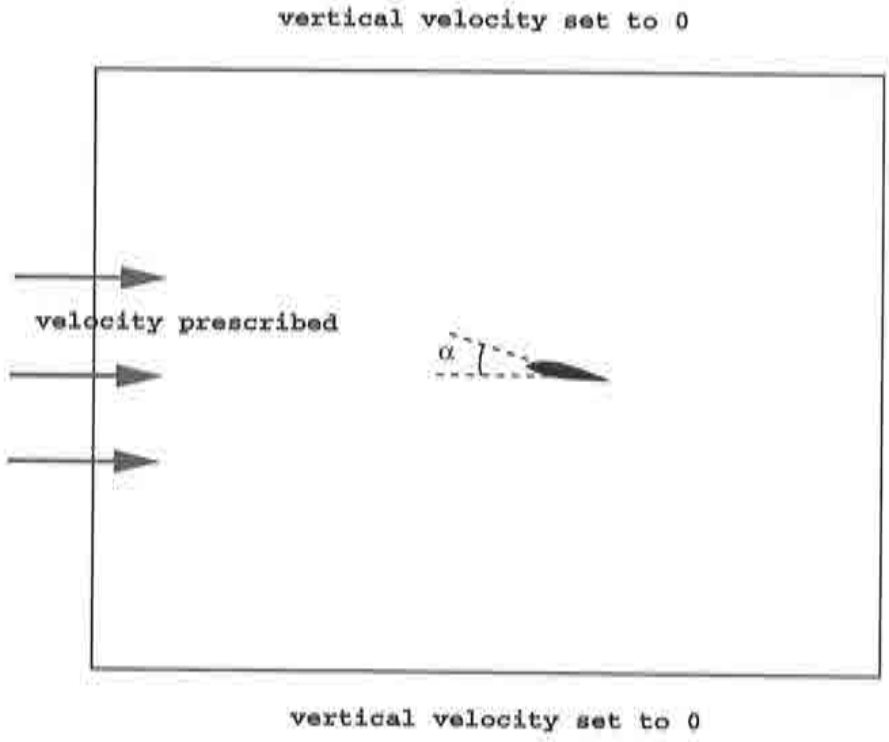

Figure 4.1: NACA 0012 profile.

Kutta condition) the final stationary solution reached is that corresponding to the viscous problem, namely with the downstream stagnation point at the very trailing edge. This fact seems to violate Kelvin's theorem, because if the initial condition is circulation free then if no diffusion is present, the final stationary state must be also circulation free. However, this is not the case, and a circulation which is different from zero appears around the airfoil. The mechanism that triggers this process is the artificial diffusion added by the numerical method, which in turn is supposed to be small. Therefore, the convergence rate to the final state could be very poor unless the equations are treated implicitly. For that reason, this is a good problem for testing the behaviour and possible advantages of the implicit form of the scheme. As no energy equation must be solved, time factors F^{TI} (see (3.78)) much larger than 1.0 can be used improving the convergence to the steady state.

The 2-D domain is discretized using a mesh made of 15075 P1 elements (7838 nodal points) slightly refined from the exterior, far from the wing, to the profile itself (fig. 4.2). The velocity is fixed to 1.0 at the inflow and the pressure to 0.0 at the outflow. Normal component of the velocity is prescribed to 0.0 at the airfoil and at the upper

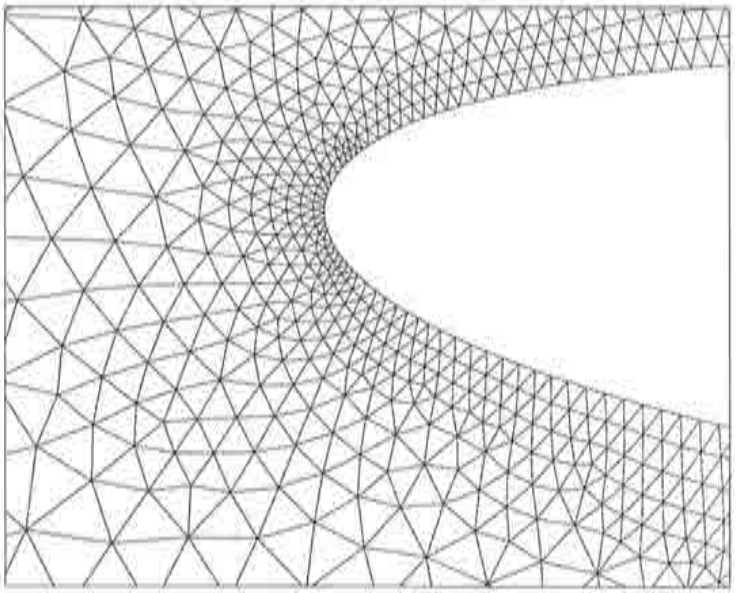

Figure 4.2: NACA 0012 profile. Detail of the mesh around stagnation point.

and lower boundaries.

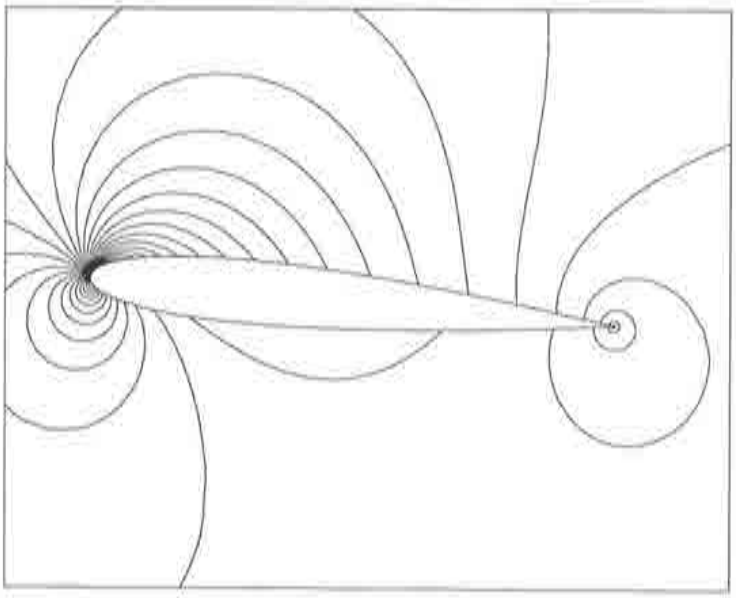

Figure 4.3: NACA 0012 profile. Pressure contours around airfoil.

Parameters θ_2 and θ_3 are in this case 1.0 (both fractional momentum and pressure equations are solved implicitly). If this is done, the time factor F^{TI} can be increased. In this particular case, using a time factor 100 times larger than when $\theta_2 = 1.0$ and $\theta_3 = 0.0$, stills produces the right solution. Although an additional linear system of equations needs to be solved per time step, the time step size may be taken much larger, making the total CPU time needed much smaller, in this problem, it is 4 times larger. This fact strongly favours the use of an implicit method for solving this equation in most of the types of flow. The stationary state reached is shown in fig. 4.3.

As time increments are here so large, our suggestion for correcting the splitting

error (see (3.47) and (3.48)) is also tested: fig. 4.4 shows the difference in pressure level contours around the stagnation point either if it is taken into account or not. The analytical value for the pressure at the stagnation point is 0.5. If the correction is done, the value is 0.515. If not, the pressure value reached there is 0.309 being much more diffusive due to the splitting error. This becomes more apparent when larger F^{TI} are used, due to the fact that this error is $O(\Delta t)$.

4.2 Incompressible Viscous Flow

Three examples of incompressible viscous flow are studied. Two of them show the behaviour of the algorithm at stationary states: the flow in a *driven cavity*, then the flow passing a *backward facing step* and the third, a periodic stationary state, formed when the *flow passes a cylinder* and a wake of vortices develops.

4.2.1 Driven cavity flow at $Re = 1000$ and 5000

This is a classical test problem to evaluate the behaviour of any algorithm which numerically solves incompressible flows. A viscous fluid is confined in a square cavity while one of its edges slides tangentially. The boundary conditions for the velocity and pressure are shown in fig. 4.5.

Initially, except at the moving wall, the velocity is set to zero everywhere, including the nodes at the left and right top corners (this boundary condition is called *non leaking* or *ramp condition*). By means of viscosity, the momentum is transferred inwards. A central vortex and two much smaller ones at the bottom corners develop when the stationary state is reached.

The numerical results are shown here for Reynolds' numbers of 1000 and 5000. In both cases, the mesh used was the same. This is shown in fig. 4.6. It is a structured mesh made of 2888 P1 elements, refined from the center to the edges. There are 1521 nodal points.

Streamlines and pressure contours are shown in fig. 4.7 and fig. 4.8.

Pressure contours are a little "wrinkled" at the top left corner, particularly when $Re = 5000$. This is so because of the singularities present at this point, due to velocity discontinuities. But this effect is bounded to that small regions and the numerical oscilations appearing in the pressure are very low.

The solutions presented were obtained using the pUT set of variables. Density and temperature are kept constant in the whole domain, and for that reason, pressure and velocity are the unknowns. Constants θ_1 and θ_2 appearing in continuity and

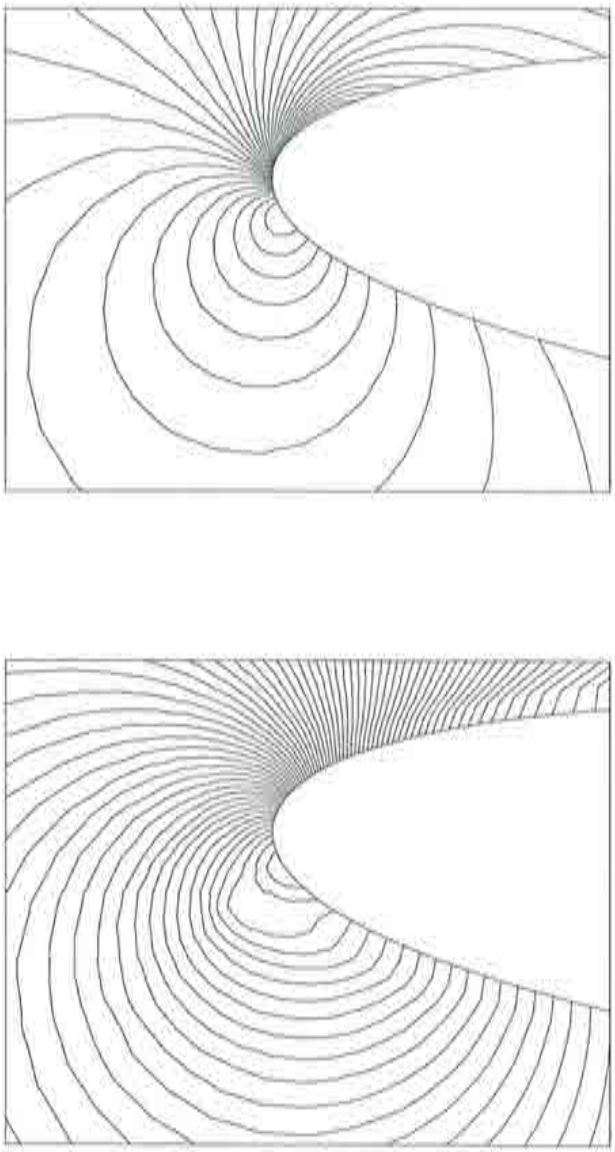

Figure 4.4: NACA 0012 profile. Pressure contours around stagnation point. Top: Splitting error of stationary state produces an overdiffusive result. Bottom: Splitting error of stationary state corrected.

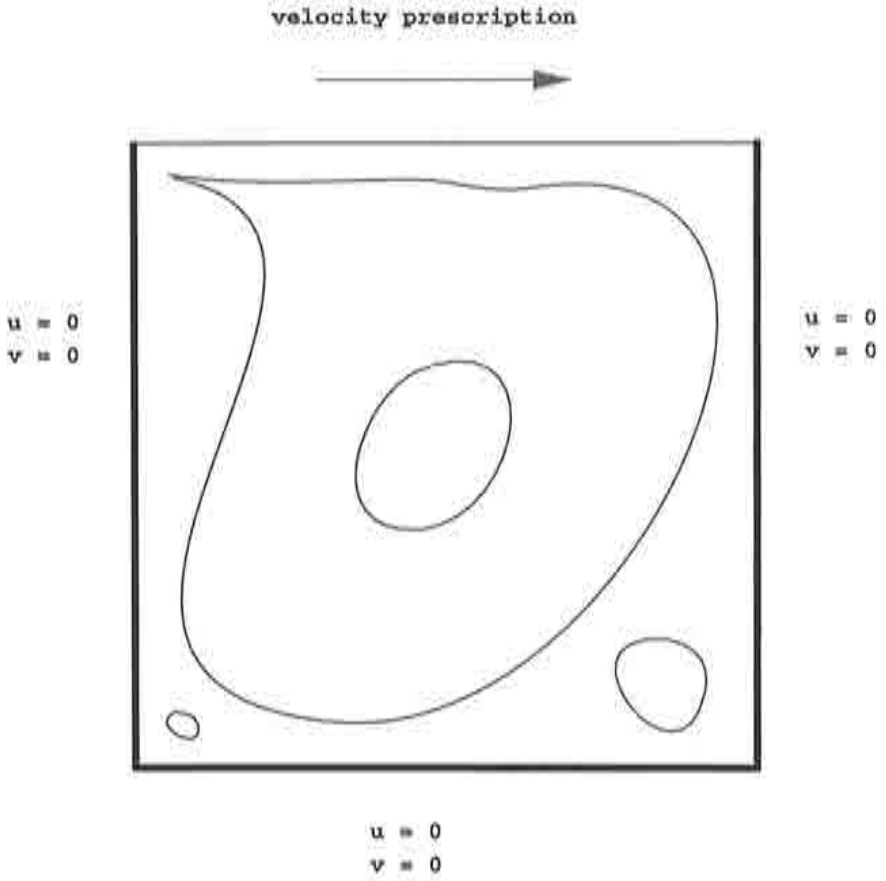

Figure 4.5: Driven cavity flow. Sketch of the problem and boundary conditions.

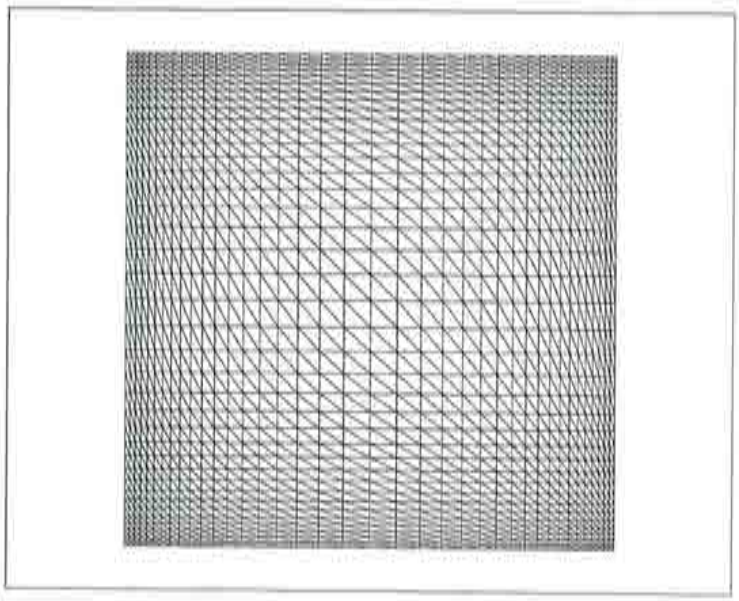

Figure 4.6: Driven cavity flow. P1 mesh.

momentum equations are 0.5 and 1.0 respectively. Pressure is solved implicitly. To speed up convergence, we tested here the implicit solution of fractional step terms like in the previous example, now adding the diffusive contribution. The time factors can rise up to 5.0 without noticing overdiffusive solutions.

These results can be compared with those obtained by Ghia *et al.* (as given in [Ghia et al., 1982]) showing the velocity x-component along a vertical central cut (see fig. 4.9). The comparison is satisfactory.

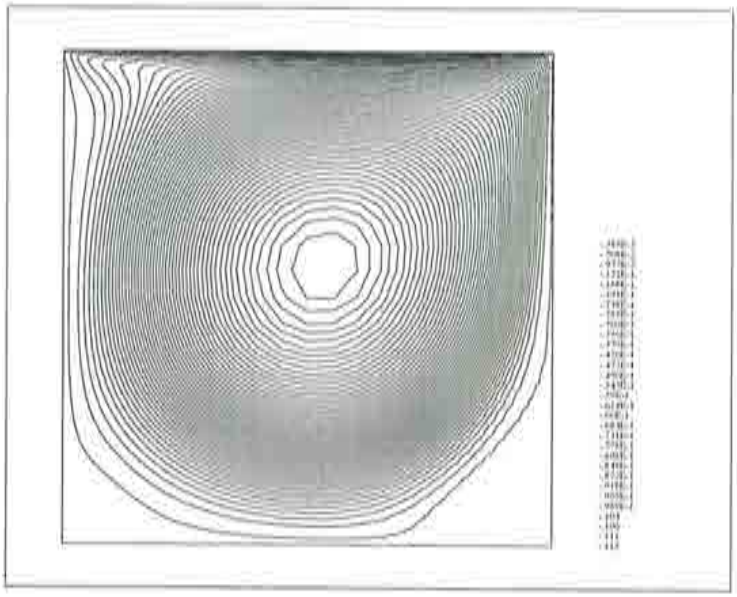

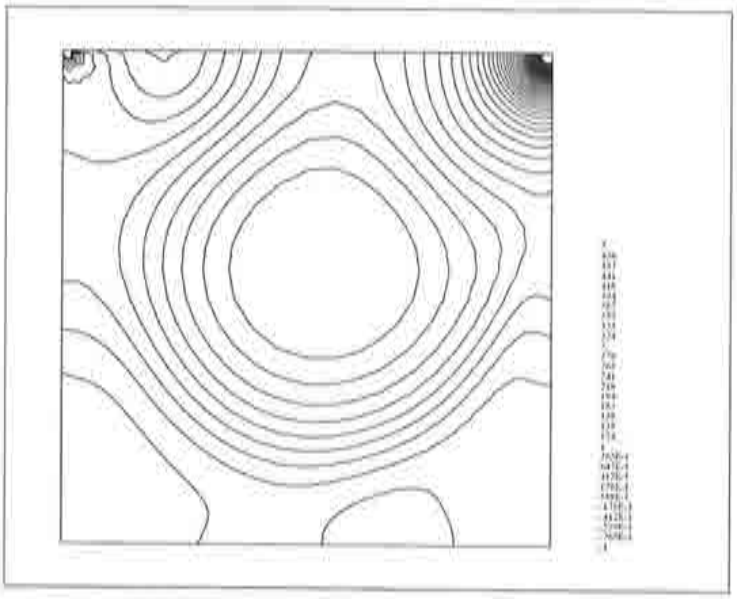

Figure 4.7: Driven cavity flow. Streamlines and pressure contours, Re=1000.

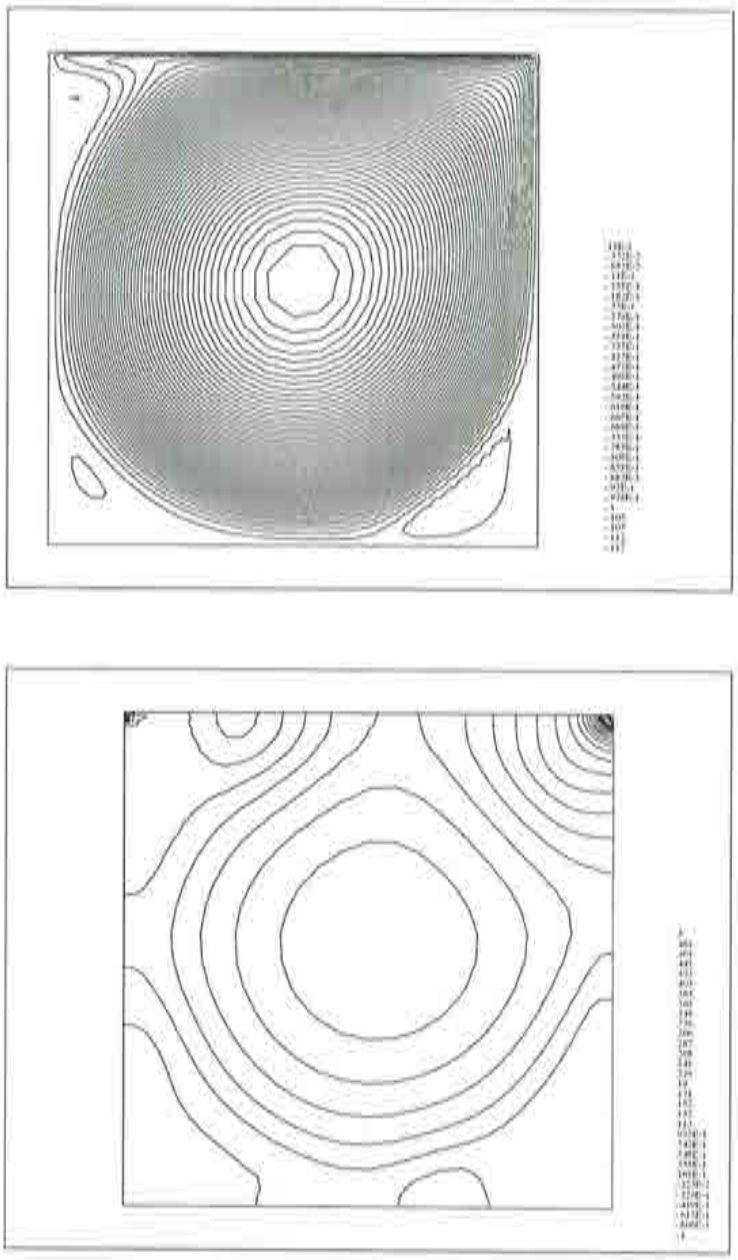

Figure 4.8: Driven cavity flow. Streamlines and pressure contours, Re=5000.

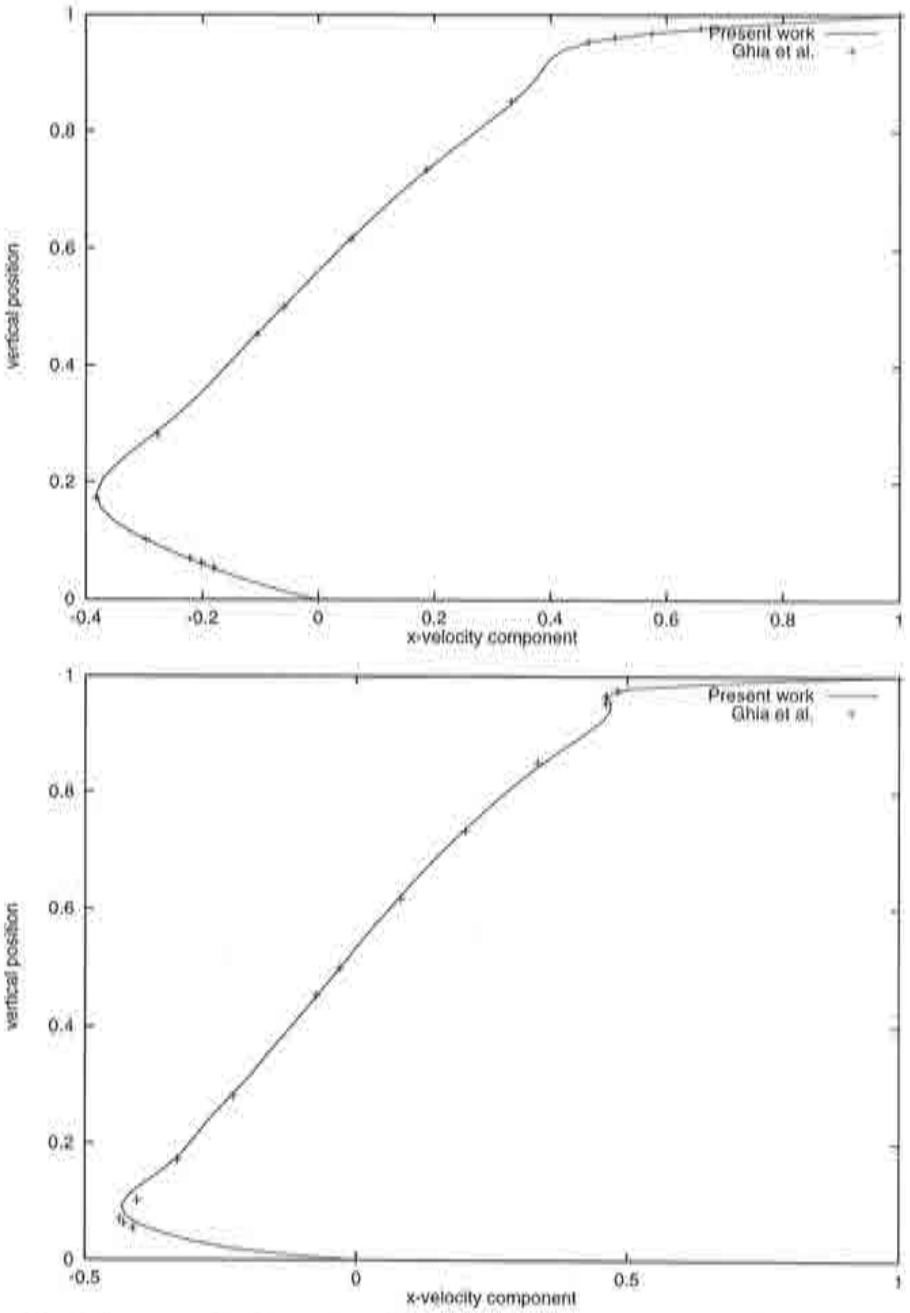

Figure 4.9: Driven cavity flow. Horizontal velocity component, Re=1000 (top) and Re=5000 (bottom).

4.2.2 Backwards facing step at $Re = 200$

In this case, the flow is constrained to move within a 2-D domain, which contains a backwards step. Right after the step, a vortex is produced. The general arrangement is seen in fig. 4.10 (not at scale). The step is one half the width of the inflow.

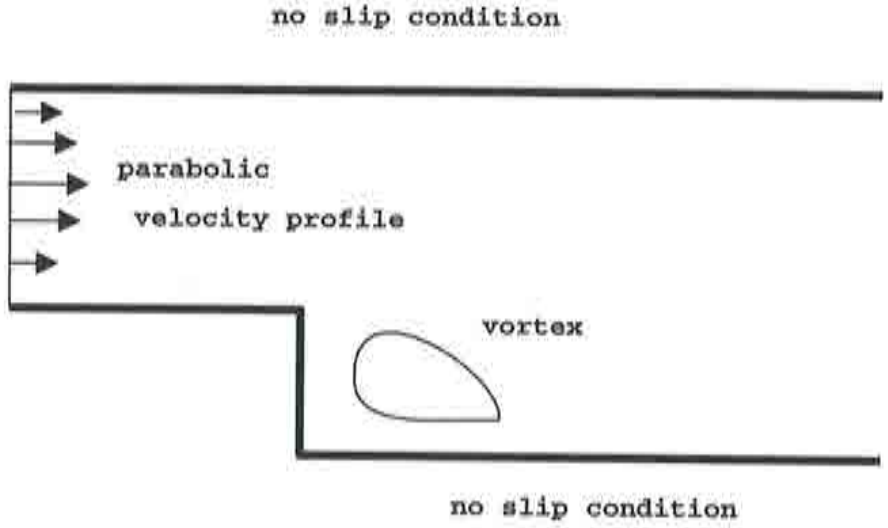

Figure 4.10: Backwards facing step.

At the inflow, a parabolic velocity profile is prescribed, while at the outflow, the pressure is prescribed to $n_i \tau_{ij} n_j$, being the velocity free there. No additional prescription is done on the pressure. Finally, the no-slip condition is used at the walls, i.e. the velocity is there set to zero. No volume forces are present.

The problem here corresponds to $Re = 200$. It was solved on a mesh made of 1632 Q1 elements and 1721 nodal points, slightly refined at the walls. The region near the step is shown in fig. 4.11. The computational domain is indeed larger, its full length is 22 times the width of the inflow.

Once the stationary state is reached, the solution shows the features seen in fig. 4.12 and fig. 4.13

Again, as in the driven cavity, we have used the pUT set of variables, and temperature and density were kept constant within the whole domain.

As it was stated on the comment on boundary conditions for the fractional momentum at section 4.1.1, the boundary integral on the weak form of the equation for the fractional momentum can be split in two, depending on the kind of contour where it is

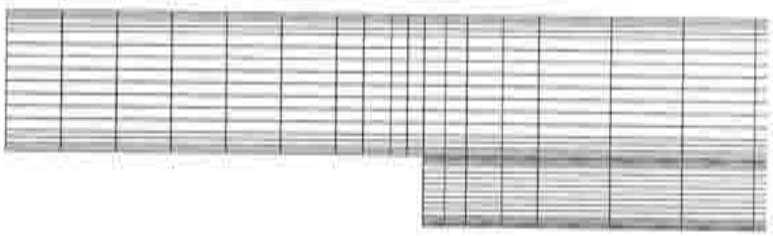

Figure 4.11: Backwards facing step. Q1 mesh (detail).

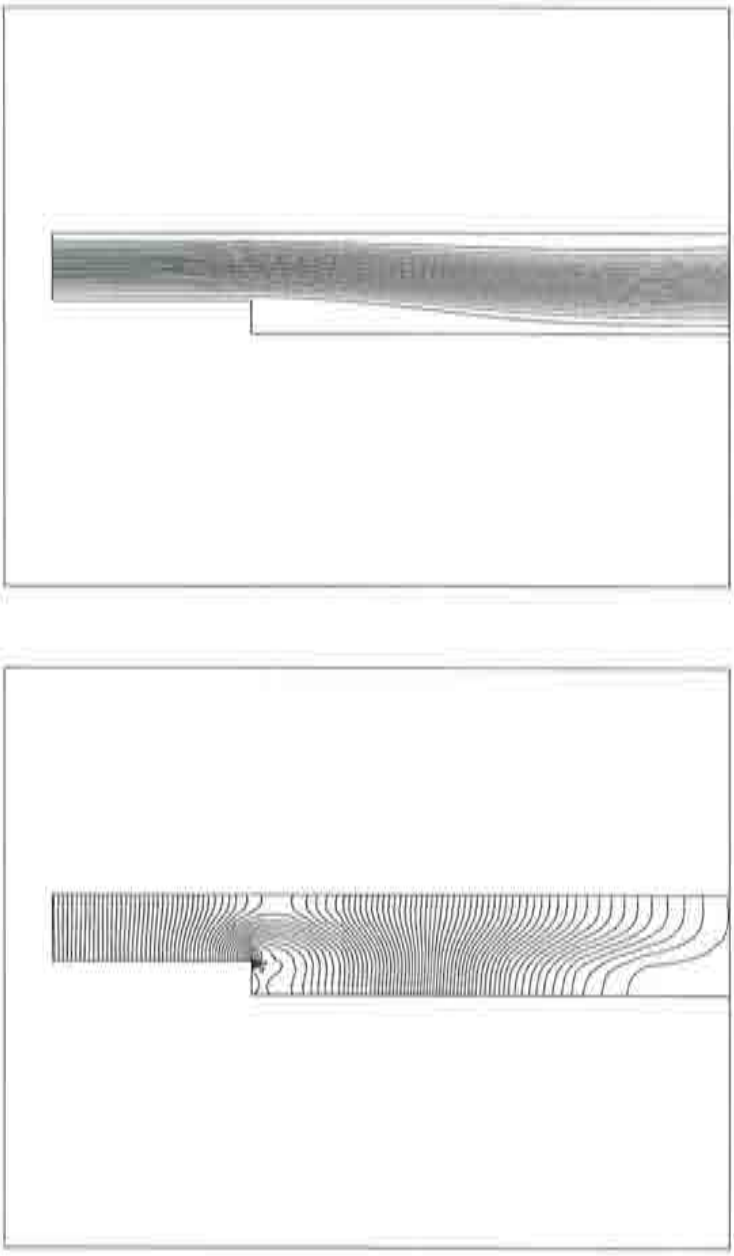

Figure 4.12: Backwards facing step. Streamlines and pressure contours, Re=200.

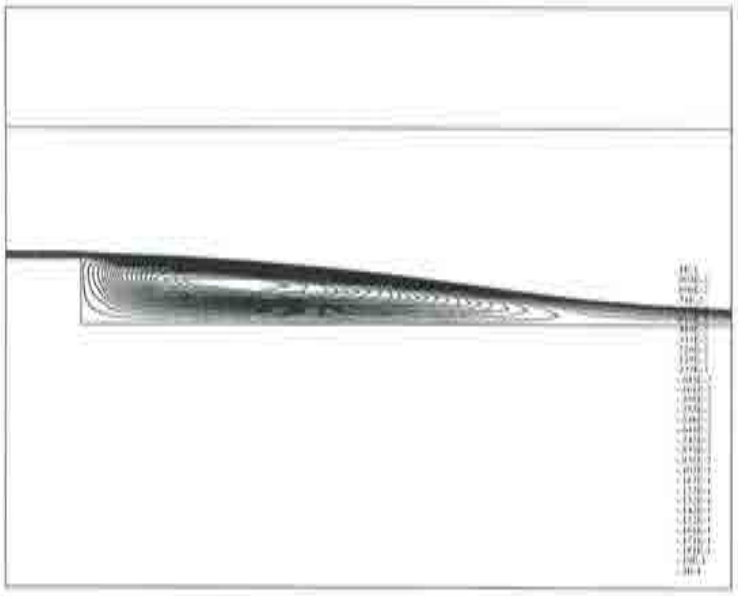

Figure 4.13: Backwards facing step. Streamlines for Re=200, detail behind the step.

evaluated. The effect is that the whole traction on a given contour can be prescribed, for instance at the outflows. There, normal and tangential traction set to zero means a "physical" contour, not just "numerical" and the flow opens like if it were getting out of a real tube, see fig. 4.14.

The numerical parameters θ_1 and θ_2 are 1.0 and 1.0 respectively.

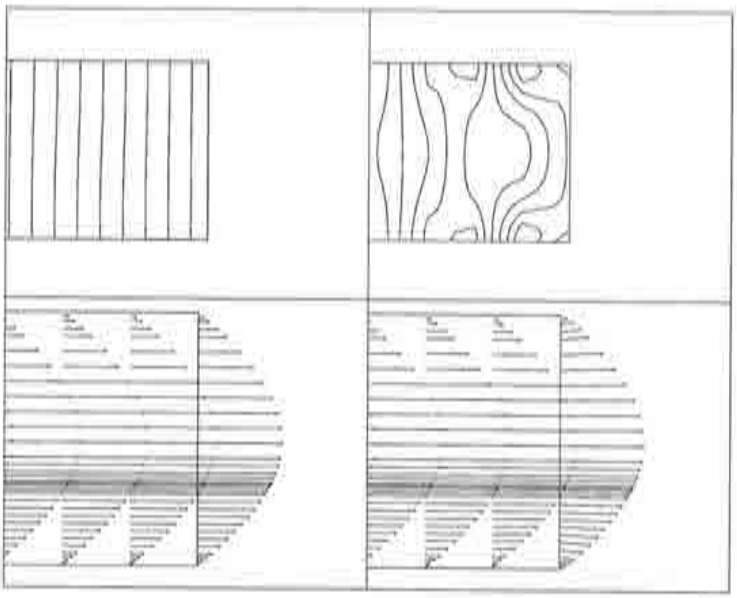

Figure 4.14: Backwards facing step. Pressure contours and velocity vectors at the outflow, left, no condition on tangential traction; right, traction zero imposed.

4.2.3 Flow passing a cylinder at $Re = 100$

This example is at Re=100. Both domain and boundary conditions are shown in fig. 4.15 and the mesh in fig. 4.16. It is made of 2000 Q1 elements (2100 nodal points). At this regime, the stationary state is oscillatory: a trail of vortices is left behind the cylinder. The cylinder's diameter D is 1.0 and the horizontal inflow velocity is $u_\infty = (1, 0)$.

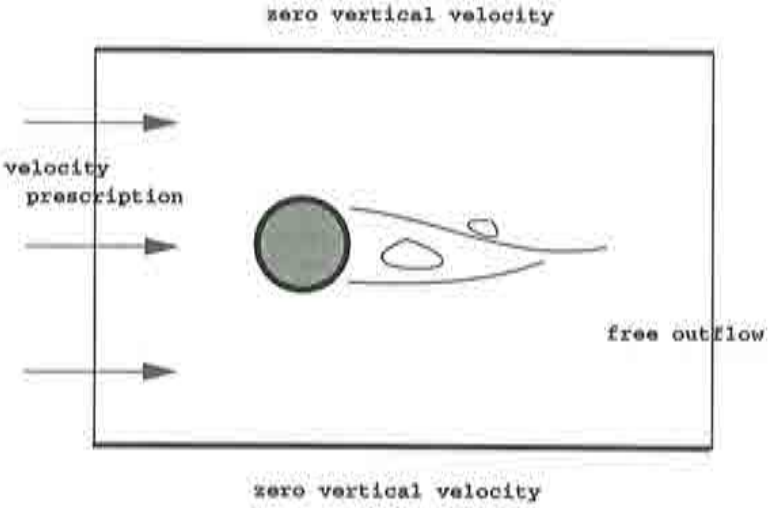

Figure 4.15: Flow passing a cylinder.

The SIM form of the algorithm is used, with $\theta_1 = 1.0$ and $\theta_2 = 1.0$. As in the preceding example, pressure is fixed to $n_j \tau_{ij} n_i$ on the outflow. In this case, normal traction cannot be considered zero; for that reason pressure can be slightly incorrect at the outflow. Temperature is fixed all over the domain, and no volume forces are present. The onset of the oscillatory behaviour was produced by a small initial perturbation on the velocity. Fully developed flow is shown in fig. 4.17.

The period T obtained is around 5.7 time units, leading to a *Strouhal number* $St = Du_\infty$ of 0.175, which is about 4% above the experimenatal value obtained in [Roshko, 1954], and very close to that obtained in [Simo and Armero, 1994]. The period can be evaluated in many ways: through the evolution of a variable at a point behind the cylinder or the net force over it, or through the evolution of the error norm, etc. In the example shown here, one period of time is covered in approximately 270 time steps. A comparison of streamlines and pressure contours separated in time by half a period is shown in fig. 4.18. We run from the perturbed initial condition aforementioned about 20 time cycles to assume the oscillatory final stated reached.

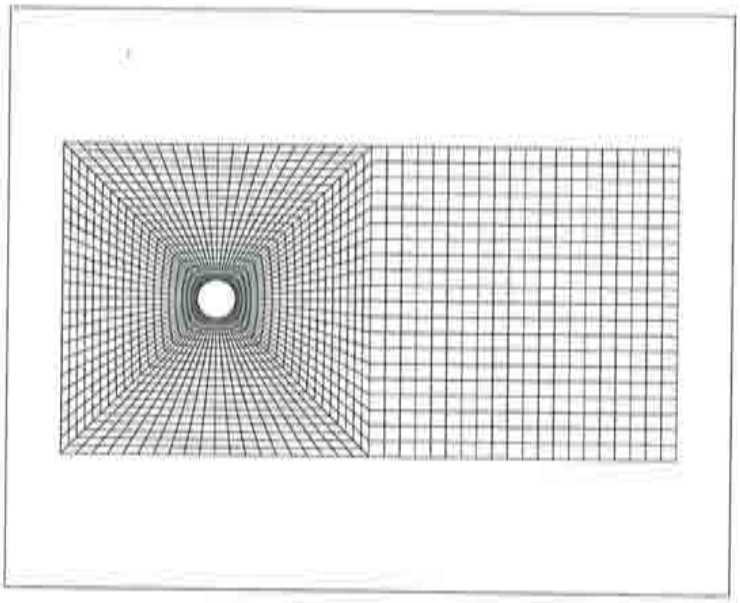

Figure 4.16: Flow passing a cylinder. Q1 mesh.

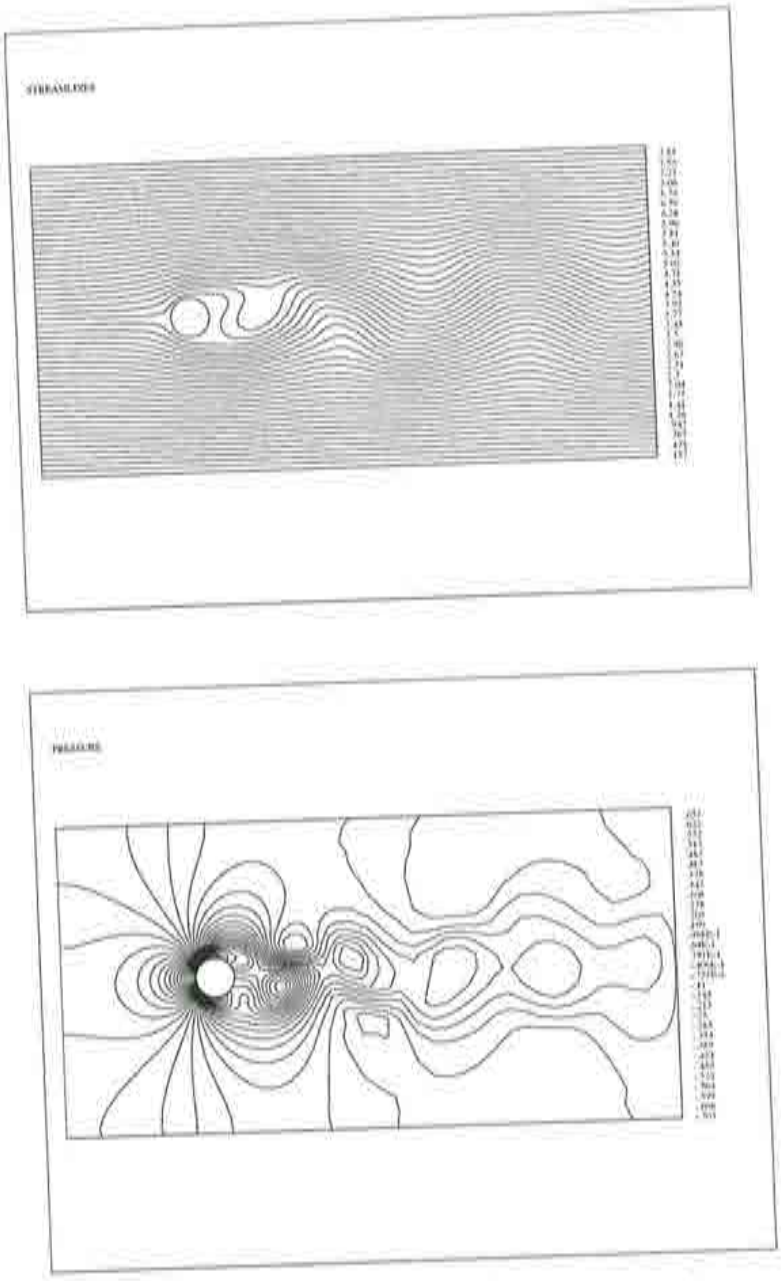

Figure 4.17: Flow passing a cylinder, Re=100. Streamlines and pressure contours.

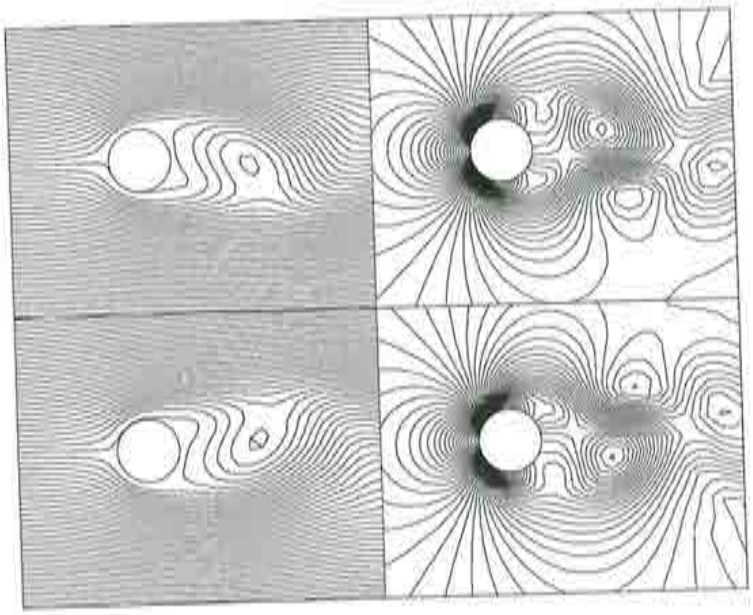

Figure 4.18: Flow passing a cylinder. Top and bottom differs half period. Left, streamlines; right, pressure contours.

4.3 Compressible Inviscid Flow

Next, three inviscid compressible flow problems are shown. One of them is subsonic $M = 0.5$, passing a NACA 0012 profile. The following two are supersonic, at $M = 3.0$: a wedge and a cylinder; in both cases a stationary shock wave is formed upstream.

4.3.1 Subsonic flow passing a NACA 0012 profile at $M = 0.5$

This example illustrates the behavior of the algorithm in the case of inviscid subsonic flow with a barotropic state law. The mesh is a rather coarse unstructured one, made of 2556 nodes arranged in 4902 P1 elements. Partial views are shown in fig. 4.19.

The angle of attack is $\alpha = 0°$. The Mach number at the inflow is $M_\infty = 0.5$. Velocity is prescribed at the inflow to 1.0 in the x direction and to 0.0 in the y direction. Density at the outflow ρ_∞ is fixed to 1.0. Also, the normal component of the velocity is fixed to 0.0 on the profile. The adiabatic exponent γ is 1.4 and the constant A in (3.70) is 2.857136. Pressure isolines are shown in fig. 4.20.

In the example shown here, the continuity equation is solved with the pressure as unknown, which gives a slightly better solution (particularly around the stagnation point) than when the density is chosen. Both schemes however give acceptable results. Although the subsonic character of the problem, an additional shock capturing diffusion is needed, due probably to the strong gradients present in the solution. But being the flow subsonic throughout the whole domain, we let act this artificial diffusion only in the fractional momentum equation using an upwind constant lower than the optimal. According what we saw in previous sections, its optimal value is 0.7, but in this case 0.3 was a better choice. This improves the convergence and smoothes the solution.

A good test for the correctness of the solution is the density at the stagnation point, which can be easily calculated inserting $M_\infty = 0.5$ and $\rho_\infty = 1.0$ in

$$\rho_o = \rho_\infty \left(1 + \frac{\gamma - 1}{2} M_\infty^2\right)^{\frac{1}{\gamma - 1}}$$

giving 1.129726. The value obtained numerically is 1.1320, which differs less than 0.02% from the analytical one.

In this particular case, we have ran the problem solving implicitly the continuity and the fractional convective terms, i.e. parameters θ_2 and θ_3 are set to 1.0. This again allows to use very large F^{TI}, up to 500. To reach the same convergence solution, total CPU time is for the implicit case about 100 times smaller than for the fully explicit scheme.

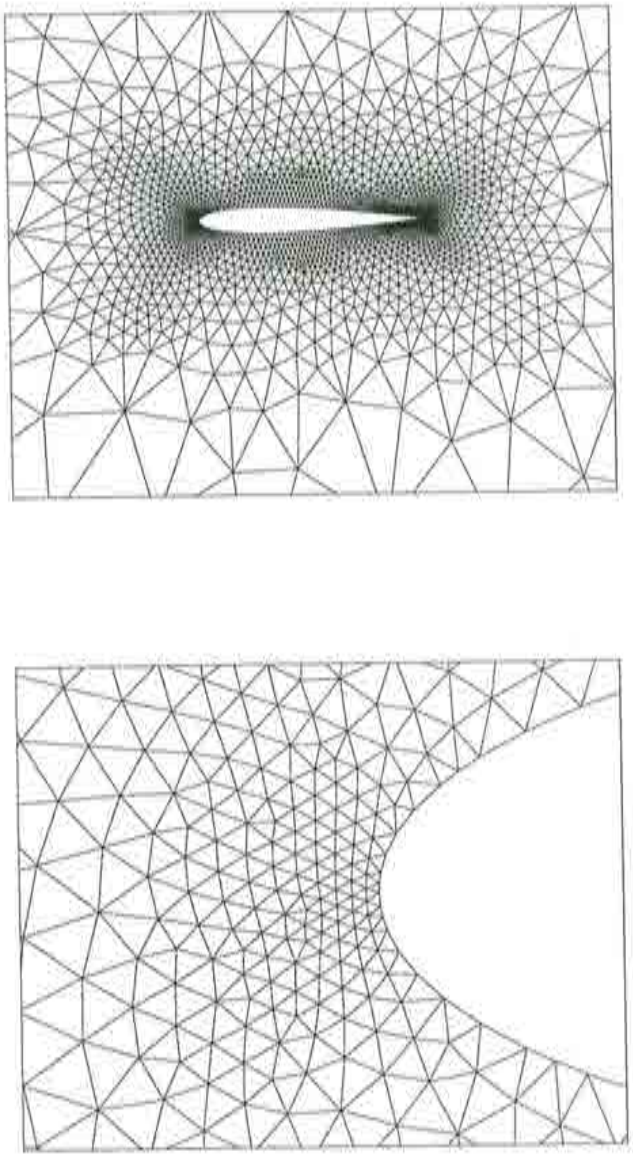

Figure 4.19: Flow over NACA0012 profile. Detail of the mesh. Botton: stagnation point close up.

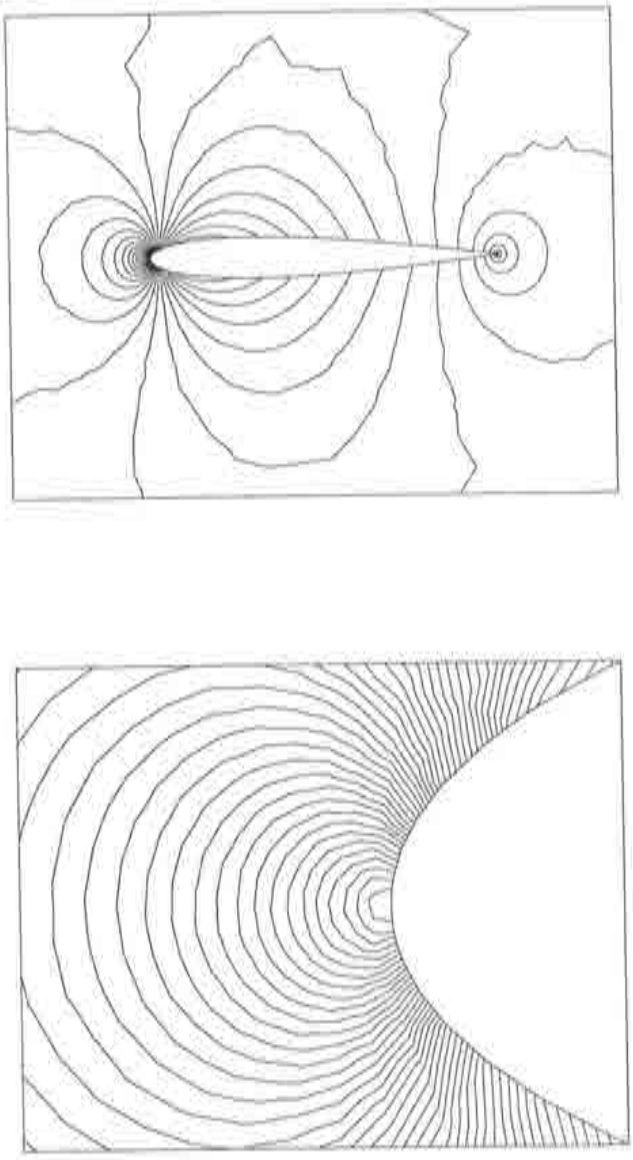

Figure 4.20: Flow over NACA0012 profile. Pressure isolines. Bottom: stagnation point close up.

4.3.2 Supersonic flow passing a wedge at $M = 3.0$

In the next example (fig. 4.21), supersonic flow passes over an oblique ramp, producing a shock . Temperature, density, and velocity are prescribed at the inflow. The outflow is left free. Zero normal velocity is fixed all along the ramp and the preceding floor.

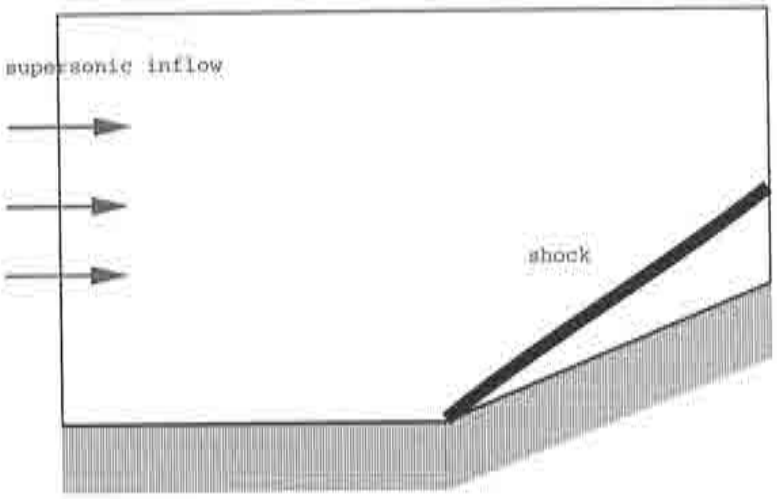

Figure 4.21: Flow passing a wedge.

The spatial domain is discretized by means of 3099 P1 elements (1621 nodal points), which form an unstructured mesh. A second discretization is done, comprising 758 P2 elements (1587 nodal points). The idea is to compare both grids fig. 4.22, containing about the same amount of nodal points.

Level contours, for the case ρUE, are shown in fig. 4.23, fig. 4.25, fig. 4.24 and fig. 4.26. This is a typical example of the behavior of P1 and P2 elements. Along many problems, we have seen that if viscosity is zero, linear triangles give smoother solutions compared to biquadratic ones, which highly concentrate the shock in very few elements. The consecuence is that P1 elements are more robust and for a new algorithm this is very important for fine tunning the constants. Numerical integration is done in both cases using an open rule. In P1 three integration points are used and in P2, six. P1 can be also solved using 1 integration, which sub-integrates but provides numerical diffusion.

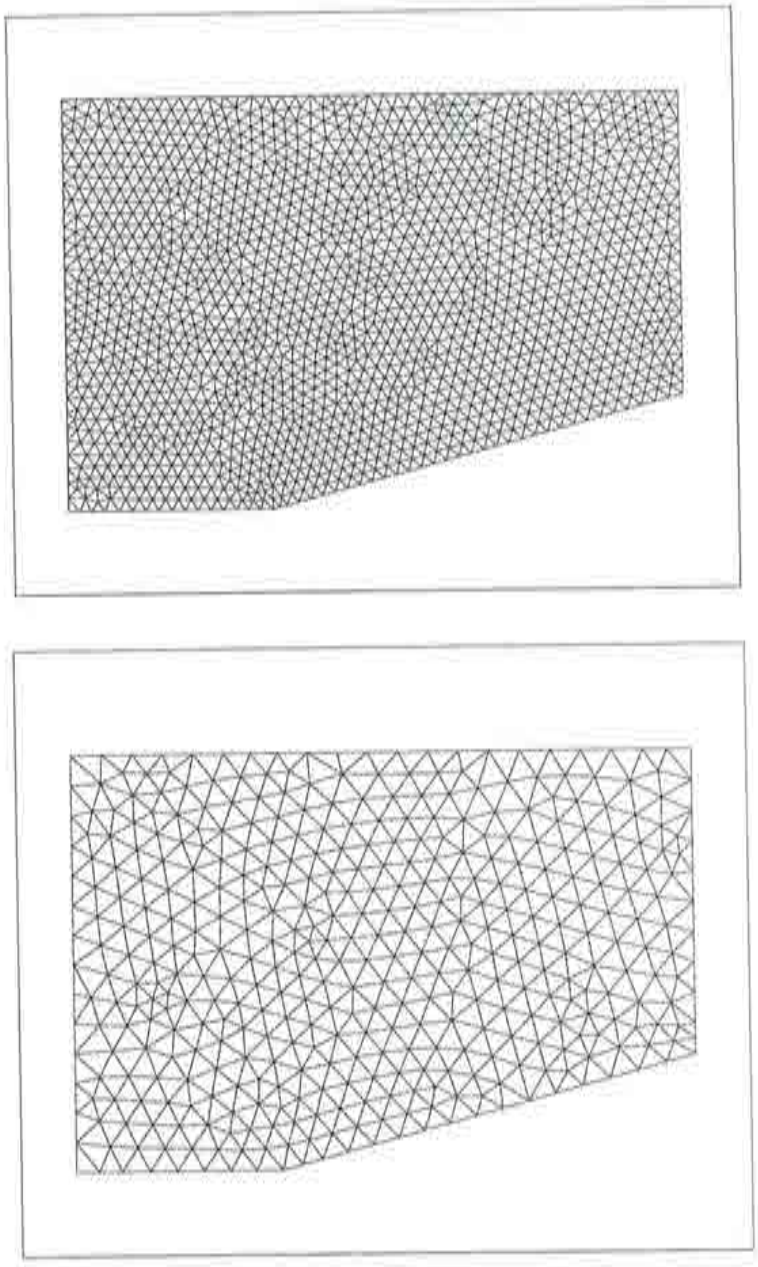

Figure 4.22: Flow passing a wedge. P1 (top) and P2 meshes.

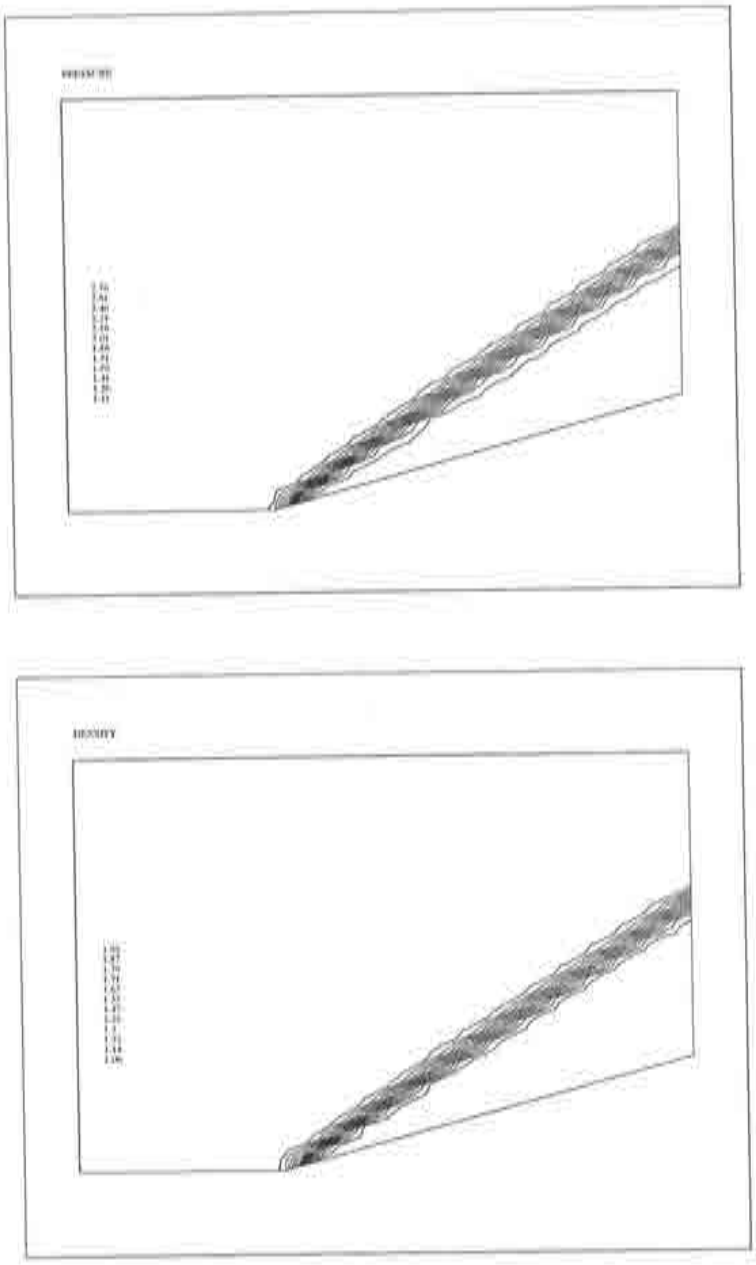

Figure 4.23: Flow passing a wedge, Mach 3. P1 mesh. Density - momentum - energy variables. Pressure and density contours.

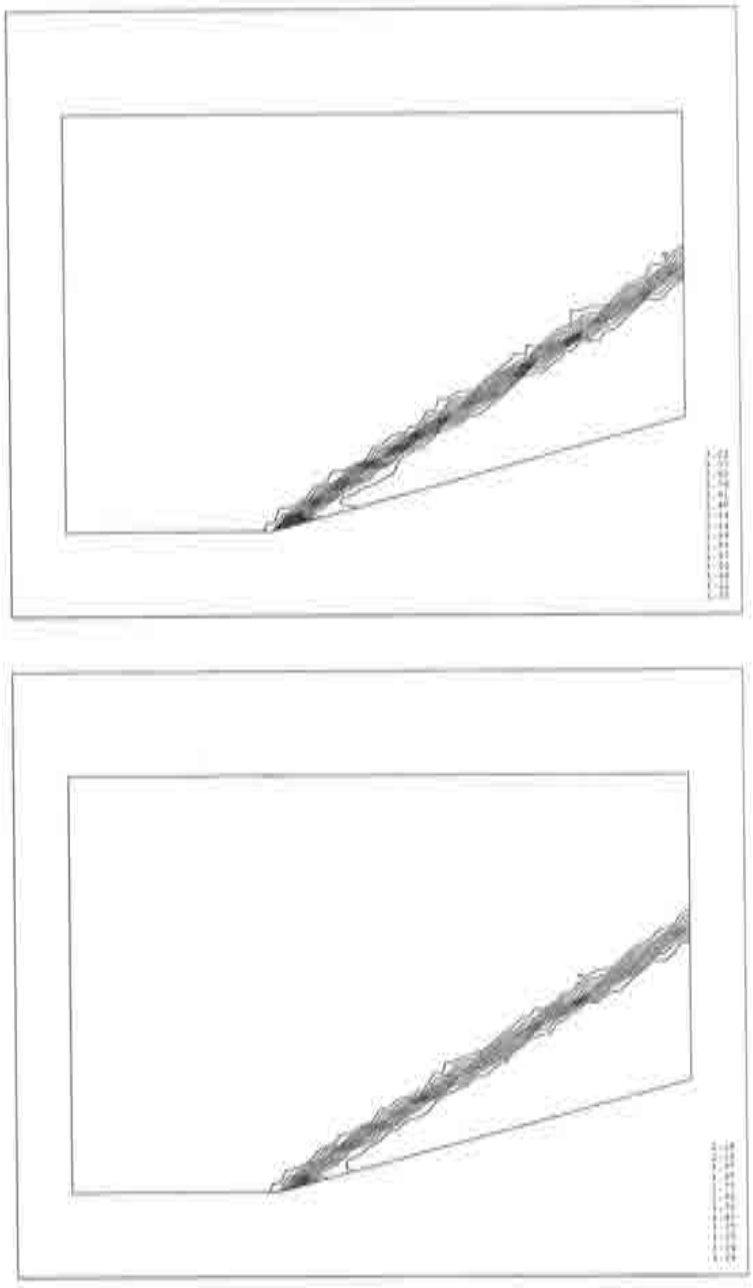

Figure 4.24: Flow passing a wedge, Mach 3. P2 mesh. Density - momentum - energy variables. Pressure and density contours.

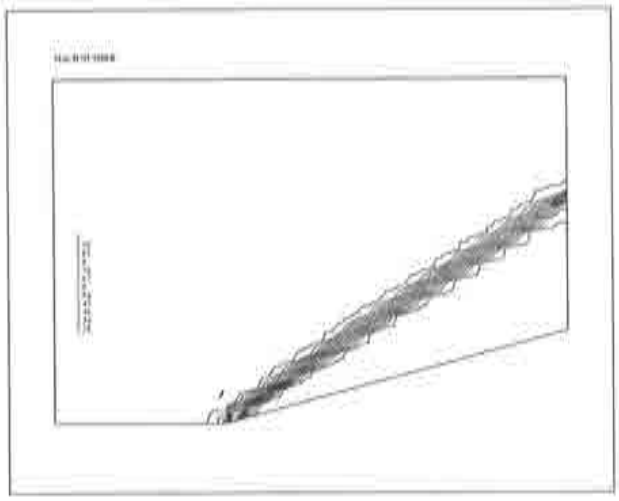

Figure 4.25: Flow passing a wedge, Mach 3. P1 mesh. Density - momentum - energy variables. Mach number contours.

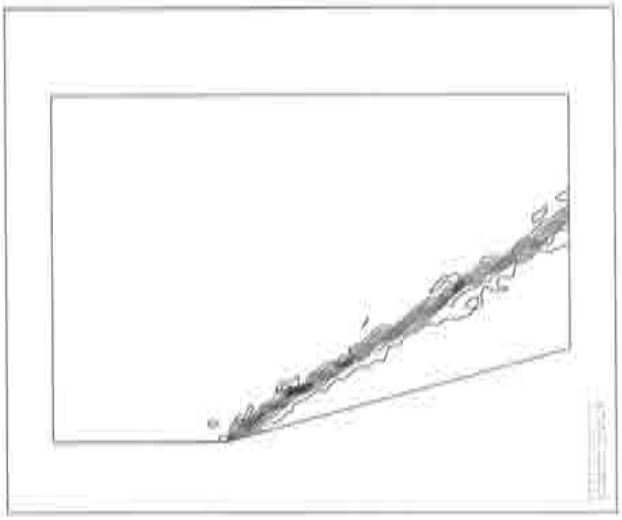

Figure 4.26: Flow passing a wedge, Mach 3. P2 mesh. Density - momentum - energy variables. Mach number contours.

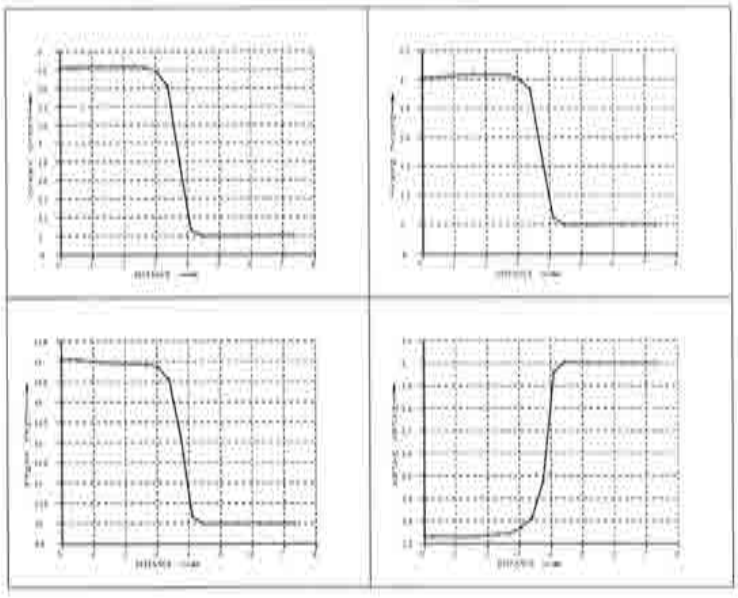

Figure 4.27: Flow passing a wedge, Mach 3. P1 mesh. Density - momentum - energy variables. Cut along the outflow: pressure, density, temperature and Mach number (clockwise, from top left)

In this example, the sets of variables are tested for fixed values of $\theta_1 = 1.0$ and $\theta_2 = 0.0$ (i.e. explicit form of the algorithm). Both ρUE and ρUT sets of variables can be compared through different Mach numbers. Here, the analysis shown is for the case Mach 3. If the temperature is chosen instead of the total energy as the third unknown, all the variables show smooth contours also, fig. 4.29, but the shock is badly placed. This behaviour is typical of non-conservative sets [Hansbo, 1994].

This fact can be seen in fig. 4.30 which show the stationary state reached for Mach 3 using both sets of variables. Only when using the total energy the shock angles obtained coincide with those predicted by the theory. Solving the equation for the temperature instead of the total energy places the shock like if it was for a bigger Mach number. As the solution given in both cases is different, jump conditions are not equally verified. This is shown in fig. 4.31. This figure shows the value of the convective flux of energy along the bottom edge of the domain, for both sets of variables and for Mach 3. As the shock is stationary, there shouldn't be any jump in the flux across the discontinuity. Appart from the over and undershoots (less than 5%) at the sharp beginning of the ramp, only the conservative set verifies the jump condition. For stationary shocks, it is [Courant and Friedrichs, 1948]:

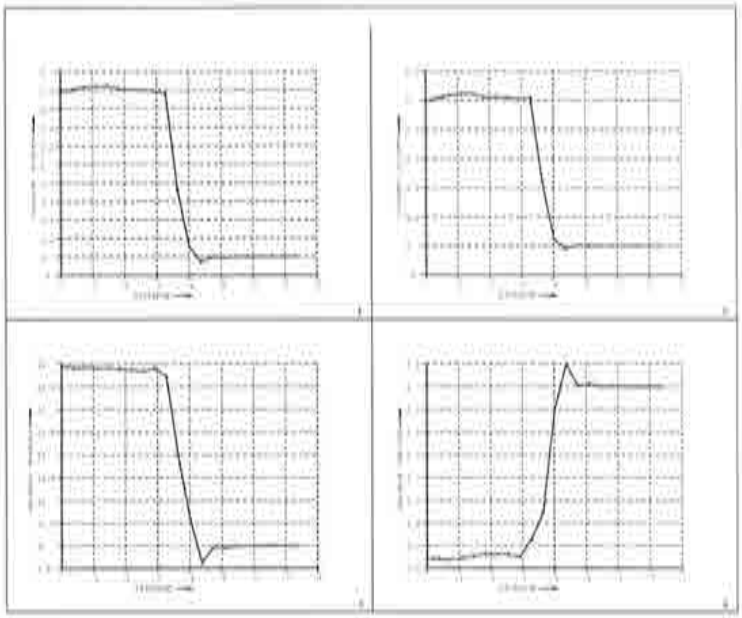

Figure 4.28: Flow passing a wedge, Mach 3. P2 mesh. Density - momentum - energy variables. Cut along the outflow: pressure, density, temperature and Mach number (clockwise, from top left)

$$\frac{1}{2}|u_1|^2 + h_1 = \frac{1}{2}|u_2|^2 + h_2, \tag{4.1}$$

where 1 and 2 labels the side of the shocks, $|u|$ is the velocity norm and h the enthalpy.

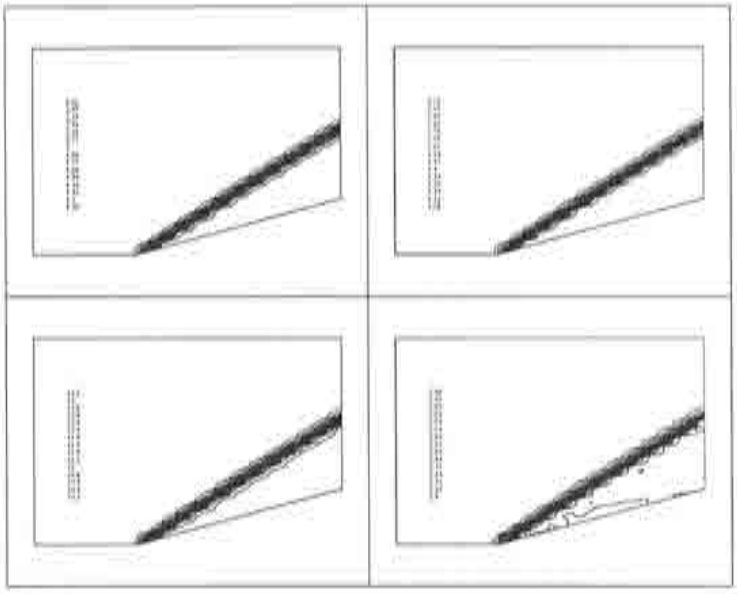

Figure 4.29: Flow passing a wedge at Mach 3. P1 mesh. Density - momentum - temperature variables. Pressure, density, temperature and Mach number (clockwise, from top left)

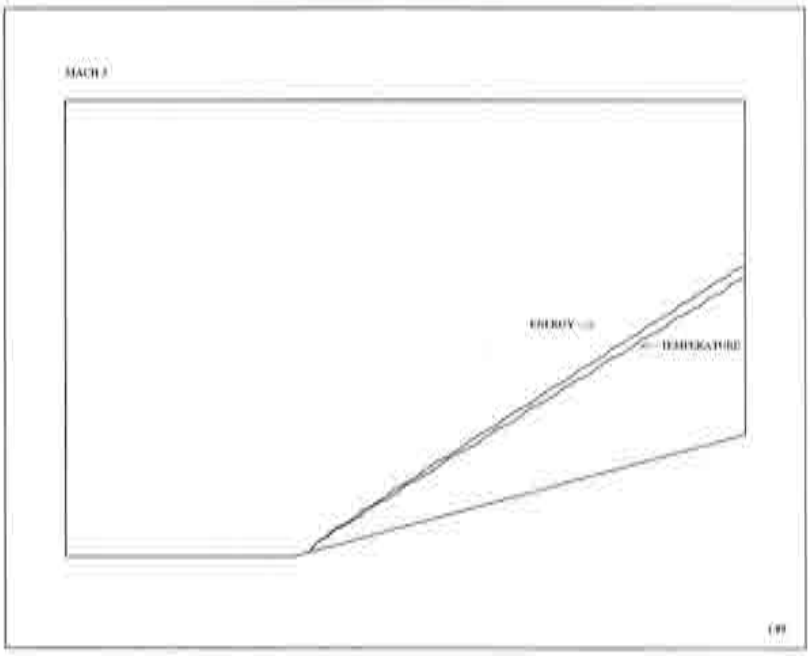

Figure 4.30: Flow passing a wedge, Mach 3. P1 mesh. Density - momentum - energy against Density - momentum - temperature variables. Different position of the shock.

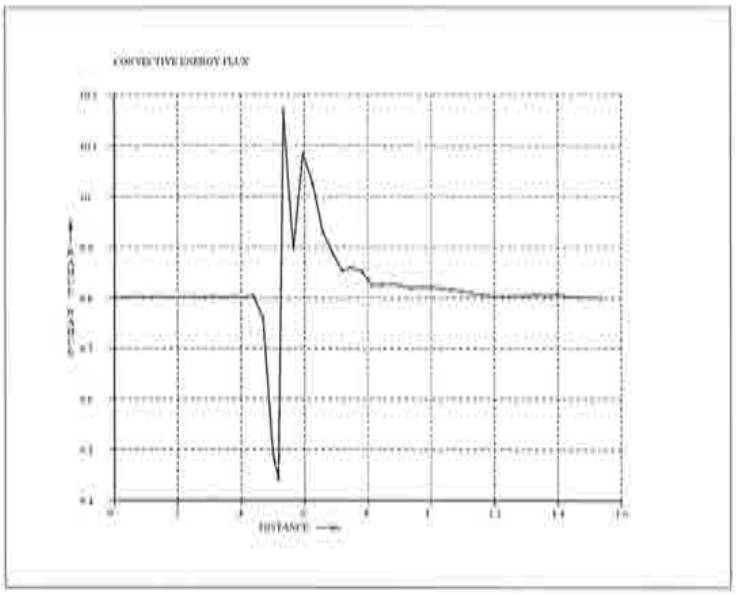

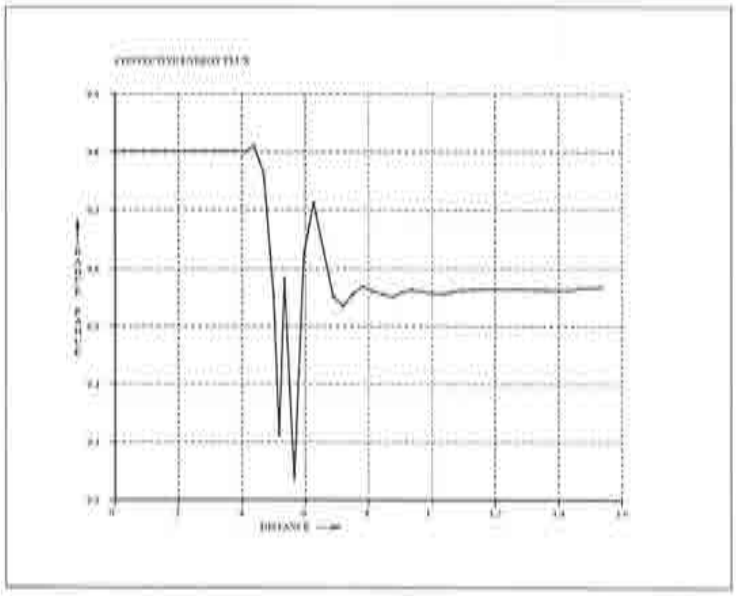

Figure 4.31: Flow passing a wedge, Mach 3, P1 mesh. Top: density - momentum - energy set. Bottom: density - momentum - temperature set. Convective flux of energy along the bottom edge.

4.3.3 Supersonic flow passing a cylinder at $M = 3$

In this example, flow at Mach 3 reachs a cylinder and a steady shock is formed in front of the cylinder fig. 4.32 . At the inflow, velocity, density and temperature are prescribed, for it is a supersonic inlet. The normal velocity on the cylinder is fixed to zero. The domain is discretized using a mesh of 5351 P1 elements (2772 nodal points) which is shown in fig. 4.33. As before, the mesh has no kind of adaptivity.

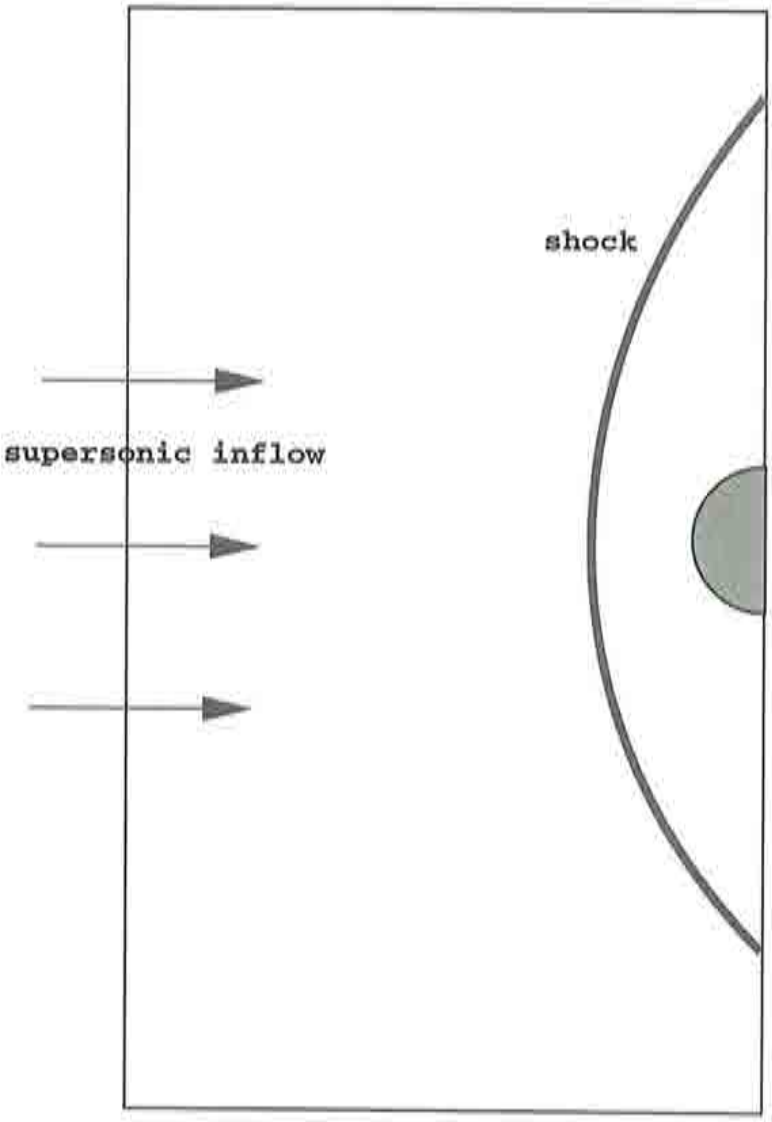

Figure 4.32: Supersonic flow passing a cylinder.

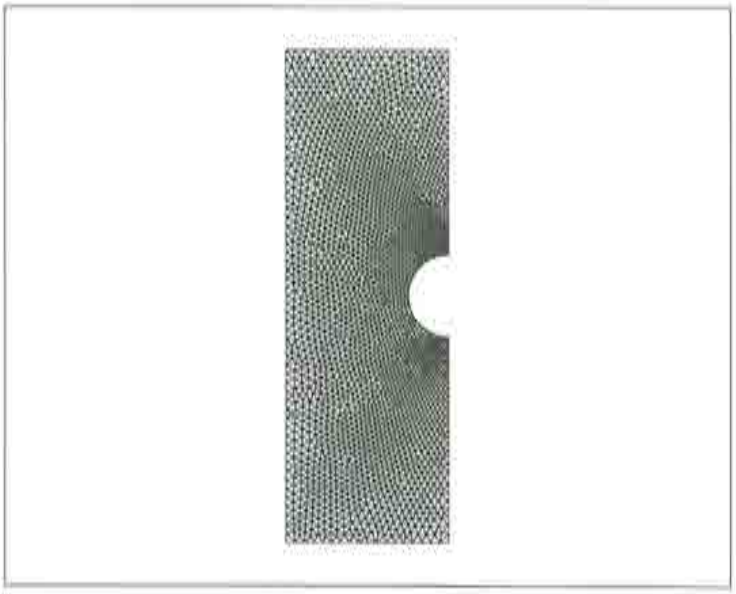

Figure 4.33: Supersonic flow passing a cylinder. P1 mesh.

Again the difference with conservative and non-conservative sets become apparent. If ρUT is used, the shock is placed in a wrong position (fig. 4.34). This problem is present whether the explicit or the semi-implicit form of the algorithm is used. For that reason the explicit form was chosen in this example.

The wrong position of the shock can be checked also evaluating the jump conditions, which in the case of ρUT set are not verified. For instance, fig. 4.35 shows the Rankine - Hugoniot condition corresponding to the conservation of energy for both sets. In this case, as the shock is stationary, the convective flux of energy must not present jumps crossing it. In this figure, its variation is tracked following the x axis at half of the domain, crossing normally to the shock. When the total energy is used, the values at both sides of the shock seem to be approximately the same, despite of some oscillations remaining behind it. Clearly, this is not the case for the ρUT set. The bump of the flux right over the discontinuity would fade away as the mesh is refined there.

Pressure coefficient and density along the same cut for the "conservative" set only are shown in fig. 4.36.

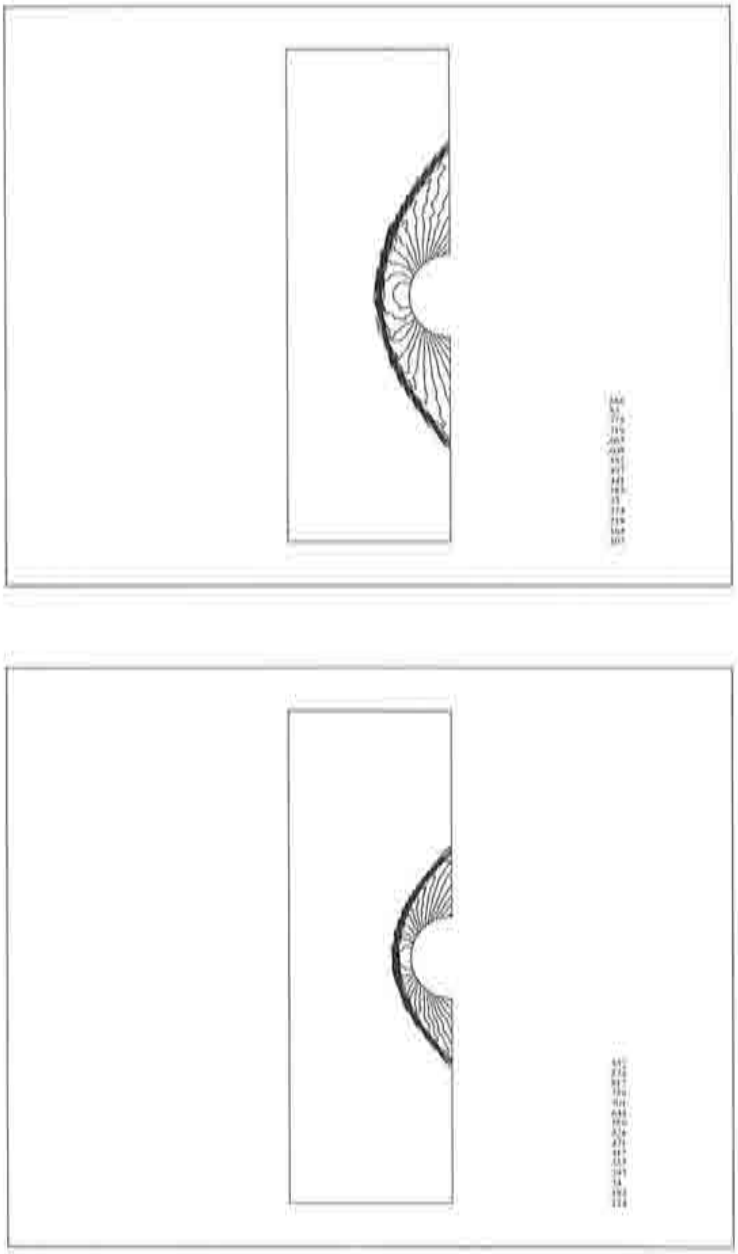

Figure 4.34: Supersoninc flow passing a cylinder, Mach 3. Pressure contours. Top: Density - momentum - energy variables. Bottom: Density - momentum - temperature variables.

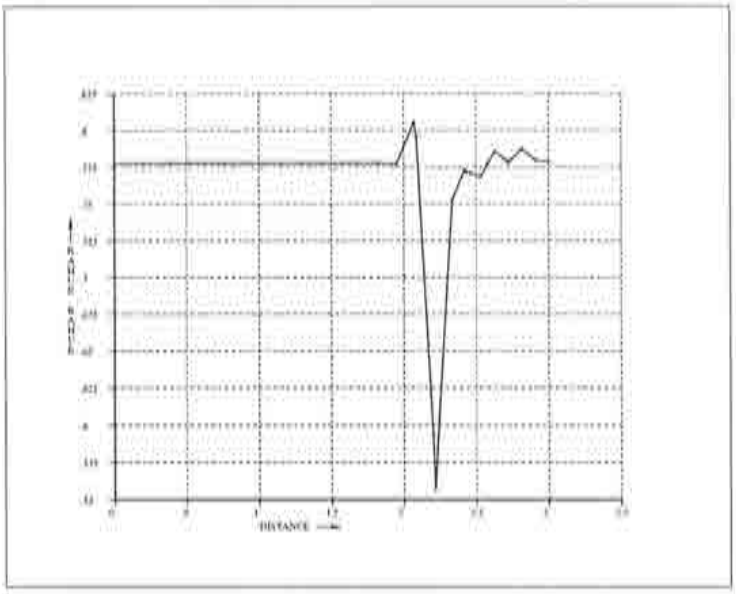

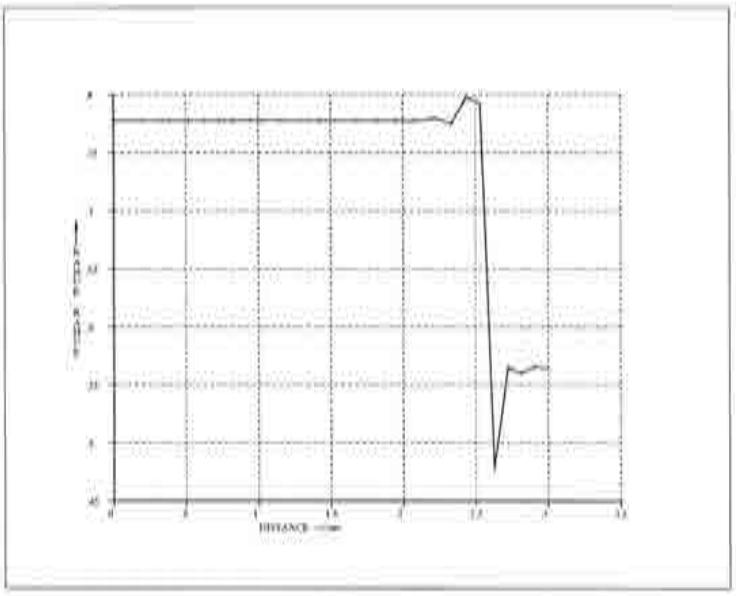

Figure 4.35: Supersonic flow passing a cylinder, Mach 3. Jump conditions: convective flux of energy across the shock. Top: Density - momentum - energy variables. Bottom: Density - momentum - temperature variables. The cut is horizontal and normal to the shock, running through the stagnation point on the cylinder.

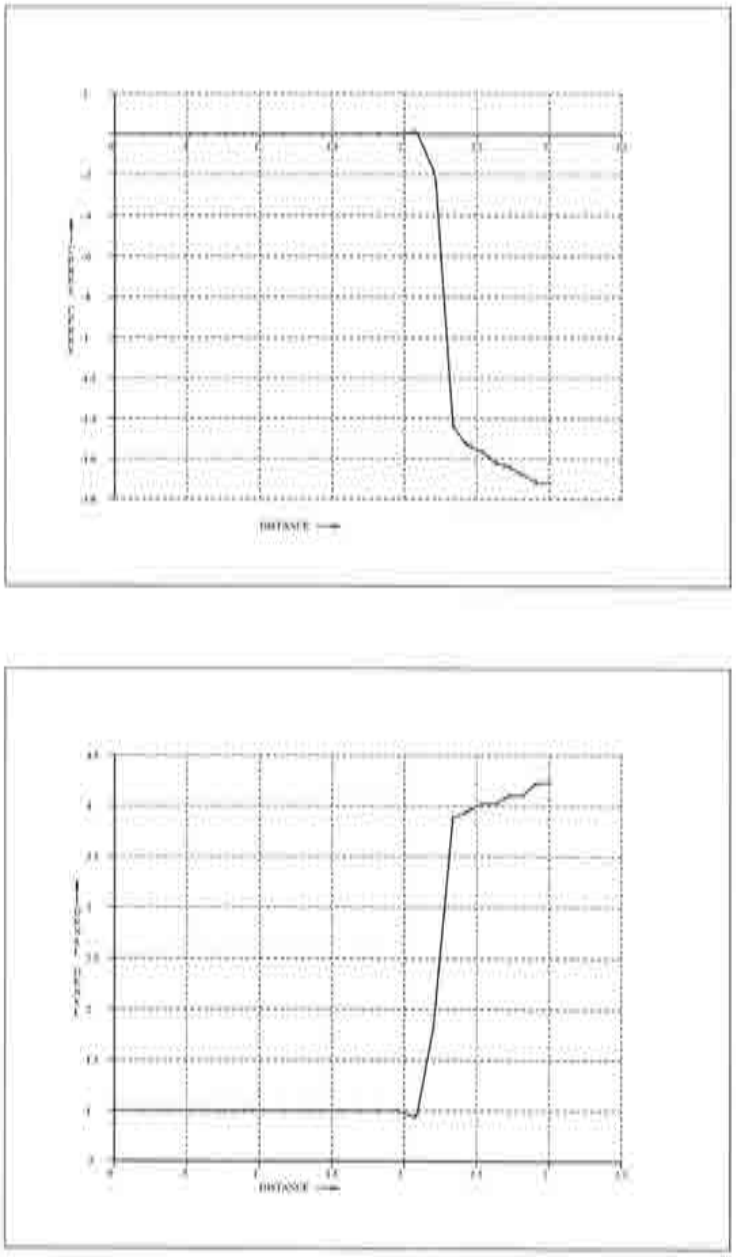

Figure 4.36: Supersonic flow passing a cylinder, Mach 3. Density - momentum - energy variables. Top: pressure coefficient. Bottom: density. The cut is done horizontally at half of domain, normal to the shock.

4.4 Compressible Viscous Flow

Two examples are shown here: the supersonic flow over a plate, known as *Carter's flow*, at $Re = 1000$ and $M = 3$, and the transonic flow passing a NACA 0012 profile at $M = 0.85$ and $Re = 500$.

4.4.1 Supersonic flow over a plate (Carter's flow)

The supersonic flow over a plate (fig. 4.37) develops all the different features that can appear when solving the complete Navier-Stokes equations. It has low compressibility regions mixed with high Mach number ones. Boundary layers interacting with shocks are a good test for the stability of the scheme. The shock itself is useful to test the behavior of the anisotropic shock capturing diffusion, now with viscosities different than zero. FEM spatial discretization allows the use of higher order elements which are also here tested. EXP and SIM forms of the algorithm are checked one against each other. Finally, the use of the temperature as unknown produces a shift in the position of the stationary shock formed.

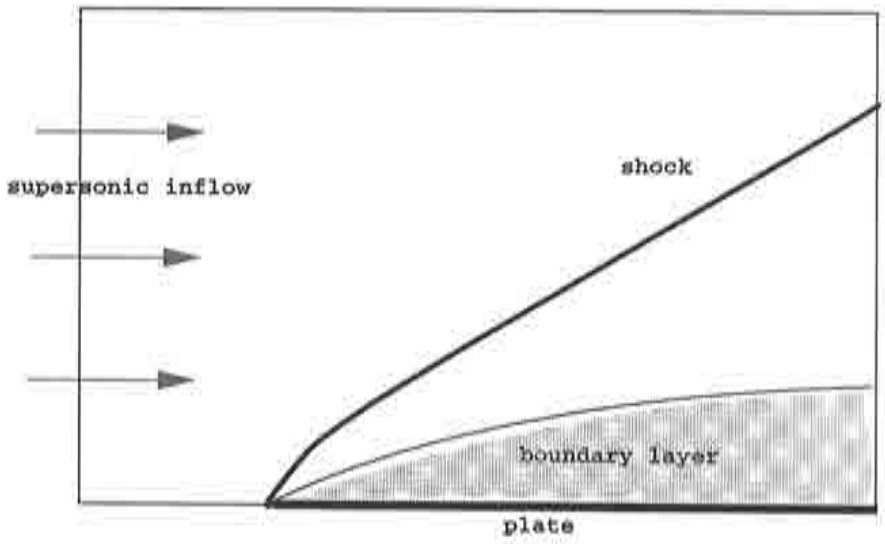

Figure 4.37: Flow over a plate.

The problem studied here is at Mach 3. The viscosity μ depends on the temperature according to the Sutherland's law:

$$\mu = \frac{0.0906T^{1.5}}{T + 0.0001406},$$

Prandtl number (cf. section 2) is 0.72. The domain is meshed in 112×64 (7168) Q1 elements, corresponding to 7345 nodal points. Also, here the results for a Q2 elements mesh are presented. This mesh was obtained from the Q1 one: it is made of 1792 biquadratic elements of 9 nodes each, while keeping the same number of nodal points. Density, velocity and temperature are prescribed at the inflow, because this inlet is supersonic. No prescriptions are made at the outflow. The *no slip* condition is imposed at the floor of the plate, wich starts at $x = 0.2$ if the length of the domain goes from $x = 0.0$ to $x = 1.4$. The stagnation temperature is calculated according to:

$$T_{\text{stag}} = T_{\text{inflow}} \left(1 + \frac{\gamma - 1}{2} M^2_{\text{inflow}}\right)$$

Testing elements: Q1 and Q2.

These first results were obtained using the Explicit form of the algorithm, and ρUT as the set of variables. θ_1 is 0.5. The results for both meshes and for this scheme are shown from fig. 4.38 to fig. 4.41.

It can be seen that both the Q1 and Q2 elements reproduce equally well the flow features. Biquadratic elements are less diffusive, and for that reason, shocks seems to be sharper if the latter elements are used to build the mesh. To correctly deal with the shocks, the anisotropic shock capturing device proposed in [Codina, 1993b] is used. A cut along the outlet is shown in fig. 4.42.

Testing forms: EXP and SIM.

The numerical results obtained using the same set of variables, but with the Semi Implicit form, compare very well to those of the Explicit one. The following graphs show the behaviour of the SIM form, with $\theta_1 = 0.5$ and $\theta_2 = 1.0$. The mesh used is

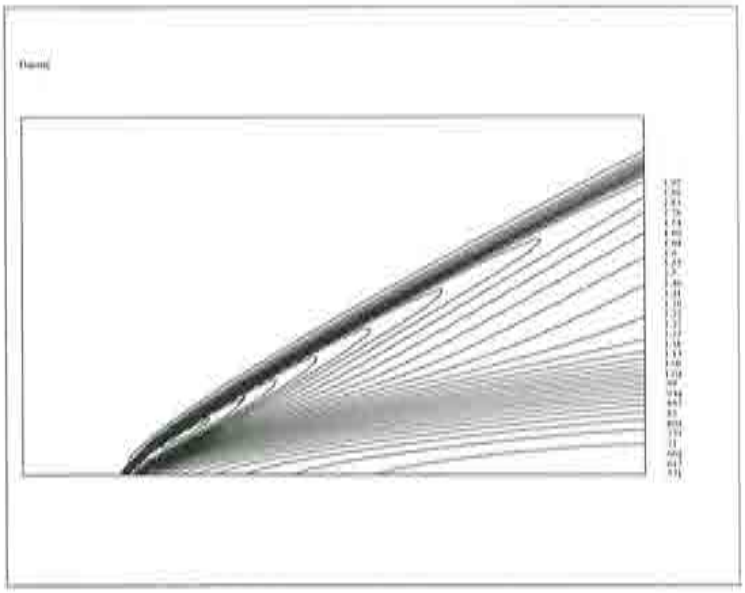

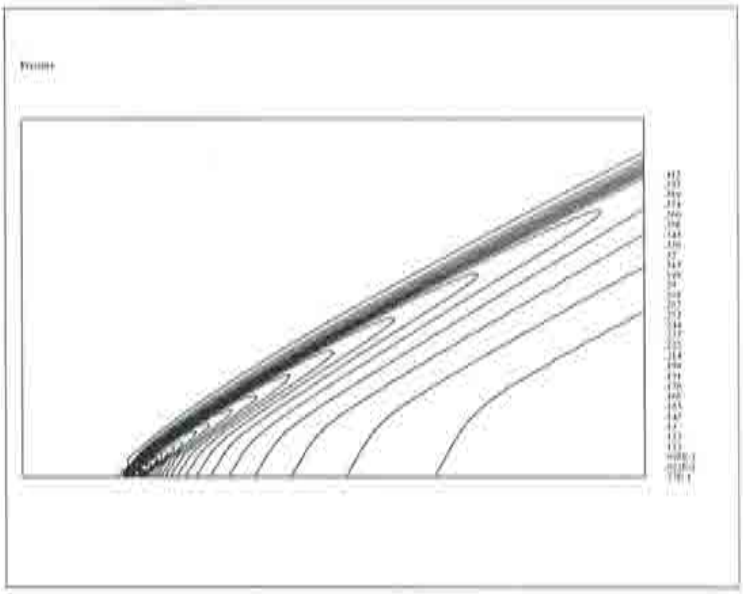

Figure 4.38: Flow over a plate. Density and pressure contours, Q1 elements. EXP form. Density - momentum - energy variables.

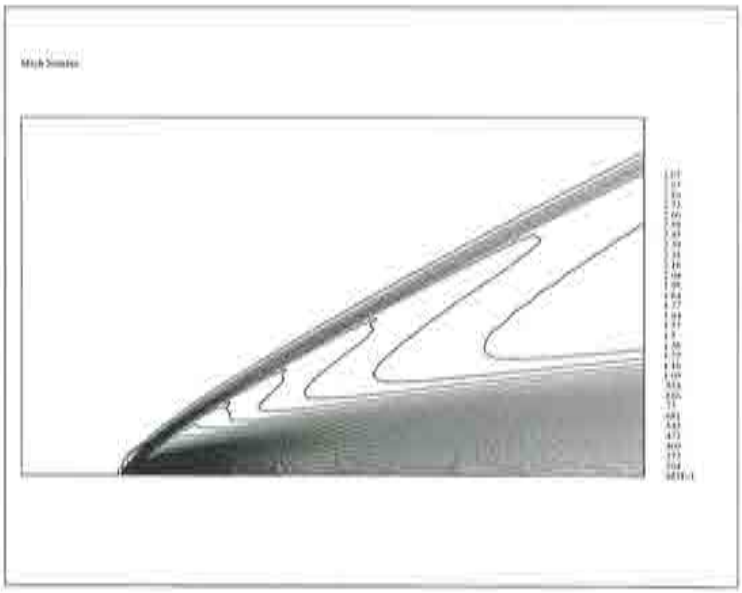

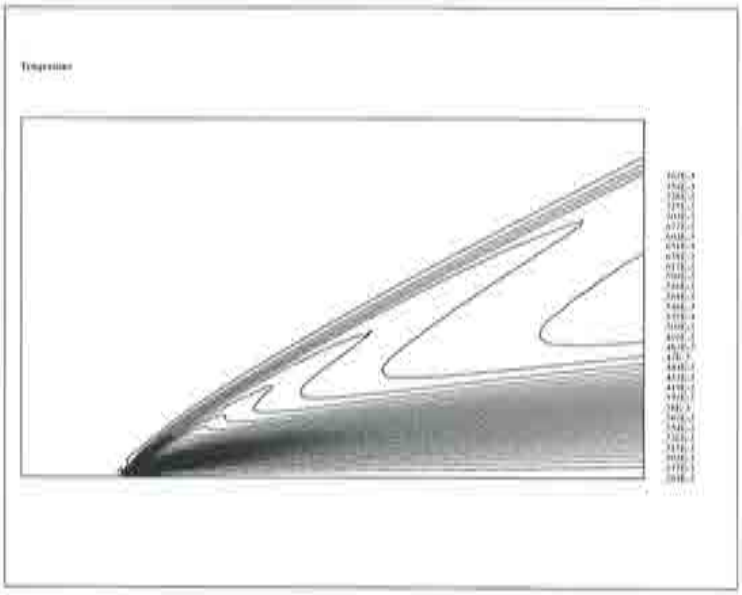

Figure 4.39: Flow over a plate. Mach number and temperature contours, Q1 elements. EXP form. Density - momentum - energy variables.

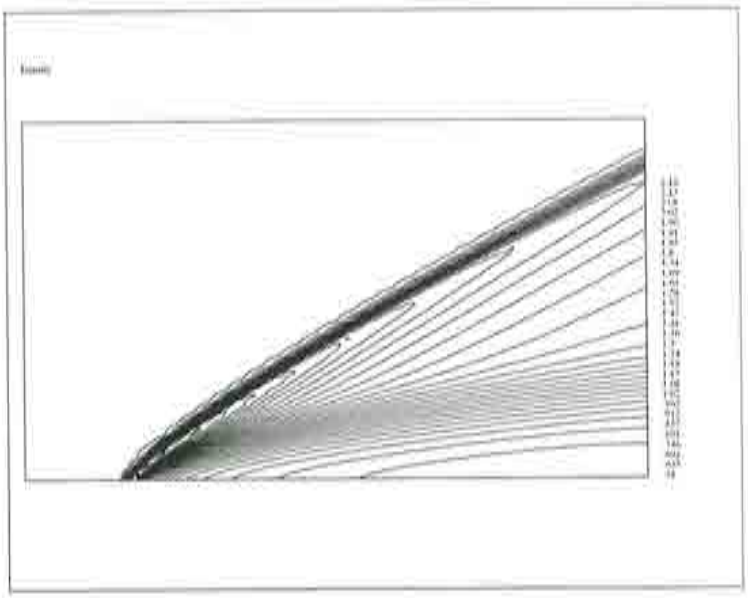

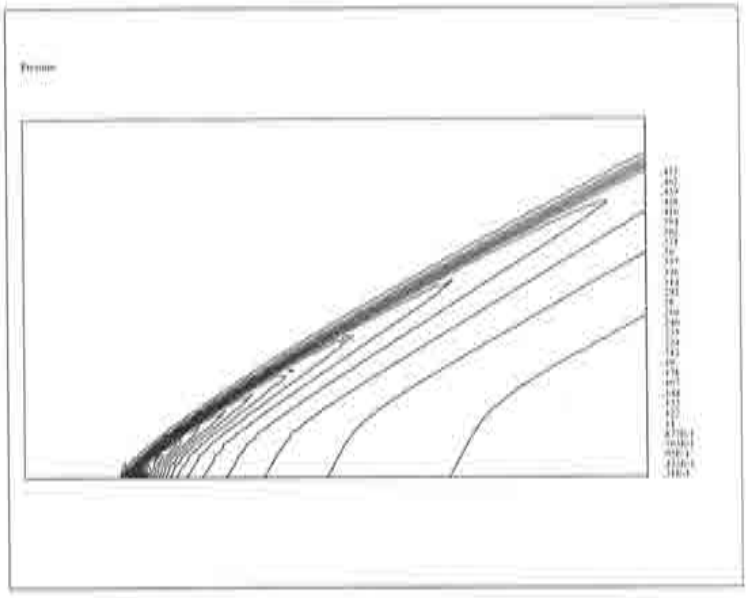

Figure 4.40: Flow over a plate. Density and pressure contours, Q2 elements. EXP form. Density - momentum - energy variables.

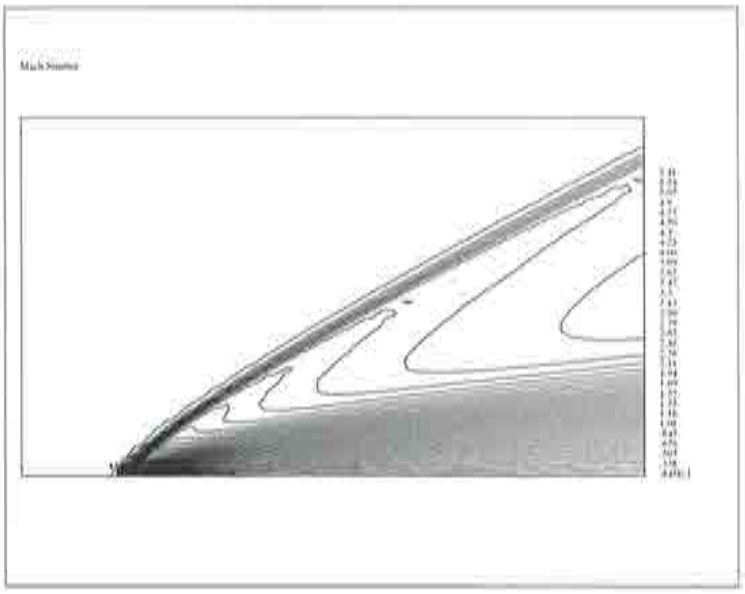

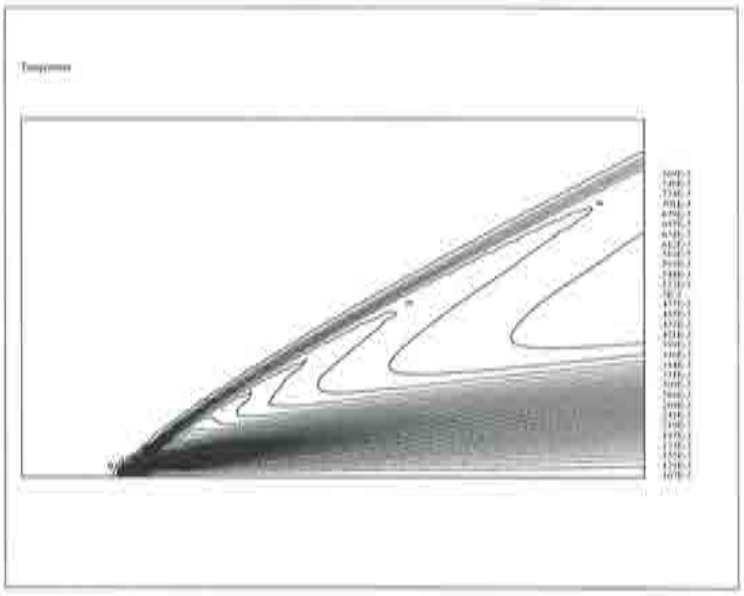

Figure 4.41: Flow over a plate. Mach number and temperature contours, Q2 elements, EXP form. Density - momentum - energy variables.

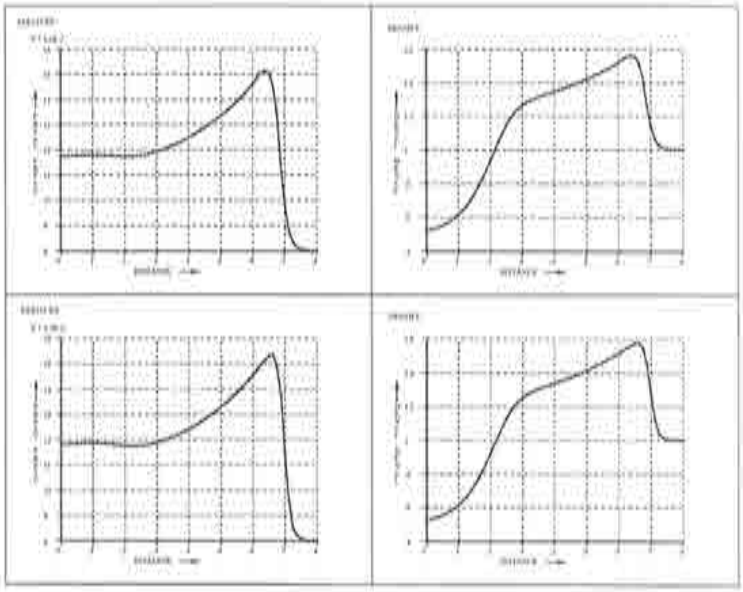

Figure 4.42: Flow over a plate. Cut along the outflow. Top, Q1 elements; bottom, Q2 elements. Left, pressure; right, density. EXP form. Density - momentum - energy variables.

again the Q1 mesh. To speed up the code as much as possible, an iterative conjugate gradient method was used to solve the continuity equation (fig. 4.43 and fig. 4.44).

The shock and the boundary layer are at the same place using both forms. Also, the values and behaviour of the variables almost coincide (fig. 4.45).

Testing sets of variables: ρUE and ρUT:

The ρUT set produces very sharp shocks but wrongly placed. Besides, it fails when modelling the boundary layer. This can be seen, for instance, at the lower right corner of the domain. The density contours there are clearly different than in the case of ρUE (fig. 4.46). On the other hand, along a cut through the outflow, the wrong position of the shock becomes apparent (fig. 4.47).

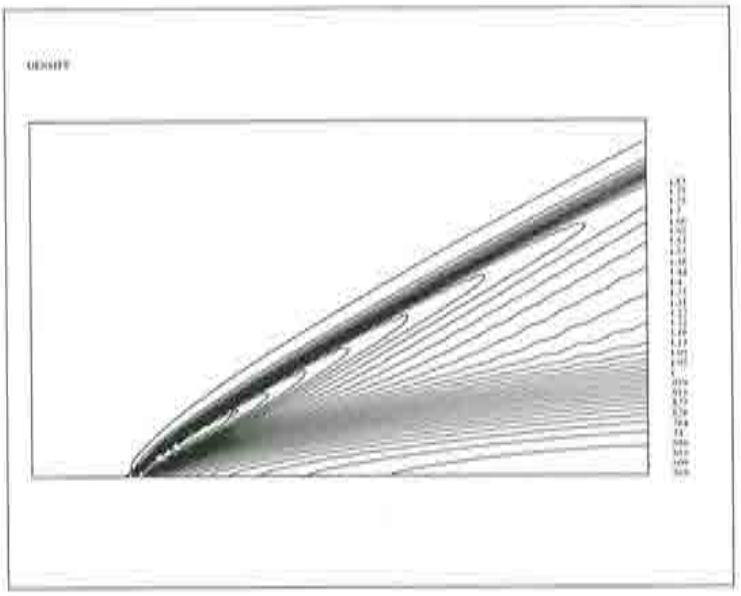

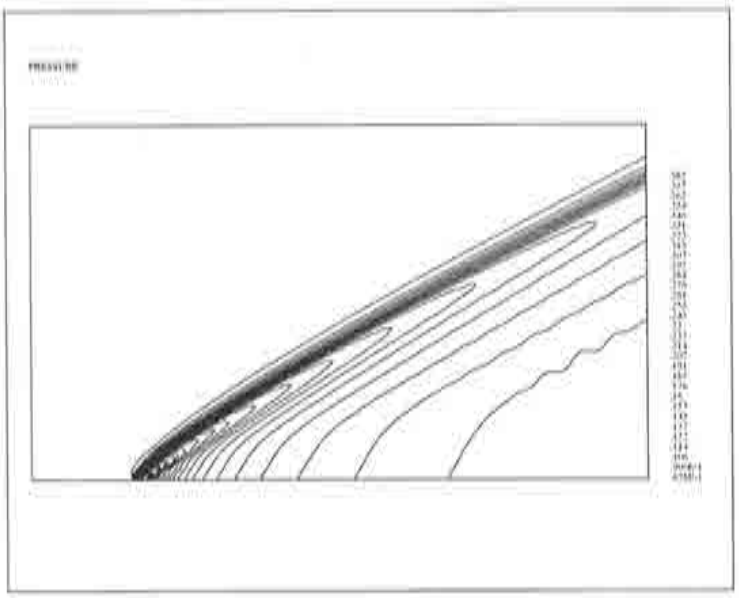

Figure 4.43: Flow over a plate. Density and pressure contours, Q1 elements. SIM form. Density - momentum - energy variables.

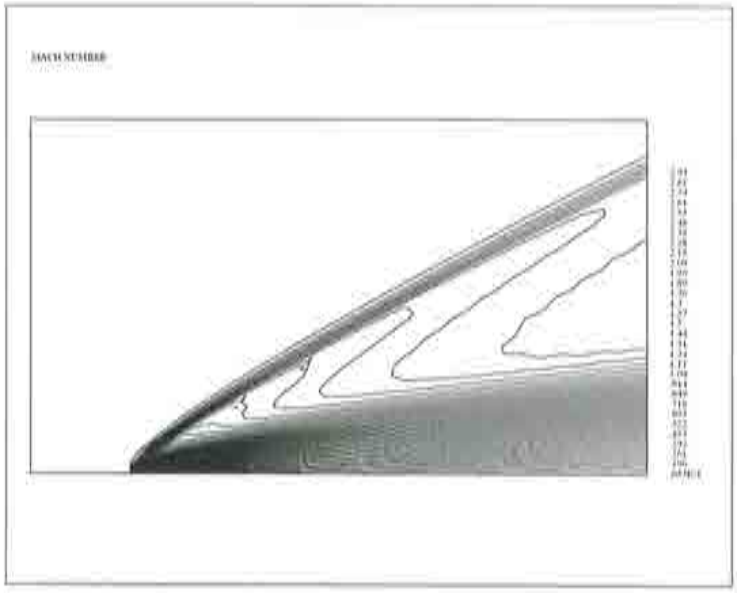

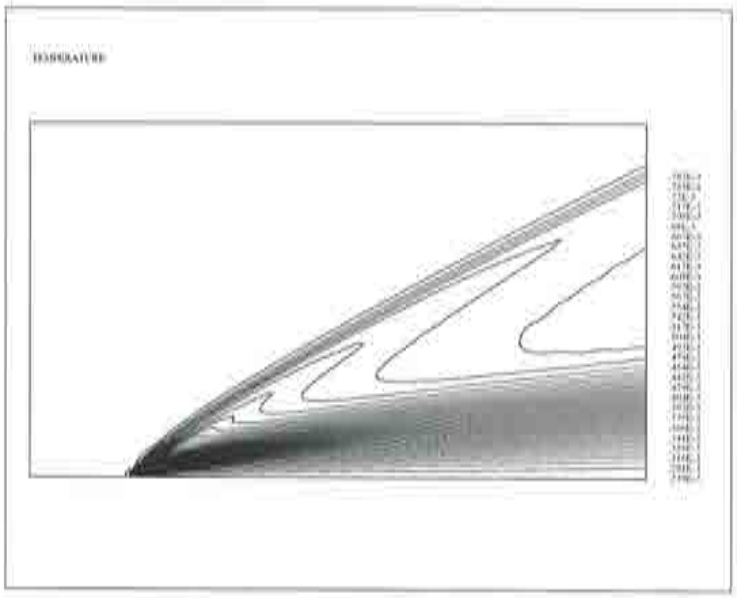

Figure 4.44: Flow over a plate. Mach number and temperature contours, Q1 elements, SIM form. Density - momentum - energy variables.

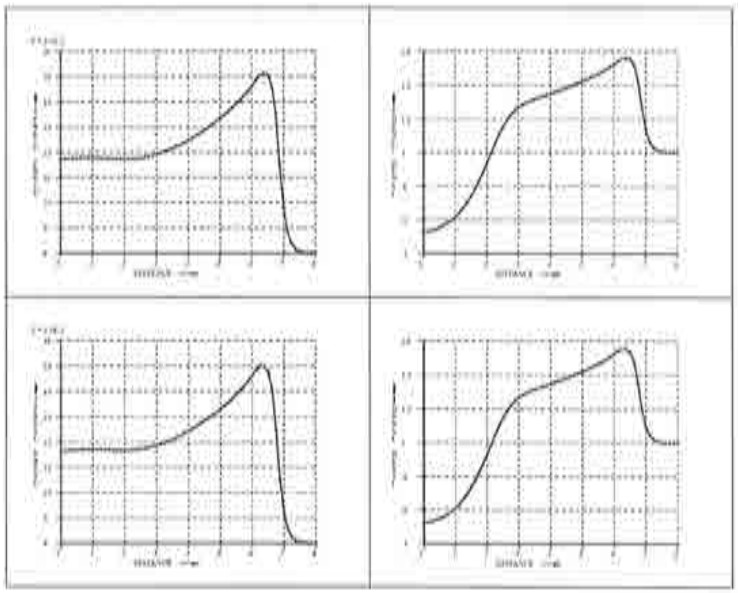

Figure 4.45: Flow over a plate. Cut along the outflow. Q1 mesh. Top, EXP form; bottom, SIM form. Left, pressure; right, density. Density - momentum - energy variables.

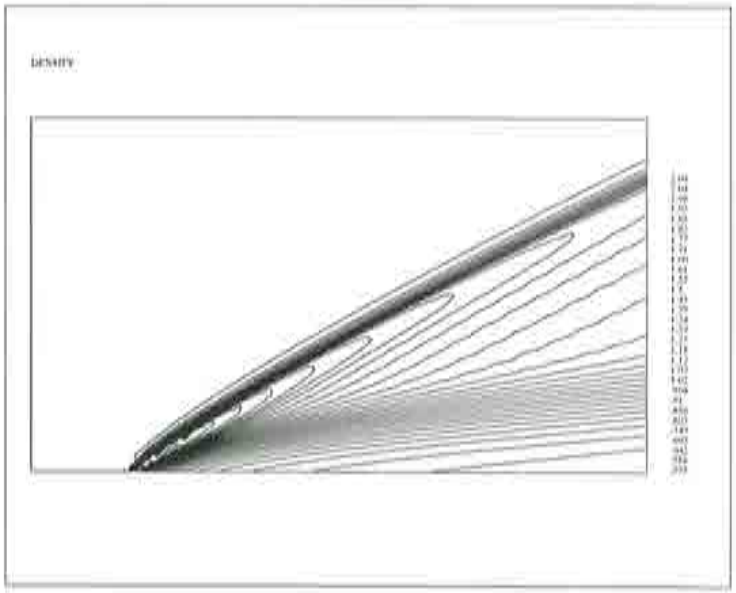

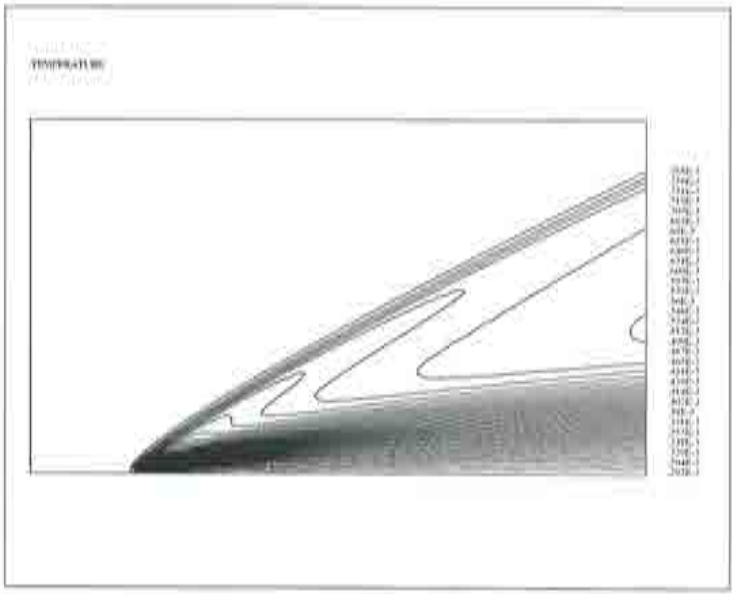

Figure 4.46: Flow over a plate. Density and temperature contours, Q1 elements. EXP form. Density - momentum - temperature variables.

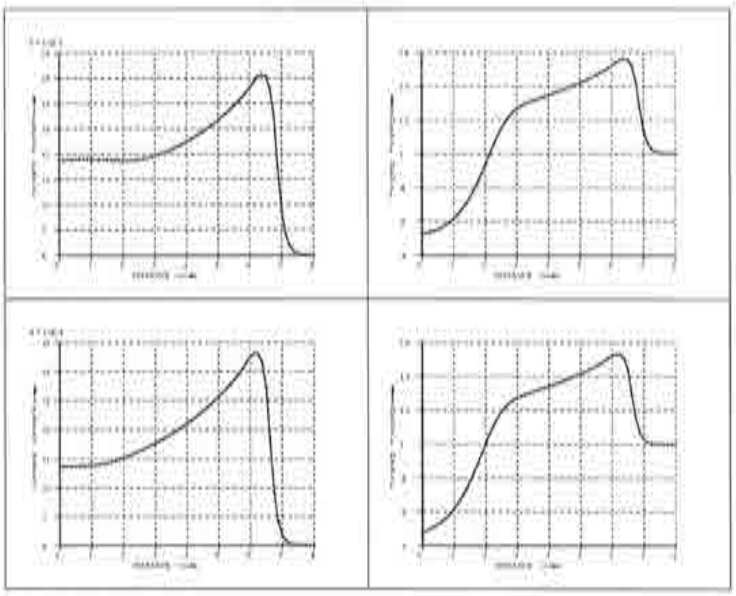

Figure 4.47: Flow over a plate. Cut along the outflow. Q1 mesh. Top, Density - momentum - energy variables; bottom, Density - momentum - temperature variables. Left, pressure; right, density. EXP form.

4.4.2 Transonic flow passing a NACA 0012 profile at $M = 0.85$ and $Re = 500$

Like in the preceding example, the no-slip condition imposed in the solid walls produces a boundary layer and its thickness is determined by the Reynolds number. This problem is reported in the GAMM workshops (reference [Bristeau et al., 1988], cited in [Mittal, 1998]). We show here the problem for $M = 0.85$ and $Re = 500$. Part of the computational domain can be seen in fig. 4.49. It is made of 8446 P1 elements, including 4359 points. It is not adapted, except for the node concentration around the profile, sligthly refined around the leading edge. The first layer of nodes following the no-slip boundary condition ones is placed ranging from $0.004L$ at the leading edge to 0.009 at the trailing one, where L is the chord of the profile. In the inflow, velocity and temperature is kept fixed according to the selected Mach number, whereas in the outflow, only the density is prescribed. In the no-slip wall, zero velocity and stagnation value temperature (like in the flat plate example) are prescribed.

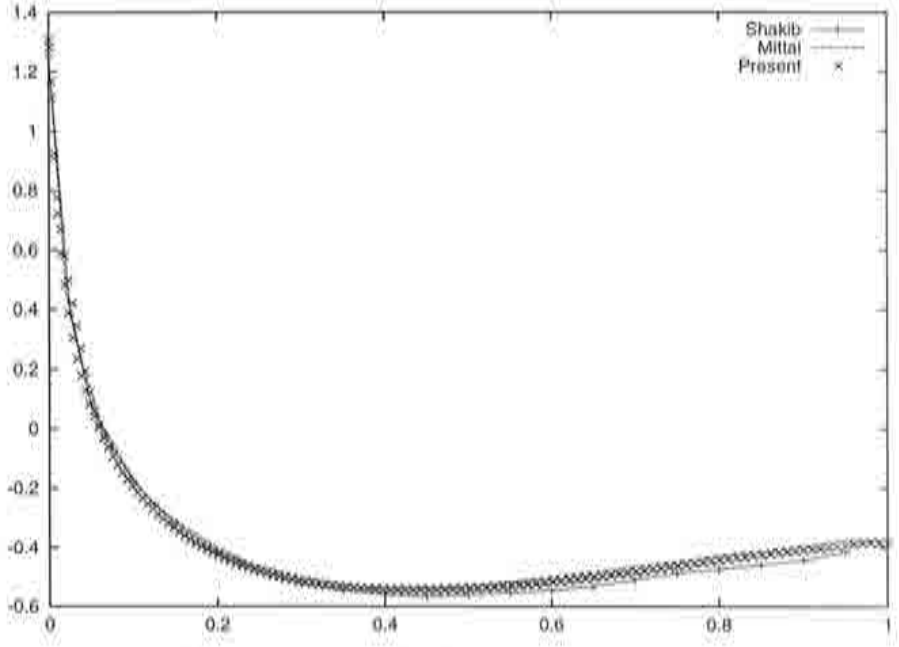

Figure 4.48: Transonic flow passing a NACA 0012. Chord-wise variation of C_p. Comparison between [Shakib, 1988], [Mittal, 1998] and the present scheme.

The C_p variation chord-wise is shown in fig. 4.48. It is compared with those results obtained by F. Shakib [Shakib, 1988] and by S. Mittal [Mittal, 1998]. In both cases, the spatial discretization used was much finer than here. In the first case, the mesh

used has 24.256 P1 elements (12.300 nodes). In the second one, it is a 18.772 Q1 elements mesh (10.014 nodes). The distribution here obtained is very close to that obtained by S. Mittal despite of the size and adaptivity differences. In this case, the coarse discretization in the wake zone has not noticeable effects in the C_p distribution on the profile.

The following figures, fig. 4.50 and fig. 4.51, show contour levels of the variables in the vicinity of the profile. In fig. 4.50, Mach number field is seen in different close-ups. Closer to the wing, the contour levels are smoother due to the refinement, becoming jagged when zoomed out, in particular in the wake zone. Due to the relatively low Mach and Reynolds numbers, shocks are not present. The boundary layer is well resolved by the discretization and there is no oscillatory behaviour downstream the profile. In fig. 4.51, pressure and temperature contours are shown. Again, in the refined region, the contour levels are smoother. In any case, it is remarkable that this fact has no influence in the inner part of the boundary layer.

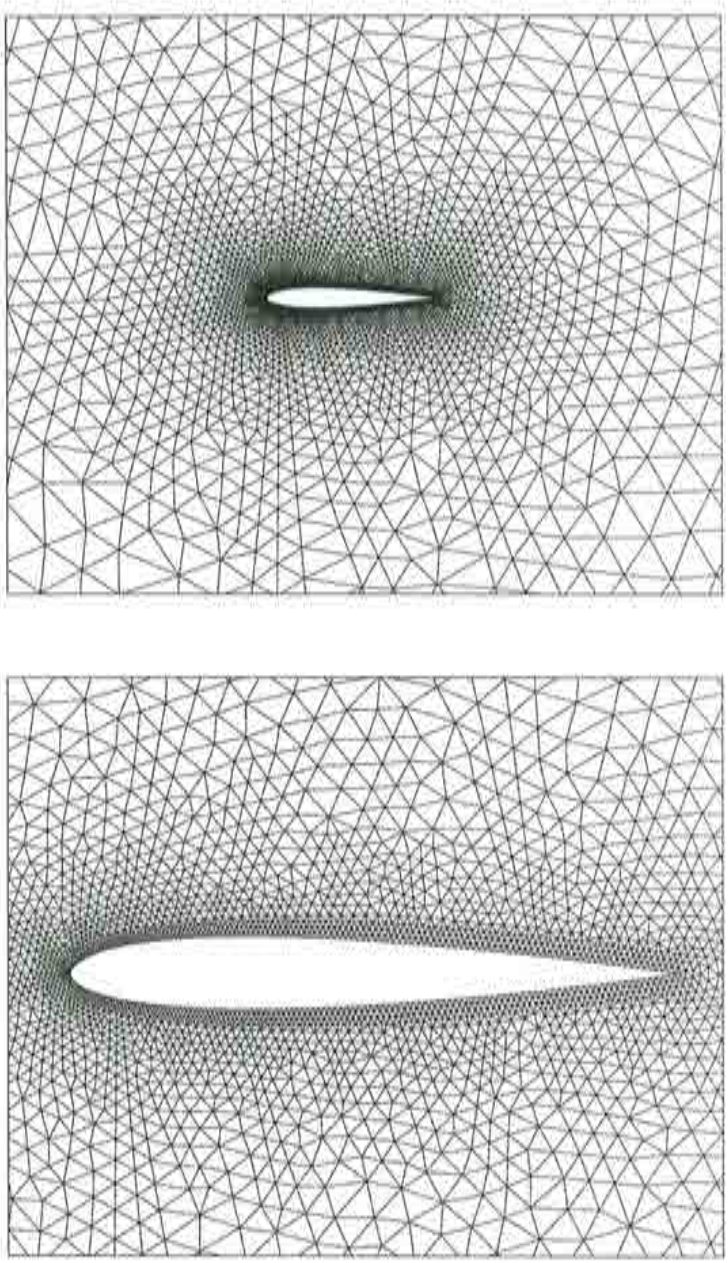

Figure 4.49: Transonic flow passing a NACA 0012. Views of the mesh.

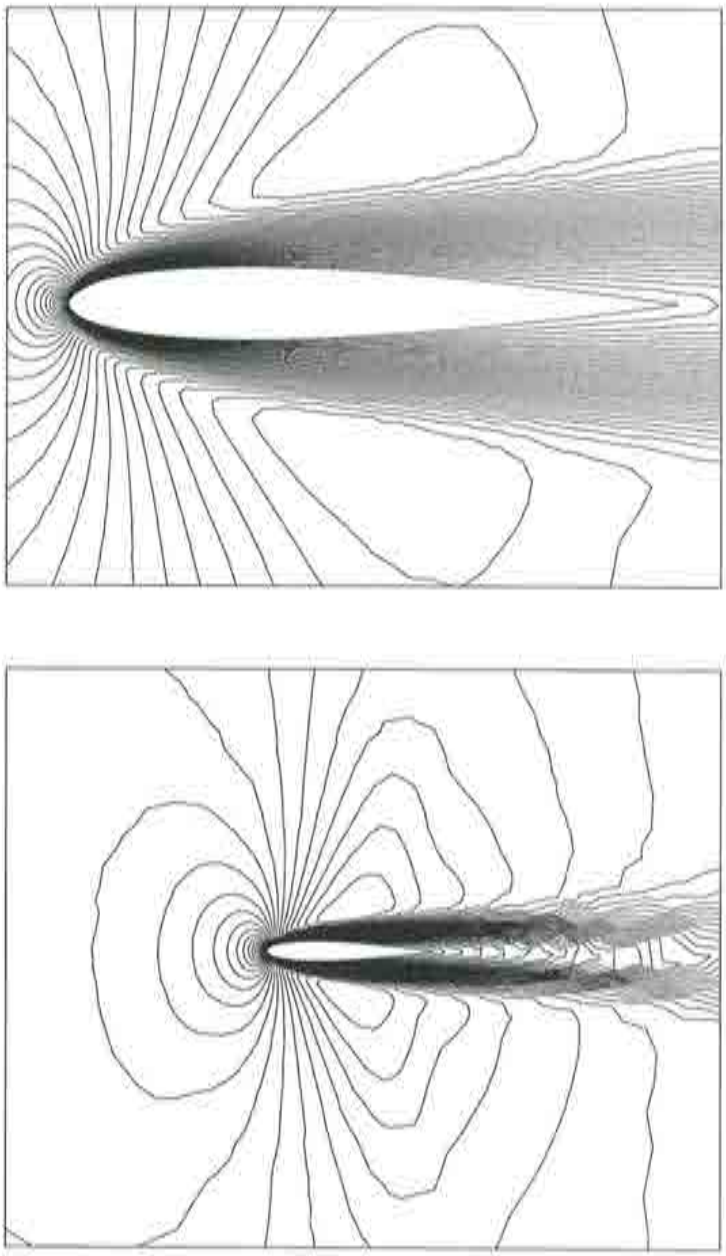

Figure 4.50: Transonic flow passing a NACA 0012. Mach number level contours. Two views.

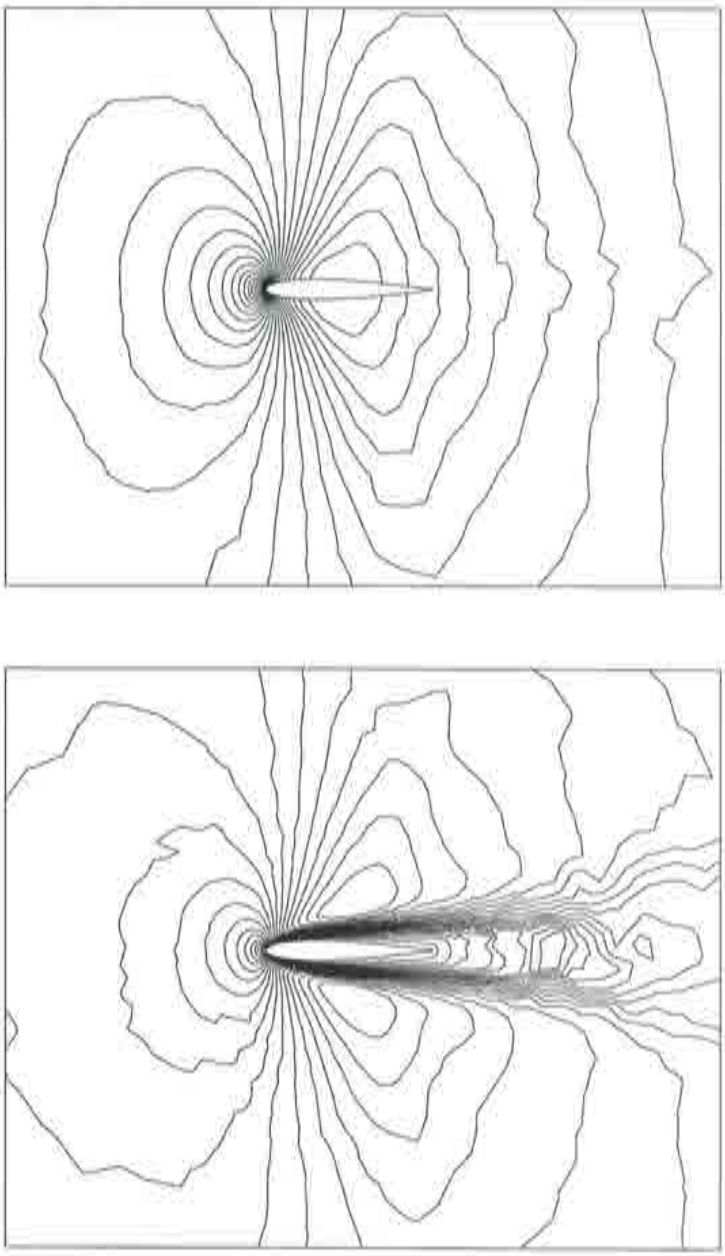

Figure 4.51: Transonic flow passing a NACA 0012. Pressure (top) and temperature (bottom) level contours.

4.5 Summary

CBS performance for laminar flow problems is evaluated through some selected 2D examples. Being a general algorithm, it must pass tests for incompressible and compressible flow with different Re numbers. The incompressible examples studied here are inviscid and viscous, stationary and transient. Triangle and quadrilateral elements are tested in structured and unstructured meshes. Continuity equation is solved implicitly, and fractional momentum either implicitly or explicitly.

Shocks and its interaction with boundary layers are a challenge in compressible flow. In this case, also both inviscid and viscous problems are considered. In the first case, the abscense of viscosity produces a less smooth solution than in the viscous case, being shocks steeper. Quadratic elements are also very difficult to tune for Euler problems. On the other hand, for Navier-Stokes equations Q2 elements work really well.

Chapter 5

The CBS Algorithm. Turbulent Flow

5.1 The physical problem

So far, we have dealt with idealized flows. As was said in the introduction to the laminar flow equations, the Navier - Stokes', starting from some general principles and hypotheses, a set of equations modeling a flow system is derived. Nothing was said about existence and uniqueness of the solutions of this set. Although for some cases these statements can be proven, this is not the general rule. The difficulties faced at this point are very challenging. For instance, for some simplified cases, a solution for the weak derived problem is proven to exist and *if* a solution for the strong set *exists* both are the same (c.f. [Lions, 1996] for results on incompressible Navier - Stokes equations, [Brézis, 1984] for general results on the heat equation or the wave equation or [Lions, 1996] for results on compressible Navier - Stokes equations).

In spite of this, many times experimental evidence leads to conclude that the solutions are there. But supposing that this is true, that the solution of a given laminar problem exists, is this solution stable? Suppose for instance that we have developed such a robust FEM numerical code that we can solve, say, an incompressible backwards facing step flow at Reynolds numbers of about 5000. The weak laminar solution exists, because we have found it. Is it real? Could we find it in nature? What is the experimental evidence saying about that? It seems that in many cases, laminar approximations work really well. But not always. At what extent laminar flow simplifications follow real cases? Which is its range of applicability?

The fact is that although our laminar solution exists, it turns to be highly *unstable* and even the most tiny perturbation at the inlet will propagate inwards and grow,

unleashing a very complex phenomenon: turbulence. Nature is as crowded of highly complex problems as science of awkward human simplifications, more available to our understanding. In 1880, Osborne Reynolds carried out a series of famous experiments ([Reynolds, 1883], cited in [McComb, 1990]) in the Owens College, in Manchester University. He experimented over the flow through a pipe, discovering that its overall behavior depends on a number (called after him Reynolds Number):

$$Re = Ud/\nu,$$

where d is the diameter of the pipe, U the inflow velocity (calculated taking into account the caudal and the section of the pipe) and ν the kinematic viscosity. For low Re, the flow remains laminar, with a parabolic profile all along the pipe. But if Re goes beyond some critical Re^{cr}, the flow suddenly becomes turbulent at some distance from the pipe entrance, being that critical value about 2000. By increasing Re number, the turbulent region extends more and more. The effect is to change the parabolic profile. Hence, it can be concluded that beyond Re^{cr}, flow is *a) unstable to small perturbations* and *b) highly sensitive to small perturbations in the inflow conditions.*

Two different approaches can be faced: to study either the transition from laminar to turbulent flow or the fully developed turbulence. Due to the inherent extreme complexity of the turbulence problem, each of these subjects can be considered almost as independent ones, and since O. Reynolds times, huge efforts were done in both directions, tackling the problems from several fronts: theoretical, experimental and, in more recent years, computational. Here, we work on a possible technique belonging to the field of CFD, analyzing a small bunch of turbulent models. In the previous sections, we have shown the development of a general algorithm for solving laminar flow problems, the CBS algorithm. Now, taking profit of its generality, we extend it to more realistic turbulent problems. Our goal is not to produce a model itself but to assess some known models by building a "numerical laboratory". The use of the same numerical algorithm over the different models provides a good gauge for testing them (e.g. [Krishnamurty and Shyy, 1997] or [Barakos and Drikakis, 1998]).

What does it mean "fully developed turbulence"? What is the fundamental difference between laminar, the kind of flow considered so far, and turbulent flow? It is very difficult and therefore very controversial to define "turbulent flow" but some of its characteristics can be pointed out ([Batchelor, 1953, Landau and Lifshitz, 1987, Lesieur, 1990, McComb, 1990]). Turbulent flow at large Re, far from Re^{cr}, is characterized by a highly fluctuating velocity field. This fluctuation seems to be random both in time and space and it is spread to the state variables: pressure, temperature and density. It is a time dependent process, developed in a wide range of scales, the larger the Re, the wider the range. $3D$ effects are very important due to vortex stretching:

energy in turbulent processes are transferred from large scale vortexes to small scales being vortex stretching, devoid of sense in $2D$, an important contribution. In principle, all the physics of the process should remain bounded to Navier - Stokes equations for turbulence is a continuum phenomenon. Much before the mean path of the molecules forming the fluid becomes important, all turbulence effects are thought to disapear due to the molecular viscosity. Also it exhibits much more efficient mixing properties than those of the molecular viscosity left alone.

In this chapter we first stress what kind of model we have chosen and why. Then, the turbulent flow equations are written down following this model. Next, CBS algorithm is extended to handle the enriched set of equations. Before the numerical examples, some of the compressible correction models are briefly described. Finally, in the next chapter, some numerical examples are shown.

5.1.1 Turbulent modelization

The amount of scales involved in real turbulence problems can be huge, increasing more and more as the Re gets larger and larger. If all the degrees of freedom are to be solved, it must be taken into account that this number can be estimated as $Re_L^{n^2/4}$, where n is the spatial dimension and Re_L is the Reynolds number calculated using as the distance the characteristic length of the energy containing eddies (see for instance the classic book by G.K. Batchelor [Batchelor, 1953]). Considering the computer power available in the days of this monograph (1998), this is a great hindrance. The finest resolution achieved using direct methods (DNS, see [Moin and Mahesh, 1998] for a recent review of these techniques), where the full set of Navier - Stokes is solved for all the scales, is 512^3 for homogeneous turbulence by J. Jiménez and co - workers ([Jiménez et al., 1993]) and S. Chen and co - workers ([Chen et al., 1993]) in 1993. This resolution corresponds to about a microscale Reynolds number of 170, orders of magnitude far away from those found in common life examples.

For that reason, one possible way out is to model the smallest scales. Following this line are many methods. The most common and most used in engineering problems are:

- **LES:** The Large Eddy Simulation (c.f. [Rogallo and Moin, 1984] or [Lesieur and Métais, 1996]) solves the Navier - Stokes equations only for the large scales, modeling the contribution of the smallest scales. The large scale flow equations are obtained by filtering the full scale equations using compact support distributions and spatial convolution.

- **N-equation models:** In these models, *mean* variables are solved and small turbulent variations effects are modeled (c.f. [Wilcox, 1993] for a wide modern review) using an eddy viscosity assumption and one, two or more evolution equa-

tions to calculate it. If instead it is calculated from some constants and mean flow properties, it is known as a 0-equation or algebraic model (mixing length models). The Averaged Navier - Stokes equations are obtained using an ensemble mean, or in practice, a spatial or temporal mean, but providing the ergodic hypothesis is accomplished [Batchelor, 1953]. Among the most common 2-equation models are $k-\varepsilon$, $k-\tau$ and $k-\omega$.

A method between DNS and LES has been very recently proposed by T. Dubois and co - workers, the Dynamic Multilevel (DML) ([Dubois et al., 1998]). Many other very different approaches are under work now. Among them are the two point closures of EDQNM (c.f [Lesieur, 1990]), the application of renormalization procedures in the RNG (c.f. [Smith and Woodruff, 1998]) or even the LBM (c.f. [Chen and Doolen, 1998]), which used simplified kinetic equations instead of Navier - Stokes ones.

We have chosen a 2-equation model: the $k-\varepsilon$, firstly proposed in
[Harlow and Nakayama, 1968] and completed in references like
[Launder and Spalding, 1974]. The reason of our choice is the simplicity for extending the CBS algorithm when the equations added have the same convection - diffusion - reaction character of the original Navier - Stokes set. Also, it is well known and used widespread in engineering and it can be corrected in many ways accounting for compressibility effects.

5.1.2 Taking averages

Suppose that a variable q can be decomposed in two parts, a mean field and a small perturbation:

$$q = \bar{q} + q'. \tag{5.1}$$

The mean part is obtained using one of the following definitions of the so called *Reynolds average*.

- Reynolds ensemble average:

$$\bar{q}(\boldsymbol{x},t) = \lim_{N\to\infty} \frac{1}{N} \sum_{1}^{N} n\, q_n(\boldsymbol{x},t)$$

- Reynolds spatial average:

$$\overline{q}(t) = \lim_{V\to\infty} \frac{1}{V} \iiint_V q(\boldsymbol{x}', t) d\boldsymbol{x}'$$

- Reynolds time average:

$$\overline{q}(\boldsymbol{x}) = \lim_{T\to\infty} \frac{1}{T} \int_{t-T}^{t+T} q(\boldsymbol{x}, t') dt'$$

The first average is taken *à la* Gibbs: not over one system, but over a collection of systems, all of them identical in composition and macroscopic condition but existing in different states. Such a collection is an *ensemble*. This average is more a construction of the mind than something that can be done in reality. Closer to the everyday experience are the next two. Spatial average is done over all the domain at the same time. Time average should be done all along the dynamical process. In this last case, when the system has very different time scales (for instance in the case of wake vortexes) instead of passing to the limit $T \to \infty$, if large scale characteristic time is T_{ls}, the small scale characteristic time is T_{ss} and it verifies that $T_{\text{ss}} \ll T_{\text{ls}}$, the average is

$$\overline{q}(\boldsymbol{x}, t) = \frac{1}{T_{\text{ls}}} \int_{t-T_{\text{ls}}}^{t+T_{\text{ls}}} q(\boldsymbol{x}, t') dt'.$$

This fact is sketched in fig. 5.1, where the thick curve represents the mean field and the thin and oscillating one represents the real field.

These definitions are important in order to understand what we mean by averaging the equations. It is possible that for a given problem, to take these averages could hide the real physics, like, for instance, in non-equilibrium turbulence. Therefore, in the problems considered here, ergodic hypothesis and large time scale separation of mean and turbulent variables are to be required.

For compressible flow problems, it is useful to define a mass weighted average, the *Favre average* ([Van Mieghem, 1949, Favre, 1965], cited in [Smits and Dussange, 1996])

$$q = \tilde{q} + q'', \tag{5.2}$$

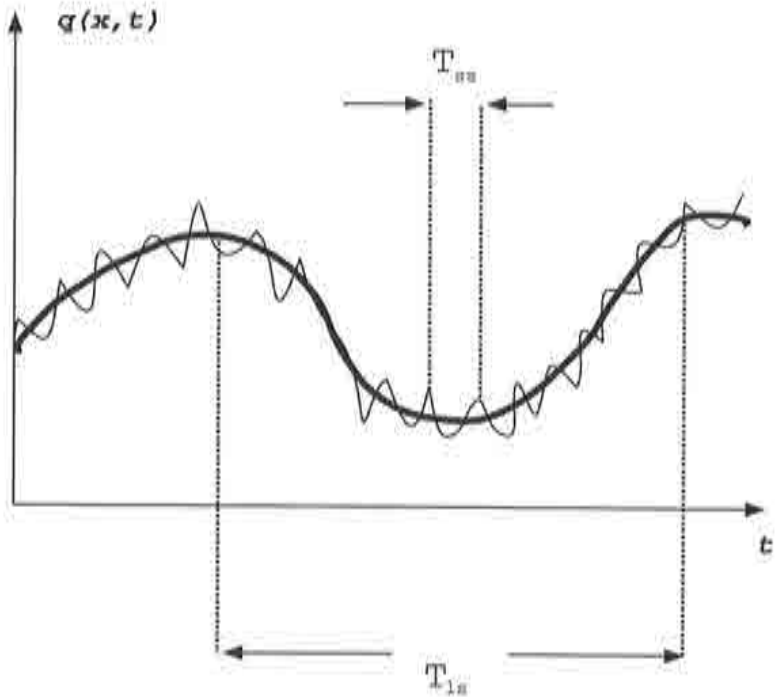

Figure 5.1: Flow time scales. The thick curve represents $\overline{q}(\boldsymbol{x},t)$ and the thin one, q($\boldsymbol{x}$,t).

according to

$$\overline{q} = \lim_{T\to\infty} \frac{1}{T\overline{\rho}} \int_{t-T}^{t+T} \rho(t')q(t')dt'.$$

As before, ensemble, spatial and time mass weighted averages can be calculated:

- Favre ensemble average:

$$\overline{q}(\boldsymbol{x},t) = \lim_{N\to\infty} \frac{1}{N\overline{\rho}} \sum_{1}^{N} n\,\rho_n(\boldsymbol{x},t)q_n(\boldsymbol{x},t)$$

- Favre spatial average:

$$\bar{q}(t) = \lim_{V\to\infty} \frac{1}{V\bar{\rho}} \iiint_V \rho(\boldsymbol{x},t')q(\boldsymbol{x}',t)d\boldsymbol{x}'$$

- Favre time average:

$$\tilde{q}(\boldsymbol{x}) = \lim_{T\to\infty} \frac{1}{T\bar{\rho}} \int_{t-T}^{t+T} \rho(\boldsymbol{x},t')q(\boldsymbol{x},t')dt'$$

And, when mean and oscillatory timescales can be separated to get time dependent mean flow,

$$\bar{q}(\boldsymbol{x},t) = \frac{1}{T_{\rm ls}} \int_{t-T_{\rm ls}}^{t+T_{\rm ls}} \rho(\boldsymbol{x},t')q(\boldsymbol{x},t')dt'.$$

From the definition of Favre average, it follows that

$$\tilde{q} = \frac{\bar{\rho q}}{\bar{\rho}} \tag{5.3}$$

$$\bar{\tilde{q}} = \bar{q} \tag{5.4}$$

$$\tilde{\bar{q}} = \bar{q} \tag{5.5}$$

By taking these averages over the flow fields, two scales can be separated. First, a scale that corresponds to the mean flow, $\bar{q}$ (or $\tilde{q}$), the large scale behavior of the system, associated with the large eddies. The bulk of the energy system is contained in these eddies, which remain in the inertial range where viscosity effects are small. As turbulent flow is seen at high Reynolds numbers, inertial range is far away from viscous range, where most of the energy is dissipated. Between them is q' (or q''), the second scale which is part of the real flow according to (5.1) (or (5.2)). It is a fluctuating field of high space or time frequencies and is characterized by small eddies, of low energy. Energy comes from large eddies and is drained through smaller and smaller ones until viscosity effects dissipate it.

The aforementioned closure models (and many more) are based on this kind of flow scales separation. As we will show in the next section, fluctuation terms are present

in the mean flow equations. Because we are not able to solve them, they should be modeled in terms of the mean values in one way or another.

5.1.3 Turbulent flow equations: Averaged Navier-Stokes

Now that we know how to take means of fields, we can study their evolution by averaging the equations governing the dynamics of the system. It is then obtained the so called *Averaged Navier-Stokes* (ANS) set. The solutions to the ANS comprise the mean flow: the mean density, momentum and total energy and the derived physical quantities. Whereas the use of Reynolds averages produces the same kind of mean fields (Reynolds mean fields), Favre average gives a mixed set: Favre mean conservative variables $\bar{\rho}$, $\tilde{U}_i$ and $\tilde{E}$ (also $\tilde{p}$) and Reynolds mean derived quantities $\bar{u}_i$, $\tilde{e}$ or $\tilde{T}$. This fact is one of the distinctive features of compressible flow.

For a given variable $q(u_i, t)$, the difference $\bar{q} - \tilde{q}$ depends on mean density gradients, because from the definitions above it follows that for constant density both averages coincide. In [Smits and Dussauge, 1996] it is shown that for some kinds of flow this difference is related to

$$M_t^2 = \left(\frac{\overline{|u''|}}{\bar{c}} \right)^2 ,$$

the turbulent Mach number, which for instance, for an adiabatic boundary layer of freestream Mach number $M = 3$ is about 0.2, or for strongly cooled wall flows at $M = 7.2$ is about 0.4. In this cases, to consider $\bar{u}_i - \tilde{u}_i \simeq 0$ produces errors below 5%. However, for mixing layers or jets, M_t can be high even for low M. Some authors, like J.R. Ristorcelli [Ristorcelli, 1993] have proposed compressibility corrections to account for this effect, which can be assessed using algorithms like the one proposed here.

The set of ANS is written below. It is obtained from the laminar set by first replacing the variables by the mean ones + the fluctuating part, and then by taking the Reynolds mean. The first step can be done using either (5.1) or (5.2), being the last one particularly useful in the case of compressible flow. In any case, both are the same for incompressible flow. In this work we have chosen (5.2).

Reynolds Averaged Continuity Equation:

$$\frac{\partial \bar{\rho}}{\partial t} + \frac{\partial}{\partial x_i}(\bar{\rho}\tilde{u}_i) = 0, \tag{5.6}$$

or

$$\frac{\partial \bar{\rho}}{\partial t} + \frac{\partial \bar{U}_i}{\partial x_i} = 0 \tag{5.7}$$

It is very clear in this equation the effect of using Favre average: fluctuating terms are absent. Therefore, $\tilde{u}_i$ can be regarded as the mean mass transport velocity. On numerical grounds, it is convenient also because the solver for this equation is exactly the same as that for laminar flow.

Reynolds Averaged Linear Momentum Conservation Equation:

$$\frac{\partial \bar{U}_j}{\partial t} + \frac{\partial}{\partial x_i}\left(\overline{u_i U_j} - \bar{\tau}_{ij} + \delta_{ij}\bar{p}\right) + \overline{\rho g_j} = 0, \tag{5.8}$$

which by expanding the convective flux by means of the (5.2) velocity decomposition,

$$\frac{\partial}{\partial x_i}\left(\overline{u_i U_j}\right) = \frac{\partial}{\partial x_i}\left(\bar{\rho}\tilde{u}_i\tilde{u}_j\right) + \frac{\partial}{\partial x_i}\left(\overline{\rho u_i'' u_j''}\right)$$

becomes

$$\frac{\partial \bar{U}_j}{\partial t} + \frac{\partial}{\partial x_i}\left(\bar{\rho}\tilde{u}_i\tilde{u}_j - \bar{\tau}_{ij} + \delta_{ij}\bar{p}\right) + \overline{\rho g_j} = \frac{\partial}{\partial x_i}\left(-\overline{\rho u_i'' u_j''}\right). \tag{5.9}$$

Again, terms containing density fluctuations are not present and thus no third order correlations of the kind

$$\frac{\partial}{\partial x_i}\left(-\overline{\rho' u_i' u_j'}\right)$$

appears. The only difference with the equation for laminar flow is the right hand side term. Unlike the continuity equation, this one contains fluctuating contributions, making evident the closure problem.

Reynolds Averaged Total Energy Conservation Equation:

$$\frac{\partial \bar{E}}{\partial t} + \frac{\partial}{\partial x_i}\left(\overline{u_i(\rho e + p)} - \overline{u_j \tau_{ij}} + \bar{q}_i\right) + \overline{\rho u_i g_i} + \overline{\rho r} = 0. \tag{5.10}$$

Some of these terms can be rearranged or simplified. We consider them separately.

- Total energy definition: total energy $\bar{E}$ can be decomposed in mean internal and kinetic energies and turbulent kinetic energy k, which is the double velocity correlation term. Its definition allows to re-write the time derivative of the energy:

$$k := \frac{\widetilde{u_i'' u_i''}}{2}, \tag{5.11}$$

$$\frac{\partial \bar{E}}{\partial t} = \frac{\partial}{\partial t}(\bar{\rho}\tilde{e}) = \frac{\partial}{\partial t}\left(\bar{\rho}(\tilde{e}_o + \frac{\tilde{u}_i \tilde{u}_i}{2} + k)\right). \tag{5.12}$$

- Convective transport of total energy: using the fact that

$$\overline{u_i E} = \overline{u_i \rho e} \tag{5.13}$$

and decomposing velocity and total energy in mean and fluctuating parts, it is obtained

$$\frac{\partial}{\partial x_i}(\overline{u_i E}) = \frac{\partial}{\partial x_i}(\bar{\rho}\tilde{u_i}\tilde{e}) = \frac{\partial}{\partial x_i}(\bar{\rho}\tilde{u_i}\tilde{e}) + \frac{\partial}{\partial x_i}(\bar{\rho}\widetilde{u_i'' e''}),$$

Then,

$$\frac{\partial}{\partial x_i}(\overline{u_i E}) = \frac{\partial}{\partial x_i}(\bar{\rho}\tilde{u}_i\tilde{e}) + \frac{\partial}{\partial x_i}\left(\bar{\rho}\widetilde{u_i'' e_o''} + \bar{\rho}\tilde{u}_j\widetilde{u_i'' u_j''} + \bar{\rho}\frac{\widetilde{u_i'' u_j'' u_j''}}{2}\right), \tag{5.14}$$

because $e'' = e_o + u_i'' u_j''/2 + \tilde{u}_i u_j''$ (the last term disapears when Favre-averaging). Note that in this equation it has appeared a third order correlation term in the velocities.

- Convective transport of pressure: Pressure is decomposed in $p = \bar{p} + p'$ and velocity $u = \tilde{u} + u''$, so

$$\frac{\partial}{\partial x_i}(\overline{u_i p}) = \frac{\partial}{\partial x_i}(\tilde{u}_i\bar{p} + \overline{u_i'' p'} + \overline{u_i''}\bar{p}). \tag{5.15}$$

Pressure and velocity are decomposed using different averages. Then, the third term is of a special kind because it follows from the mean definitions that $\overline{u_i''} \neq 0$ in compressible flow.

- Heat dissipated by thermal flux: from the Fourier law, and taking $T = \tilde{T} + T''$,

$$\frac{\partial \bar{q}_i}{\partial x_i} = \frac{\partial}{\partial x_i}(-\kappa\overline{\frac{\partial T}{\partial x_i}}) = \frac{\partial}{\partial x_i}(-\kappa\frac{\partial \tilde{T}}{\partial x_i}) + \frac{\partial}{\partial x_i}(-\kappa\overline{\frac{\partial T''}{\partial x_i}}). \tag{5.16}$$

We suppose $\kappa \simeq \bar{\kappa}$.

- Heat dissipated by Joule effect: again, $u = \tilde{u} + u''$. Then

$$\frac{\partial}{\partial x_i}(-\overline{\tau_{ij}u_j}) = -\frac{\partial}{\partial x_i}(\bar{\tau}_{ij}\tilde{u}_j + \overline{\tau_{ij}u_j''}). \tag{5.17}$$

The last term of this and the previous equations represent heat transported and dissipated by turbulence phenomena.

- Source terms: finally, the power of volume sources and heat sources are

$$\overline{\rho u_i g_i} = \bar{\rho}\tilde{u}_i g_i \tag{5.18}$$

$$\overline{\rho r} = \bar{\rho} r. \tag{5.19}$$

Then,

$$\frac{\partial \hat{E}}{\partial t} + \frac{\partial}{\partial x_i}(\bar{\rho}\tilde{u}_i\tilde{e}) + \frac{\partial}{\partial x_i}(\tilde{u}_i\bar{p} - \kappa\frac{\partial \tilde{T}}{\partial x_i} - \bar{\tau}_{ij}\tilde{u}_j) + \bar{\rho}\tilde{u}_i g_i + \bar{\rho} r$$

$$= -\frac{\partial}{\partial x_i}(\bar{\rho}\widetilde{u_i''e_o''} + \overline{u_i''p'} + \overline{u_i''}\bar{p} + \bar{\rho}\frac{\widetilde{u_i''u_j''u_j''}}{2} + \overline{\rho u_i''u_j''}\tilde{u}_j - \kappa\overline{\frac{\partial T''}{\partial x_i}} - \overline{\tau_{ij}u_j''}). \tag{5.20}$$

As in the momentum equation, all the terms containing fluctuations are placed at the right hand side. Again, no density fluctuation is present and the ANS have the same form as the laminar set plus the divergence of a flux. As written here, the set keeps the same conservation form which is very convenient for numerical purposes.

Hitherto, it can be seen that right members present the difficulty that they cannot be evaluated directly and must be modeled in some way. Keeping this in mind, to the ANS set, a new transport equation is added: the turbulence kinetic energy transport one. Multiplying u'' times the momentum equation and taking the Reynolds average, an exact equation for k is obtained.

$$\frac{\partial}{\partial t}(\bar{\rho}k) + \frac{\partial}{\partial x_i}(\bar{\rho}\tilde{u}_i k) = \frac{\partial}{\partial x_i}(-\bar{\rho}\frac{\widetilde{u_i''u_j''u_j''}}{2} - \overline{u_i''p'} + \overline{\tau_{ij}u_j''})$$

$$+\overline{\rho u_i''u_j''}\frac{\partial \tilde{u}_j}{\partial x_i} - \overline{\tau_{ij}\frac{\partial u_j''}{\partial x_i}} + \overline{p'\frac{\partial u_i''}{\partial x_i}} - \overline{u_i''}\frac{\partial \bar{p}}{\partial x_i}. \tag{5.21}$$

This additional transport equation is motivated by the fact that through the definition of total energy, where quadratic terms in the velocity are present, it was obtained a new variable, k, defined as the turbulent kinetic energy, and that an exact transport equation for it can be derived.

By adding equations in this way, it is very clear the closure problem: the correlation order of the left hand sides is one less respect to the order of the right hand sides. Hence, for the momentum equation, a second order term is in the right member and for the mean total energy and the turbulent energy equations, the right hand side contains third order terms. By modeling correlation terms this process is stopped. If done now, the model is called a 1-equation model. We go a little farther. The *dissipation rate* ε is defined as [Wilcox, 1993]:

$$\varepsilon := \overline{\tau_{ij} \frac{\partial u_i''}{\partial x_j}}, \tag{5.22}$$

which will turn to be an additional variable. This definition follows from the concept of *energy disipation* in laminar flow, which is defined as $\tau_{ij} \frac{\partial u_i}{\partial x_j}$. Some authors take an alternative definition [Launder and Spalding, 1974, Lele, 1994]:

$$\varepsilon_{\text{alt}} := \overline{\tau_{ij}'' \frac{\partial u_i''}{\partial x_j}}, \tag{5.23}$$

where

$$\begin{aligned}
\tau_{ij}'' &= 2\mu(s_{ij}'' - \frac{1}{3}\theta''\delta_{ij}), \\
s_{ij}'' &= \frac{1}{2}\left(\frac{\partial u_i}{\partial x_j}'' + \frac{\partial u_j}{\partial x_i}''\right), \\
\theta'' &= \frac{\partial u_i}{\partial x_i}''.
\end{aligned}$$

In [Tennekes and Lumley, 1972] it is shown that in general, $\tilde{\tau}_{ij}$ and τ_{ij}'', where $\tau_{ij} = \tilde{\tau}_{ij} + \tau_{ij}''$, correspond to very separate scales: the strain rate of large eddies and of small ones respectively. For that reason, $\tilde{\tau}_{ij}$ and $\overline{\frac{\partial u_i''}{\partial x_j}}$ are almost uncorrelated, and ε_{alt} is a good approximation to ε as defined in (5.22). We prefer to take (5.22) because in this form appears in the equation for k. However, ε_{alt} can be understood as a closer analogy to the mean flow energy dissipation $\tilde{\tau}_{ij} \frac{\partial \tilde{u}_i}{\partial x_j}$ due to the fact that no crossed terms fluctuation-mean flow appear.

The k-ε model, first proposed in [Harlow and Nakayama, 1968], is one of many possibilities of completing one-equation models. The most common two-equation models are based in that the turbulent viscosity μ_T is function of k and another variable, for which is derived a transport equation. Instead of ε, it can be chosen the specific dissipation rate ω [Kolmogorov, 1942], the turbulent length scale l [Rotta, 1951] or the turbulent dissipation time τ [Zeierman and Wolfshtein, 1986]. (all of them cited in [Wilcox, 1993]). These variables are related to each other [Launder and Spalding, 1974]:

$$l \sim k^{3/2} \qquad w \sim \varepsilon^2/k^2 \qquad \tau \sim k/\varepsilon, \tag{5.24}$$

Hence, evolution equations for each variable are also related and modelized terms can be compared. The relations above are obtained through dimensional analysis, which only said the kind of proportion but not what is the proportionality constant. An equation for ε evolution is then (c.f. [Launder and Spalding, 1974], [Wilcox, 1993], etc.) obtained:

$$\frac{\partial \bar{\rho}\varepsilon}{\partial t} + \frac{\partial}{\partial x_i}\left(\tilde{u}_i\bar{\rho}\varepsilon - (\mu + \frac{\mu_T}{\sigma_\varepsilon})\frac{\partial \varepsilon}{\partial x_i}\right) = \omega_\varepsilon(k,\varepsilon) \tag{5.25}$$

where

$$\omega_\varepsilon(k,\varepsilon) = C_{\varepsilon 1}\frac{\varepsilon}{k}P_k - C_{\varepsilon 2}\frac{\bar{\rho}\varepsilon^2}{k}, \tag{5.26}$$

$$P_k = R_{ij}\frac{\partial \tilde{u}_i}{\partial x_i}. \tag{5.27}$$

We will see in the next section the values of the constants and the meaning of R_{ij}.

The use of Favre instead of Reynolds average has allowed us to obtained a somewhat cleaner form of the ANS. For instance, using Reynolds average, the $\bar{U}_i$ equation becomes

$$\frac{\partial}{\partial t}\left(\bar{\rho}\tilde{u}_j + \overline{\rho' u'_j}\right) + \frac{\partial}{\partial x_i}\left(\bar{\rho}\tilde{u}_i\tilde{u}_j - \bar{\tau}_{ij} + \delta_{ij}\bar{p}\right) + \overline{\rho g_j}$$

$$= \frac{\partial}{\partial x_i}\left(-\overline{\rho u'_i u'_j} - \bar{\rho}\widetilde{u'_i u'_j} - \tilde{u}_i\overline{\rho u'_j} - \tilde{u}_j\overline{\rho u'_i}\right). \tag{5.28}$$

But Favre average is no more than a mathematical artifice, the difficulties still remain there. Sometimes terms present using the Reynolds average are easier to understand on physical grounds than Favre's. This matter is deeply analyzed in the references [Spina et al., 1994] and [Smits and Dussauge, 1996].

Closure modeled terms

In the context of k - ε models, the following hypotheses can be used to close the set of equations ([Wilcox, 1993, Smits and Dussauge, 1996, Krishnamurty and Shyy, 1997]):

Reynolds stress tensor:

In compressible flow, using Favre means, it holds

$$R_{ij} := -\overline{\rho u''_i u''_j} \approx 2\mu_T\left(\tilde{s}_{ij} - \frac{1}{3}(\tilde{\theta} + k\bar{\rho})\delta_{ij}\right), \tag{5.29}$$

which is the so called Boussinesq approximation. It assumes that the Reynolds stress tensor R_{ij} is proportional in its principal axes to the mean strain-rate tensor $\tilde{s}_{ij}$, with the turbulent viscosity μ_T as the proportionality constant, in analogy with the laminar stress τ_{ij} and strain-rate tensor s_{ij}. Mean strain tensor $\tilde{s}_{ij}$ and dilatation $\tilde{\theta}$ are calculated as in the laminar case, but using $\tilde{u}_i$. Turbulent viscosity is

$$\mu_T := C_\mu f_\mu \bar{\rho}\frac{k^2}{\varepsilon}, \tag{5.30}$$

Where C_μ is a constant which depends on the model (0.9 in k-ε model), and f_μ is a function used when so called Low Reynolds models are used. In that case, the equations are integrated down to the physical wall, where gradients of mean and turbulent variables can be strong. f_μ then depends on some kind of distance to the wall. When the law of the wall is used, it takes the constant value 1.0.

Next, the modelized terms corresponding to total mean energy and turbulent kinetic energy transport equations are briefly described. Some of them are due to compressibility effects and in incompressible problems they are absent. In [Lele, 1994], an analysis of energy transfers between turbulent and mean ranges is done. There are some terms appearing in both $\tilde{E}$ and k equations which couple their evolution. The analysis is done by separating the effects of turbulence on mean kinetic and internal energies and turbulent kinetic energy.

Phenomenological, dimensional or simply based on experience arguments are behind these hypotheses. The goal is to model fluctuation containing terms as functions of mean variables. In [Wilcox, 1993], it is stated a triple rule-of-thumb for any assumption on this matter:

1. All closure approximations should approach the proper limiting value for Mach number and density fluctuations tending to zero.
2. All closure terms should be written in proper tensor form, e.g., not dependent upon a specific geometrical configuration.
3. All closure approximations should be dimensionally consistent and invariant under a Galilean transformation.

Following these ideas, the hypothesis chosen in this work are:

Turbulence heat flux:

It is usually approximated as

$$\widetilde{\bar{\rho} u_i'' e_o''} \approx \frac{C_v \mu_T}{Pr_T} \frac{\partial \tilde{T}}{\partial x_i}, \tag{5.31}$$

where the *turbulent thermal diffusivity* can be taken as $\kappa_T = \dfrac{C_v \mu_T}{Pr_T}$, being Pr_T the *turbulent Prandtl number*. This coefficient is usually a constant (0.89 or 0.90 for boundary layers). Sometimes, instead of $\widetilde{\bar{\rho} u_i'' e_o''}$, the approximation is done including pressure convection, upon the enthalpy h, defined for ideal polytropic gases as

$$h = e_o + \frac{p}{\rho} = C_p T,$$

by taking

$$\bar{\rho}\widetilde{u_i''h''} \approx \frac{C_p\mu_T}{Pr_T}\frac{\partial \tilde{T}}{\partial x_i}. \tag{5.32}$$

Pressure correlation terms:

$$\overline{u_i''}\bar{p} = 0. \tag{5.33}$$

As seen before, the turbulent mass flux $\overline{u_i''}$ can be neglected in some cases like when considering low Mach number boundary layers for instance. When this is not possible, there exist some alternative models, like the mentioned of [Ristorcelli, 1993] or that studied in [Speziale and Sarkar, 1991].

Enthalpic production of turbulence:

Concerning turbulent mass flux $\overline{u_i''}$, the same comments as in the preceding term can be done here. In this case, this term corresponds more to inertial response of the turbulent flow upon mean pressure gradients than to compressibility effects [Lele, 1994]. The work done by pressure gradients produces a gain in kinetic energy both of mean and turbulent flows. As a simple approximation for low Mach number flows, we assume here

$$\overline{u_i''}\frac{\partial \bar{p}}{\partial x_i} \approx 0. \tag{5.34}$$

Pressure dilatation correlation:

In this case, too, we take as a simple first approximation

$$\overline{p' \frac{\partial u_i''}{\partial x_i}} \approx 0 \tag{5.35}$$

which seems to be reasonable in low Mach number shear flows. In reviews like that of [Krishnamurty and Shyy, 1997] or [Speziale et al., 1994], some models like that of [Sarkar, 1992] are assessed. Depending on its sign, it represents a loss from k and a gain of mean internal energy or vice versa [Lele, 1994].

Turbulent transport of k:

In [Krishnamurty and Shyy, 1997] it is suggested to model together

$$\overline{\tau_{ij} u_j''} - \overline{u_i'' p'} - \frac{\overline{u_i'' u_j''} u_j''}{2} = \left(\mu + \frac{\mu_T}{\sigma_k}\right) \frac{\partial k}{\partial x_i}. \tag{5.36}$$

The first term corresponds to $\mu \dfrac{\partial k}{\partial x_i}$, the molecular diffusion of turbulence and the next two, to $\dfrac{\mu_T}{\sigma_k} \dfrac{\partial k}{\partial x_i}$, the turbulent transport itself.

Turbulent heat diffusion:

In [Smits and Dussauge, 1996], it is stressed that, for boundary layer compressible flows, when MM_t and M_t^2 are small compared to one, it seems reasonable to take

$$\overline{\kappa \frac{\partial T}{\partial n}} \approx \bar{\kappa} \frac{\partial \tilde{T}}{\partial n},$$

where n represents the direction normal to the wall. Considering the fact that in boundary layers streamline gradients of T are generally much smaller than crosswind ones, i.e. normal to the wall, it can be assumed that

$$\overline{\kappa \frac{\partial T}{\partial x_i}} \approx \bar{\kappa} \frac{\partial \tilde{T}}{\partial x_i},$$

and hence

$$\overline{\kappa \frac{\partial T''}{\partial x_i}} \approx 0. \tag{5.37}$$

Turbulence dissipation:

It is defined as

$$\overline{\tau_{ij} \frac{\partial u_i''}{\partial x_i}} = \bar{\rho}\varepsilon \tag{5.38}$$

according to the remarks done above.

Reynolds tensor flux:

With the definition of Reynolds tensor, it follows

$$\bar{\rho}\tilde{u}_j \widetilde{u_i'' u_j''} = R_{ij}\tilde{u}_j. \tag{5.39}$$

In 5.1.3, the complete set to solve is written down. There, per - unit - volume turbulence kinetic energy and dissipation are defined as

$$\begin{aligned} K &:= k\bar{\rho}, \\ D &:= \varepsilon\bar{\rho}. \end{aligned} \tag{5.40}$$

The turbulence sources $\omega_k(k,\varepsilon)$ and $\omega_\varepsilon(k,\varepsilon)$ depend on the k - ε model used. According to the standard Jones and Launder model (e.g. see [Launder and Spalding, 1974]),

$$\frac{\partial \bar{\rho}}{\partial t} + \frac{\partial \bar{U}_i}{\partial x_i} = 0$$

$$\frac{\partial \bar{U}_j}{\partial t} + \frac{\partial}{\partial x_i}\left(\bar{\rho}\tilde{u}_i\tilde{u}_j - \bar{\tau}_{ij} + \delta_{ij}\bar{p}\right) + \rho\bar{g}_j = \frac{\partial R_{ij}}{\partial x_i}$$

$$\frac{\partial \bar{E}}{\partial t} + \frac{\partial}{\partial x_i}\left(\tilde{u}_i\bar{E} + \tilde{u}_i\bar{p} - \kappa\frac{\partial \tilde{T}}{\partial x_i} - \bar{\tau}_{ij}\tilde{u}_j\right) + \bar{U}g_i + \bar{\rho}r =$$

$$= \frac{\partial}{\partial x_i}\left(-\kappa_T\frac{\partial \tilde{T}}{\partial x_i} + (\mu + \frac{\mu_T}{\sigma_k})\frac{\partial k}{\partial x_i} + \tilde{u}_j R_{ij}\right)$$

$$\frac{\partial K}{\partial t} + \frac{\partial}{\partial x_i}\left(\tilde{u}_i K - (\mu + \frac{\mu_T}{\sigma_k})\frac{\partial k}{\partial x_i}\right) = \omega_k(k,\varepsilon)$$

$$\frac{\partial D}{\partial t} + \frac{\partial}{\partial x_i}\left(\tilde{u}_i D - (\mu + \frac{\mu_T}{\sigma_\varepsilon})\frac{\partial \varepsilon}{\partial x_i}\right) = \omega_\varepsilon(k,\varepsilon)$$

Table 5.1: Averaged compressible Navier-Stokes equations

$$\omega_k = P_k - D, \tag{5.41}$$

$$\omega_\varepsilon = C_{\varepsilon 1}\frac{D}{K}P_k - C_{\varepsilon 2}\frac{D^2}{K}, \tag{5.42}$$

$$P_k = R_{ij}\frac{\partial \tilde{u}_i}{\partial x_j}, \tag{5.43}$$

and the constants are

$$C_\mu = 0.09, \quad \sigma_k = 1.0, \quad \sigma_\varepsilon = 1.3, \quad C_{\varepsilon 1} = 1.44, \quad C_{\varepsilon 2} = 1.92,$$
$$f_\mu = 1.0. \tag{5.44}$$

5.1.4 Boundary conditions. The law of the wall

Turbulent models like k-ε , the one adopted here, were devised with one objective: the reduction of the range of significant problem scales in high Re turbulent flow, because should all the physical scales had to be solved, the huge number of degrees of freedom involved would make the problem unsolvable, at least with the computing facilities available nowadays. Another way of still reduce the degrees of freedom of a given turbulent problem is to avoid regions very close to walls, where very strong velocity gradients are present. There, a lot of grid points must be placed to solve flow behavior properly. A useful and widespread technique for doing this is the so called *law of the wall*. By means of this technique, a *numerical* wall is placed in an off position from the real physical wall, where no-slip condition should be imposed in velocities. Where to place it and what conditions are appropriate there can be analyzed following this reasoning [Wilcox, 1993, Smits and Dussauge, 1996, Landau and Lifshitz, 1987].

Flow at high Re number, whether compressible or not, around a rigid body can be separated in two regions: an outer region, where turbulent viscous effects dominate over molecular viscosity ones, and an inner region, where molecular viscosity reigns over turbulence effects. Momentum flow equations can then be simplified as one gets closer to one region coming from the other if some assumptions are done.

In fig. 5.1.4 it is shown the vicinity of a flat plate. Within the inner layer, it is assumed that [Smits and Dussauge, 1996]:

1. Convective terms are small against viscous ones.

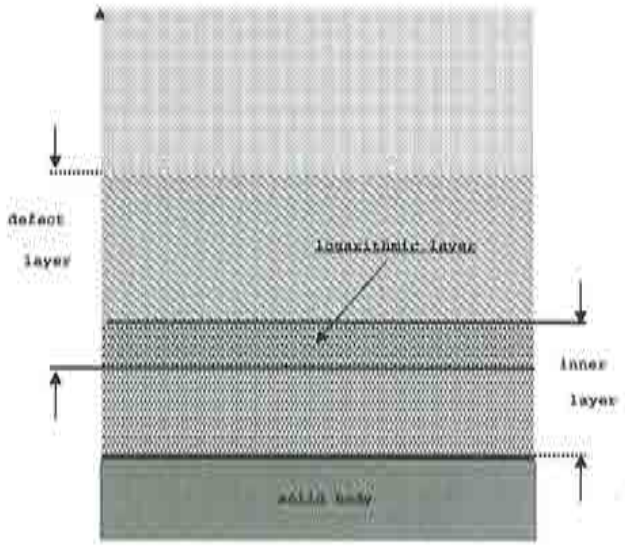

Figure 5.2: Defect layer, inner layer and their overlapping zone: the log layer.

2. Pressure gradients are small too and can be ignored.
3. Total stress

$$\tau = \mu \frac{\partial \bar{u}_x}{\partial y} - \rho R_{xy} = \tau_w$$

is constant. As for the moment we ignore compressibility effects, we consider $\bar{u} = \tilde{u}$. Subscript w means "evaluated on the wall",

Closer to the wall, where $\mu_T \ll \mu$ the solution of the momentum equation gives

$$u^+ \quad := \frac{\bar{u}}{u_*} = \frac{\rho u_*}{\mu} =: \quad y^+ \tag{5.45}$$

that is the velocity increases linearly with the normal distance to the wall. u^+ and y^+ are velocity and distance normalized according to (5.45). u_* is the friction velocity, which provides an estimate of the inner layer length scale l_{rmscin},

$$l_{rmscin} = \frac{\mu}{\rho u_*},$$

being $\sqrt{\frac{\tau_w}{\rho_w}}$.

On the other hand, in the neighboring region of the inner layer, viscous effects still are much stronger than convective ones, but $\mu_T \sim \mu$. This region is called the defect layer and have a more complicated velocity scaling with distance. The outer and inner limits of the defect layer are blurred and so the outer limits of the viscous inner layer. But what is certain (generally assumed, at least) is what C.B.A. Millikan ([Millikan, 1938], referenced in [Smits and Dussauge, 1996]) proposed: both regions are expected to have an overlapping zone for large Re numbers. By imposing some matching conditions, a logarithmic law of the wall can be obtained. This law relates again mean velocity with distance to the wall through friction velocity, and is independent of inner and outer length scales. Its expression is

$$\frac{\tilde{u}}{u_*} = \frac{1}{\chi} \log\left(\frac{u_* \Delta}{\nu}\right) + C, \tag{5.46}$$

where Δ is the approximate length of the viscous sub layer, or the distance from the "numerical" wall to the physical one, $\chi = 0.41$ is the so called von Karman constant and C is around 5.5. It is usually assumed that the logarithmic, *log*, layer holds approximately in the range $30 \leq y^+ \leq 100$.

The knowledge of the velocity distribution in this region has been a great aid for many years ([Launder and Spalding, 1974], for instance) because the numerical computation domain wall can be transported inwards upto these regions, where velocity gradients are not so high. Table 5.2 shows the boundary conditions for the k-ε model imposed there and in the rest of the contours. Suppose the domain described in the fig. 5.1.4, where Γ_D is a Dirichlet (velocity) contour, Γ_N, a Neumann (velocity) contour and Γ_M, a mixed (velocity) contour. The first one corresponds to inflows or far field conditions. The last one, to wall law contours. Neumann boundaries are the rest: the condition on the normal gradients imposed to zero is widespread used.

Whereas at the physical wall no slip condition is imposed, up in the logarithmic region, tangential velocity is set free, normal imposed to zero and traction is imposed to a value evaluated using the wall law. Besides, k and ε conditions can also be fixed there in a consistent way. k condition value is taken from considering there that turbulent energy production equals turbulent energy dissipation and ε, from using dimensional arguments. Using the law of the wall, lot of computational time and storage could be saved, for the spatial grid can be coarser in the boundary layers. This law is used equally with other turbulence models ([Wilcox, 1993], [Grotjans and Menter, 1998], [Frink, 1998], etc.).

In compressible flow, things can be much more complex (see [Wilcox, 1993] or

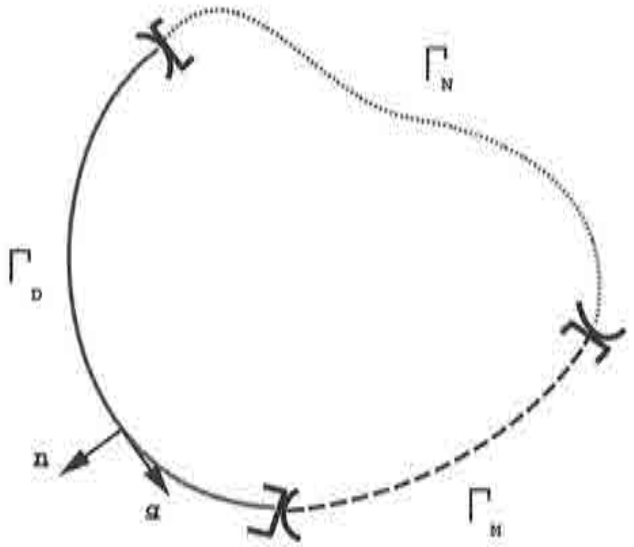

Figure 5.3: Numerical domain sketch.

	Γ_D	Γ_N	Γ_M
Velocity u_i	$u_i = u_i^p$	$n_i \tau_{ij} = t_j^p$	$u_i n_i = u_n^p$ $n_i \tau_{ij} g_j = t_s^p$
$k-\varepsilon$	$k = C_{bc} u_i u_i$ $\varepsilon = C_\mu \frac{k^{3/2}}{L}$ or $\varepsilon = C_\mu f_\mu \rho \frac{k^2}{\mu_T^{rel}}$	$\frac{\partial k}{\partial x_i} = 0$ $\frac{\partial \varepsilon}{\partial x_i} = 0$	$t_i = -\rho u_*^2 \frac{\tilde{u}_i}{\tilde{u}}$ $k = \frac{u_*^2}{\sqrt{C_\mu}}$ $\varepsilon = \frac{u_*^3}{\chi \Delta}$

Table 5.2: Boundary conditions for the k-ε model.

[Smits and Dussauge, 1996]). But in some cases, density variations can have a negligible effect within the viscous layer, allowing the use of the incompressible wall law. It seems that this happens when Morkovin Hypothesis holds: compressible effects may not have strong effects on turbulent compressible boundary layers at least at non-hypersonic flow (up to freestream $M = 5.0$) [Smits and Dussauge, 1996]. Many compressible corrections to the law of the wall were proposed by many authors for problems were this hypothesis is false (since pioneering work of [Van Driest, 1951], to [So et al., 1994] or [Huang et al., 1994]) which can be tested using CBS method.

On the other hand, the ANS equations can be integrated down to the wall. Within the inner viscous layer the strong gradients are solved by agglomerating more nodes. There lays the additional difference. Turbulent variables meaning, specially that of ε, becomes fuzzy due to the increment of molecular viscosity against turbulent eddy viscosity. In this case, a damping function f_μ is needed and constructed in many different ways (see [Barakos and Drikakis, 1998], [Mavriplis and Martinelli, 1994], [Bardina et al., 1997], [Hanine and Kourta, 1991], etc.)

As was said before, in CBS method Neumann conditions can be easily imposed through traction prescriptions (fig. 5.1.4). The first node of the numerical domain is slightly off the physical wall. There, a Neumann prescription can be weakly imposed on the traction in the equivalent to the equation (3.48) for turbulent cases ((5.55) ahead). Parameter Δ controls that the first nodes in the domain discretization (now nodes C) are within the log layer. The values of k-ε prescribed at inflows will determine the amount of turbulent kinetic energy which feeds the domain. This can be evaluated as a percentage of the mean flow kinetic energy, through the constant C_{tu}. Once k is fixed, ε and μ_{T} are to be calculated as their functions. One possibility is to fix inflow ε as a function of k and the mixing length L characteristic of the problem. Then the mixing length, which can be in turn set to a fraction of the characteristic length of the problem must be known *a priori*. Another option is to estimate a $\mu_{\text{T}}^{\text{inf}}$ for the inflow, which could be evaluated as a fraction of the reference laminar viscosity, or the laminar Re number. The inflow ε is calculated then as its function. We choose one or the other according to the kind of problem we are dealing with or from other researchers experience.

5.1.5 Weak form of the turbulent equations

As was said before, the turbulent equations of the k-ε model has the same convection - diffusion - reaction form of the original Navier - Stokes set, making the CBS model worth to be extended including them. Hence, time discretization along the characteristics, as was described for the laminar case in previous section, could be applied to the new transport equations and FEM used for spatial discretization. In order to keep the same spirit, both are explicitly advanced, using the same Δt that is calculated for the momentum equation except when reaction terms are thought to affect the stability of

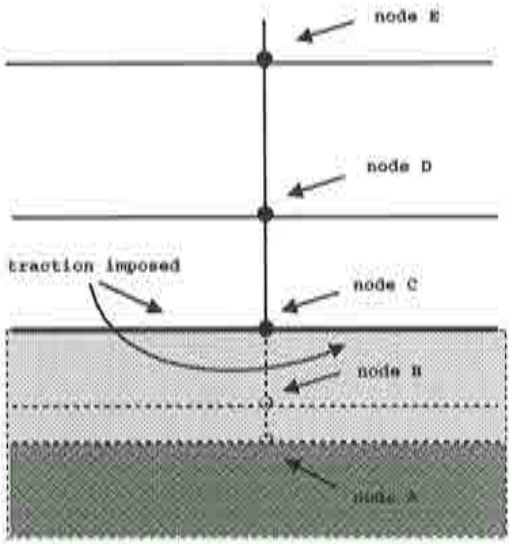

Figure 5.4: Law of the wall boundary conditions. First nodes are placed off the physical wall. u_* is evaluated at nodes C and traction is weakly prescribed there.

the enriched scheme.

The time discretized (along the characteristics) k-ε equations are

$$\frac{\Delta K^n}{\Delta t} = R_{\mathrm{K}}^n - \frac{\Delta t}{2} u_i^n \frac{\partial R_{\mathrm{K}}^n}{\partial x_i}, \tag{5.47}$$

$$\frac{\Delta D^n}{\Delta t} = R_{\mathrm{D}}^n - \frac{\Delta t}{2} u_i^n \frac{\partial R_{\mathrm{D}}^n}{\partial x_i}, \tag{5.48}$$

where R_{K}^n and R_{D}^n are the spatial residuals of the equations as are written in set 5.1.3.

The weak form of (5.47) and (5.48) can be obtained in the usual way. For both equations we project on the space of tests functions W, integrate the diffusion terms by parts and set the residuals to zero in the boundaries. Then

$$\int_\Omega W \frac{\Delta K^n}{\Delta t} d\Omega = -\int_\Omega W \frac{\partial}{\partial x_i}(\tilde{u}_i K) d\Omega - \int_\Omega \frac{\partial W}{\partial x_i}(\mu + \frac{\mu_T}{\sigma_k}) \frac{\partial k}{\partial x_i} d\Omega$$
$$+ \int_\Omega W \omega_\varepsilon(k, \varepsilon) d\Omega - \frac{\Delta t}{2} \int_\Omega \frac{\partial}{\partial x_i}(W \tilde{u}_i) R_K d\Omega, \tag{5.49}$$

$$\int_\Omega W\frac{\Delta D^n}{\Delta t}d\Omega = -\int_\Omega W\frac{\partial}{\partial x_i}(\tilde{u}_i D)d\Omega - \int_\Omega \frac{\partial W}{\partial x_i}(\mu+\frac{\mu_T}{\sigma_\varepsilon})\frac{\partial \varepsilon}{\partial x_i}d\Omega$$
$$+\int_\Omega W\omega_\varepsilon(k,\varepsilon)d\Omega - \frac{\Delta t}{2}\int_\Omega \frac{\partial}{\partial x_i}(W\tilde{u}_i)R_D d\Omega. \qquad (5.50)$$

In these equations, it is not present the boundary integral coming from the integration by parts of the diffusive terms. This should be calculated along the contours where both k and ε are freed. By not doing it, we are imposing that $n_i\frac{\partial k^n}{\partial x_i}$ and $n_i\frac{\partial \varepsilon^n}{\partial x_i}$ are zero. In the cases were this assumption is not correct a small localized $O(\Delta t)$ error would be present.

Diffusion terms can be slightly modified considering that the unkowns are K and D instead of k and ε:

$$\begin{aligned}\frac{\partial k}{\partial x_i} &= \frac{1}{\bar{\rho}}\frac{\partial K}{\partial x_i} - \frac{K}{\bar{\rho}^2}\frac{\partial \bar{\rho}}{\partial x_i},\\ \frac{\partial \varepsilon}{\partial x_i} &= \frac{1}{\bar{\rho}}\frac{\partial D}{\partial x_i} - \frac{D}{\bar{\rho}^2}\frac{\partial \bar{\rho}}{\partial x_i},\end{aligned} \qquad (5.51)$$

Now, renaming

$$\tilde{u}_i^c := \tilde{u}_i + (\mu+\frac{\mu_T}{\sigma})\frac{1}{\bar{\rho}^2}\frac{\partial \rho}{\partial x_i}$$

where σ is either σ_k or σ_ε according to which equation are we working on, (5.50) and (5.49) can be re written as

$$\int_\Omega W\frac{\Delta K^n}{\Delta t}d\Omega = -\int_\Omega W\frac{\partial}{\partial x_i}(\tilde{u}_i^c K)d\Omega - \int_\Omega \frac{\partial W}{\partial x_i}(\mu+\frac{\mu_T}{\sigma_k})\frac{1}{\bar{\rho}}\frac{\partial K}{\partial x_i}d\Omega$$
$$+\int_\Omega W\omega_\varepsilon(k,\varepsilon)d\Omega - \frac{\Delta t}{2}\int_\Omega \frac{\partial}{\partial x_i}(W\tilde{u}_i^c)R_K d\Omega, \qquad (5.52)$$

$$\int_\Omega W \frac{\Delta D^n}{\Delta t} d\Omega = -\int_\Omega W \frac{\partial}{\partial x_i}(\tilde{u}_i^c D) d\Omega - \int_\Omega \frac{\partial W}{\partial x_i}(\mu + \frac{\mu_T}{\sigma_\varepsilon}) \frac{1}{\bar{\rho}} \frac{\partial D}{\partial x_i} d\Omega$$
$$+ \int_\Omega W \omega_\varepsilon(k, \varepsilon) d\Omega - \frac{\Delta t}{2} \int_\Omega \frac{\partial}{\partial x_i}(W \tilde{u}_i^c) R_D d\Omega. \tag{5.53}$$

5.2 The CBS algorithm extension to turbulent flows

Now that we have written the weak form of the turbulent variables equations, let us take a look at the ANS for the mean variables. By using Favre average, we have gotten rid of the fluctuating field in the continuity equation. Then, the continuity equation for mean variables is the same as the original, except, of course that now the unknowns are mean ones. Its discretization, solution, and boundary conditions are therefore treated in the same way as was done for the laminar case. The only slight exception is that for incompressible cases, we could replace the mean pressure by an effective mean pressure

$$\bar{p}^{\text{eff}} := \bar{p} + \frac{2}{3} k \tag{5.54}$$

before solving it, motivated by the fact that in the diagonal of the Reynolds stress tensor appears $\frac{2}{3} k \delta_{ij}$. This is no more than a programming advantage, because effective pressure is not physical at all. In this way, continuity equation solver need not any information about turbulent variables. Pressure fluctuations also are absent because fractional step stabilization is done only using mean pressure. In compressible flow, the same comments stands, except for the fact that we generally put boundary conditions upon the density, so (5.54) is not necessary.

Being the split the same as before, the linear momentum equation is divided in two. Momentum correction equation is also free of fluctuations. The only two ANS equations with turbulent contributions are fractional momentum and energy ones.

5.2.1 Fractional momentum equation

The weak form of the ANS for the fractional momentum is

$$\int_\Omega \tilde{W}_i \frac{\Delta \tilde{U}_i^n}{\Delta t} d\Omega = -\int_\Omega \tilde{W}_i \frac{\partial}{\partial x_i}(\tilde{u}_i \bar{U}_j) d\Omega - \int_\Omega \frac{\partial W}{\partial x_i}(\bar{\tau}_{ij} + R_{ij}) d\Omega + \int_\Gamma \tilde{W}_i n_i (\bar{\tau}_{ij} + R_{ij}) \, \mathrm{d}\Gamma - \int_\Gamma \tilde{W}_i \bar{p} g_j \, \mathrm{d}\Gamma - \frac{\Delta t}{2} \int_\Omega \frac{\partial}{\partial x_i}(W \tilde{u}_i) \hat{R}_j d\Omega. \tag{5.55}$$

Now, boundary and volume integrals of diffusive terms contain a contribution coming from $\bar{\tau}_{ij} + R_{ij}$. From the definition of R_{ij}, it is clear that the strain rate tensor is now multiplied by $\mu_{tot} = \mu + \mu_T$ instead of μ. The consequence is that different time steps than those that would be obtained if only the molecular viscosity were used are obtained. Finally, $\hat{R}_j$ should be evaluated considering the spatial residual of the ANS equation, which again is set to zero at the boundaries.

5.2.2 Total Energy Equation

We use the total energy equation. Now the turbulent contribution is present in more terms. Heat flux and Joule effect terms are modified to account for the increased viscosity. Diffusion of the turbulent part of the total energy, the turbulent kinetic energy, also appears. The weak form is

$$\int_\Omega W_E \frac{\Delta \tilde{E}^n}{\Delta t} d\Omega = -\int_\Omega W_E \frac{\partial}{\partial x_i}(\tilde{u}_i(\tilde{E} + \tilde{p})) d\Omega - \int_\Omega W_E(\bar{U}_i g_i + \bar{\rho} r) d\Omega - \int_\Omega \frac{\partial W_E}{\partial x_i} \left((\kappa + \kappa_T) \frac{\partial \tilde{T}}{\partial x_i} + \tilde{u}_j(\bar{\tau}_{ij} + R_{ij}) + (\mu + \frac{\mu_T}{\sigma_k}) \frac{\partial k}{\partial x_i} \right) d\Omega + \int_{\Gamma_H} W_E H \, \mathrm{d}\Gamma - \frac{\Delta t}{2} \int_\Omega \frac{\partial}{\partial x_i}(W \tilde{u}_i) R_E d\Omega. \tag{5.56}$$

Again, like in the laminar case, on $\Gamma - \Gamma_H$ we assume that $W_E = 0$, that is, the energy is known there. Also, we have taken

$$\int_\Gamma W n_i(\mu + \frac{\mu_T}{\sigma_k})\frac{\partial k}{\partial x_i}\, d\Gamma = 0 \tag{5.57}$$

following the same reasoning than in k-ε equations.

5.2.3 Discrete form of extended CBS

The discrete set of ANS equations + the 2-equation model is shown in table 5.2.3. Matrixes and nodal vectors are defined as before. Turbulent contributions are included in the right hand side force terms, being the unknowns mean variables. In the first line, the discrete form of both the k-ε equations is solved explicitly. It is done in one line remarking the fact that due to the explicit character of the method, they are decoupled and time advancing can be done simultaneously for both the turbulent variables. They are noted as a nodal vector $\bar{\boldsymbol{X}}_{k\text{-}\varepsilon}$ of length (2 X number of free nodes). $\boldsymbol{M}_{2,0}$ accounts also for that fact, it is the scalar mass matrix for each of the unknowns, with decreased rank for the Dirichlet boundary conditions are already included in the force term.

5.2.4 Anisotropic Discontinuity Capturing Technique applied to turbulence equations

We have based the extension of CBS algorithm to k-ε equations in the fact that convection - diffusion - reaction character is shared by all the intervening equations. By inspection of turbulence equations, it is clear that in compressible cases, non linear velocity terms are present which can lead to the appearance of shock waves. Strong gradients are also present near boundary layers inasmuch as turbulence is characterized by high Re numbers. Finally, strong (non linear) reaction terms can favor all this phenomena. In incompressible flow, its use can bring the advantage of speeding up convergence and smoothing the solutions. Therefore, it seems reasonable to implement the ASC technique described in the chapters devoted to laminar flow also on the k-ε equations. This is done exactly as described in 3.1.3, replacing scalar V by ρk and $\rho\varepsilon$. The only basic difference is that in this case reaction coefficient s is a linearized term plus the $\nabla \cdot \boldsymbol{u}$ contribution from writing the convective term in non conservative way. It is linearized in fact only in the ε equation

$$s_k = -\frac{2}{3}\frac{\partial u_i}{\partial x_i}$$
$$s_\varepsilon = C_{\varepsilon 1}\frac{1}{\rho k}P_k - 2C_{\varepsilon 2}\frac{\varepsilon}{k},$$

$$\boldsymbol{M}_{2,0}\frac{\tilde{\boldsymbol{X}}_{k\text{-}\varepsilon}^{n+1}}{\Delta t} = \boldsymbol{M}_{2,0}\frac{\tilde{\boldsymbol{X}}_{k\text{-}\varepsilon}^{n}}{\Delta t} + \boldsymbol{F}_{k\text{-}\varepsilon},$$

$$\boldsymbol{M}\frac{\tilde{\boldsymbol{U}}^{n+1}}{\Delta t} + \boldsymbol{K}\tilde{\boldsymbol{U}}^{n+\theta_3} = \boldsymbol{M}\frac{\tilde{\boldsymbol{U}}^{n}}{\Delta t} + \boldsymbol{F}_1,$$

$$\boldsymbol{M}_{\alpha}\frac{\tilde{\boldsymbol{X}}_{\text{cont}}^{n+1}}{\Delta t} + \theta_1\Delta t\boldsymbol{L}_{\beta}\tilde{\boldsymbol{X}}_{\text{cont}}^{n+\theta_2} = \boldsymbol{M}_{\alpha}\frac{\tilde{\boldsymbol{X}}_{\text{cont}}^{n}}{\Delta t} + \boldsymbol{F}_{\text{cont}},$$

$$\boldsymbol{M}_0\frac{\tilde{\boldsymbol{U}}_0^{n+1}}{\Delta t} = \boldsymbol{M}_0\frac{\tilde{\boldsymbol{U}}_0^{n+1}}{\Delta t} - \boldsymbol{G}_0\tilde{\boldsymbol{p}}^{n+\theta_2} + \boldsymbol{F}_2,$$

$$\boldsymbol{M}_{8,0}\frac{\tilde{\boldsymbol{X}}_{\text{heat}}^{n+1}}{\Delta t} = \boldsymbol{M}_{8,0}\frac{\tilde{\boldsymbol{X}}_{\text{heat}}^{n}}{\Delta t} + \boldsymbol{F}_{\text{heat}},$$

Table 5.3: Discrete set of ANS + k-ε equations.

according to (5.21) and (5.27).

5.3 Two - equation models under study.

In this work we have chosen the k-ε model, as it is described in classical papers and books: see for example [Launder and Spalding, 1974] or [Wilcox, 1993]. A great effort is put in trying to understand the effects of compressibility in turbulent flows, the physics of the process. With the aid of experimental data and DNS algorithms [Moin and Mahesh, 1998], some insight is step by step being obtained. These corrections can be transferred to simpler models, like the k-ε , generally used in applied or industial problems. It then happens a recurrent thing in science: highly complex models are used to (try to) understand very simple and symmetric problems and then their results are extended to simpler models to study much more complicated flow. The more you read on the subject, the more you become convinced of this fact: turbulence is one of the most challenging problems in modern physics, still unsolved and open, where this technique that goes from *simpler problem, complex model* to *complex problem, simpler model* seems to slowly drain clues to understand the problem.

Relating to k-ε models, some of the corrections that can be studied for flows beyond Morkovin approximation using CBS in the next future are:

- K. Chien's damping function for low Reynolds [Chien, 1982].
- J. Hu and A. Rizzi's correction to K. Chien in production terms [Hu and Rizzi, 1995].
- Turbulent mass flux evaluation of J.R. Ristorcelli [Ristorcelli, 1993].
- O. Zeman or S. Sarkar's decomposition and modeling $\varepsilon = \varepsilon_s + \varepsilon_d$ solenoidal and dilatation dissipation respectively [Sarkar et al., 1991, Zeman, 1990].
- S. Sarkar and co-worker's pressure dilatation [Sarkar, 1992] and baroclinic torque of V.S. Krishnamurty and W. Shyy [Krishnamurty and Shyy, 1997].
- And a long etcetera.

The kind of assessment we want to carry out is that found in [Bardina et al., 1997], [Barakos and Drikakis, 1998], [Hanine and Kourta, 1991] or
[Krishnamurty and Shyy, 1997].

5.4 Summary

In this section, turbulence is briefly described. Its physics can be modeled in many ways and from different points of view due to its extreme complexity. We focused in the so called fully developed turbulence, leaving aside the transition problem. Out of all the models we know to exist, we choose a two-equation model: k-ε , to work with. Once the averaging process is described, it can be applied to the Navier-Stokes set and the Averaged Navier-Stokes equations are now those which rules the dynamics of the mean flow. Small scale effects are modeled and two new equations for the turbulent variables are derived. Modelization is needed to deal with the fact that we have more unknowns than equations (the closure problem). To finish with the differential problem, boundary conditions are discussed, among them the law of the wall. Finally, after writting the weak form of the ANS set + k-ε equations, the discretized equations of the CBS + k-ε model are derived. Some compressibility corrections are very briefly described.

Chapter 6

Turbulent Flow: Numerical Examples

We present some incompressible turbulent problems solved using CBS and a k-ε two-equation model. A mixing layer, where no law of the wall is needed, a Poiseuille flow, in 2D and 3D arrangements, where physical walls are present and a classical backwards facing step are the examples shown.

6.1 Incompressible turbulent flow

6.1.1 Mixing layer

This example shows the stationary flow developed from two layers of flow at different velocities fig. 6.1. The computational domain is a rectangle with the proportion 5:1:length:height. In the inflow, a discontinuous horizontal mean velocity is imposed. This produces a shear stress effect which propagates to the interior due to the viscosity, both turbulent and laminar. In the lower half of the inlet and all along the bottom contour a mean horizontal velocity (2,0) is imposed. In the upper half of the inlet and along the top contour, the mean horizontal velocity is fixed to (1,0). The velocity at the outflow has no imposition, where the mean effective pressure is set to 0. According to (5.54), by imposing $\bar{p}^{\text{eff}} = 0$ in fact we are setting $\bar{p} = \frac{2}{3}k$. Turbulent kinetic energy is prescribed where velocity is, to a constant value $k = 0.01$, no matter the velocity value imposed. ε is there evaluated according to table 5.2 using $L = 0.009$. The kinematic viscosity is $\nu = 10^{-4}$.

In fig. 6.2 and fig. 6.3 are shown some level contours for different variables, both

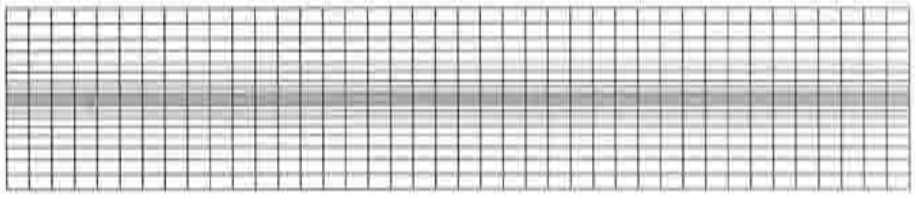

Figure 6.1: Mixing layer. Q1 mesh.

mean and turbulent. When compared to results shown in [Soto, 1997], it seems that they compare well, obtaining approximately the same spreading rate of about 0.060 - 0.070 [Wilcox, 1993]. In this example, no shock-capturing is needed because turbulent variables gradients are not to strong.

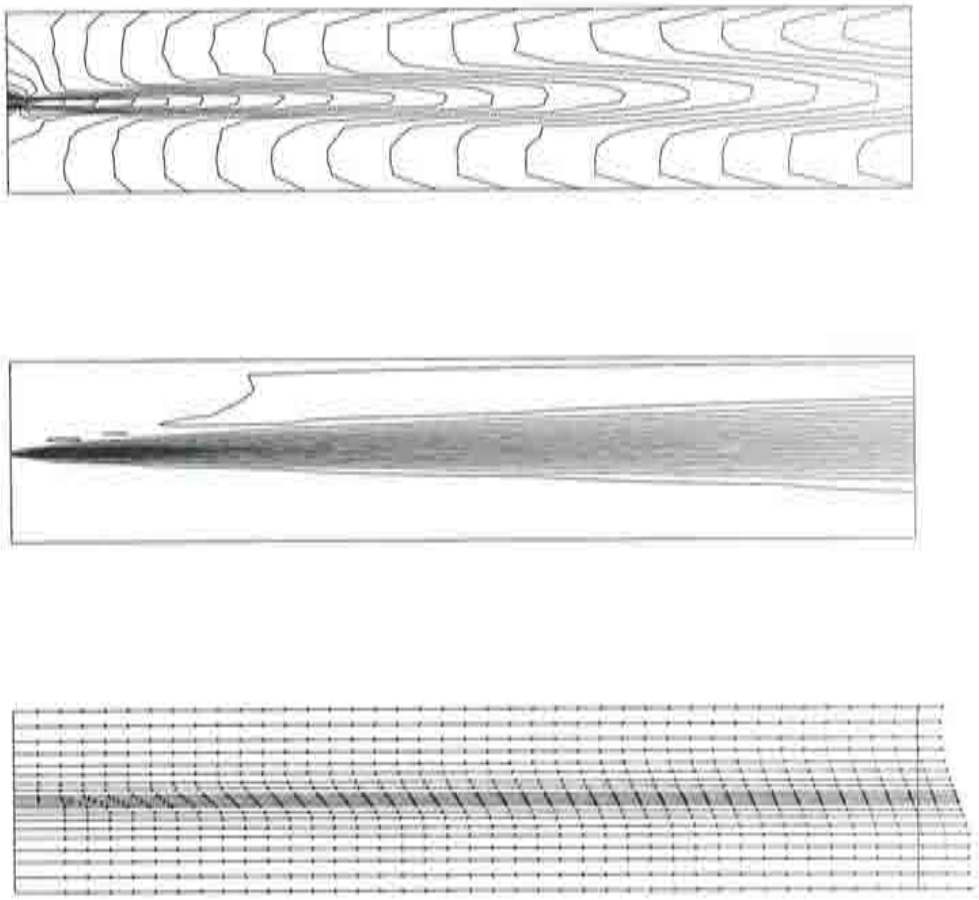

Figure 6.2: Mixing layer. From top to bottom: pressure and velocity contours, and velocity vectors.

The following are the value ranges for the mean and turbulent variables: velocity module, [0.903 , 2.01]; pressure, [-0.152 , -0.00092]; turbulent kinetic energy, [0.00148 , 0.0576], turbulent dissipation, [0.000907 , 0.141]; turbulent viscosity, [0.000179 , 0.00502].

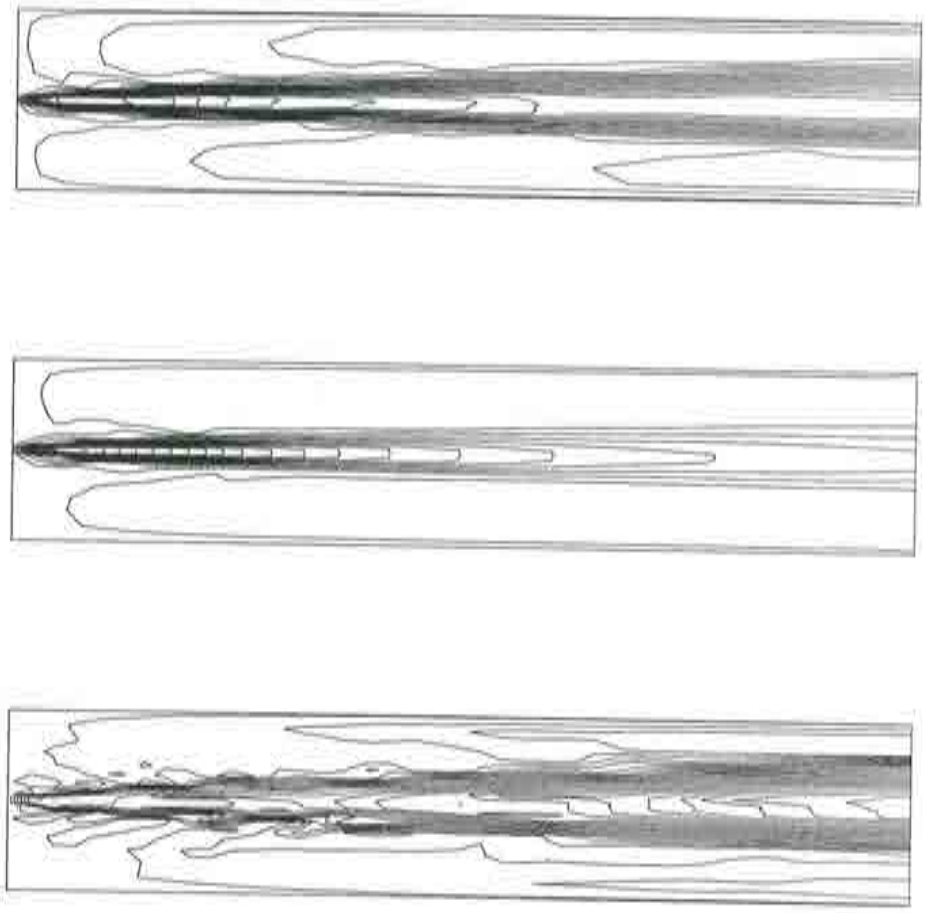

Figure 6.3: Mixing layer. From top to bottom: k, ε and turbulent viscosity level contours.

6.1.2 Boundary layer, 2D

A stationary boundary layer is studied in this example. Turbulent effects are modeled using the law of the wall. The numerical domain and its discretization is shown in fig. 6.4. Structured and refined to account for boundary layer effects, the spatial grid is made of 840 Q1 elements and 915 nodes. Its ratio is 30:1.5 : length:height. The left vertical contour is the inflow. With the exception of the left bottom corner node, the velocity is there prescribed to (1,0). In the top segment vertical velocity is prescribed to zero, in the outflow left free. Pressure is again imposed in the outflow using $\bar{p} = \frac{2}{3}k$. The bottom rigth corner node is included in both the wall and the outflow, with their boundary conditions.

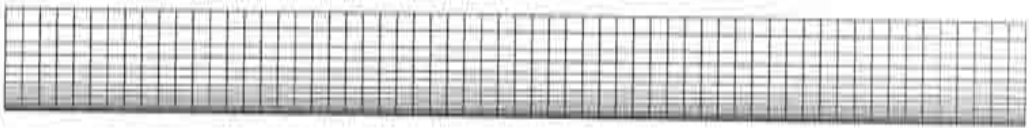

Figure 6.4: 2D Boundary layer. Q1 mesh.

The bottom contour is the numerical wall, a distance Δ off the physical one. In this boundary, traction coming from the law of the wall is imposed by means of (5.46). Boundary conditions for k-ε follows table 5.2. The data for this problem where taken from [Soto, 1997]. The mixing length is 0.009 and $\Delta = 0.05$, which in this case corresponds to $y^+ \simeq 20$. In the inflow, $k = 0.01u^2$, and ε is calculated as set in the table. In the rest of the contours, k and ε are free. The kinematic viscosity is again $\nu = 10^{-4}$.

Several contour level graphs are shown in fig. 6.5. Again, in this example, results are very close to those of [Soto, 1997]. The obtained value ranges for the mean and turbulent variables are: pressure, [-0.0051 , 0.0517]; turbulent kinetic energy, [0.00025 , 0.0134], turbulent dissipation, [0.000007 , 0.0124]; turbulent viscosity, [0.000589 , 0.00305]. In fig. 6.6 is shown the velocity vector in the domain and its norm profile

along the outflow.

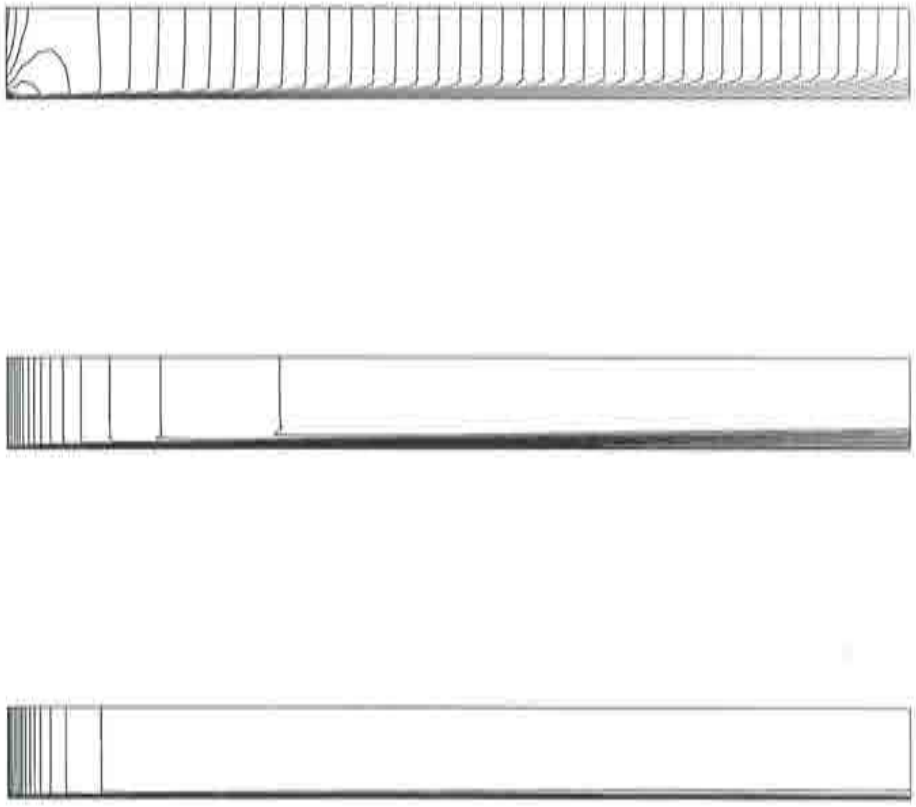

Figure 6.5: 2D Boundary layer. From top to bottom: pressure, k, and ε level contours.

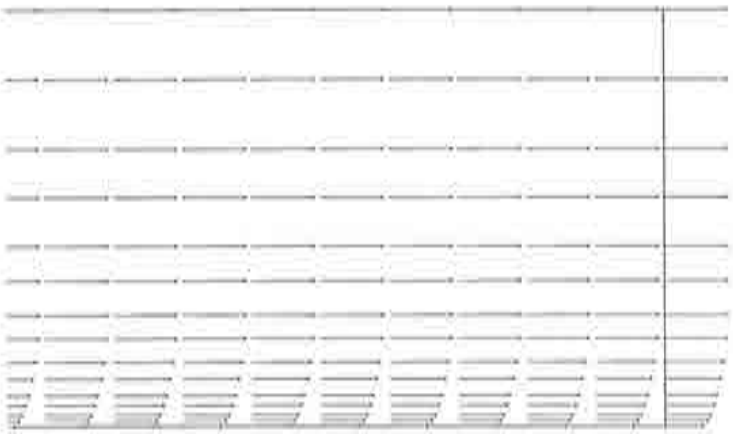

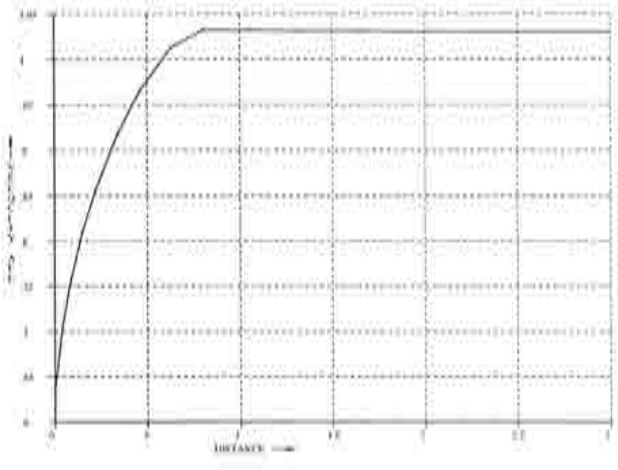

Figure 6.6: 2D Boundary layer. Velocity along the outflow.

6.1.3 Boundary layer, 3D

This is a simple 3D example to show the behavior of a boundary layer, like above. In fact, the grid is generated from the previous one, by replicating five times towards z-direction. The domain is formed by 3360 Q1 elements and 4575 nodal points. A view of it is in fig. 6.7. The same parameters and boundary conditions as before are taken. Along the edges and lateral walls, symmetry conditions, i.e. $u_z = 0$ are imposed.

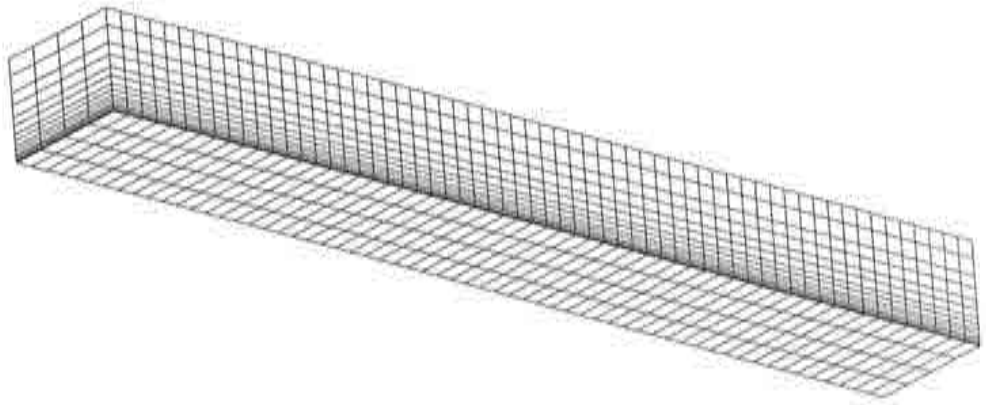

Figure 6.7: 3D Boundary layer. Q1 mesh.

In fig. 6.8 are shown the k, turbulent viscosity and pressure level contours for this problem. They are basically the same as in the previous 2D example.

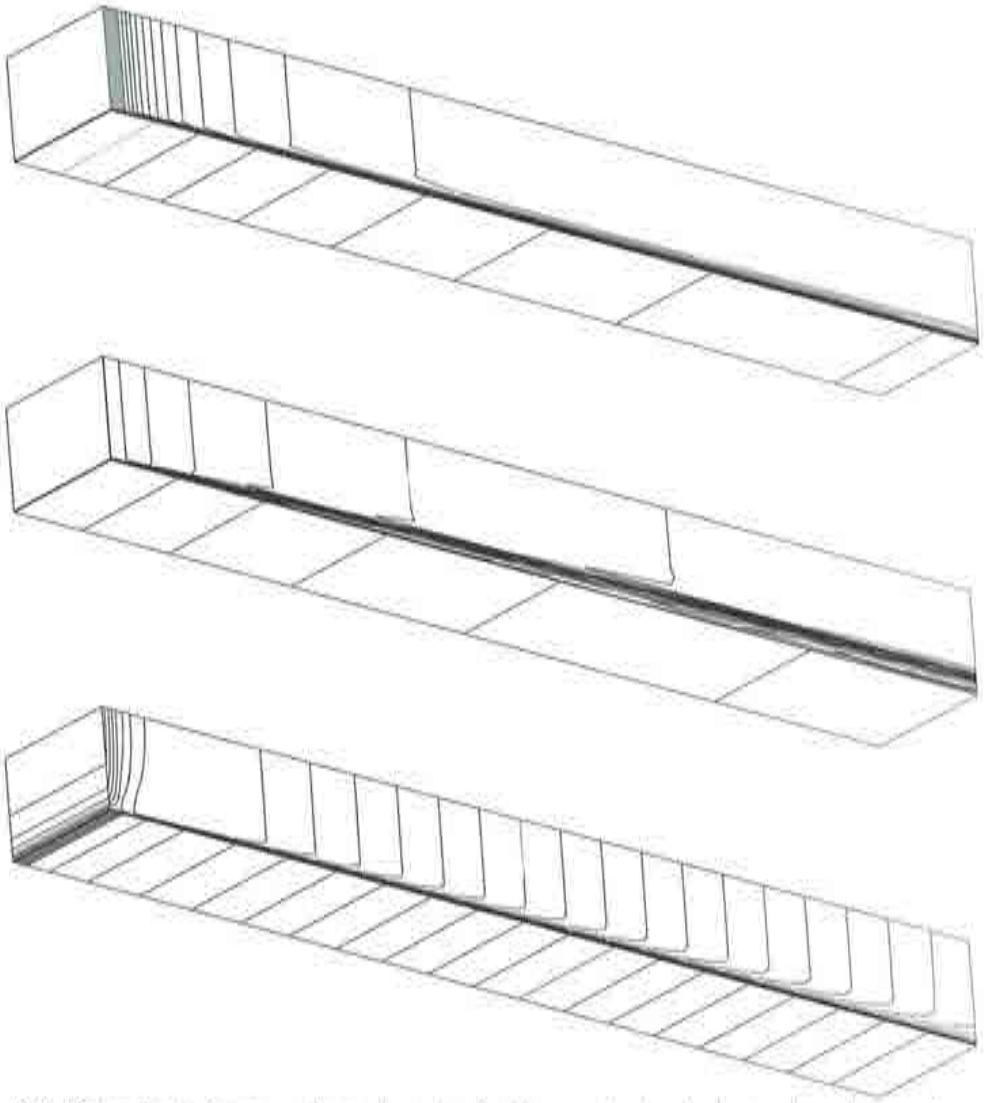

Figure 6.8: 3D Boundary layer. From top to bottom: k, turbulent viscosity and pressure level contours.

6.1.4 Backwards facing step at $Re = 7 \times 10^5$

This is a classical example. At this regime, turbulence is fully developed, unlike the backwards facing step flow presented in the section devoted to laminar examples. The step-to-inlet ratio is 1:2 : step:inlet and the ratio between the up-step part and the long down-step tail is 1:7 : up-part:down-tail. The data for this example is taken from [Soto, 1997] (in turn, referencing [Sohn, 1986]). With this Reynolds number, the step height $h = 0.5$ and the inflow velocity norm $u_{inf} = 1.0$, it is obtained a molecular viscosity $\mu = 7.143e-06$. The spatial discretized domain is shown in fig. 6.9. It is a structured, refined grid made of 1632 Q1 elements and 1721 nodal points.

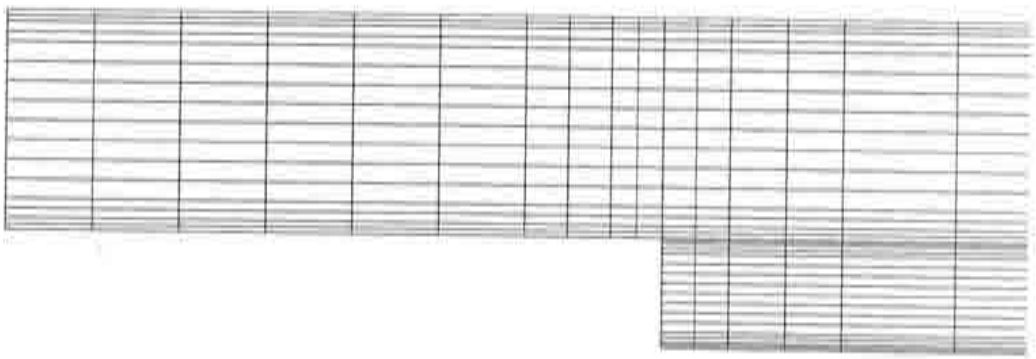

Figure 6.9: Backwards facing step. Q1 mesh (detail).

At the inflow, a horizontal constant velocity (1,0) is prescribed. The mesh refinement is done considering the boundary layer contours, where the traction prescriptions according to the law of the wall are put. This comprises all the upper boundary and the bottom one, including the up-step segment, the down-step tail and the vertical step itself. The mixing length is 0.03 and $\Delta = 0.03$. In the inflow, $k = 0.003u^2$, being ε evaluated from table 5.2. In the outflow, k and ε are free and the pressure is prescribed as before.

This example gives an approximate idea about the effect of turbulence. First, we solve the problem keeping k, ε and μ_T to constant values, those of the inflow: $k = 0.003$,

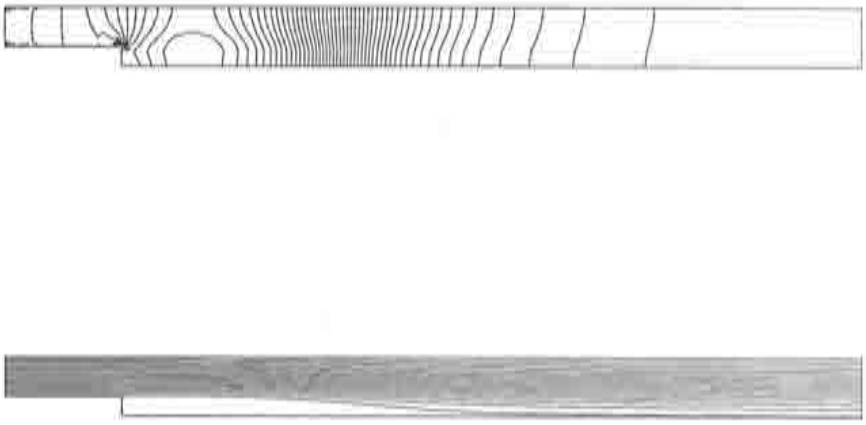

Figure 6.10: Backwards facing step. From top to bottom: pressure contours and streamlines, laminar solution.

$\varepsilon = 0.000493$ and $\mu_T = 0.00164 = \mu$. On the walls, we prescribe a traction calculated from the law of the wall, which gives a velocity on the wall closer to that of the turbulent case. This problem is equivalent to to a laminar one with Reynolds number around 300. Once converged, we use this solution as initial condition to get the developed stationary turbulent solution. In fig. 6.10, mean pressure contours and streamlines are shown for the laminar solution. As expected, the main vortex down the step is larger. From fig. 6.12, where the horizontal velocity along the contour behind the step is plotted, it follows that the vortex length is in this case about $15h$. It is taken as the position where velocity crosses from negative to positive values the $y = 0$ axis. Horizontal axis is in units of $h/2$.

Turbulent developed flow is studied next, starting from the laminar solution. Mean pressure contours and streamlines are shown in fig. 6.11, and turbulent variables in fig. 6.13. Due to the fact that in the upper step edge velocity values have strong gradients and no grid refinement is there, shock capturing for the turbulent variables is necessary. Also, a relaxation factor 0.1 for the turbulent variables is used.

In fig. 6.14 are shown the streamlines and velocity vectors of the main vortex down stream the step. Both previous numerical and experimental results seems to be

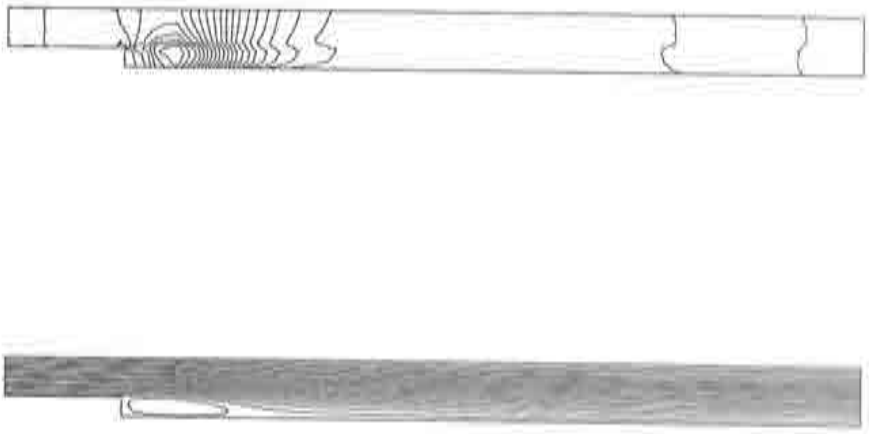

Figure 6.11: Backwards facing step. From top to bottom: pressure contours and streamlines, turbulence developed.

quite similar to those obtained here. The experiments depicted in [Kim et al., 1980] give a value of $(7.0 \pm 1.0)h$ for the length of the vortex. In [Stanford, 1982], numerical simulations produce a value of $(5.2-5.8)h$ and in [Soto, 1997], $6.57h$. Here, we obtained about $7.10h$. As in the laminar initial solution, this value is given approximately because in fig. 6.12, the curve has no points in $y = 0$, so it is a linear interpolation considering two points below and above.

6.2 Summary

CBS extension to turbulent flows is introduced through a few numerical examples. All of them are incompressible, leaving compressible problems as future work. 2D mixing layer, boundary layer and backwards facing step and a simple 3D boundary layer are the chosen tests. It can be concluded that this algorithm is, at least, very promising for the assessment and development of turbulence models.

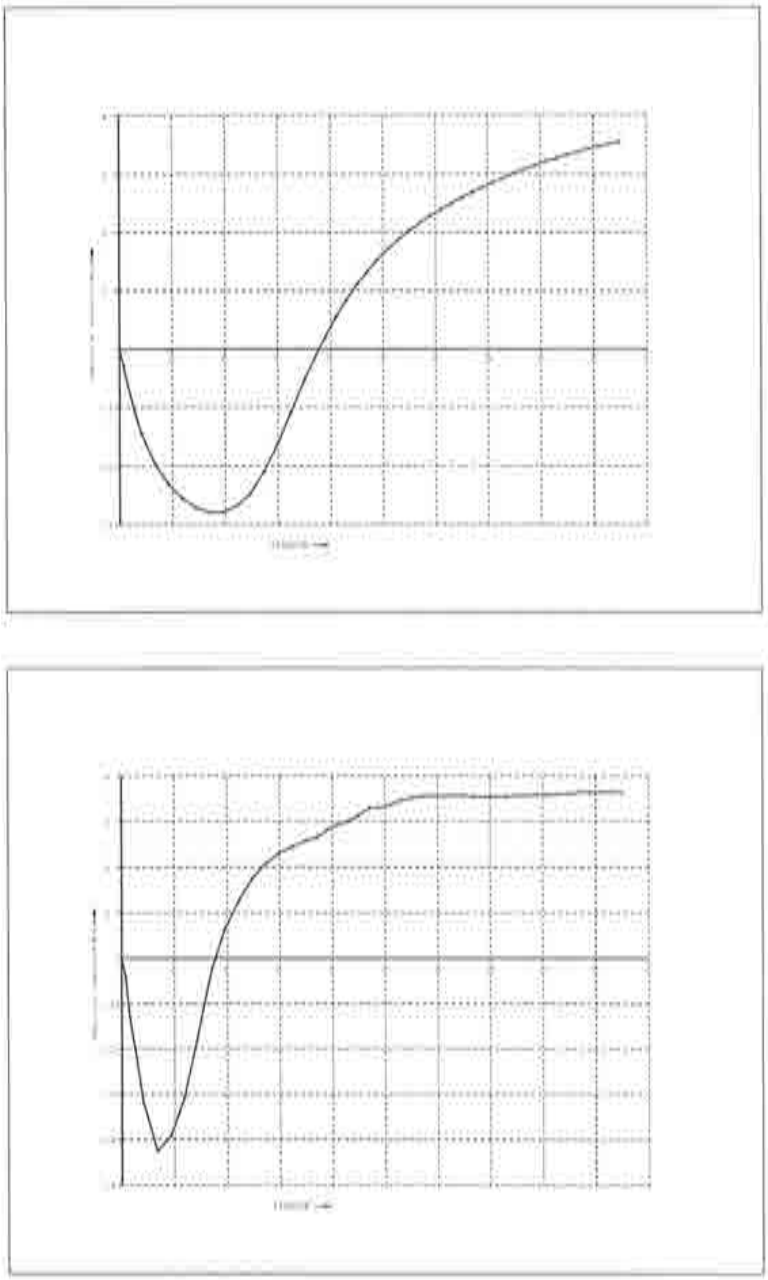

Figure 6.12: Backwards facing step. Horizontal velocity along the bottom contour. Top, laminar; bottom, turbulent.

Figure 6.13: Backwards facing step. From top to bottom: k, and ε level contours.

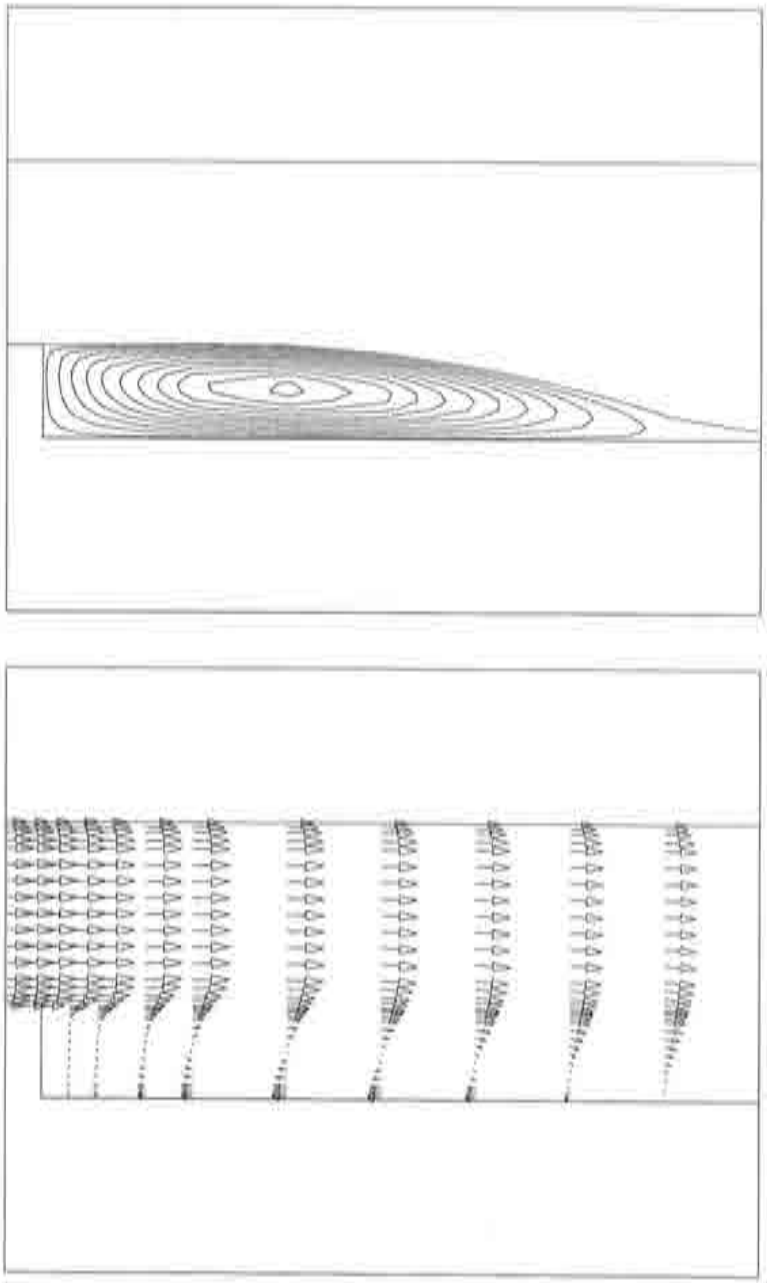

Figure 6.14: Backwards facing step. Down-step vortex. From top to bottom: Streamlines and velocity vectors.

Chapter 7

Multigrid techniques applied to the CBS algorithm

Multigrid (MG) methods are an important tool for accelerating convergence rates to stationary solutions of systems of equations with a great number of degrees of freedom [Hackbusch, 1994, Wesseling, 1995, Mavriplis, 1995]. Its application in the field of Computational Fluid Dynamics goes from algebraic MG, where matrixes are reduced by eliminating rows and columns following some criteria (e.g. in [Hackbusch, 1994]), to geometric MG, where this effect is achieved by formulating the continuous original problem in different grain discretizations (e.g. in [Mavriplis, 1988]). This is the case whether finite differences or finite element methods are used to discretize the numerical domain. These methods are very popular and widespread, both for solving explicit (e.g. [Mavriplis, 1988] or [Peraire et al., 1993]) or implicit schemes (for instance, see [Kanarchos and Pantelelis, 1994], [Kanarchos and Vournas, 1993] or [Dutto et al., 1997]). Even there exist special cites in Internet devoted to multigrid techniques (for instance, see *http://na.cs.yale.edu/mgnet/www/mgnet.html*, which has more than 3000 entries - winter 1998 -).

In this chapter we present a MG method for the CBS in laminar problems. When fluid dynamics is studied using fixed Eulerian spatial discretizations the construction of the connecting operators between the grids can be done once, remaining unchanged until the end of the process. FEM provides a natural way for constructing these operators because interpolations of nodal vectors through shape functions are inherent to the solution method. Besides, the structured or unstructured character of the meshes involved loses its influence in the final results and also mixed order interpolations can be used. As previously noted, multigrid is thought for speeding up the convergence of the explicit forms when stationary solutions are sought. The main difficulty is the fractional step, because many options can be implemented. The question is open, and

as work on the subject evolves, new approaches are very likely to be found, more efficient and accurate. Here, through numerical experiments over different ideas, we have achieved a reasonable convergence acceleration, specially when boundary layers are present. This is shown in through two examples, previously studied in its converged state: the Carter's flow and the flow passing a NACA 0012 profile.

Originally, we started the work on this point aiming to convergence rates improvement. While carrying on, we noticed that other more general algorithmic and original aspects can be focused. For instance, due to the flexibility of the spatial discretization of finite element methods and CBS itself, the set of domain partitions can be rather diverse. Not only coarse and fine meshes, but of different order and kind of interpolation, structured and unstructured, different solutions schemes and so on. All of this is done for laminar problems, leaving aside turbulence by the moment. To apply MG techniques to any fractional step algorithm is in a very embrionary state and much more work is needed prior to step into turbulent problems, like for instance in [Mavriplis and Martinelli, 1994] and [Dick and Steelant, 1997] for k-ε models.

The chapter is organized as follows. First, the general idea is depicted. Then, more insight is gained through the description of both the ingredients and the scheme. These ideas are applied then to CBS method. Finally, two compressible laminar viscous problems, supersonic and transonic, are studied, preferred for its complexity and richness.

7.1 Multigrid Techniques

7.1.1 Statement of the general problem

The discretized set in table 3.2 leads to a problem of the kind: solve the inhomogeneous system

$$\boldsymbol{A}(\boldsymbol{x})\boldsymbol{x} = \boldsymbol{b}, \tag{7.1}$$

with given boundary conditions already incorporated on the right hand side. $\boldsymbol{A}(\boldsymbol{x})$ is the matrix, maybe large, which comes from the convective, diffusive and reactive terms. $\boldsymbol{b}$ is the source vector, including source terms and boundary contributions. $\boldsymbol{x}$ is the unknown vector. We are going to solve this problem through an iterative procedure, motivated by the fact that (7.1) are the steady state equations of an evolution problem. The iterative technique is based precisely on the time stepping of these problems towards the steady state of the kind

$$\boldsymbol{M}\boldsymbol{x}^{j+1} = \boldsymbol{M}\boldsymbol{x}^{j} + \eta^{j}(\boldsymbol{b} - \boldsymbol{A}(\boldsymbol{x})\boldsymbol{x})^{j}, \tag{7.2}$$

where $\boldsymbol{M}$ is the mass matrix and η^j a scaling parameter. The former can be either lumped or consistent and the latter is identified with the time step increment Δt, evaluated for each time step according to stability criteria. Suppose that the right hand side of (7.2) is evaluated explicitly. When $\boldsymbol{M}$ is a diagonal lumped mass matrix the unknown $\boldsymbol{x}^{j+1}$ is directly calculated, being simply

$$\boldsymbol{x}^{j+1} = \boldsymbol{x}^{j} + \eta^{j}\boldsymbol{M}_{L}^{-1}(\boldsymbol{b} - \boldsymbol{A}(\boldsymbol{x})\boldsymbol{x})^{j}. \tag{7.3}$$

On the other hand, when $\boldsymbol{M}$ is a consistent non-diagonal matrix, for each step j, equation (7.2) can be solved using Jacobi iterations. Taking

$$\Delta\boldsymbol{x}^{j+1,\alpha} = \boldsymbol{x}^{j+1,\alpha} - \boldsymbol{x}^{j,\alpha}$$

where greek supraindices are the Jacobi iterations counter, then

$$\Delta\boldsymbol{x}^{j+1,\alpha+1} = \Delta\boldsymbol{x}^{j+1,\alpha} + \boldsymbol{M}_{L}^{-1}\left(\eta^{j,0}(\boldsymbol{b} - \boldsymbol{A}(\boldsymbol{x})\boldsymbol{x})^{j,0} - \boldsymbol{M}\Delta\boldsymbol{x}^{j+1,\alpha}\right). \tag{7.4}$$

In order to grasp the concepts behind MG procedures, let us re-write the original problem in a slightly different way:

$$\boldsymbol{A}(\boldsymbol{x})\boldsymbol{x} - \boldsymbol{A}(\boldsymbol{x})\boldsymbol{x}^{0} = \boldsymbol{b} - \boldsymbol{A}(\boldsymbol{x})\boldsymbol{x}^{0}.$$

Naming $\Delta\boldsymbol{x} = \boldsymbol{x} - \boldsymbol{x}^0$ and $\boldsymbol{d} = \boldsymbol{b} - \boldsymbol{A}(\boldsymbol{x})\boldsymbol{x}^0$, where $\boldsymbol{x}^0$ is a given vector, the original problem can be restated as follows: solve

$$\boldsymbol{A}(\boldsymbol{x})\Delta\boldsymbol{x} = \boldsymbol{d}. \tag{7.5}$$

The iterative procedure set in (7.2) is then be applied to (7.5):

$$\boldsymbol{M}\Delta\boldsymbol{x}^{j+1} = \boldsymbol{M}\Delta\boldsymbol{x}^{j} + \eta^{j}(\boldsymbol{d} - \boldsymbol{A}(\boldsymbol{x})\Delta\boldsymbol{x})^{j}, \tag{7.6}$$

taking the same $\boldsymbol{M}$ and η as before, and

$$\begin{aligned} \Delta\boldsymbol{x}^{j} &= \boldsymbol{x}^{j} - \boldsymbol{x}^{0} \\ \boldsymbol{d} &= \boldsymbol{b} - \boldsymbol{A}(\boldsymbol{x})\boldsymbol{x}^{0}. \end{aligned} \tag{7.7}$$

Using these definitions, (7.6) becomes

$$\boldsymbol{M}\boldsymbol{x}^{j+1} = \boldsymbol{M}\boldsymbol{x}^{j} + \eta^{j}(\boldsymbol{d} - \boldsymbol{A}(\boldsymbol{x})\boldsymbol{x}^{j} + \boldsymbol{A}(\boldsymbol{x})\boldsymbol{x}^{0}). \tag{7.8}$$

As it is written now, equations (7.8) and (7.2) are exactly the same because $\boldsymbol{d} + \boldsymbol{A}(\boldsymbol{x})\boldsymbol{x}^{0} = \boldsymbol{b}$. But when $\boldsymbol{d}$ is evaluated in a grid and transferred by some means to another grid, where equation (7.8) is set, this identity is not any more verified (unless the two grids are coincident). The difference between both terms becomes the new source.

7.1.2 Multigrid methods

These methods are of the kind of fastest convergence rates (see [Hackbusch, 1994], [Wesseling, 1995]). Their properties are based on two facts. First, different spatial frequency errors are damped at different rates according to the following: the higher the frequency, the higher the rates. Second, higher frequencies are resolved only by finer grids.

Let us suppose that the original continuum problem is discretized as was said above in a given spatial grid labeled l. The eigenvectors of $\boldsymbol{A}_l$ form a basis where the error

$$\boldsymbol{e}_l^{j} = \boldsymbol{x}_l^{j} - \tilde{\boldsymbol{x}}_l,$$

can be expanded in, being $\boldsymbol{x}_l^j$ the outcome of j iterations of the type (7.2) or (7.8) and $\tilde{\boldsymbol{x}}_l$ the solution of the problem $\boldsymbol{A}_l\boldsymbol{x}_l = \boldsymbol{b}_l$ .The highest convergence rates for an iterative procedure like the one above are attained by the components of $\boldsymbol{e}_l^j$ belonging to the space spanned by the eigenvectors corresponding to the highest eigenvalues [Hackbusch, 1994] . These eigenvalues in turn correspond to the highest spatial frequencies that can be resolved by the chosen discretization.

For that reason, alternative advance of the iterative procedure in grids of different element sizes damps the errors acting selectively over the whole frequency spectrum, because for a given mesh, the highest spatial frequency "corresponds" to lower eigenvalues in a finer mesh. Therefore each grid out of a set of discretizations with different spacings smooths the error damping at the highest rate at different frequencies. After some iterative steps in the finest grid, which smooth the error, the solution can be well approximated in the next coarser mesh. There, some more iterative steps are performed, the error is smoothed again and the solution is transferred to the following coarser mesh. This process continues until the coarsest mesh is reached and the coarse grid correction is transferred back to the finest grid. The whole process is repeated until some convergence criterium is accomplished. In this sense, multigrid algorithms applied to explicit schemes act like other convergence speed up techniques which by the introduction of a preconditioning mass matrix of a certain kind prompt each of the error modes to move at the maximum allowed speed, reaching the boundaries as fast as possible. There, the bulk of them are either absorbed or expelled out of the domain. See for instance [Baumann et al., 1992, Storti et al., 1992]. These kind of algorithms are probably less bruising with the error than multigrid, but much easier to program. In chapter 1, the same idea was cited but in the context of implicit methods for general type algorithms ([Turkel and Radespiel, 1996, Turkel, 1992]). All these methods share the same strategy: preconditioning the matrix which carries the weight of the solution procedure. It goes from diagonal lumped mass matrix, like in explicit algortihms, to highly complex ones, coming from convective or diffusive terms. Explicit methods, specially when lumped mass matrix is used, can be thougth as an iterative method for getting stationary solutions, and preconditioning is a usual accelerating technique for methods solved iteratively.

The basic scheme of a multigrid algorithm is shown in fig. 7.1.2. It is needed a hierarchy of systems of equations, coming from discretizations of the same continuum problem but formulated in different grids and transfer operators between the components of the hierarchy.

- **The hierarchy of systems.** The original continuum problem is discretized in a series of grids, having different (mean) cell sizes, thus allowing an ordering according to the sizes. Let the mean size of the grid l be labelled by a characteristic length h_l. If

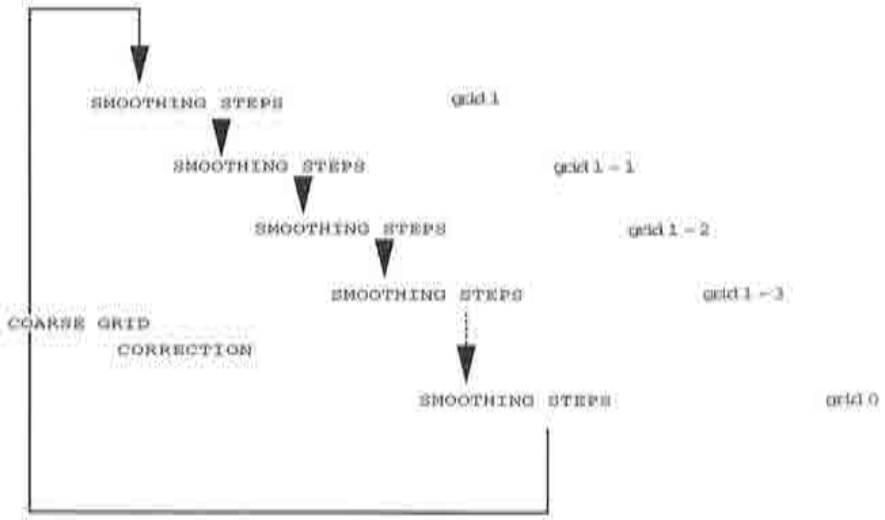

Figure 7.1: Multigrid general scheme.

$$h_0 > h_1 > h_2 > \cdots > h_{l-2} > h_{l-1} > h_l > \cdots$$

where

$$\lim_{l \to \infty} h_l = 0,$$

then the set $\mathcal{H}$ is the needed hierarchy

$$\mathcal{H} = \{\Omega^{h_l}, \Omega^{h_{l-1}}, \Omega^{h_{l-2}}, \Omega^{h_{l-3}}, \ldots\} \tag{7.9}$$

- **The transfer operators.** Data transferring between two given elements of $\mathcal{H}$ is done through two kinds of operators: a *restriction* r, which does it from fine to coarse grid and a *prolongation* p , which does the opposite. Transferring between the elements is done both ways, through the preceding operators and their adjoints r^* and p^*, all of them operating over discrete functions defined on the partitions.

  Consider Ω^{h_l} and $\Omega^{h_{l-1}}$. Let x_l, x_{l-1} be two vectors of the discrete spaces $X_l \cong \mathbb{R}^{d_l}$ and $X_{l-1} \cong \mathbb{R}^{d_{l-1}}$. Then let

restriction r :

$$\mathrm{r} : X_l \to X_{l-1} \;/\; x_{l-1} = \mathrm{r}\, x_l \tag{7.10}$$

prolongation p :

$$\mathrm{p} : X_{l-1} \to X_l \;/\; x_l = \mathrm{p}\, x_{l-1}. \tag{7.11}$$

Having presented the ingredients, a multigrid procedure can be built up as follows: let a hierarchy $\mathcal{H}$, the restriction and prolongation operators defined as above and let $l = k$ be the finest mesh label. Then the basic algorithm follows the steps:

1. Set $l = k$.
2. Do m iterations, *smoothing steps*, on system l according either to equation (7.2) if $l = k$ or to equation (7.8) if $l < k$. In this case, take as unknown vector the initial value that has been transferred from the upper finer system. Once step m is reached set

$$\boldsymbol{d}_l^m := (\boldsymbol{b}_l - \boldsymbol{A}_l(\boldsymbol{x}_l)\boldsymbol{x}_l)^m. \tag{7.12}$$

3. Transfer variable $\boldsymbol{x}_l^m$ and residual $\boldsymbol{d}_l^m$ to the coarser following grid $l - 1$.
4. Set $l = l - 1$ and go to 2. Repeat until $l = 0$, thus exhausting the hierarchy. Continue.
5. Transfer the *coarse grid correction* $\Delta\boldsymbol{x}_l$ to the upper following grid.
6. Set $l = l + 1$ and go to 5. Repeat until $l = k$. Continue.
7. Go to 1. Repeat until a given convergence criterium is reached, like not letting a norm of the residual to surpass a certain tolerance.

These steps represent the plain scheme of the algorithm. In this form, it belongs to the so called *V-cycle* type (see fig. 7.1.2). It goes from the finest to the coarsest

grids in steps 2,3 and 4 and back straight to the finest in 5 and 6. But sometimes the performance improves by changing to a *W-cycle* type. There the way up to the finest grid is not straight but "bouncing back" in some of the intermediate grids. Besides, for both cycling types, each of the subsidiary grids when receiving the coarse grid correction can do some additional iterations. These are called *post-smoothing steps*.

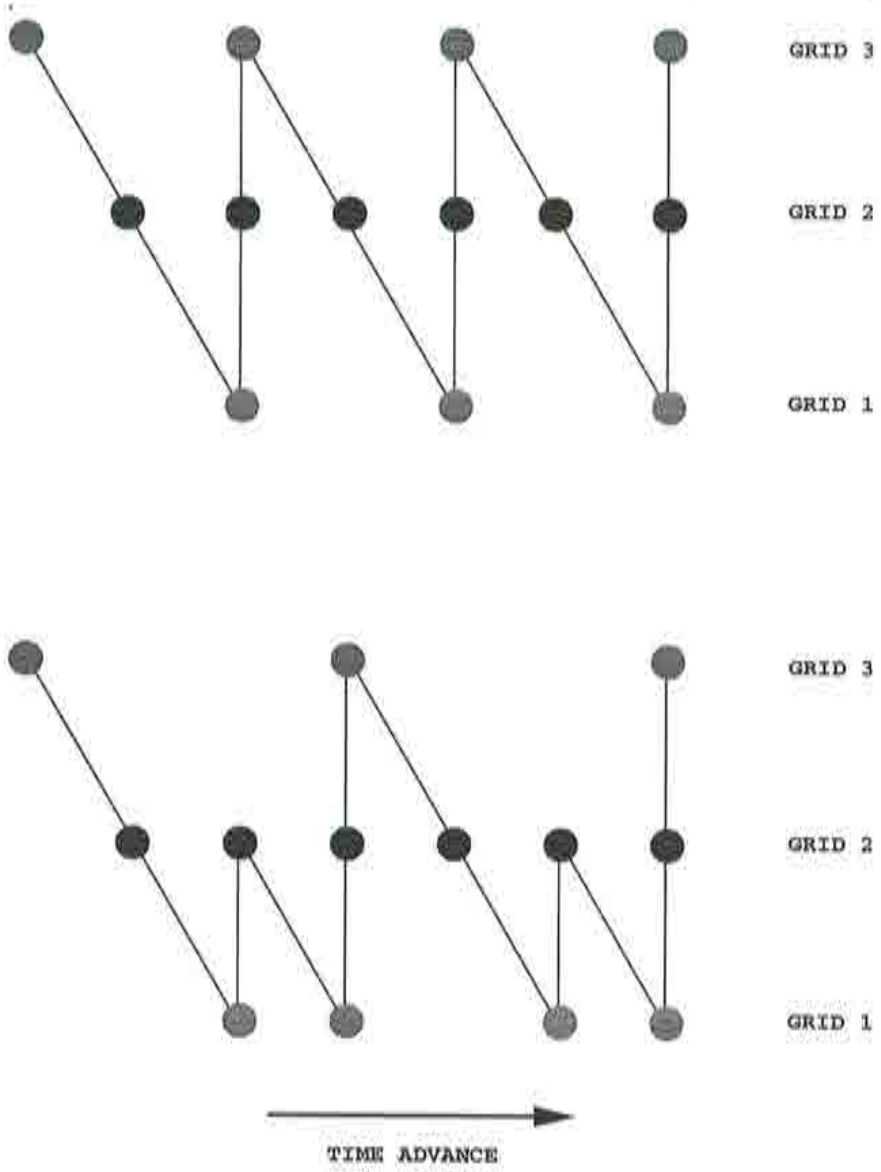

Figure 7.2: Numerical domain sketch.

Transfer operators can be constructed in many ways [Hackbusch, 1994, Wesseling, 1995,

Mavriplis, 1988]. If the grids remain unchanged along the whole process they are constructed once, at the beginning. In this work we did it by first identifying in which element of the upper and lower partitions are each node of each of the grids in $\mathcal{H}$. Then the entries of the interpolation matrix are calculated using the same finite element shape functions which was used to discretize the spatial domain.

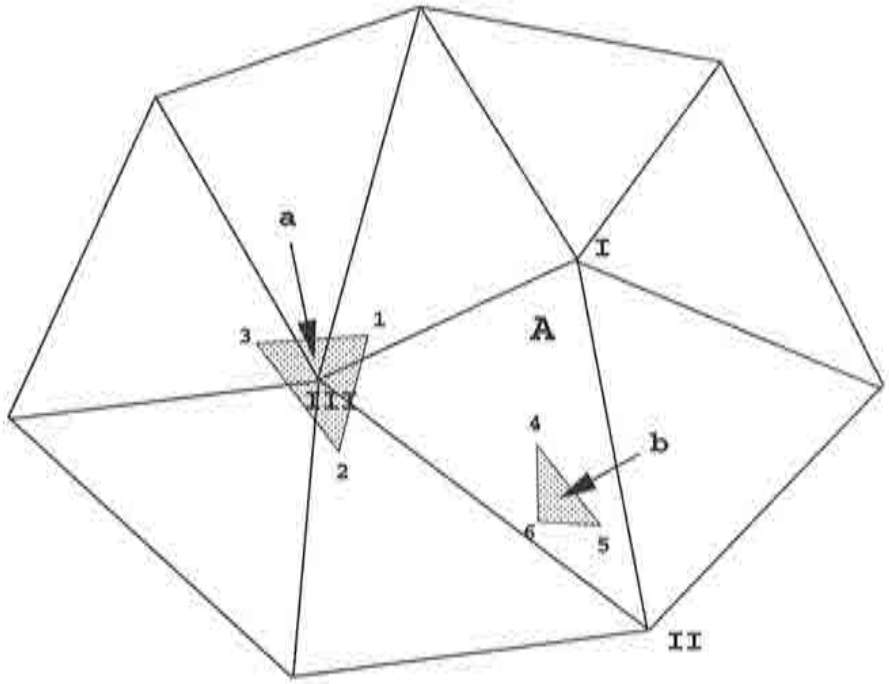

Figure 7.3: Interpolation between grids.

In fig. 7.1.2 it is sketched the interpolation procedure. The coarse mesh is shown complete while two elements of the fine one are drawn filled with a grey pattern. Element **A** of coarse grid is formed by nodes **I**, **II**, **III**. Elements **a** and **b** of the fine grid are formed by nodes **1**, **2**, **3** and **4**, **5**, **6** respectively. Consider node **III** of element **A** of the coarse grid. The value of the variable in it is transferred from the fine grid by first identifying node **III** as placed within element **a**. It is calculated as

$$u_{\mathrm{III}} = N_1(x_{\mathrm{III}})u_1 + N_2(x_{\mathrm{III}})u_2 + N_3(x_{\mathrm{III}})u_3, \tag{7.13}$$

where $N(x)$ are the FEM interpolating functions evaluated at x. In this case they are linear and vary from 1.0 at the labelling node to 0.0 at the other two nodes of the triangle. Alternatively, for example u_2 is

$$u_2 = W_{\rm I}(x_2)u_{\rm I} + W_{\rm II}(x_2)u_{\rm II} + W_{\rm III}(x_2)u_{\rm III}, \tag{7.14}$$

and $W(x)$ are the interpolating functions again.

The first of these two equations reflects how restriction operator works whereas the second one shows the action of prolongation. See that through restriction "information" is lost in the sense that not all the fine grid elements contain one node of the coarse grid. Therefore the values of u at nodes **4**, **5**, **6** of element **b** has no influence at all in the coarse grid, i.e. restriction is not conservative. When unknowns are transferred from fine to coarse, this is not relevant: we only need a starting value which follows as close as possible the fine grid. On the other hand, residuals must be transferred conservatively. Suppose that throughout all the fine grid the residual is zero except at nodes **4**, **5**, **6** of element **b**. Then, if plain restriction is used, transferred residuals at **I**, **II** and **III** are zero. For that reason, a conservative interpolation must be build up from contributions of *all* the fine grid nodes placed *within* each coarse grid element. The prolongation operator contains this information, being its adjoint the one chosen for residual transferring from fine to coarse [Wesseling, 1995, Peraire et al., 1993, Mavriplis, 1988].

Table 7.1.2 presents an example of a complete MG cycle showing the individual advance iterations for the principal and subsidiary systems. Total number of systems is set to $k = 3$ and it is of the so called *V-cycle* type.

The process is divided into two stages, considering the direction of advance from grid to grid. The *smoothing stage* is carried out going from finer to coarser meshes. It starts on the finest one and evolves passing the interpolated last variables and last residual obtained through the whole hierarchy. The triad m, p, q depends on the problem considered. It will be treated again in the next sections.

On the other hand, the *coarse grid correction stage* goes from coarser to finer meshes. Once the coarsest one is reached, the correction $\Delta\boldsymbol{x}_1$ obtained in it is transferred and then added to $\Delta\boldsymbol{x}_2$. This tranferring and adding process is repeated up to the finest grid.

It is important to see that the final stationary solution of subsidiary systems does not always match the solution of the principal one. Consider system 2 of table 7.1.2. Suppose that at iteration p it is reached a stationary state, i.e. $\boldsymbol{x}_2^{i+1} = \boldsymbol{x}_2^i := \boldsymbol{x}_2^p$. It verifies

$$\begin{aligned} 0 &= \overline{\boldsymbol{d}_2} - \boldsymbol{A}_2(\boldsymbol{x}_2^p)\boldsymbol{x}_2^p + \boldsymbol{A}_2(\boldsymbol{x}_2^p)\overline{\boldsymbol{x}_2} \\ &= \mathrm{p}_{23}^* \left((\boldsymbol{b}_3 - \boldsymbol{A}_3(\boldsymbol{x}_3)\boldsymbol{x}_3)^m\right) - \boldsymbol{A}_2(\boldsymbol{x}_2^p)\boldsymbol{x}_2^p + \boldsymbol{A}_2(\boldsymbol{x}_2^p)\mathrm{r}_{32}\left(\boldsymbol{x}_3^m\right). \end{aligned} \tag{7.15}$$

This final state $\boldsymbol{x}_2^p$ will be different from the solution $\tilde{\boldsymbol{x}}_2$ of the original problem set in grid 2. It is also different from $\mathrm{r}_{32}(\tilde{\boldsymbol{x}}_3)$. This is so because terms number 2 and 4 of equation (7.15) are not the same for operator $\boldsymbol{A}$ is non linear. Besides, should $\boldsymbol{A}$ be linear, the interpolating functions used to construct restriction and prolongation operators are very likely uncapable of exact interpolation of the fields obtained in grid 3, to grid 2. Thus, the number of iterations done in subsidiary systems need not to be high.

7.2 MG applied to CBS scheme

The split of the momentum equation, the number of different unknowns, the coupling of the equations, allow many possible ways to applying MG techniques in order to improve convergence rates to stationary state. Also, the spectrum of possibilities even increases more when considering the different regimes of flow that can be modeled using NS equations. For these reasons we are going to set the main ideas we propose while analyzing only one problem from different points of view.

In order to get a deeper insight of the method, let us consider a compressible viscous problem, solved fully explicitly and formulated in the conservative form. In this case, for each time step, $\check{\boldsymbol{U}}$ is first advanced. Then, the rest of the variables is evaluated at time $n+1$ using their values at time n in addition to $\check{\boldsymbol{U}}$ just obtained. Following table 3.2, in compact form, for each time step evaluate

$$\boldsymbol{M}\frac{\check{\boldsymbol{U}}^{n+1}}{\Delta t} = \boldsymbol{M}\frac{\bar{\boldsymbol{U}}^{n}}{\Delta t} + \boldsymbol{R}_1^n + \boldsymbol{b}_1^n, \tag{7.16}$$

firstly and then

$$\boldsymbol{\mathcal{M}}\frac{\boldsymbol{\mathcal{X}}^{n+1}}{\Delta t} = \boldsymbol{\mathcal{M}}\frac{\boldsymbol{\mathcal{X}}^{n}}{\Delta t} + \boldsymbol{\mathcal{R}}^n + \boldsymbol{\mathcal{B}}^n. \tag{7.17}$$

In the first equation, let

$$\boldsymbol{R}_1^n = -\boldsymbol{K}\bar{\boldsymbol{U}}^n + \boldsymbol{F}_1 - \boldsymbol{b}_1^n,$$

Smoothing stage:

Do $j = 0$ to m

$$\vdots \quad \boldsymbol{M}_3 \boldsymbol{x}_3^{j+1} = \boldsymbol{M}_3 \boldsymbol{x}_3^{j} + \eta_3^{j} (\boldsymbol{b}_3 - \boldsymbol{A}_3(\boldsymbol{x}_3)\boldsymbol{x}_3)^{j}$$

End Do

$$\begin{aligned} \boldsymbol{d}_3^m &:= (\boldsymbol{b}_3 - \boldsymbol{A}_3(\boldsymbol{x}_3)\boldsymbol{x}_3)^m \\ \overline{\boldsymbol{x}_2} &:= \mathrm{r}_{32}\, \boldsymbol{x}_3^m \\ \overline{\boldsymbol{d}_2} &:= \mathrm{p}_{23}^{*}\, \boldsymbol{d}_3^m \end{aligned}$$

Do $i = 0$ to p

$$\vdots \quad \boldsymbol{M}_2 \boldsymbol{x}_2^{i+1} = \boldsymbol{M}_2 \boldsymbol{x}_2^{i} + \eta_2^{i} (\overline{\boldsymbol{d}_2} - \boldsymbol{A}_2(\boldsymbol{x}_2^{i})\boldsymbol{x}_2^{i} + \boldsymbol{A}_2(\boldsymbol{x}_2^{i})\overline{\boldsymbol{x}_2})$$

End Do

$$\begin{aligned} \boldsymbol{d}_2^p &:= \overline{\boldsymbol{d}_2} - \boldsymbol{A}_2(\boldsymbol{x}_2^{p})\boldsymbol{x}_2^{p} + \boldsymbol{A}_2(\boldsymbol{x}_2^{p})\overline{\boldsymbol{x}_2} \\ \overline{\boldsymbol{x}_1} &:= \mathrm{r}_{21}\, \boldsymbol{x}_2^m \\ \overline{\boldsymbol{d}_1} &:= \mathrm{p}_{12}^{*}\, \boldsymbol{d}_2^m \end{aligned}$$

Do $l = 0$ to q

$$\vdots \quad \boldsymbol{M}_1 \boldsymbol{x}_1^{l+1} = \boldsymbol{M}_1 \boldsymbol{x}_1^{l} + \eta_1^{l} (\overline{\boldsymbol{d}_1} - \boldsymbol{A}_1(\boldsymbol{x}_1^{l})\boldsymbol{x}_1^{l} + \boldsymbol{A}_1(\boldsymbol{x}_1^{l})\overline{\boldsymbol{x}_1})$$

End Do

Coarse grid correction stage:

$$\begin{aligned} \Delta \boldsymbol{x}_1 &:= \boldsymbol{x}_1^{q} - \overline{\boldsymbol{x}_1} \\ \Delta \boldsymbol{x}_2 &:= \boldsymbol{x}_2^{p} - \overline{\boldsymbol{x}_2} + \mathrm{p}_{12}\, \Delta \boldsymbol{x}_1 \\ \Delta \boldsymbol{x}_3 &:= \mathrm{p}_{23}\, \Delta \boldsymbol{x}_2 \\ \boldsymbol{x}_3^{m+1} &:= \boldsymbol{x}_3^{m} + \Delta \boldsymbol{x}_3 \end{aligned}$$

Table 7.1: Multigrid V-cycle example

according to the right hand side of the fractional momentum equation. b_1^n are simply the volume forces written down explicitly. In the second one, we note $\mathcal{M}$ the consolidated matrix of mass matrixes and $\mathcal{B}$ the consolidated vector of volume forces.

$$\begin{aligned} \mathcal{X}^{n+1} &= \left[\boldsymbol{\rho}^{n+1}; \tilde{\boldsymbol{U}}^{n+1}; \bar{\boldsymbol{E}}^{n+1}\right]^{\mathrm{T}} \\ \mathcal{X}^{n} &= \left[\boldsymbol{\rho}^{n}; \tilde{\boldsymbol{U}}^{n+1}; \bar{\boldsymbol{E}}^{n}\right]^{\mathrm{T}}, \end{aligned} \tag{7.18}$$

are the vectors of unknowns. The second component of the unknowns at step n is the fractional momentum, which has become an already updated unknown at this moment. Finally, vector $\mathcal{R}^n$ is built up from the right hand sides of the continuity, momentum correction and energy equations except for the volume forces, which again are written down separately. The first and second components of $\mathcal{R}^n$ (corresponding to the continuity and the momentum equations) have also contributions from the just calculated $\tilde{\boldsymbol{U}}^{n+1}$. In this sense, the momentum splitting step couples (7.16) and (7.17). This is the price that has to be paid for obtaining the additional stabilizing diffusion in the continuity equation.

Equations (7.16) and (7.17) are now properly set up for the use of MG techniques. Table 7.2 shows the general scheme of a complete MG V-cycle applied to the CBS. For the sake of simplicity, $k = 2$.

In table 7.2, overbars mean transferred variables again. The coupling mentioned above introduced by the splitting of the momentum equation doesn't allow the straightforward use of MG techniques. After discussions and numerical experiments we have reached the present state. Obviously, it is opened to new ideas to improve the algorithm.

We have chosen to treat $\hat{\boldsymbol{U}}$ and $\bar{\boldsymbol{U}}$ as separate variables as far as possible, considering their equations also separately. The coupling arises when considering the initial value for $\tilde{\boldsymbol{U}}$ in the subsidiary systems. While the initial values for $\mathcal{X}$ (and the rest of physical variables needed to determinate the state) are the tranferred set $(\overline{\boldsymbol{\rho}}, \overline{\tilde{\boldsymbol{U}}}, \overline{\bar{\boldsymbol{E}}})$, i.e. the last values obtained in the preceding finer grid, say l, to the present one $l-1$, $\tilde{\boldsymbol{U}}_{l-1}^0$ is the first value obtained in $l-1$ itself. This is done so because the fractional momentum $\tilde{\boldsymbol{U}}$ is nothing but an auxiliar variable used to calculate the real physical momentum. Therefore, while $\boldsymbol{R}_1^0$ and the last component (heat equation) of $\mathcal{R}^0$ are evaluated from "overlined" first values, the continuity and momentum equation components of $\mathcal{R}^0$ are mixed.

Smoothing stage:

Do $j = 0$ to m

$$\begin{aligned} \boldsymbol{M}_2 \frac{\bar{\bar{\boldsymbol{U}}}_2^{j+1}}{\Delta t_2} &= \boldsymbol{M}_2 \frac{\bar{\boldsymbol{U}}_2^{j}}{\Delta t_2} + \boldsymbol{R}_{1,2}^{j} + \boldsymbol{b}_{1,2}^{j} \\ \boldsymbol{\mathcal{M}}_2 \frac{\boldsymbol{\mathcal{X}}_2^{j+1}}{\Delta t_2} &= \boldsymbol{\mathcal{M}}_2 \frac{\boldsymbol{\mathcal{X}}_2^{j}}{\Delta t_2} + \boldsymbol{\mathcal{R}}_2^{j} + \boldsymbol{\mathcal{B}}_2^{j}. \end{aligned}$$

End Do

$$\begin{aligned} \boldsymbol{d}_{1,2}^{m} &:= \boldsymbol{R}_{1,2}^{m} + \boldsymbol{b}_{1,2}^{m} \\ \boldsymbol{\mathcal{D}}_2^{m} &:= \boldsymbol{\mathcal{R}}_2^{m} + \boldsymbol{\mathcal{B}}_2^{m} \\ \overline{\bar{\boldsymbol{U}}_1} &:= \mathrm{r}_{21}\, \bar{\bar{\boldsymbol{U}}}_2^{m} \\ \overline{\boldsymbol{\mathcal{X}}_1} &:= \mathcal{R}_{21}\, \boldsymbol{\mathcal{X}}_2^{m} \\ \overline{\boldsymbol{d}_{1,1}} &:= \mathrm{p}_{12}^{*}\, \boldsymbol{d}_2^{m} \\ \overline{\boldsymbol{\mathcal{D}}_1} &:= \mathcal{P}_{12}^{*}\, \boldsymbol{\mathcal{D}}_2^{m} \end{aligned}$$

Do $i = 0$ to p

$$\begin{aligned} \boldsymbol{R}_{1,1}^{0} &:= \boldsymbol{R}_{1,1}^{0}(\overline{\boldsymbol{\mathcal{X}}_1}) \\ \boldsymbol{M}_1 \frac{\bar{\bar{\boldsymbol{U}}}_1^{i+1}}{\Delta t_1} &= \boldsymbol{M}_1 \frac{\bar{\boldsymbol{U}}_1^{i}}{\Delta t_1} + \overline{\boldsymbol{d}_{1,1}} - \boldsymbol{R}_{1,1}^{0} + \boldsymbol{R}_{1,1}^{i} + \boldsymbol{b}_{1,1}^{i} \\ \star \qquad \boldsymbol{\mathcal{R}}_1^{0} &:= \boldsymbol{\mathcal{R}}_1^{0}(\overline{\boldsymbol{\mathcal{X}}_1}, \bar{\bar{\boldsymbol{U}}}_1^{0}) \\ \boldsymbol{\mathcal{M}}_1 \frac{\boldsymbol{\mathcal{X}}_1^{i+1}}{\Delta t_1} &= \boldsymbol{\mathcal{M}}_1 \frac{\boldsymbol{\mathcal{X}}_1^{i}}{\Delta t_1} + \overline{\boldsymbol{\mathcal{D}}_1} - \boldsymbol{\mathcal{R}}_1^{0} + \boldsymbol{\mathcal{R}}_1^{i} + \boldsymbol{\mathcal{B}}_1^{i}. \end{aligned}$$

End Do

Coarse grid correction stage:

$$\begin{aligned} \Delta \boldsymbol{\mathcal{X}}_1 &:= \boldsymbol{\mathcal{X}}_1^{p} - \overline{\boldsymbol{\mathcal{X}}_1} \\ \Delta \boldsymbol{\mathcal{X}}_2 &:= \mathcal{P}_{12} \Delta \boldsymbol{\mathcal{X}}_1 \\ \boldsymbol{\mathcal{X}}_2^{m+1} &:= \boldsymbol{\mathcal{X}}_2^{m} + \Delta \boldsymbol{\mathcal{X}}_2 \end{aligned}$$

Table 7.2: Multigrid V-cycle applied to CBS

7.2.1 Programming notes

The computer code written for testing the CBS algorithm is briefly described in a previous chapter. Once this code was done and tested for laminar flow problems and after chosing multigrid as speed up technique, the question was: should we program together CBS + MG in a new, larger code? Or can we write a different program only for MG which in turn controls the CBS running on the hierarchy grids? These options are depicted in fig. 7.4 and fig. 7.5 respectively.

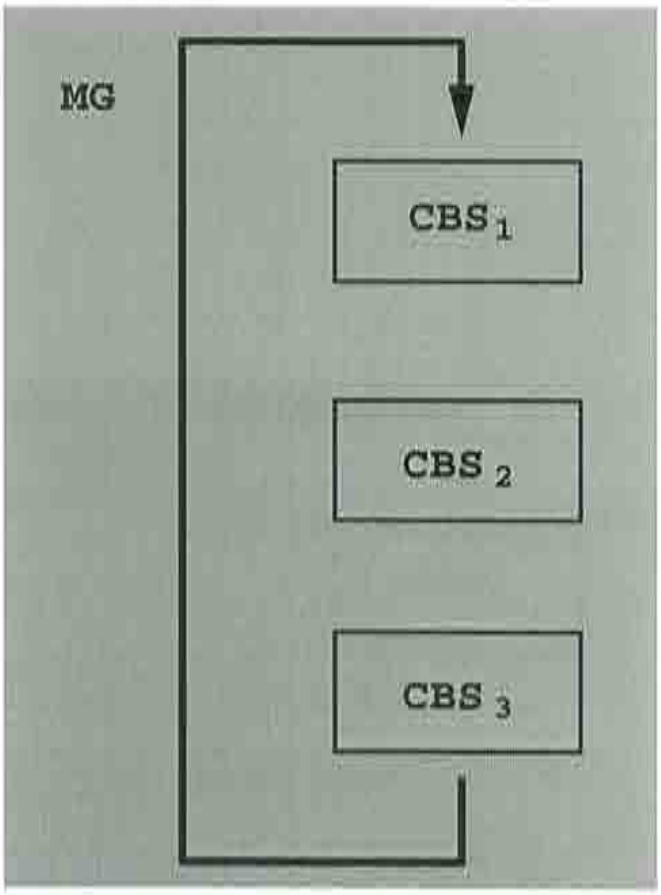

Figure 7.4: MG+CBS: "1-Code" strategy.

The first procedure, the "1-Code" strategy, is particulary recommended for implicit schemes, because everything can be within the solver. On the other hand, for explicit algorithms it is apparent that both solutions can be equally adopted. Multigrid techniques applied to fractional step methods in compressible flow is something

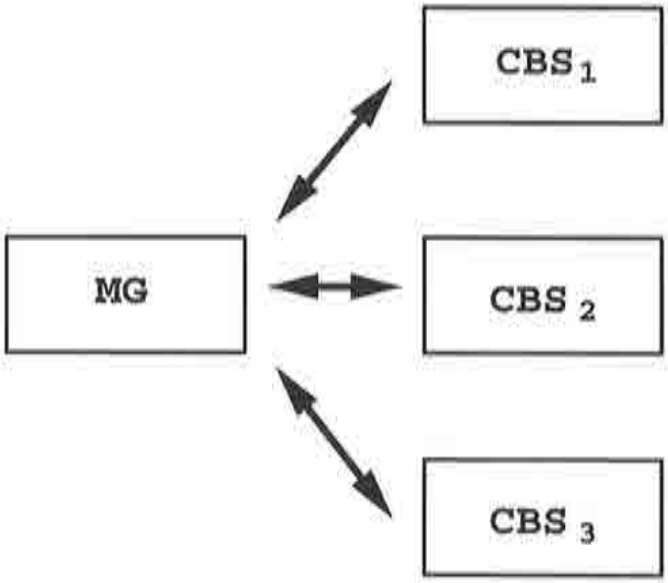

Figure 7.5: MG+CBS: "Master-slaves" strategy.

quite original and in a very embrionary state. Thus, a separate code provides an easier way of study different possibilities as they change. We preferred the "Master-Slaves" strategy: a individual multigrid code plays the role of a "master" controlling different equivalent CBS codes, running as if were independent problems, with their own time advance strategies, interpolation spaces, stabilizing diffusion, time step evaluation and so on. Each problem runs unnoticed of the existence of the rest of "slaves", except for the fact that at the beginning of each time step each CBS codes receives the transferred residuals and unknowns and at the end, either it transfers to the master or it keeps time advancing until the master commands it.

The multigrid code can communicate with the chain of CBS's in many ways. It can be done using PVM (Parallel Virtual Machine, a communication protocol created for data tranference between computers of different kinds) or, with less portable capabilities, using inter-process communication of UNIX operative system (the so-called *socket* function). A third possibility is between both strategies cited above: a master-slaves procedure in which MG and CBS programs are in fact subroutines of an integrating code. We have chosen the "master-slaves" option combined with socket UNIX functions with very good results: in machines with multiple processors and shared memory, data tranfer can be up to 10 times faster (!) with sockets than with PVM. Of course, PVM portability characteristics are unbeatable by sockets, at least as it is presented here. In any case, CPU time spent in communication was of about 1% in the problems studied.

Multigrid master code controls the general MG procedure. First it contructs transfer operators between the discretizations like is here described. Then it releases the CBS's one at a time. Paralellization degree is very small because while one CBS is working the rest must wait until the following in the hierarchy receives data. Next, this one works and the rest keeps standing by.

7.3 Numerical Examples

We test multigrid ideas in two compressible flow problems, previously shown in chapter 4: the supersonic Carter's flow and the transonic flow passing a NACA 0012, which is shown in chapter 4. Boundary conditions and numerical parameters are the same as there. The first case shows how Multigrid ideas work when combined with the CBS algorithm in the way proposed above by using different order discretizations. The Q2 grid is particularly interesting. In chapter 4 we have shown that biquadratic elements are a great choice for solving shock-boundary layer interactions. Here, its very slow convergence is highly improved, making them very competitive against bilinear elements. Finally, in the second example, the concepts are again put to a test.

7.3.1 Carter's flow

Problem description The finer mesh both for Q1 and Q2 elements, is the one used previously too. New coarser P1 and Q1 meshes are added to form the required hierarchy. This meshes are not refined at all. The purpose here is just to show the scheme behavior using the MG techniques in the way we propose.

Multigrid implementation For the analysis of the Carter's problem, we discretize the problem using five different partitions, shown in figure fig. 7.6. G1 is made of bilinear (G1a) or biquadratic (G1b) elements, being the nodes coincident in both cases. G2a and G3a are bilinear element grids, and G4c is linear. Also, G4c it is the only one unstructured.

- **G1a:** 7345 nodal points, 7168 Q1 elements, 4 nodes each
- **G1b:** 7345 nodal points, 1792 Q2 elements, 9 nodes each
- **G2a:** 1881 nodal points, 1792 Q1 elements, 4 nodes each
- **G3a:** 493 nodal points, 448 Q1 elements, 4 nodes each
- **G4c:** 684 nodal points, 1274 P1 elements, 3 nodes each

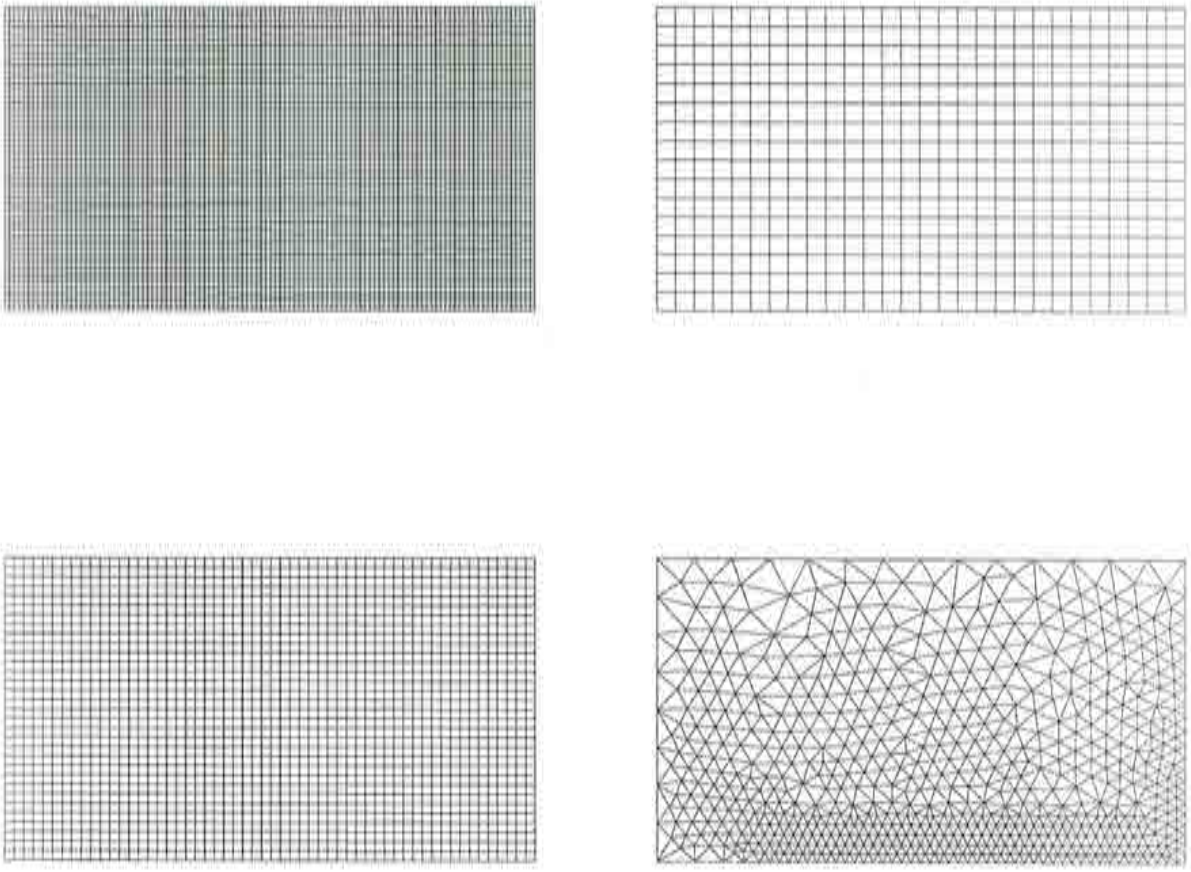

Figure 7.6: Carter problem. Spatial grids. Clockwise, from top-left: G1a (G1b also), G3a, G4c and G2a.

Figure fig. 7.7 shows the convergence of the spatial RHS for the continuity equation in the case G1a or G1b are used as principal grids. The former graph compares several combinations of linear and bilinear element grids. For the double combination (G1a + G2a) a V-Cycling strategy was used, being $m = 3$ and $p = 4$ (see table 7.2). For the triple (G1a + G2a + G3a), W-Cycling turned to be a better option, with $m = 3$, $p = 4$ and $q = 4$. Also, 4 steps of postsmoothing in G2a are done prior to pass to G3a, which improves the performance. At about step 50 G3a leaves the process.

In this graph, it can be seen a rather surprising fact. Before 2000 CPU time units, the convergence of the 3-grid multigrid is much steeper than that of the other two. But at about this time value, the curve crosses the 2-grid one. How can this be possible? The answer is easy and it was cited above: the mixture of transferred and "in situ" calculated variables in $\mathcal{R}_1^0$ (the starred line in table 7.2). This is inherent to fractional step methods, because when the stationary state is reached, the residual of fractional momentum equation is different from zero due to the lacking pressure gradient term. Hence, a threshold residual value had to be put in order to disconnect the coarser discretizations once the residual modul goes below it. In the 3-grid configuration, only the coarsest grid leaves the multigrid arrange.

The second convergence plot shows the performance of the procedure when the principal mesh is made of Q2 elements. The triple MG (G1b + G2a + G4c) is W-Cycling, with $m = 2$, $p = 2$ and $q = 4$ and 2 postsmoothing steps in G2a. Appart from this MG combination and the single G1b curve, it is here replotted the single G1a curve to show the even lower convergence rate of the biquadratic elements. The flexibility provided by the FEM in which CBS method is based is here clearly shown. Three element types (biquadratic Q2, bilinear Q1 and linear P1) are combined in order to speed up the convergence of the worst of them, namely Q2. Left alone, spatial grids made of Q2 elements are extemely slow. In the same graph it is repeated the curve for the Q1 grid for comparison. When both grids made of quadrilaterals are combined with a P1 coarser grid, the speed up is the highest. Therefore, in the way proposed here, a multigrid method can make higher order elements more appealing and worth studying, at least in compressible flow problems.

Figures fig. 7.8 and fig. 7.9 show qualitatively the convergence degree reached at a given value of CPU time units by comparing level contours in different cases. In fig. 7.8 a single Q1 grid against two of them are compared. Then, (fig. 7.9) the same is done for a single Q2 and the Q2-Q1-P1 multigrid. Although the multigrid solution is not totally converged (some oscillations are still there), the speed up is clearly observed. The shock is the structure developed first and then the boundary layer, at least for this initial conditions. At $t = 0$, all the variables are set to the inflow values.

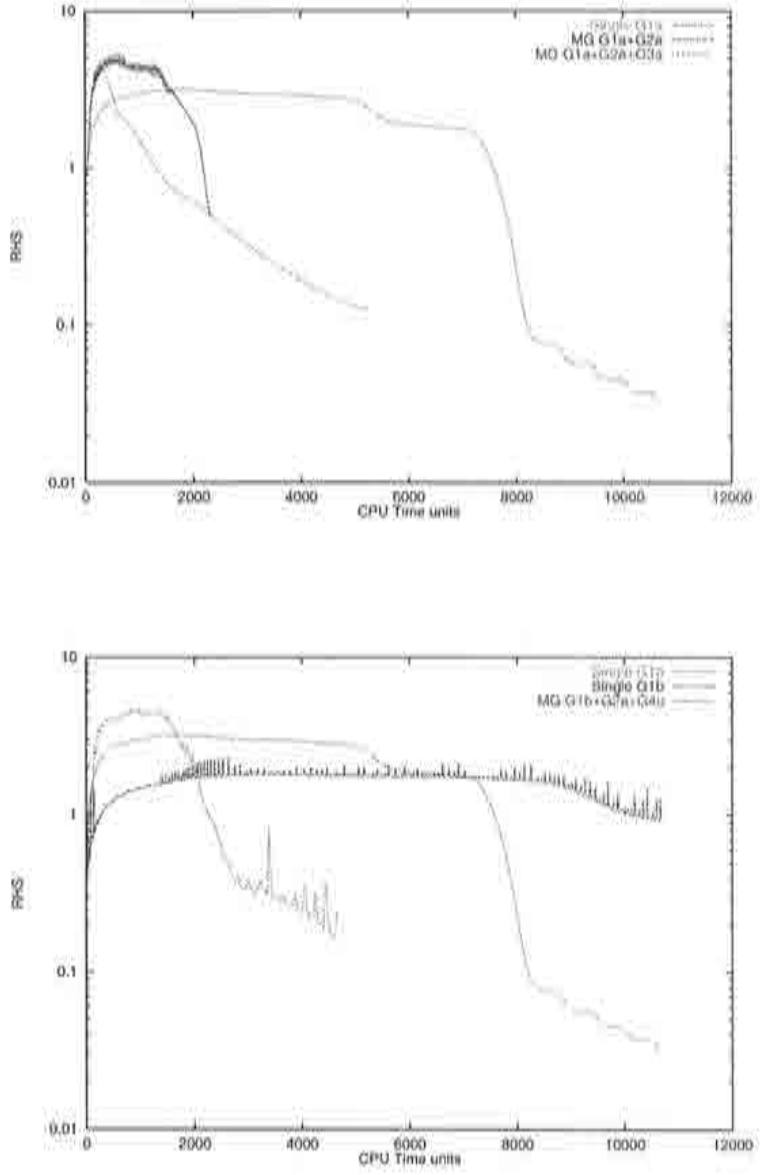

Figure 7.7: Carter problem. Convergence history with G1a (top) and G1b (bottom) as principal meshes.

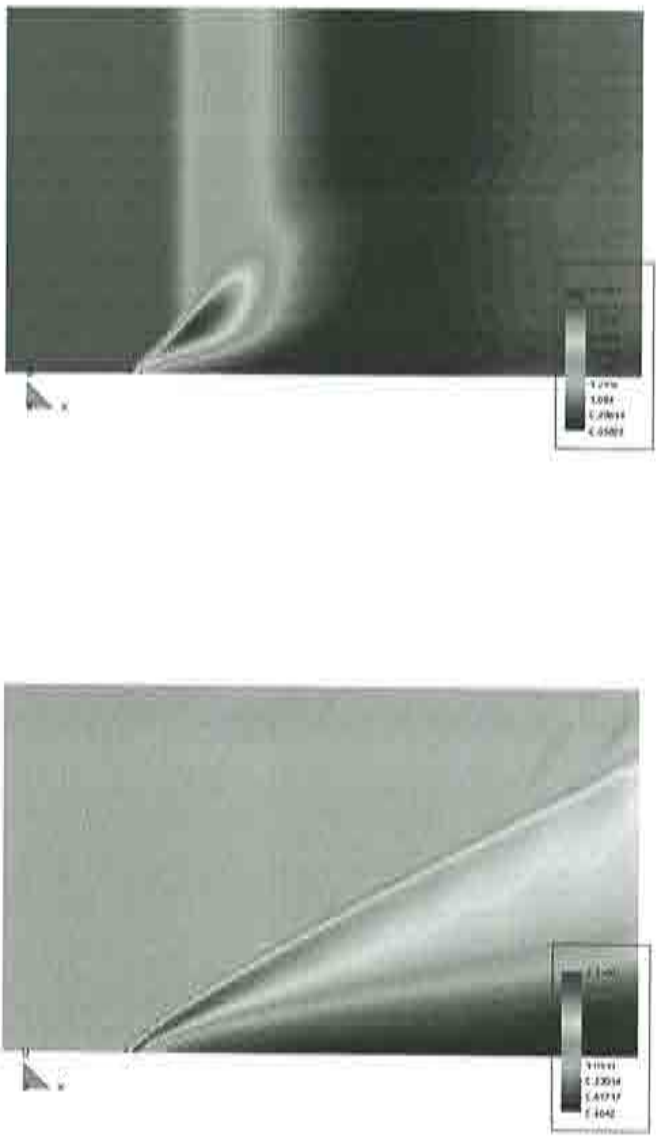

Figure 7.8: Carter problem. Density contours shown at CPU time units=2300 for both a single grid (G1a) (top) and a two grid MG (G1a + G2a) (bottom).

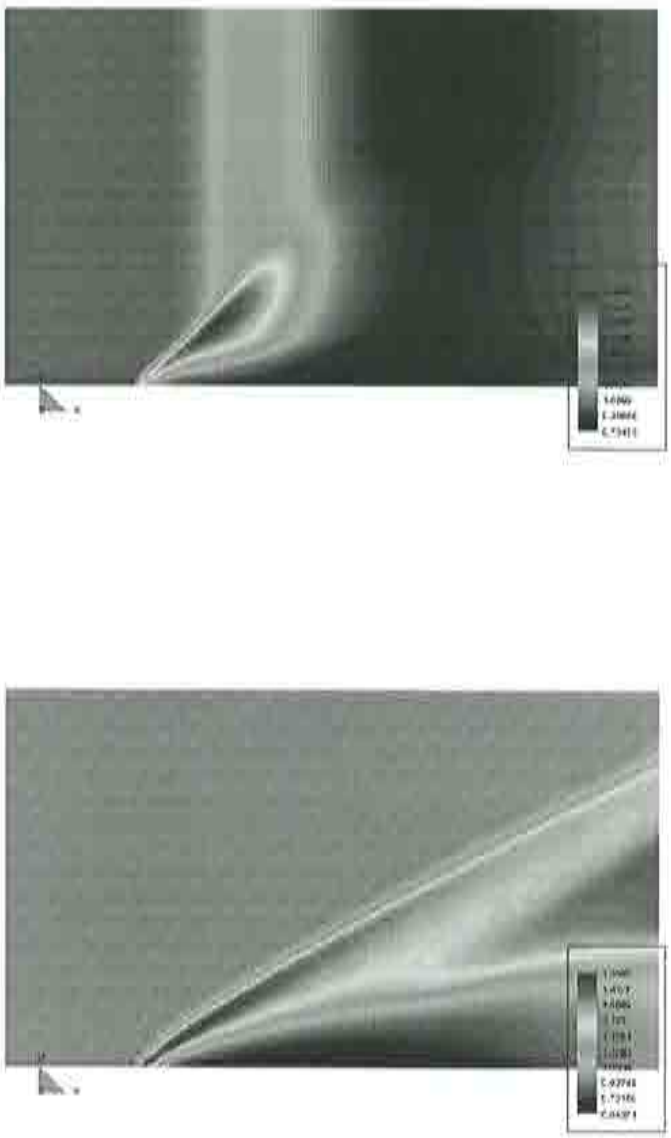

Figure 7.9: Carter problem. Density contours shown at CPU time unit=4600 for both a single grid (G1b) (top) and a three grid MG (G1b + G2a + G4c) (bottom).

7.3.2 Transonic flow passing a NACA 0012 profile

Problem description Again, the finest discretization is that of section 4. Two more coarser grids are used to construct the hierarchy. All three are unstructured and made of P1 elements, slightly refined in the boundary layer, not in the wake.

Multigrid implementation The grids used are shown in fig. 7.10. Next their sizes are written:

- **G1c:** 4359 nodal points, 8446 P1 elements, 3 nodes each
- **G2c:** 1284 nodal points, 2450 P1 elements, 3 nodes each
- **G3c:** 805 nodal points, 1565 P1 elements, 3 nodes each

History convergence is shown in fig. 7.11. In order to compare the real convergence status, both the single grid and multigrid problems are stopped at the same CPU time, at about 310 units. In this case, we adopted the multigrid strategy found to be best in the previous example: W-Cycling, using 4 steps of postsmoothing in the second mesh and $m = 3$, $p = 4$ and $q = 4$. In order to get more speed up, no shock capturing is activated G2c and G3c, thus decreasing the CPU time needed by these discretizations. In this figure, it can be seen a steep jump at the first steps. This is so because the residual is normalized using the first step value, obtained in the finest grid *before* starting the multigrid process. Clearly, the first step residual *after* multigrid activation is larger. Again, as in the previous case, after some time if the coarsest mesh keeps working the solution could be worsened by it. Now the effect could be stronger due to the fact that the coarsest discretization is really coarse, specially in the wake region. This can be avoided by disconnecting G3c once some residual norm criteria is reached or by using a wake-refined grid. In any case, fig. 7.12 and fig. 7.13 shows at what extent multigrid accelerates the convergence to stationary states. The chord-wise C_p distribution is compared for the converged solution and those solutions obtained with and without multigrid at the same CPU time (around 310 units). With MG applied, it is very close to the converged distribution. On the other hand, the Mach number level contours shown in fig. 7.13 are again, like in the Carter's case, an impressive signal of the convergence degree: the boundary layer is almost developed in the accelerated process.

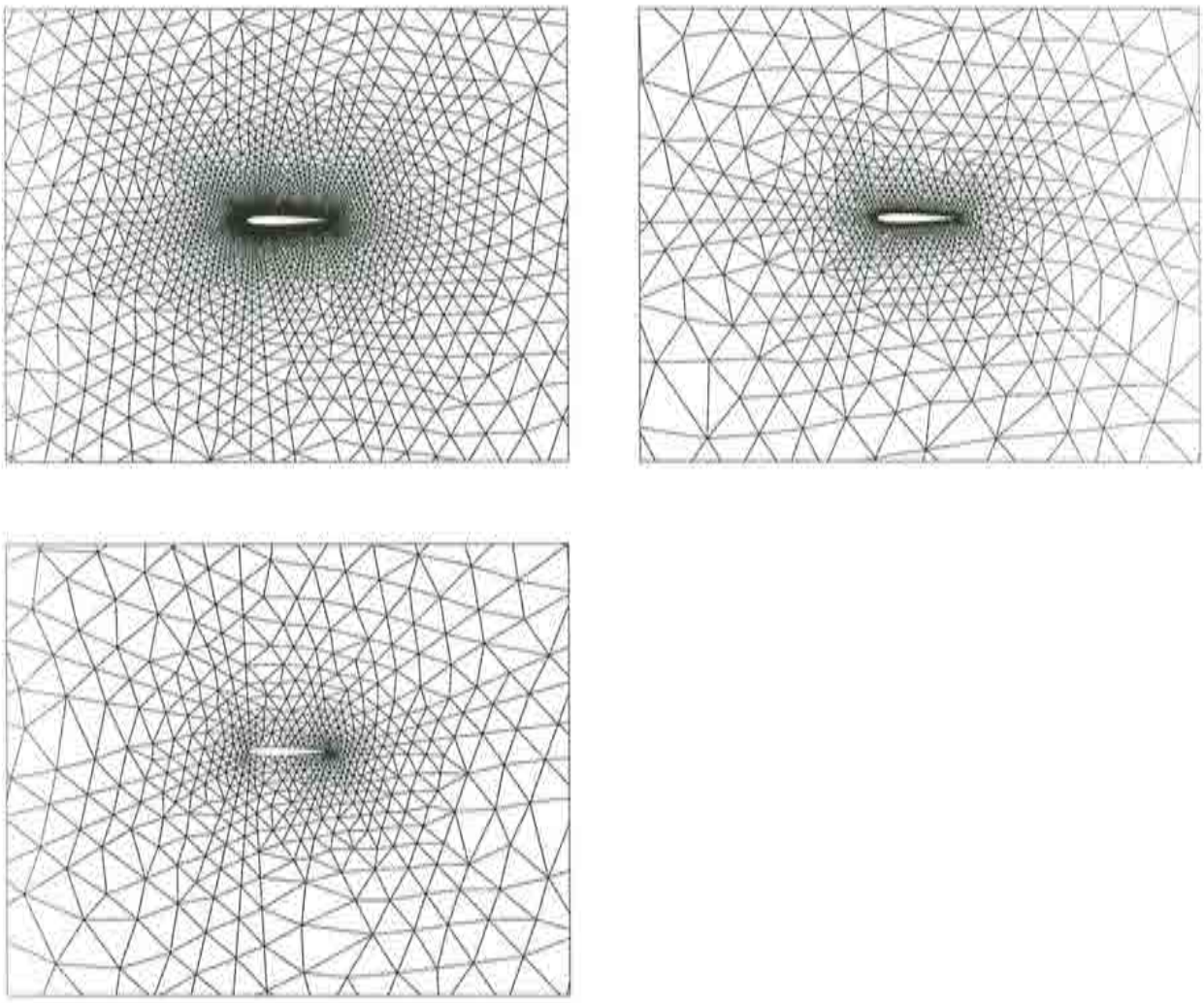

Figure 7.10: NACA 0012. Spatial grids. Clockwise, from top-left: G1c, G2c and G3c.

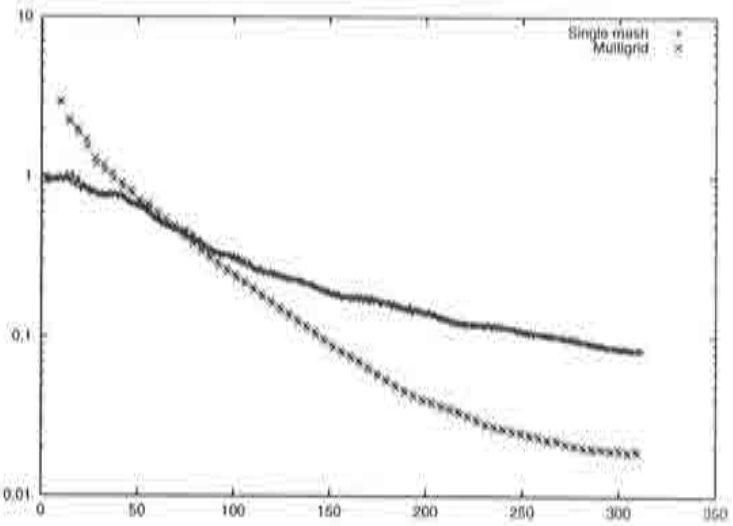

Figure 7.11: NACA 0012. Convergence history until CPU Time = 300.

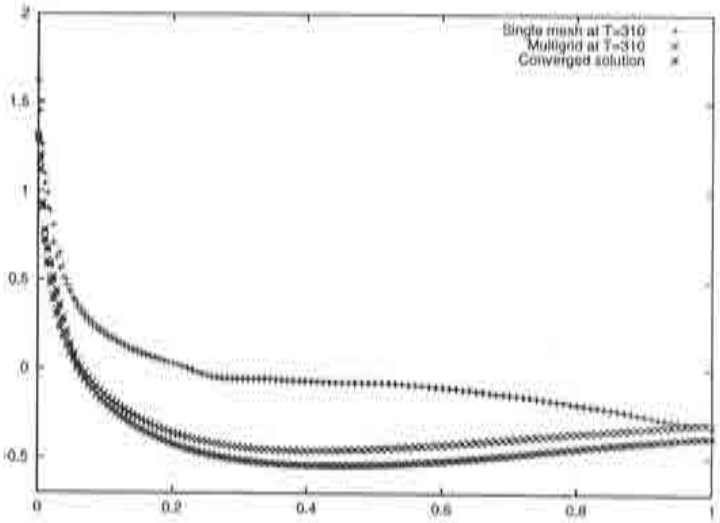

Figure 7.12: NACA 0012. C_p distribution at CPU Time = 300 for a single mesh, for MG using 3 meshes and converged solution.

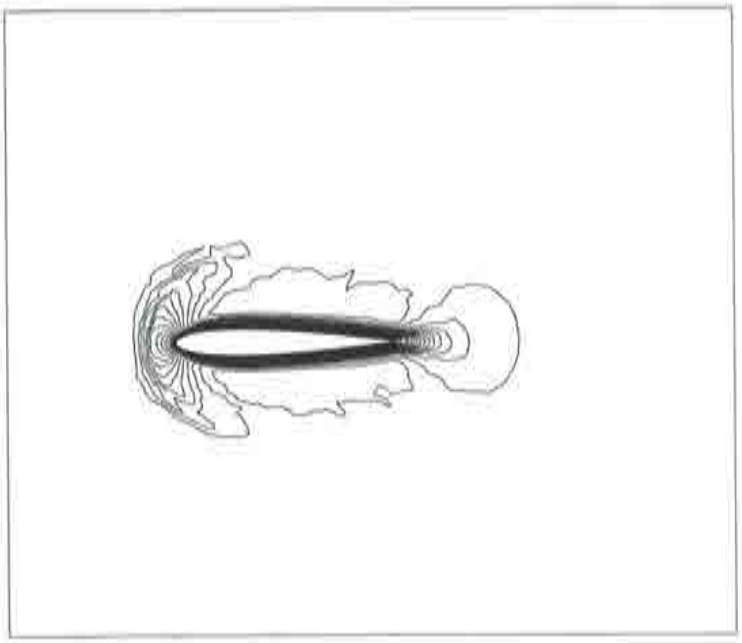

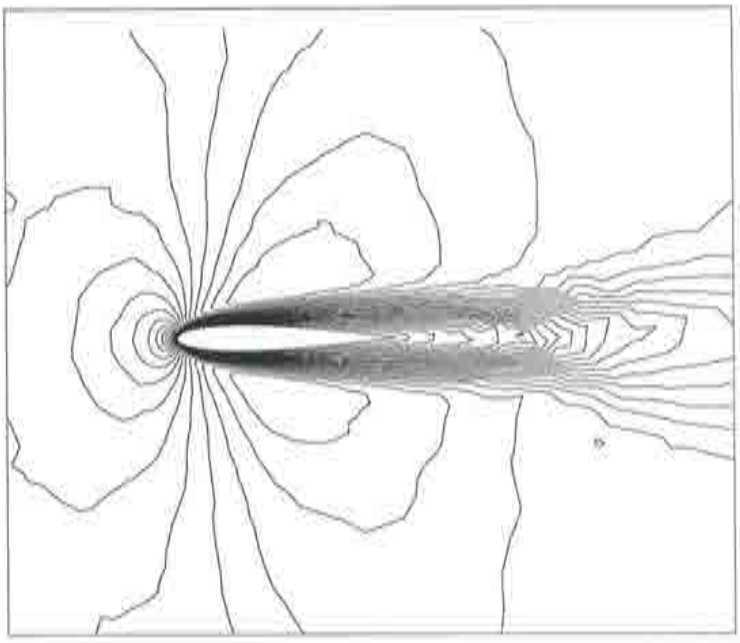

Figure 7.13: NACA 0012. Mach number contours at CPU Time = 300 for a single mesh (top) and for MG using 3 meshes (bottom).

7.4 Summary

Multigrid techniques combined with CBS algorithm are discussed. MG speed up convergence effects are well known and CBS scheme left alone can be quite slow to reach stationary states. First, MG general idea is introduced. Then, its main ingedients, flow diagram and characteristics are described. One of many different possibilities for implement a fractional step scheme with multigrid is next suggested. Taking profit of the finite element features, it is proposed to use the new CBS+MG new scheme with spatial discretizations of different order. Finally, a Navier-Stokes viscous compressible problem, the Carter's flow over a plate, is analyzed. It is demonstrated the great advantages of the proposed method, specially when the finest discretization is of higher order than the rest.

Chapter 8

Conclusions. Future lines

This monograph presents the development of a general algorithm for compressible and incompressible flow: the CBS. The three main chapters (Laminar Flow, Turbulent Flow and Accelerating Technique) describe the evolution of our work throughout the years. The original idea of all these kind of algorithms is to bridge the gap which lays between incompressible and compressible flow, a traditional challenge in computational fluid mechanics. CBS is a possible, real attempt, with some great advantages and a few drawbacks. Lot of work has been done by all the group working to develop CBS method and lot of work is waiting to be done. Step by step, the algorithm has been (and it is) successfully tackling a broad range of problems, once incompressibility limit is solved. Some of them are shown here, but a great deal is done outside this context by Prof. O.C. Zienkiewicz and his co-workers, being the lucky author of this manuscript one of them.

The extension to compressible flow of fractional steps techniques, which have their origin in incompressible flow problems is a powerful tool for bridging the cited gap. The general method is described here. The Navier-Stokes equations for laminar flow are first written in their weak form and then projected to the finite element space functions. CBS flexibility, inherited from the finite element method, allowed to test the algorithm in different kinds of elements, integration rules, time advance schemes. A computer code, christened *Alamak*, was written to implement the algorithm. We believe that the comparison of several element types done for all the problems here considered is a quite innovative approach. This comparison is done for at least one problem of every kind. Quadratic triangles has shown its "wildest" side for being much more difficult to fine tune than linear triangles. Perhaps, out of all the elements here tested (P1, P2, Q1, Q2) this type is the least reliable. On the other hand, biquadratic Q2 elements has demonstrated a great performance, particularly in the Carter's flat plate problem. Non linear elements can be a good solution for boundary layers with high gradients, like those found in turbulence.

The fractional step technique allows us to solve the incompressibility limit. However, its slow convergence rate, common to all projection schemes, can be a great disadvantage. We propose here an algorithm with many degrees of implicitness, which can be adapted to many situations. Full explicit form can be widely used in compressible Euler or Navier-Stokes problems. By solving implicitly some terms we can reach greater and greater safety factors, in this case called simply *time* factors. The "record" of all this monograph is 500 or more, spurious diffusion unnoticed, for the barotropic NACA compressible profile. For the fractional momentum equation, we propose a simple linearization for the convective term and a innovative implicit treatment. In the way depicted here, the typical *fractional step error* can be eliminated from the convective term. A second original aspect of this is that by a careful handling of the stress tensor, the left hand side matrix is the same for all the spatial dimensions, considering each fractional momentum vector component as an scalar. Finally, the energy equation (or heat transport one) allows a similar treatment.

Boundary conditions treatment is also considered carefully in this monograph. For compressible flow, the usual subsonic-supersonic / outlet-inlet relationships are used for Dirichlet boundary conditions. On the other hand, incompressible boundary conditions are analyzed in a deeper way. In these problems, Neumann boundary conditions for one unknown (the velocity, for instance) can become Dirichlet ones for another (the pressure) and vice versa. This allows different new combinations. The well known open boundary condition is for the fractional step method, as it is stressed in this monograph, a natural condition, coming from the weak form itself. In the incompressible problems, all of these points are exemplified.

Anisotropic shock capturing provides an elegant and effective way of controlling localized instabilities near shock waves. Also for incompressible Euler or high Re number flow, ASC becomes a useful tool for either accelerate the convergence to a stable state or smooth discontinuities created at the boundaries and which can propagate inwards. Clear examples are, in the first case, the setting of the so-called Kutta condition in the NACA tilted profile, the first of the series of laminar examples. And in the second case, the turbulent backwards facing step, where very strong gradients are produced in the problem boundaries. In its origin, ASC was devised for much simpler equations. All along this work, its action in Navier-Stokes or Euler equations is extensively tested, and some rules for its application to each of the set's equations are proposed.

It follows the extension to turbulent flow of the CBS method. Being rather new the idea of extending fractional step techniques to compressible flow, to include turbulent terms in the laminar, now averaged, Navier-Stokes equations and enrich the model with two equations for k-ε , the turbulent variables, is really innovative. Both stabilization techniques of CBS can be applied to turbulence equations: ASC and CG. Law of the wall type boundary conditions can be applied in a natural way through boundary integrals, a fact coming from the weak form of the equations and typical of finite

element methods. In this monograph, this extension is in a quite preliminary state. Due to a lack of both time and inspiration (inspiration on the author's side) turbulence compressible problems could not be included in the original manuscript. However, all the motivation (motivation on the author's side too) is put in use the algorithm as numerical laboratory for test and develop turbulence models. In any case, the turbulent incompressible flow examples shown here give us some confidence in future task.

Finally, multigrid techniques are faced. The objective is to improve the convergence rates of the algorithm. In this case, a one example study shows the potential of the method. A search in an Internet site devoted to multigrid methods (cited in the multigrid chapter) of any method which combines both MG and fractional step techniques for compressible flow gives 0 entries out of more than 3000 (October, 1998). The same result holds for MG and mixed element type discretizations. These two aspects are treated and developed in this monograph. Of course, also, lot of work has to be done.

Many examples are here examined. But many more are to be treated. *Alamak*, the algorithm code, is written independent of the space dimensions. It can handle either 2D or 3D problems. In this monograph only a simple 3D problem is shown. Also, no hypersonic problems are included and we feel prompted to study them. Turbulence study must be deepened. To cover a wider model panorama in incompressible flow and to move into compressible turbulence modelization should be the two ways to follow. Finally convergence speed up is a must. Multigrid methods seems to be a powerful tool, and it is our intention, once a quite effective procedure is achieved, to integrate MG and CBS in a unique code, by separated subroutines. On a different way, but aiming at the same objective is the implicit form of the algorithm. Extensive testing in the energy and heat transport equation, and in the turbulence variable equations is to be done in the near future.

Appendix A

Appendix

A.1 Time step evaluation

As was stated when discussing the convection - diffusion - reaction (CDR) character of the equations, an extension from stability conditions for scalar CDR equations is used to evaluate multidimensional CDR time steps, according to

$$\Delta t = \frac{F_S}{\left(\frac{1}{\Delta t_c} + \frac{1}{\Delta t_u}\right)} \tag{A.1}$$

where both Δt_c and Δt_u are calculated independently. If the CDR equation

$$\frac{\partial V}{\partial t} + \beta \frac{\partial V}{\partial x} - \epsilon \frac{\partial^2 V}{\partial x^2} + \sigma V = Q, \tag{A.2}$$

with $\epsilon, \sigma > 0$, is discretized in space by means of the SUPG method, the following term is added

$$\alpha \frac{h}{2} \frac{\partial N(x)}{\partial x}$$

to the weighting function $N(x)$ when discretized in time using a forward Euler method, the limiting time step, for which a stability condition holds, must verify ([Codina, 1992])

$$\Delta t^{\mathrm{L}} \leq \frac{1}{A(\frac{2\epsilon}{h^2} + \frac{\alpha\beta}{h}) + \frac{\sigma}{2}}. \tag{A.3}$$

In this inequality, A depends on the order of the interpolation ($A = 1$, if linear or $A = 8$, if quadratic). The mass matrix used in the calculation of the stability condition is the lumped mass matrix. [1] Defining the *Peclet number* as

$$Pe = \frac{h\beta}{2\epsilon}, \tag{A.4}$$

the optimal upwind function α is a dependent on Pe. Its asymptotic approximation can be used instead of the function itself. This approximation is different whether the order of the interpolation is linear or quadratic:

- Linear: $\alpha = \min(Pe/3, 1)$
- Quadratic: $\alpha = \min(Pe/12, 1)$

As was said previously, to calculate Δt_c, the diffusive limit is used, and Δt_{u} is obtained directly by means of (A.3). Then (A.1) becomes:

$$\Delta t = \frac{F_{\mathrm{S}}}{A(\frac{4\epsilon}{h^2} + \frac{\alpha\beta}{h}) + 2B\sigma}, \tag{A.5}$$

where, now, $\beta^2 = \beta_i\beta_i$.

We can turn back to Navier-Stokes equations. Plain use of this last equation to calculate the time increment could be quite difficult, because Navier-Stokes equations must be disentangled to show a "CDR character". To rewrite the original equations in a CDR fashion can become a very subjective matter, and many possibilities are able to be adopted. What we have used seemed to be efficient, but better choices are likely to

[1] If the consistent mass matrix is used instead of the lumped one, it can be proved that for the linear case the last term of the denominator is $\sigma/6$ instead of $\sigma/2$.

be found. In any case, as the shock capturing diffusion used here was derived also for a CDR equation, the same criteria to transform the original equations is used for it.

One last observation. In Navier-Stokes compressible equations, the reaction σ can be identified with the divergence of the velocity. In that case, it is not guaranteed at all that $\nabla \cdot \boldsymbol{u} > 0$. For that reason, we simply neglect the reaction, when Δt is calculated.

For each equation, we adopted the following identifications for $\boldsymbol{\beta}$ and ϵ (σ is equaled to zero) to be used in (A.5) to calculate the time increment:

- Continuity equation:

$$\begin{aligned} \beta_i &= u_i \\ \epsilon &= 0 \end{aligned}$$

- Linear momentum equation:

$$\begin{aligned} \beta_i &= u_i - \frac{1}{\rho}\frac{\partial}{\partial x_i}\mu \\ \epsilon &= \frac{\mu}{\rho} \end{aligned}$$

- Total energy equation:

$$\begin{aligned} \beta_i &= u_i - \frac{1}{\rho}\frac{\partial}{\partial x_i}\mu \\ \epsilon &= \frac{\mu}{\rho} + \frac{k}{C_v \rho} \end{aligned}$$

- Temperature equation:

$$\begin{aligned} \beta_i &= u_i^{\mathrm{Rea}} \\ \epsilon &= \frac{k}{C_v \rho} \end{aligned}$$

A.2 Matrix B: a pressure stabilizer

In the section devoted to the continuity equation discretization, matrix $\boldsymbol{B} := \boldsymbol{L} - \boldsymbol{G}_0^t \boldsymbol{M}_0^{-1} \boldsymbol{G}_0$ appearing was discussed. It is a matrix that appears in the incompressible, space discretized, form of the algorithm, which allows equal interpolation for both velocity and pressure and stabilizes the pressure. This is partly explained because $\boldsymbol{B}$ is positive semidefinite. We will prove it now.

To simplify the notation, let us write $\boldsymbol{B} := \boldsymbol{L} - \boldsymbol{G}^T \boldsymbol{M}^{-1} \boldsymbol{G}$. Let two different interpolating finite element spaces for $\boldsymbol{U}$ and p: V_h and $Q_h \subset C^0(\Omega)$ respectively. Let us consider the space $E_h = V_h + \nabla Q_h$ and see how $\boldsymbol{B}$ operates with elements belonging to it. ∇Q_h denotes the space of vector functions gradients of Q_h. We can split

$$E_h = V_h \oplus V_h^{\perp} = \mathrm{Span}\{\boldsymbol{v}_1, \ldots, \boldsymbol{v}_n\} \oplus \mathrm{Span}\{\boldsymbol{v}'_1, \ldots, \boldsymbol{v}'_m\} \tag{A.6}$$

and we need to prove that

$$\bar{\boldsymbol{p}}^T \boldsymbol{B} \bar{\boldsymbol{p}} = \bar{\boldsymbol{p}}^T \boldsymbol{L} \bar{\boldsymbol{p}} - \bar{\boldsymbol{p}}^T \boldsymbol{G}^T \boldsymbol{M}^{-1} \boldsymbol{G} \bar{\boldsymbol{p}} \tag{A.7}$$

is non-negative. If we consider the decomposition

$$\nabla p = \boldsymbol{s} + \boldsymbol{t} = \bar{s}_i \boldsymbol{v}_i + \bar{t}_j \boldsymbol{v}'_j \tag{A.8}$$

where $\boldsymbol{s} \in V_h$,$\boldsymbol{t} \in V_h^{\perp}$, $i = 1, \ldots, n$, and $j = 1, \ldots, m$, then

$$\bar{\boldsymbol{p}}^T \boldsymbol{L} \bar{\boldsymbol{p}} = \int_\Omega |\nabla p|^2 \, d\Omega = \bar{\boldsymbol{s}}^T \boldsymbol{M} \bar{\boldsymbol{s}} + \int_\Omega \boldsymbol{t} \cdot \boldsymbol{t} d\Omega \tag{A.9}$$

Besides, if M_{ij}^{-1} are the components of $\boldsymbol{M}^{-1}$,

$$\bar{\boldsymbol{p}}^T \boldsymbol{G}^T \boldsymbol{M}^{-1} \boldsymbol{G} \bar{\boldsymbol{p}} \;=\; \sum_{i,j=1}^{n} \left(\int_\Omega \nabla p \cdot \boldsymbol{v}_i d\Omega \right) M_{ij}^{-1} \left(\int_\Omega \nabla p \cdot \boldsymbol{v}_j d\Omega \right)$$

$$
\begin{aligned}
&= \sum_{i,j=1}^{n} \sum_{k,l=1}^{n} \bar{s}_k \left(\int_\Omega \boldsymbol{v}_k \cdot \boldsymbol{v}_l d\Omega \right) M_{ij}^{-1} \bar{s}_l \left(\int_\Omega \boldsymbol{v}_l \cdot \boldsymbol{v}_j d\Omega \right) \\
&= \bar{\boldsymbol{s}}^T \boldsymbol{M} \bar{\boldsymbol{s}} \qquad \text{(A.10)}
\end{aligned}
$$

And then, finally

$$
\bar{\boldsymbol{p}}^T \boldsymbol{B} \bar{\boldsymbol{p}} = \int_\Omega \boldsymbol{t} \cdot \boldsymbol{t} d\Omega \geq 0 \qquad \text{(A.11)}
$$

Bibliography

[Ames Research Staff, 1953] Ames Research Staff (1953). Equations, tables and charts for compressible flow. Technical report, NASA.

[Barakos and Drikakis, 1998] Barakos, G. and Drikakis, D. (1998). Assessment of various low-Reynolds number turbulence models in shock-boundary layer interaction. *Comp. Meth. Appl. Mech. Eng.*, 160:155–174.

[Bardina et al., 1997] Bardina, J., Huang, P., and Coakley, T. (1997). Turbulence modeling validation, testing and development. NASA Technical Memorandum 110446, NASA.

[Batchelor, 1953] Batchelor, G. (1953). *The theory of homogeneous turbulence.* Cambridge University Press.

[Batchelor, 1967] Batchelor, G. (1967). *An Introduction to Fluid Dynamics.* Cambridge University Press.

[Baumann et al., 1992] Baumann, C., Storti, M., and Idelsohn, S. (1992). Improving the convergence rate of Petrov-Galerkin techniques for the solution of transonic and supersonic flows. *Int. J. Num. Meth. Eng.*, 34:543–568.

[Brézis, 1984] Brézis, H. (1984). *Análisis Funcional.* Alianza Editorial. Spanish translation of the french original *Analyse Fonctionnelle*, published by Masson, Paris, in 1983.

[Brezzi and Bathe, 1990] Brezzi, F. and Bathe, K. (1990). A discourse on the stability conditions for mixed finite element formulations. *Comp. Meth. Appl. Mech. Eng.*, 82:27–57.

[Bristeau et al., 1990] Bristeau, M., Glowinski, R., Dutto, L., Périaux, J., and Rogé, R. (1990). Compressible viscous flow calculations using compatible finite element approximations. *Int. J. Num. Meth. Fluids.*, 11:719–749.

[Bristeau et al., 1988] Bristeau, M., Glowinski, R., Périaux, J., and Viviand, H. (1988). GAMM-workshop: Numerical simulation of compressible Navier-Stokes flows: Presentation of problems and discussion of results. In *Proceedings of the 7th. GAMM*

Conference on Numerical Methods on Fluid Mechanics, volume 20, pages 442–450, Wiesbaden.

[Brooks and Hughes, 1982] Brooks, A. and Hughes, T. (1982). Streamline upwind/Petrov-Galerkin formulations for convection dominated flows with particular emphasis on the incompressible Navier-Stokes equation. *Comp. Meth. Appl. Mech. Eng.*, 32:199–259.

[Chen and Doolen, 1998] Chen, S. and Doolen, G. (1998). Lattice Boltzmann method for fluid flows. *Annu. Rev. Fluid Mech.*, 30:329–364.

[Chen et al., 1993] Chen, S., Doolen, G., Kraichnan, R., and She, Z. (1993). On statistical correlations between velocity increments and locally ... dissipation in homogeneous turbulence. *Phys. Fluids A*, 5(2):458–463.

[Chien, 1982] Chien, K. (1982). Predictions of channel and boundary-layer flows with a Low-Reynolds number turbulence model. *AIAA Journal*, 20(1).

[Chorin, 1967] Chorin, A. (1967). A numerical method for solving incompressible viscous problems. *Journ. Comp. Phys.*, 2:12–26.

[Chorin, 1969] Chorin, A. (1969). On the convergence of discrete approximation to the Navier-Stokes equations. *Math. Comput.*, 23.

[Codina, 1992] Codina, R. (1992). *A Finite Element Model for Incompressible Flow Problems*. PhD thesis, Escola Tècnica Superior d'Enginyers de Camins, Canals i Ports, Universitat Politècnica de Catalunya, Barcelona.

[Codina, 1993a] Codina, R. (1993a). A discontinuity-capturing crosswind-dissipation for the finite element solution of the convection-diffusion equation. *Comp. Meth. Appl. Mech. Eng.*, 110:325–342.

[Codina, 1993b] Codina, R. (1993b). A shock-capturing anisotropic diffusion for the finite element solution of the diffusion-convection-reaction equation. In *Proc. VIII International Conference on Finite Elements in Fluids*, volume Part I, pages 67–75, Barcelona, Spain. Ed. CIMNE/Pineridge Press.

[Codina, 1998a] Codina, R. (1998a). Comparison of some finite element methods for solving the diffusion - convection - reaction equation. *Comp. Meth. Appl. Mech. Eng.*, 156:185–210.

[Codina, 1998b] Codina, R. (1998b). Numerical solution of the incompressible Navier-Stokes equations with Coriolis forces based on the discretization of the total time derivative. *Journ. Comp. Phys.*

[Codina et al., 1995] Codina, R., Vázquez, M., and Zienkiewicz, O. (1995). A fractional step method for compressible flows: Boundary conditions and incompressible limit. In *Proc. 9th International Conference on Finite Elements in Fluids, Venice, Italy*, volume Part 1, pages 409–418. Dip. di Matematica Pura ed Applicata, Università di Padova.

[Codina et al., 1998a] Codina, R., Vázquez, M., and Zienkiewicz, O. (1998a). *A fractional step method for the solution of compressible Navier - Stokes equations* . Computational Fluid Dynamics Review. World Scientific Publishing Co. Edited by M. Hafez and K. Oshima.

[Codina et al., 1998b] Codina, R., Vázquez, M., and Zienkiewicz, O. (1998b). A general algorithm for compressible and incompressible flow–Part III. The semi-implicit form. *Int. J. Num. Meth. Fluids.*, 27:13–32.

[Codina et al., 1998c] Codina, R., Vázquez, M., and Zienkiewicz, O. (1998c). An implicit fractional step finite element method for incompressible and compressible flows. In Hafez, M. and Heinrich, J., editors, *Proc. 10th International Conference on Finite Elements in Fluids*, pages 519–524, Tucson, EE.UU. University of Arizona.

[Courant and Friedrichs, 1948] Courant, R. and Friedrichs, K. (1948). *Supersonic Flow and Shock Waves*. Springer-Verlag.

[Demkowicz et al., 1990] Demkowicz, L., Oden, J., and Rachowicz, W. (1990). A new finite element method for solving compressible Navier-Stokes equations based on an operator splitting method and h-p adaptivity. *Comp. Meth. Appl. Mech. Eng.*, 84:275–326.

[Dick and Steelant, 1997] Dick, E. and Steelant, J. (1997). Coupled solution of the steady compressible Navier-Stokes equations and the k-ε turbulence equations with a multigrid method. *Appl. Num. Math.*, 23:49–61.

[Donea, 1984] Donea, J. (1984). A taylor - galerkin method for convective transport problems. *Int. J. Num. Meth. Eng.*, 20:101–119.

[Douglas and Russel, 1982] Douglas, J. and Russel, T. (1982). Numerical methods for convection dominated problems based on combining the method of characteristics with finite elements or finite difference procedures. *SIAM J. Numer. Anal.*, 19:871–885.

[Dubois et al., 1998] Dubois, T., Jaberteau, F., and Temam, R. (1998). Incremental unknowns, multilevel methods and the numerical simulation of turbulence. *Comp. Meth. Appl. Mech. Eng.*, 159:123–189.

[Dutto et al., 1997] Dutto, L., Habashi, W., and Fortin, M. (1997). An algebraic multilevel parallelizable preconditioner for large-scale CFD problems. *Comp. Meth. Appl. Mech. Eng.*, 149:303–318.

[Eriksson et al., 1996] Eriksson, K., Estep, D., Hansbo, P., and Johnson, C. (1996). *Computational Differential Equations*. Cambridge University Press.

[Faber, 1995] Faber, T. (1995). *Fluid Dynamics for Physicists*. Cambridge University Press.

[Favre, 1965] Favre, A. (1965). Equations des gaz turbulents compressibles. *Journal de Mécanique*, 4:361–421.

[Frink, 1998] Frink, N. (1998). Tetrahedral unstructured Navier-Stokes method for turbulent flows. *AIAA Journal*, 36(11).

[Ghia et al., 1982] Ghia, U., Ghia, K., and Shin, C. (1982). High-Re solutions for incompressible flow using the Navier-Stokes equations and a multi-grid method. *Jour. Com. Phys.*, 48:387–441.

[Gresho, 1990] Gresho, P. (1990). On the theory of semi-implicit projection methods for viscous incompressible flow and its implementation via a finite element method that also introduces a nearly consistent mass matrix. Part I: Theory. *Int. J. Num. Meth. Fluids.*, 11:587–620.

[Grotjans and Menter, 1998] Grotjans, H. and Menter, F. (1998). Wall functions for general application cfd codes. In *Proceedings of the Fourth ECCOMAS Computational Fluid Dynamics Conference*, pages 1112–1117, Athens, Greece. John Wiley & Sons Ltd.

[Guermond, 1994] Guermond, J. (1994). Remarques sur les méthodes de projection pour l'approximation des équations de Navier - Stokes. *Numer. Math.*, 67:465–473.

[Guermond and Quartapelle, 1995] Guermond, J. and Quartapelle, L. (1995). Analyse de convergence d'une approximation par éléments finis et méthode de projection pour les équations de Navier - Stokes instationnaires. Notes et Documents Limsi 95 - 06 and 14, LIMSI - CNRS.

[Hackbusch, 1994] Hackbusch, W. (1994). *Iterative Solution of Large Sparse System of Equations*. Springer - Verlag.

[Hanine and Kourta, 1991] Hanine, F. and Kourta, A. (1991). Performance of turbulence models to predict supersonic boundary layer flows. *Comp. Meth. Appl. Mech. Eng.*, 89:221–235.

[Hansbo, 1994] Hansbo, P. (1994). Aspects of conservation in finite element flow computations. *Comp. Meth. Appl. Mech. Eng.*, 117:423–437.

[Harlow and Nakayama, 1968] Harlow, F. and Nakayama, P. (1968). Transport of turbulence energy decay rate. University California Report LA-3854, Los Alamos Science Lab.

[Harten et al., 1983] Harten, A., Lax, P., and Leer, B. (1983). On upstream differencing and Godunov-type schemes for hyperbolic conservation laws. *SIAM Review*, 25(1):35–61.

[Hawke, 1995] Hawke, G. (1995). *A unified approach to compressible and incompressible flows and a new entropy-consitent formulation of the k-ε model*. PhD thesis, Department of Mechanical Engineering, Stanford University.

[Hawke and Hughes, 1998] Hawke, G. and Hughes, T. (1998). A comparative study of different sets of variables for solving compressible and incompressible flows. *Comp. Meth. Appl. Mech. Eng.*, 153:1–44.

[Hedstrom, 1979] Hedstrom, G. (1979). Nonreflecting boundary conditions for nonlinear hyperbolic systems. *Journ. Comp. Phys.*, 30:222–237.

[Higdon, 1986] Higdon, R. (1986). Initial-boundary value problems for linear hyperbolic systems. *SIAM Review*, 28(2):177–217.

[Hindmarsh et al., 1984] Hindmarsh, A., Gresho, P., and Griffiths, D. (1984). The stability of explicit Euler time-integration for certain finite-difference approximation of the multidimensional advection-diffusion equations. *Int. J. Num. Meth. Flaids.*, 4:853–897.

[Hirsch, 1990] Hirsch, C. (1990). *Numerical Computation of Internal and External Flows - Vol. 2*. John Wiley & sons.

[Hu and Rizzi, 1995] Hu, J. and Rizzi, A. (1995). Turbulent flow in supersonic and hypersonic nozzles. *AIAA Journal*, 33(9).

[Huang et al., 1994] Huang, P., Bradshaw, P., and Coakley, T. (1994). Turbulence models for compressible boundary layers. *AIAA Journal*, 32(4):735–739.

[Hughes, 1987] Hughes, T. (1987). *The Finite Element Method*. Prentice-Hall.

[Hughes, 1995] Hughes, T. (1995). Multiscale phenomena: Green's function, the Dirichlet-to-Neumann formulation, subgrid scale models, bubbles and the origins of stabilized formulations. *Comp. Meth. Appl. Mech. Eng.*, 127:387–401.

[Hughes and Mallet, 1986] Hughes, T. and Mallet, M. (1986). A New Finite Element Method for Computational Fluid Dynamics: III. The Generalized Streamline Operator for Multidimensional Advective-Diffusive Systems. *Comp. Meth. Appl. Mech. Eng.*, 58:305–328.

[Jiménez et al., 1993] Jiménez, J., Wray, A., Saffman, P., and Rogallo, R. (1993). The structure of intense vorticity in isotropic turbulence. *J. Fluid Mech.*, pages 65–90.

[Johnson, 1987] Johnson, C. (1987). *Numerical Solution of Partial Differential Equations by the Finite Element Method*. Cambridge University Press.

[Kanarchos and Pantelelis, 1994] Kanarchos, A. and Pantelelis, N. (1994). A multigrid scheme for the implicit solution of the compressible flow equations. *Comp. Mech.*, 14:235–248.

[Kanarchos and Vournas, 1993] Kanarchos, A. and Vournas, I. (1993). Multigrid technique for the compressible Euler and Navier-Stokes equations. *Eng. Comp.*, 10:123–137.

[Karimian and Schneider, 1995] Karimian, S. and Schneider, G. (1995). Pressure-based control-volume finite element method for flow at all speeds. *AIAA Journal*, 33(9).

[Kawahara and Ohmiya, 1985] Kawahara, M. and Ohmiya, K. (1985). Finite element analysis of density flow using the velocity correction method. *Int. J. Num. Meth. Fluids*, 5:981–993.

[Kim et al., 1980] Kim, J., Kline, S., and Johnston, J. (1980). Investigation of a reattaching turbulent shear layer: Flow over a backwards facing step. *J. Fluid. Eng. ASME Tran.*, 102:302–308.

[Kolmogorov, 1942] Kolmogorov, A. (1942). Equations of turbulent motion of an incompressible fluid. *Izvestia Academy of Sciences, USSR, Physics*, 6(1-2):56–58.

[Kreiss, 1970] Kreiss, H. (1970). Initial boundary value problems for hyperbolic systems. *Comm. Pure Appl. Math.*, 23:277–298.

[Krishnamurty and Shyy, 1997] Krishnamurty, V. and Shyy, W. (1997). Study of compressibility modifications to the $k-\varepsilon$ turbulence model. *Phys. Fluids*, 9(9):2769–2788.

[Landau and Lifshitz, 1987] Landau, L. and Lifshitz, E. (1987). *Fluid Mechanics*. Butterworth - Heinemann, 2nd. edition.

[Launder and Spalding, 1974] Launder, B. and Spalding, D. (1974). The numerical computation of turbulent flows. *Comp. Meth. Appl. Mech. Eng.*, 3:269–289.

[Laval and Quartapelle, 1990] Laval, H. and Quartapelle, L. (1990). A fractional - step Taylor - Galerkin method for unsteady incompressible flows. *Int. J. Num. Meth. Fluids.*, 11:501–513.

[Lee et al., 1987] Lee, J., Peraire, J., and Zienkiewicz, O. (1987). The Characteristic-Galerkin method for advection-dominated problems – an assessment. *Comp. Meth. Appl. Mech. Eng.*, 61:359–369.

[Lele, 1994] Lele, S. (1994). Compressibility effects on turbulence. *Annu. Rev. Fluid Mech.*, 26:211–254.

[Lesieur, 1990] Lesieur, M. (1990). *Turbulence in fluids*. Kluwer Academic Publishers.

[Lesieur and Métais, 1996] Lesieur, M. and Métais, O. (1996). New trends in Large - Eddy Simulations of turbulence. *Annu. Rev. Fluid Mech.*, 28:45–82.

[Lions, 1996] Lions, P. (1996). *Mathematical Topics in Fluid Mechanics. Volume 1. Incompressible Models.* Oxford University Press.

[Loehner et al., 1984] Loehner, R., Morgan, K., and Zienkiewicz, O. (1984). The solution of non-linear hyperbolic equations system by the finite element method. *Int. J. Num. Meth. Fluids.*, 4:1043–1063.

[Mavriplis, 1988] Mavriplis, D. (1988). Multigrid solution of the two - dimensional Euler equations on unstructured triangular meshes. *AIAA Journal*, 26(7):824–831.

[Mavriplis, 1995] Mavriplis, D. (1995). Multigrid techniques for unstructured meshes.

[Mavriplis and Martinelli, 1994] Mavriplis, D. and Martinelli, L. (1994). Multigrid solution of compressible turbulent flow on unstructured meshes using a two-equation model. *Int. J. Num. Meth. Fluids.*, 18:887–914.

[McComb, 1990] McComb, W. (1990). *The physics of fluid turbulence.* Oxford University Press.

[Millikan, 1938] Millikan, C. (1938). A critical discussion on turbulent flows in channels and circular tubes. Proc. 5th International Congress of Applied Mechanics.

[Mittal, 1998] Mittal, S. (1998). Finite element computation of unsteady viscous compressible flows. *Comp. Meth. Appl. Mech. Eng.*, 157:151–175.

[Mittal and Tezduyar, 1998] Mittal, S. and Tezduyar, T. (1998). A unified finite element formulation for compressible and incompressible flows using augmented conservation variables. *Comp. Meth. Appl. Mech. Eng.*, 161:229–243.

[Moin and Mahesh, 1998] Moin, P. and Mahesh, K. (1998). Direct numerical simulation: A tool in turbulence research. *Annu. Rev. Fluid Mech.*, 30:539–578.

[Nithiarasu et al., 1998] Nithiarasu, P., Zienkiewicz, O., Satyasai, B., Morgan, K., Codina, R., and Vázquez, M. (1998). Shock capturing viscosities for the general algorithm. In Hafez, M. and Heinrich, J., editors, *Proc. 10th International Conference on Finite Elements in Fluids, Venice, Italy*, pages 350–356, Tucson, EE.UU. University of Arizona.

[Oliger and Sundstrom, 1978] Oliger, J. and Sundstrom, A. (1978). Theoretical and practical aspects of some initial boundary value problems in fluid dynamics. *SIAM J. Appl. Math.*, 25:419–.

[Papanastasiou et al., 1992] Papanastasiou, T., Malamataris, N., and Ellwood, K. (1992). A new outflow boundary condition. *Int. J. Num. Meth. Fluids.*, 14:587–608.

[Peraire et al., 1993] Peraire, J., Peiro, J., and Morgan, K. (1993). Multigrid solution of the 3-D compressible Euler equations on unstructured tetrahedral grids. *Int. J. Num. Meth. Eng.*, 36:1029–1044.

[Pironneau, 1982] Pironneau, O. (1982). On the transport-diffusion algorithm and its application to the Navier-Stokes equations. *Numer. Math.*, 38:309–332.

[Pironneau et al., 1992] Pironneau, O., Liou, J., and Tezduyar, T. (1992). Characteristic-Galerkin and Galerkin/least-squares space-time formulations for the advection-diffusion equation with time-dependent domains. *Comp. Meth. Appl. Mech. Eng.*, 100:117–141.

[Reynolds, 1883] Reynolds, O. (1883). An experimental investigation of the circumstances which determine whether the motion of water shall be direct or sinuous, and of the law of resistance in parallel channels. *Royal Society, Phil. Trans.*, A175:935.

[Ristorcelli, 1993] Ristorcelli, J. (1993). A representation for the turbulent mass flux contribution to Reynolds-stress and two-equation closures for compressible turbulence. CR - 191569 ICASE, NASA.

[Roe, 1986] Roe, P. (1986). Characteristic-Based schemes for the Euler equations. *Annu. Rev. Fluid Mech.*, 18:337–365.

[Rogallo and Moin, 1984] Rogallo, R. and Moin, P. (1984). Numerical simulation of turbulent flows. *Annu. Rev. Fluid Mech.*, 16:99–137.

[Roshko, 1954] Roshko, A. (1954). On the development of turbulent wakes from vortex streets. Technical Report 1194, NACA.

[Rotta, 1951] Rotta, J. (1951). Statistische Theorie nichthomogener Turbulenz. *Zeitschrift fur Physik*, 129:547–572.

[Rudy and Strikwerda, 1980] Rudy, D. and Strikwerda, J. (1980). A nonreflecting outflow boundary condition for subsonic Navier-Stokes calculations. *Journ. Comp. Phys.*, 36:55–70.

[Sarkar, 1992] Sarkar, S. (1992). The pressure-dilatation correlation in compressible flows. *Phys. Fluids A*, 4(12):1606–1610.

[Sarkar et al., 1991] Sarkar, S., Erlebacher, G., and Hussaini, M. (1991). The analysis and modeling of dilatation terms in compressible turbulence. *J. Fluid Mech.*, 227:473.

[Schneider et al., 1978] Schneider, G., Raithby, G., and Yovanovich, M. (1978). Finite element analysis of incompressible fluid flow incorporating equal order pressure and velocity interpolation. In *Numerical Methods in Laminar and Turbulent Flow* (C. Taylor, K. Morgan, C.A. Brebbia eds). Pentech Press, Plymouth.

[Shakib, 1988] Shakib, F. (1988). *Finite element analysis of the compressible Euler and Navier-Stokes equations.* PhD thesis, Department of Mechanical Engineering, Stanford University.

[Shakib et al., 1991] Shakib, F., Hughes, T., and Johan, Z. (1991). A New Finite Element Method for Computational Fluid Dynamics: X. The compressible Euler and Navier-Stokes equations. *Comp. Meth. Appl. Mech. Eng.*, 89:141–219.

[Simo and Armero, 1994] Simo, J. and Armero, F. (1994). Unconditional stability and long term behavior of transient algorithms for the incompressible Navier-Stokes equations. *Comp. Meth. Appl. Mech. Eng.*, 111:111–154.

[Sloan, 1980] Sloan, D. (1980). On boundary conditions for the numerical solution of hyperbolic differential equations. *Int. J. Num. Meth. Fluids.*, 15:1113–1127.

[Smith and Woodruff, 1998] Smith, L. and Woodruff, S. (1998). Renormalization - Group analysis of turbulence. *Annu. Rev. Fluid Mech.*, 30:329–364.

[Smits and Dussauge, 1996] Smits, A. and Dussauge, J. (1996). *Turbulent Shear Layers in Supersonic Flow.* AIP Press.

[So et al., 1994] So, R., Zhang, H., Gatski, T., and Speziale, C. (1994). Logarithmic laws for compressible turbulent boundary layers. *AIAA Journal*, 32(11).

[Sohn, 1986] Sohn, J. (1986). *Evaluation of Fidap on some classical laminar and turbulent benchmarks.* Universities Space Research Association. Fluid Dynamics Branch. NASA / Marshall Space Flight Center.

[Soto, 1997] Soto, O. (1997). *Estabilización de la solución por elementos finitos de problemas de flujo incompresible con rotación, turbulencia, superficie libre y temperatura.* PhD thesis, Escola Tècnica Superior d'Enginyers de Camins, Canals i Ports, Universitat Politècnica de Catalunya, Barcelona.

[Soulaimani and M.Fortin, 1994] Soulaimani, A. and M.Fortin (1994). Finite element solution of compressible viscous flows using conservative variables. *Comp. Meth. Appl. Mech. Eng.*, 118:319–350.

[Speziale et al., 1994] Speziale, C., Abid, R., and Mansour, N. (1994). Evaluation of Reynolds stress turbulence closures in compressible homogeneous shear flows. TR - ICASE 94 - 17, NASA.

[Speziale and Sarkar, 1991] Speziale, C. and Sarkar, S. (1991). Second order closure models for supersonic turbulent flows. CR - 187508 ICASE 91 - 9, NASA.

[Spina et al., 1994] Spina, E., Smits, A., and Robinson, S. (1994). The physics of supersonic turbulent boundary layers. *Annu. Rev. Fluid Mech.*, 26:287–319.

[Stanford, 1982] Stanford (1982). AFOSR-HTTM-Stanford Conference on Complex Turbulent Flows: Comparison of Computation and Experiment. Vol. 1 and 2.

[Storti et al., 1992] Storti, M., Baumann, C., and Idelsohn, S. (1992). A preconditioning mass matrix to accelerate the convergence to the steady state Euler solutions using explicit schemes. *Int. J. Num. Meth. Eng.*, 34:519–541.

[Storti et al., 1997] Storti, M., Nigro, N., and Idelsohn, S. (1997). Equal-order interpolations: a unified approach to stabilize the incompressible and advective effects. *Comp. Meth. Appl. Mech. Eng.*, 143:317–331.

[Strang, 1968] Strang, G. (1968). On the construction and comparison of difference schemes. *SIAM J. Numer. Anal.*, 5(3):506–517.

[Temam, 1969] Temam, R. (1969). Sur l'approximation de la solution des équations de Navier–Stokes par la méthode des pas fractionaires (I). *Arch. Rat. Mech. Anal.*, 32:135–153.

[Tennekes and Lumley, 1972] Tennekes, H. and Lumley, J. (1972). *A first course in turbulence*. MIT Press.

[Turkel, 1992] Turkel, E. (1992). Review of preconditioning methods for fluid dynamics. CR 92-47, NASA.

[Turkel and Radespiel, 1996] Turkel, E. V. V. and Radespiel, R. (1996). Preconditioning methods for low-speed flows. CR -201605 ICASE 96-57, NASA.

[Van den Burg et al., 1992] Van den Burg, J., Kuerten, J., and Zandbergen, P. (1992). Improved shock - capturing of Jameson's scheme for the Euler equations. *Int. J. Num. Meth. Fluids.*, 15:649–671.

[Van Driest, 1951] Van Driest, E. (1951). Turbulent boundary layer in compressible fluids. *Journal of Aeronautical Sciences*, 18:145–160.

[Van Mieghem, 1949] Van Mieghem, J. (1949). Les équations générales de la mécanique et de l'énergétique des milleux turbulents en vue des applications à la météorologie. *Mémoires Institut Royal Météo. de Belgique*, 34.

[Vázquez and Codina, 1998] Vázquez, M. and Codina, R. (1998). Numerical solution of the Navier - Stokes equations using a splitting technique with Multigrid acceleration. In *Proc. 4th World Congress on Computational Mechanics, Buenos Aires, Argentina*, volume Part 2, page 663. International Asociation for Computational Mechanics.

[Vázquez et al., 1996] Vázquez, M., Codina, R., and Zienkiewicz, O. (1996). A fractional step method for the solution of the Navier-Stokes equations. Technical Report 103, CIMNE.

[Weiss and Smith, 1995] Weiss, J. and Smith, W. (1995). Preconditioning applied to variable and constant density flows. *AIAA Journal*, 33(11).

[Wesseling, 1995] Wesseling, P. (1995). Introduction to Multi - Grid methods. CR - 195045 ICASE 95 - 11, NASA.

[Wilcox, 1993] Wilcox, D. (1993). *Turbulence Modeling for CFD*. DCW Industries.

[Zeierman and Wolfshtein, 1986] Zeierman, S. and Wolfshtein, M. (1986). Turbulent time scale for turbulent-flow calculations. *AIAA Journal*, 24(10):1606–1610.

[Zeman, 1990] Zeman, O. (1990). Dilatation dissipation: the concept and applicacion in modeling compressible mixing layers. *Phys. Fluids A*, 2(2):178–188.

[Zienkiewicz, 1977] Zienkiewicz, O. (1977). *The Finite Element Method*. Mc. Graw - Hill, London.

[Zienkiewicz and Codina, 1995] Zienkiewicz, O. and Codina, R. (1995). A general algorithm for compressible and incompressible flow - Part I. The Split, Characteristic-Based Scheme. *Int. J. Num. Meth. Fluids.*, 20:869–885.

[Zienkiewicz et al., 1995] Zienkiewicz, O., Morgan, K., Satya Sai, B., Codina, R., and Vázquez, M. (1995). A general algorithm for compressible and incompressible flow - Part II. Tests on the Explicit Form. *Int. J. Num. Meth. Fluids.*, 20:887–913.

[Zienkiewicz et al., 1996] Zienkiewicz, O., Satya Sai, B., Morgan, K., and Codina, R. (1996). Split characteristic based semi - implicit algorithm for laminar / turbulent incompressible flows. *Int. J. Num. Meth. Fluids.*, 23:1–23.

[Zienkiewicz et al., 1990] Zienkiewicz, O., Szmelter, J., and Peraire, J. (1990). Compressible and incompressible flow; an algorithm for all seasons. *Comp. Meth. Appl. Mech. Eng.*, 78:105–121.

[Zienkiewicz and Wu, 1992] Zienkiewicz, O. and Wu, J. (1992). A general explicit or semi-explicit algorithm for compressible and incompressible flows. *Int. J. Num. Meth. Fluids.*, 35:457–479.